TOWARDS A BETTER UNDERSTANDING OF *ERG11* BIOLOGY IN THE MODEL ORGANISM *SACCHAROMYCES CEREVISIAE* AND IN THE OPPORTUNISTIC HUMAN PATHOGEN *CANDIDA ALBICANS*

Winnie KERSTENS

Supervisor:
Prof. P. Van Dijck

Members of the
Examination Committee:
Prof. R. Lavigne
Prof. S. Rupp
Prof. L. Temmerman
Prof. J. Thevelein
Prof. A. Voet

Dissertation presented in partial fulfilment of the requirements for the degree of Doctor of Science (PhD): Biochemistry and Biotechnology

February 2019

© 2019 WINNIE KERSTENS
Uitgegeven in eigen beheer, WINNIE KERSTENS, LEUVEN

Alle rechten voorbehouden. Niets uit deze uitgave mag worden vermenigvuldigd en/of openbaar gemaakt worden door middel van druk, fotokopie, microfilm, elektronisch of op welke andere wijze ook zonder voorafgaandelijke schriftelijke toestemming van de uitgever.

All rights reserved. No part of the publication may be reproduced in any form by print, photoprint, microfilm, electronic or any other means without written permission from the publisher.

Acknowledgements

I am excited about the fact that I have reached the very final phase of PhD writing and by extension also of the PhD itself. It has been an experience from which I have learned a lot and in which I have grown both on a professional and personal level. I am very grateful to my supervisor Prof. Van Dijck for having given me this opportunity and for his continuous support and positive mindset.

I would like to thank the members of the Examination Committee, Prof. Thevelein, Prof. Lavigne, Prof. Voet, Prof. Rupp and Prof. Temmerman for the time they have put into the evaluation of this thesis and for all comments and suggestions, which have significantly improved this work. I would also sincerely like to thank Griet, for all the effort and time put into correcting the preliminary version of the thesis. Thank you.

I would like to thank the two post docs who have worked on this project, Dr. A Fiori, for starting up the work and Dr. M. Holtappels, for going through some challenging scientific times with me. I would also like to thank the master and bachelor students who have contributed to this work. The biggest 'THANK YOU' however goes to Ilse, who has since the very beginning offered the greatest of help and not only through technical assistance. Thank you for all your hard work! You deserve a medal! I would also like to thank all the other members of the *Candida* lab. Thank you Ana - for all your great advice and encouragement, Floris - for the awesome food tips, Celia - for technical assistance and interesting cultural talks, Ona - for more nice small(&bigger) talk, Liesbeth - for scientific tips&tricks, Yuke - for the laughs at the end of the working day, Tran - for the funny encounters in the hallway, Sanne - for even more tips and Lotte, Cindy, Soña, Erwin, Adam, Wouter, Jurgen, Mieke, Stefanie, Selien and Katrien for the good vibe and the interesting scientific discussions. I thank my office mates Sanne, Griet, Thomas and Stefanie for the nice working atmosphere and the occasional breaks. I would also like to thank all other members of the MCB lab for scientific or other help, for amusing conversations and for the fact that almost always, any time of day and night, there would be someone in the lab. That made it less spooky to walk around. Thank you also to Leni, Hilde, Jan and all technicians for everything they do to keep the lab functional and to Nico for all the IT help! I would like to thank all the members of the MCB lab (MCBall) for the positive atmosphere they bring to the lab. Lastly, I would like to thank Bea for being not just an amazing colleague but also a very good friend, you have helped me in so many ways!

I would like to thank all my friends for being truly amazing and for being a great support, even though they might not realize it. Thank you Sary, Sara, Britt, Deirdre, Ming, Wen, Ying Ying, Lynn and Ditte. Thank you Dominique and Lieselot. Thank you Margot. Thank you awesome Biochemie vriendjes, especially Bea, Goele and Hanne.

Lastly, I would like to thank my family. I take a lot of inspiration from you. I enjoy our cosy get-togethers and I would like to thank you for all your support! Thank you mams and paps for all the good things you have brought to my life, for always believing in me and for all your love. Thank you bomma and bompa for being the superbest grandparents in the whole world. Your support and love is limitless. I am so grateful for everything you have done. This brings me to the last but biggest THANK YOU of all… Thank you Superman Maciej for being the very best partner I could have ever wished for! You have guided me through this PhD, with joy, laughter, crazy moments, dancing and singing and I am so grateful for all your support! I am the luckiest person for having you in my life!

February 1st, 2019 - Leuven

Winnie

Table of contents

Table of contents I

Summary V

Samenvatting VII

List of abbreviations IX

CHAPTER 1
Literature overview 1

1.1 Introduction 3

1.2 An introduction to fungi and fungal infections 4

1.2.1 The yeast model *Saccharomyces cerevisiae*: a vow to molecular biology in sickness and in health 4

1.2.2 Human fungal pathogens 5

1.2.2.1 'Hear, hear': awareness of human fungal infections 5

1.2.2.2 Superficial and invasive human fungal infections 5

1.2.2.3 Most wanted: the top four fungal criminals 6

1.2.3 Antifungal drugs and challenges for their efficacy 8

1.2.3.1 The antifungal armamentarium 8

1.2.3.2 Antifungal drug resistance and tolerance 12

1.3 The bimodal targeting of cytochrome P450s 18

1.3.1 What are cytochrome P450s? 18

1.3.2 CYP51 alias Erg11 in yeast: a conserved lanosterol demethylase important for sterol biosynthesis 18

1.3.2.1 The conserved CYP51 protein 18

1.3.2.2 The CYP51 protein of yeast 20

1.3.2.3 The function of ergosterol and other sterols in yeast 20

1.3.2.4 Regulation of *ERG11* expression in *Saccharomyces cerevisiae* and *Candida albicans* 22

1.3.3 From mono to multi: protein targeting to subcellular compartments 24

1.3.4 Bimodal targeting of cytochrome P450s to the endoplasmic reticulum and mitochondria in mammals 25

1.3.5 Bimodal targeting in yeast: exploring the possibility of mitochondrial Erg11 26

1.4 The degradation of cytochrome P450s 28

1.4.1 The vacuolar proteases of *Saccharomyces cerevisiae*: seven actors on duty to preserve protein homeostasis 28

1.4.2 The vacuolar proteases Pep4 and Prb1 are important for autophagic breakdown in *Saccharomyces cerevisiae* 29

1.4.2.1 A general introduction to autophagy in *Saccharomyces cerevisiae* 29

1.4.2.2 The role of Pep4 and Prb1 in *Saccharomyces cerevisiae* autophagy 29

1.4.2.3 Non-vacuolar, autophagy-independent activities of *Saccharomyces cerevisiae* Pep4 and Prb1 30

1.4.2.4 ER-phagy: a specific type of autophagy that sequesters and degrades excess proteins of the endoplasmic reticulum 30

Aim of this study **33**

CHAPTER 2
***Saccharomyces cerevisiae* Erg11 is detected as multiple bands on western blot** **35**

2.1 Defining the conditions of Erg11 detection on western blot 37

2.2 Identification of the truncated Erg11 forms detected on western blot 43

2.3 Discussion 45

CHAPTER 3
Erg11 contains a mitochondrial targeting signal in *Saccharomyces cerevisiae* **47**

3.1 Construction of truncated Erg11 products in *Saccharomyces cerevisiae* 49

3.2 Is Erg11 bimodally targeted to ER and mitochondria in *Saccharomyces cerevisiae*? 51

3.2.1 Restoration of arginine auxotrophy by mitochondrial targeting of Erg11-Arg8$^{\Delta 13}$ chimeras 51

3.2.2 Analysis of the subcellular localization of the Erg11 variants by microscopy 53

3.2.2.1 Fluorescence microscopy 53

3.2.2.2 Focused ion beam scanning electron microscopy 56

3.3 Is mitochondrially localized, truncated Erg11 functional? 59

3.4 Does the mitochondrial targeting signal have a function in full-length Erg11? 69

3.5 Discussion 75

CHAPTER 4
The vacuolar proteases Pep4 and Prb1 are important for the generation of multiple Erg11 bands on western blot **79**

4.1 Testing the cleavage hypothesis: is a protease responsible for the generation of multiple Erg11 bands on western blot? 81

4.2 *ERG11* overexpression triggers ER stress in *Saccharomyces cerevisiae* 87

4.3 Discussion 90

CHAPTER 5
Translating the results to the opportunistic human pathogen *Candida albicans* **93**

5.1 *Candida albicans* Erg11 is detected as multiple bands on western blot 95

5.2 *In silico* analysis of a putative MTS of *Candida albicans* Erg11 98

5.3 Creation of null mutants of the *Candida albicans* homologs to the *Saccharomyces cerevisiae* proteases responsible for Erg11 cleavage products 100

5.4 Discussion 104

CHAPTER 6
General conclusion and future perspectives **107**

6.1 The Erg11 MTS: a determinant of mitochondrial localization? 109

6.2 Multiple Erg11 protein forms: a story of degradation 113
6.3 The contribution of this study to optimized antifungal therapy 115
CHAPTER 7
Materials and methods **117**
7.1 Materials 119
7.1.1 Growth media and conditions 119
7.1.2 Strains 119
7.1.3 Plasmids 121
7.1.4 Primers 123
7.2 Methods 130
7.2.1 Protein extraction and western blotting 130
7.2.2 Spot assay 131
7.2.3 Fluorescence microscopy 131
7.2.4 Focused ion beam scanning electron microscopy 131
7.2.5 Tetrad analysis 132
7.2.6 Ergosterol measurement 132
7.2.7 Real time quantitative reverse transcription PCR 133
7.2.8 Determination of the mitochondrial DNA copy number 133
7.2.9 FLC susceptibility by Etest 134
7.2.10 FLC susceptibility by MIC broth microdilution assay 134
7.2.11 Tolerance assay 134
7.2.12 Protease/peptidase screening 134
7.2.13 Growth analysis 135
7.2.14 *In silico* analysis of Erg11 structure 135
7.2.15 Alignment of CYP51 sequences 135
7.2.16 Mass spectrometry analysis of the free N-termini of purified *S. cerevisiae* Erg11 135
Appendix I. MS data on the identification of putative cleavage sites in *Saccharomyces cerevisiae* Erg11 **141**
Appendix II. List of genes annotated with a protease or peptidase function **143**
References **152**
CV and list of publications **163**

Summary

Fungal species are an important cause of life-threatening invasive infections. With a yearly mortality rate of more than 1.5 million people, they are responsible for more than three times the number of deaths caused by malaria (Bongomin *et al.*, 2017). Yet, the antimalarial drug arsenal exceeds that of antifungal drug classes used to treat invasive infections. In fact, only four classes are used in the clinic to treat life-threatening fungal infections, with the azoles as the predominant agents. Alarmingly, the antifungal potential of these drug classes is being threatened by the increasing prevalence of drug resistance. With an urgent need for the development of new antifungal drugs and only few in the pipeline, improvement of the activity of existing drug classes is imperative.

Previous studies in our lab have identified synergism between the azole antifungal drug class and the tetracyclines, a class of antibacterials. In particular, the combination of doxycycline (DOX) and the azole fluconazole (FLC) has proven to enhance the antifungal activity of azoles on the opportunistic human fungal pathogen *Candida albicans* (Fiori and Van Dijck, 2012). During further studies, it has been observed that the target of the azole drugs, Erg11 is detected as multiple protein bands on western blot in the presence of FLC, both in *Candida albicans* and in the model organism *Saccharomyces cerevisiae*. As the additional protein products have only been detected during FLC therapy, it has been suggested that these extra Erg11 products might affect azole therapy in a way that cells would become less susceptible to the drugs in the presence of the additional Erg11 products.

Erg11 is a member of the class of cytochrome P450 (CYP) proteins, which are conserved over all biological kingdoms. Other labs have reported that some mammalian CYPs can be bimodally targeted to the endoplasmic reticulum (ER), their usual site of residence and the mitochondria, the latter additionally under the induction of drug treatment (Avadhani *et al.*, 2011). However, the function of the mitochondrially targeted pool remains unknown. In this study, it has been investigated whether Erg11 products can be targeted to mitochondria in yeast, in addition to their ER localization, under azole treatment in analogy to the mammalian model. Furthermore, it has been examined whether mitochondrial Erg11 affects azole drug potency, as the phenomenon of bimodal targeting in mammals is especially observed under drug treatment.

Our study has indicated that the *S. cerevisiae* Erg11 protein possesses a cryptic mitochondrial targeting signal (MTS). However, the mitochondrial targeting of ER-resident Erg11 has not been detected *in vivo*, undermining the hypothesis of Erg11 bimodal targeting. Furthermore, it has been identified that the substitution of four positively charged lysine residues to alanines in the cryptic MTS abrogates the mitochondrial targeting of the $Erg11^{\Delta 150}$ construct, a truncated form of Erg11 in which the cryptic MTS is exposed. These substitutions also affect the ergosterol production of full-length Erg11, suggesting that these residues are important to the biology of the Erg11 protein.

Three of these positively charged residues are conserved in the Erg11 sequence from yeast to mammals. It has been hypothesized that these positively charged residues are important for Erg11 activity through interaction with the redox partner. In the course of these studies, the technique of focused ion beam scanning electron microscopy (FIB-SEM) has been implemented for the first time in *S. cerevisiae* for localization studies of a tagged protein of interest, Erg11.

Furthermore, the *S. cerevisiae* vacuolar proteases Pep4 and Prb1 and the *C. albicans* homologs Apr1 and Prb12 have been identified as responsible factors for the process of generating multiple Erg11 protein products, suggesting that the extra Erg11 forms are degradation products. It has been demonstrated that overexpression of the Erg11 protein induces expansion of ER membranes and ER stress, observed on electron micrographs as the production of multilayered ER membrane concentric structures, termed whorls. They are eliminated by the process of ER-phagy, which targets them to the vacuole for degradation. Most likely, this autophagic process is responsible for the degradation of Erg11, leading to the detection of the shorter Erg11 forms on western blot, especially under fluconazole treatment which induces Erg11 protein production. Correspondingly, a mass spectrometric analysis of purified Erg11 has identified 23 putative cleavage sites in Erg11.

Lastly, it has been hypothesized that *S. cerevisiae ERG11* is not essential on minimal synthetic medium, as *erg11* mutants are viable. The molecular mechanisms behind this observation have not been underpinned, however on rich medium the gene remains essential, as no viable *erg11* mutants could be obtained. Possibly, the availability of amino acids in the medium has an effect on the essentiality of the *ERG11* gene. The further validation and clarification of this finding will be important for *e.g. erg11* mutant studies, as it enables their examination under aerobic conditions, which is up to now only possible in an *erg3Δ* background strain or under anaerobic conditions in the presence of sterol supplementation.

Samenvatting

Fungale infecties vormen een belangrijke oorzaak van levensbedreigende systemische infecties, met een mortaliteitscijfer dat meer dan drie keer hoger ligt dan dat van malaria en jaarlijks meer dan anderhalf miljoen mensen bedraagt (Bongomin *et al.*, 2017). Nochtans overstijgt het aantal klassen van antimalariamiddelen dat van antifungale middelen. Er worden slechts vier klassen van antifungale middelen gebruikt om systemische fungale infecties te behandelen, waarvan de azolen het meest gebruikt worden. De behandeling van fungale infecties wordt ondermijnd door de toenemende resistentie tegen deze gelimiteerde groep. De zoektocht naar nieuwe middelen is daarom hoogstnoodzakelijk, maar slechts enkele moleculen zijn momenteel in klinische testfase. In parallel is daarom ook een verbetering van de activiteit van de huidige middelen belangrijk.

Tijdens voorgaande studies werd een synergistisch effect waargenomen tussen azolen en tetracyclines, een klasse van antibacteriële medicatie. Meer bepaald de combinatie van doxycycline (DOX) en azolen zoals fluconazol (FLC) verbeterde de antifungale activiteit van de azolen tegen de opportunistische humane pathogeen *Candida albicans* (Fiori and Van Dijck, 2012). Verdere karakterisering van dit effect leidde tot de bevinding dat het proteïne dat geïnhibeerd wordt door de azolen, Erg11, wordt waargenomen als meerdere proteïneproducten op western blot, wanneer cellen behandeld worden met fluconazol, zowel in *C. albicans* als in het modelorganisme *Saccharomyces cerevisiae*. De hypothese ontstond dat deze Erg11 fragmenten belangrijk zouden kunnen zijn tijdens azolentherapie, door de gevoeligheid van de fungi voor de azolen te verminderen wanneer ze aanwezig zijn.

Erg11 behoort tot de klasse van cytochroom P450 (CYP) proteïnen, die geconserveerd zijn over alle biologische domeinen. Sommige CYPs in zoogdieren kunnen gelokaliseerd worden in twee organellen, het ER waar zij zich normaal bevinden en de mitochondriën, waar zij naartoe kunnen worden gestuurd tijdens een behandeling met medicatie. De functie van de mitochondriale fractie is niet gekend. In deze studie wordt onderzocht of de kortere vormen van Erg11, die geobserveerd worden tijdens de behandeling met azolen, kunnen lokaliseren naar de mitochondriën in fungi, gelijkaardig aan het model in zoogdieren. Bovendien wordt onderzocht of mitochondriaal Erg11 een effect heeft op de behandeling met azolen, aangezien de mitochondriale lokalisatie van CYPs specifiek wordt waargenomen bij zoogdieren tijdens een behandeling met medicatie.

Ondanks dat een bimodale lokalisatie van Erg11 in *S. cerevisiae* niet is vastgesteld *in vivo*, wordt er wel aangetoond dat Erg11 een cryptisch mitochondriaal-lokalisatie signaal (MTS) draagt. Bovendien worden vier positief geladen aminozuren gekarakteriseerd die essentieel zijn voor de MTS. Wanneer deze veranderd worden naar alanines reduceert dit de mitochondriale lokalisatie van Erg11$^{\Delta 150}$, waarin de cryptische MTS is blootgesteld. Ook beïnvloeden deze mutaties de ergosterolproductie van een stam die deze mutaties draagt in wildtype Erg11. Drie van deze lysines

zijn geconserveerd tussen fungi en zoogdieren, wat erop wijst dat ze belangrijk kunnen zijn voor de biologie van het Erg11 proteïne. Er wordt verondersteld dat deze aminozuren betrokken zijn in de interactie met de redox partner. Tijdens deze studies wordt bovendien voor de eerste keer de *focused ion beam scanning electron microscopy* (FIB-SEM) techniek toegepast in *S. cerevisiae* voor lokalisatiestudies van een getagde versie van het proteïne van interesse, Erg11.

Het proces dat verantwoordelijk is voor de afbraak van Erg11 in *S. cerevisiae* wordt in deze studie in kaart gebracht en lijkt behouden in *C. albicans*. Een screening toont aan dat de vacuolaire proteasen Pep4 en Prb1 verantwoordelijk zijn voor de vorming van de additionele Erg11 bandjes op western blot. Een gelijkaardig resultaat wordt gevonden voor de Apr1 en Prb12 homologen in *C. albicans*, respectievelijk. Bovendien wordt aangetoond dat overexpressie van Erg11 leidt tot de expansie van het ER-membraan en ER-stress, wat waargenomen wordt gedurende elektronenmicroscopie als gelaagde, concentrische ER-membraanstructuren, die 'whorls' genoemd worden. Deze worden geëlimineerd door het proces van ER-fagie, waarbij de structuren naar de vacuole gestuurd worden voor afbraak. Er wordt verondersteld dat dit proces verantwoordelijk is voor de observatie van de extra Erg11 bandjes op western blot, aangezien fluconazolbehandeling leidt tot een verhoogde expressie van het Erg11 proteïne. Bovendien worden via massaspectrometrie analyse 23 mogelijke knipplaatsen geïdentificeerd in opgezuiverd *S. cerevisiae* Erg11.

Verder wordt aangetoond dat het *S. cerevisiae ERG11* gen niet essentieel is wanneer cellen opgroeien op minimaal synthetisch medium. *erg11* mutanten zijn echter niet leefbaar op verrijkt medium. De moleculaire mechanismen die verantwoordelijk zijn voor deze waarneming zijn niet geïdentificeerd. Mogelijks heeft de aanwezigheid van aminozuren in het medium een effect op de noodzakelijkheid van het *ERG11* gen in *S. cerevisiae*. Verdere opheldering van deze bevinding zal een impact hebben op toekomstige studies, aangezien *erg11* mutanten voorlopig enkel kunnen opgegroeid worden in een *erg3Δ* deletiestam of onder anaerobe condities in de aanwezigheid van sterolen.

List of abbreviations

3D	Three Dimensional
5-FC	Flucytosine
AmB	Amphotericin B
ANI	Anidulafungin
ANOVA	Analysis Of Variance
ATC	Anhydrotetracycline
BLAST	Basic Local Alignment Search Tool
CASP	Caspofungin
CDC	Centers for Disease Control and Prevention
CFU	Colony Forming Unit
CLSI	Clinical and Laboratory Standards Institute
CPR	Cytochrome P450 Reductase
CPS	Carboxypeptidase S
CRISPR	Clustered Regularly Interspaced Short Palindromic Repeats
CSM	Complete Synthetic Medium
C_T	Threshold Cycle
CYP	Cytochrome P450
DAB	Diaminobenzidine
DIC	Differential Interference Contrast
(c/g)DNA	(complementary/genomic) Deoxyribonucleic Acid
DOX	Doxycycline
DTT	Dithiothreitol
EMC	ER Membrane protein Complex
ER	Endoplasmic Reticulum
ERAD	ER-Associated Degradation
ERMES	ER-Mitochondria Encounter Structure
EsB	Energy selective Backscattered
EUCAST	European Committee on Antimicrobial Susceptibility Testing
EV	Empty Vector
FAD	Flavin Adenine Dinucleotide
FIB-SEM	Focused Ion Beam Scanning Electron Microscopy
FLC	Fluconazole
FMN	Flavin Mononucleotide
FRT	FLP Recombination Target
GBrowse	Generic Genome Browser
GFP	Green Fluorescent Protein
GOI	Gene Of Interest
HA	Hemagglutinin
HDR	Homology-Directed Repair
HIV	Human Immunodeficiency Virus
HRP	Horseradish Peroxidase
IM	Inner Membrane

IMS	Intermembrane Space
kDa	kilodalton
KETO	Ketoconazole
LMP	Lysosomal Membrane Permeabilization
MAM	Mitochondria Associated Membrane
MFC	Minimal Fungicidal Concentration
MIC	Minimal Inhibitory Concentration
MICA	Micafungin
MS	Mass Spectrometry
mtDNA	Mitochondrial DNA
mtGFP	Mitochondrial GFP
MTS	Mitochondrial Targeting Signal
M_w	Molecular Weight
$O.D._{600nm}$	Optical Density at 600 nm
OM	Outer membrane
ORF	Open Reading Frame
PAM	Protospacer Adjacent Motif
PEC	Proteomics Expertise Center
PKA	Protein Kinase A
POS	Posaconazole
PrA	Proteinase A
PrB	Proteinase B
PSM	Peptide Spectrum Match
qRT-PCR	quantitative Reverse Transcription Polymerase Chain Reaction
(m/t)RNA	(messenger/transfer) Ribonucleic Acid
rpm	revolutions per minute
RT	Room Temperature
SD	Synthetic Defined
sgRNA	single guide RNA
SRP	Signal Recognition Particle
TEM	Transmission Electron Microscopy
TET	Tetracycline
TOM	Translocase of the Outer Membrane
TSS	Transcription Start Sites
UPR	Unfolded Protein Response
UPS	Ubiquitin-Proteasome System
UV	Ultraviolet
VOR	Voriconazole
YPD	Yeast Peptone Dextrose
YPEG	Yeast Peptone Ethanol Glycerol

CHAPTER 1
LITERATURE OVERVIEW

1.1 Introduction

This research is based on initial experiments performed in our lab by postdoc A. Fiori. He has discovered that the efficacy of the azole antifungal drug class is enhanced *in vitro* when tetracyclines, a class of antibacterial drugs that inhibit bacterial protein synthesis, are added to *C. albicans* cultures, specifically the drug doxycycline (DOX) (Fiori and Van Dijck, 2012). DOX is typically used in molecular genetics to regulate the expression of genes of interest, when these are placed under the control of tetracycline-regulatable gene expression systems. In the course of such, unpublished studies with *C. albicans* strains carrying tetracycline-regulatable promoters in the presence of DOX, the enhanced effect on azole drug activity has been observed.

The effect of tetracyclines on azole activity has been studied further. It has been found that the combination of azoles with DOX is more potent than with tetracycline (TET) (Fiori and Van Dijck, 2012). Furthermore, the effect of DOX on the growth of FLC-treated *C. albicans* has been identified as dosage-dependent, with complete loss of growth on spot assays with 10 µg/mL fluconazole and 50 µg/mL DOX. Treatment of *C. albicans* cells with DOX alone had no effect on cell growth. Furthermore, it has been identified that a DOX concentration of 50 µg/mL inhibits the ability of *C. albicans* to grow at high azole drug concentrations, a phenomenon that has also been described as 'tolerance' to azoles or 'trailing growth' and is further discussed in paragraph 1.2.3. It has been hypothesized that the effect of DOX on FLC activity is due to its iron chelating capacity.

Furthermore, Dr. A. Fiori has noticed the presence of several distinct protein forms of the azole target, Erg11 on western blot from *C. albicans* azole-treated cells. The Erg11 protein is important to the biosynthetic pathway of ergosterol production, which is the fungal homolog of mammalian cholesterol (as further discussed in paragraph 1.3). These additional protein forms of Erg11 have not been detected during azole-DOX combination therapy or in the absence of drugs. Therefore, these findings have led to the hypothesis that the presence of extra forms of Erg11 might undermine azole antifungal therapy, possibly by contributing to the phenomenon of tolerance. Also in *S. cerevisiae*, additional Erg11 products have been observed on western blot in the presence of azole therapy.

During my doctoral studies, I have tried to repeat several experiments of Dr. A. Fiori and have studied the hypothesis that the additional Erg11 products might affect azole therapy. However, I have never been able to repeat the results of loss of the additional *C. albicans* Erg11 protein forms on western blot with azole-DOX combination therapy, compared to azole therapy alone. Therefore, the effect of DOX on *C. albicans* tolerance to azoles has not been studied further, as this is probably independent of the additional Erg11 products observed on western blot.

1.2 An introduction to fungi and fungal infections

1.2.1 The yeast model *Saccharomyces cerevisiae*: a vow to molecular biology in sickness and in health

Saccharomyces cerevisiae is also known as brewer's or baker's yeast. The former function can be deduced from its name, as *Saccharomyces* stands for sugar mold or fungus and *cerevisiae* comes from the Gaelic word *kerevigia* and the old French word *cervoise*, which both mean beer (Mortimer, 2000). The single-celled eukaryote divides by the process of budding, by which daughter cells pinch off the mother cell. Because of this property, *S. cerevisiae* is also referred to as budding yeast. *S. cerevisiae* is an efficiently culturable organism. The cells have a size of approximately five micrometers and cell divisions occur every 90 minutes in optimal growth conditions (Bergman, 2001). It can be found either in a haploid or a diploid state, both of which are able to undergo mitosis. When two haploids of the opposite mating type mate, the resulting diploid can undergo meiosis and subsequently sporulate to produce four haploid spores, which can re-enter the mitotic cell cycle and resume vegetative growth under appropriate conditions, a process referred to as germination (Joseph-Strauss *et al.*, 2007).

The haploid yeast genome is divided over sixteen chromosomes and was the first eukaryotic genome to be fully sequenced (Goffeau *et al.*, 1996). It is generally accepted that around one hundred million years ago, *S. cerevisiae* underwent a whole-genome duplication event, where the ancestor lost about 85% of the duplicated genes, leading to the current ~6,000 genes, of which about 10–20% are duplicated (Botstein and Fink, 2011). Not long after the genome sequencing cooperative, the yeast community undertook the challenge to produce a haploid deletion collection, containing *S. cerevisiae* mutants that carry single deletions in nearly every open reading frame (ORF). Moreover, the drug resistance marker-replaced ORFs have been tagged with a unique barcode sequence to enable large-scale screenings with the deletion collection, resulting in a wealth of information on yeast biology (Winzeler *et al.*, 1999; Giaever *et al.*, 2002; Giaever and Nislow, 2014).

The first studies on yeast date back from the late eighteenth to the beginning of the nineteenth century (Barnett, 1998; Barnett and Robinow, 2002b; Barnett and Robinow, 2002a). Since then, the knowledge about and the toolbox on how to work with *S. cerevisiae* has expanded to the point that it has become one of the pioneering model organisms in the study of molecular cell biology (Botstein and Fink, 2011; Duina *et al.*, 2014). This is due to its excellent genetic tractability, the ease of manipulation and the plethora of tools, techniques and equipment that are available for yeast research. Because of the considerable degree of homology between eukaryotes, lessons learnt in the unicellular yeast can often be translated to mammalian models and the other way

around. In this way, invaluable insights have been gathered on the processes of aging, autophagy, lipid metabolism, mitochondrial biology, organelle contact sites *etc.*, which have significantly contributed to the definition of molecular mechanisms of diseases. In this regard, engineered yeast models can be used to study complex human diseases like neurodegeneration, or serve as screening systems in the identification of novel therapies against various human diseases (Longo *et al.*, 2012; Pereira *et al.*, 2012; Klug and Daum, 2014; Ohsumi, 2014; Lasserre *et al.*, 2015; Rutter and Hughes, 2015; Elbaz-Alon, 2017; Herrera-Cruz and Simmen, 2017). In the ever-expanding list of *S. cerevisiae* hallmarks in cell biology studies, we here address its use to the study of the fungal pathogen *Candida albicans* and the molecular framework around its Erg11 protein.

1.2.2 Human fungal pathogens

1.2.2.1 'Hear, hear': awareness of human fungal infections

The global disease burden caused by fungal infections is not widely recognized, although in the last few years, progress has been made concerning an increased understanding of the threat presented by fungal infections. Together with their partners, the U.S. Centers for Disease Control and Prevention (CDC) have organized for the second time the 'Fungal Disease Awareness Week' (October 1–5, 2018). This campaign aims to encourage both patients and medical staff to consider fungi as the cause of an infection, especially when symptoms are not improving with the used antibiotic treatment. Unfortunately, sensitive, fast and cheap diagnostics are lacking to identify fungal infections, which delays the startup of antifungal treatment and impacts on the survival rate of patients (Brown *et al.*, 2012a). Also in Belgium, the disease burden of fungal infections is underappreciated, while it has been estimated that annually one in fifty Belgians suffers from a severe fungal infection (Lagrou *et al.*, 2015). Therefore, it is important to inform people on the ubiquity of fungal infections and on the discomforts and dangers that can be associated with specific fungal diseases.

1.2.2.2 Superficial and invasive human fungal infections

Among the estimated 0.6 – 5 million fungal species that inhabit our planet, only some six hundred are able to colonize humans (Brown *et al.*, 2012b; Mayer *et al.*, 2013; Kohler *et al.*, 2014). Fungal infections can occur in various sites of the body, ranging from superficial infections of the outer skin and mucosa to invasive and life-threatening infections of inner organs and the bloodstream. While superficial infections are universal, invasive fungal infections occur primarily in people with a weakened immune system. Infections of the skin or nails affect approximately one out of four persons globally and are the most common human fungal infections. Mucosal infections of the vulvovaginal tract are also common, affecting 50 to 75% of women in their childbearing years. Invasive fungal infections occur less frequently. They are accompanied by a high mortality rate, even when antifungal treatment is provided (see Table 1.1). More than 1.5 million people die from

invasive fungal infections every year, which equals the number of deaths caused by tuberculosis and is threefold higher than that caused by malaria (Brown *et al.*, 2012a; Bongomin *et al.*, 2017).

1.2.2.3 Most wanted: the top four fungal criminals

The primary species causing fungal infections in humans belong to four genera: *Candida*, *Cryptococcus*, *Aspergillus* and *Pneumocystis*. Together, they are responsible for over 90% of all reported fungal-related deaths (Table 1.1). *Candida* species are commensals of the human flora but can cause overgrowth under favorable conditions. They are often associated with superficial infections, such as oral thrush or vulvovaginitis. However, in immunocompromised patients *Candida* is the primary cause of opportunistic invasive mycoses, most often infecting the bloodstream, a condition referred to as candidemia (Antinori *et al.*, 2016). More than 90% of invasive *Candida* infections are caused by *C. albicans*, *C. glabrata*, *C. parapsilosis*, *C. tropicalis* and *C. krusei* with *C. albicans* playing a leading role, causing generally about half of the *Candida* infections (Guinea, 2014). CDC has also reported on *C. auris* as a drug-resistant emerging pathogen. Recent studies have indicated shifts in the occurrence of disease-causing *Candida* species. On a global scale, the frequency of *C. albicans* infections is decreasing, while those caused by *C. glabrata* and *C. krusei* remain constant and infections caused by *C. parapsilosis* and *C. tropicalis* increase. This seems to be dependent on several parameters, such as geographical distribution, age of the patients and prior antifungal therapy (Pfaller and Diekema, 2007; Diekema *et al.*, 2012; Guinea, 2014). *Cryptococcus neoformans* and *Cryptococcus gattii* are the two most prominent species causing cryptococcal disease. Although they mainly affect immunocompromised patients, immunocompetent hosts are also frequently associated with *C. gattii* infections (Brown *et al.*, 2012a). Invasive fungal infections by *Aspergillus* species in immunocompromised patients are mainly caused by *A. fumigatus*, *A. flavus*, *A. niger*, *A. terreus*, *A. versicolor* and *A. nidulans* and are generally associated with high mortality rates (Shapiro *et al.*, 2011; Brown *et al.*, 2012a). *Pneumocystis jirovecii* causes pneumonia in immunocompromised patients. So far, it has been impossible to culture *Pneumocystis* in a laboratory environment, which makes it hard to study this pathogen and the molecular mechanisms that underly its pathogenicity (Brown *et al.*, 2012a; Kohler *et al.*, 2014).

Table 1.1. Most frequent occurring invasive fungal infections and their estimated infection and mortality rates (adapted from Brown *et al.* (2012a)).

	Estimated life-threatening infections/year worldwide	Mortality rate (% in infected population)
Candidiasis	>400,000	46 – 75
Cryptococcosis	>1,000,000	20 – 70
Aspergillosis	>200,000	30 – 95
Pneumocystis	>400,000	20 – 80

A close-up of *Candida albicans* and its dissimilarities with *Saccharomyces cerevisiae*

Fungal cell biology studies rely on *S. cerevisiae* as a model, because the molecular toolbox for pathogenic fungi is not as elaborate and genetic manipulations are often not as straightforward as in *S. cerevisiae*. However, it should be mentioned that the recent introduction of the CRISPR-Cas9 technique (Clustered Regularly Interspaced Short Palindromic Repeats and CRISPR-associated protein 9) has greatly enhanced the feasibility of gene manipulations in *C. albicans* and has been an important step forward in fungal genetic engineering in general (Vyas *et al.*, 2015; Nguyen *et al.*, 2017).

Despite many conserved processes, significant differences exist between the model organism *S. cerevisiae* and the opportunistic human pathogen *C. albicans*, as their lineages diverged 140 to 841 million years ago (Berman and Sudbery, 2002). For example, *C. albicans* lacks a complete sexual cycle, which complicates genetic studies (Berman and Sudbery, 2002). Furthermore, *C. albicans* is an obligate diploid organism, with eight pairs of chromosomes. The haploid genome is slightly larger than that of *S. cerevisiae* and it encodes large families of proteases, lipases and cell wall proteins that are not as abundant in *S. cerevisiae* (Berman and Sudbery, 2002). Another trait that has hindered molecular biology studies is the unconventional *C. albicans* codon usage, whereby the CUG codon is translated as serine, rather than leucine. This implies that molecular markers often do not function in *C. albicans* and require codon optimization. Similarly, this means that *C. albicans* genes are often only partially functional in *S. cerevisiae*, which can interfere with molecular studies (Berman and Sudbery, 2002). Additionally, *C. albicans* displays a multitude of virulence factors that are less pronounced or absent in the rarely observed pathogenic *S. cerevisiae*.

In general, *S. cerevisiae* is considered a non-pathogenic species. However, in recent years, some concern has been raised about its harmless status (Perez-Torrado and Querol, 2015). *S. cerevisiae* has been identified as a commensal of the human microbiome, found in the gastrointestinal, respiratory and genital tract (Pfaller *et al.*, 2009). Furthermore, over the last three decades, *S. cerevisiae* has been associated sporadically with mucosal and invasive infections (Enache-Angoulvant and Hennequin, 2005; Pfaller *et al.*, 2009; Perez-Torrado and Querol, 2015). Population-based studies have estimated that 0.1% to 3.6% of fungal blood infections are caused by *S. cerevisiae*, with an attributed crude mortality rate of 28% (Pfaller and Diekema, 2010). However, virulence factors of *S. cerevisiae* are not well known and do not seem as elaborate as those displayed by *C. albicans* (Phadke *et al.*, 2018).

The factors that attribute to the virulence of *C. albicans* concern a wide range of properties. Morphologically, *C. albicans* can grow in the yeast form, but it can also form hyphae and pseudohyphae. This is different from *S. cerevisiae*, which does not form hyphae (Berman and Sudbery, 2002). The morphological variance is thought to help the survival and spreading of *C. albicans*, as the yeast form is believed to be important for dissemination throughout the host, while

the hyphal form is important for disruption of host membrane barriers. Furthermore, *C. albicans* is assisted by robust stress responses and it can adapt to various conditions. It can reside in the intestine at high pH or in the vaginal tract at low pH and it can colonize aerobic surfaces to anaerobic regions (Kohler *et al.*, 2014). Other factors such as expression of adhesins, secretion of hydrolytic enzymes and formation of biofilms are all believed to contribute to the pathogenicity of *C. albicans* (Mayer *et al.*, 2013). A biofilm is a community of microbial cells that can form on implanted medical devices such as catheters, pacemakers, dentures, contact lenses and prosthetic joints or on mucosal surfaces. The biofilm has distinct properties compared to free-floating or planktonic cells, this is especially important with regard to the increased difficulty of clearing biofilm infections by antimicrobial therapy and the host immune system. *C. albicans* relies on its morphologically distinct cell types to build up the biofilm, consisting of a basal layer of yeast cells that adhere to the biotic or abiotic substrate from which hyphae and pseudohyphae build up the mass of the structure and produce an extracellular matrix. *C. albicans* yeast cells can then disperse from the biofilm to form new sites of infection and seed disseminated bloodstream infections and invasive infections of tissues and organs (Nobile and Johnson, 2015).

1.2.3 Antifungal drugs and challenges for their efficacy

1.2.3.1 The antifungal armamentarium

The classes of antifungal drugs that are used to treat invasive fungal infections can unfortunately be counted on one hand. The azole drug class is the most widely used (Roemer and Krysan, 2014). The other drug classes are the polyenes, flucytosine and the echinocandins (Perlin *et al.*, 2017). The cellular targets of these four drug classes are schematically represented in Fig. 1.1. The azoles can be divided in two subclasses: the imidazoles and the triazoles. All possess five-membered heterocyclic, nitrogen-containing structures that target Erg11, an enzyme in the ergosterol biosynthesis pathway. Over time, the imidazole group of azole drugs has been replaced by the triazole group, with enhanced specificity for the fungal target, improved drug formulations, better safety and pharmacokinetic profiles and an increased antifungal activity spectrum (Ostrosky-Zeichner *et al.*, 2010; Perfect, 2017). The imidazoles, such as clotrimazole, ketoconazole and miconazole are only considered for topical use, because of their toxicity and bioavailability problems, which limits their potential as systemic agents. Triazoles, such as fluconazole, voriconazole and posaconazole on the other hand are essential in the treatment of invasive fungal infections (Ostrosky-Zeichner *et al.*, 2010). The oldest antifungal drug class, the polyenes, has been introduced to the market in the 1950s. The polyenes consist of amphotericin B and nystatin, which are amphipathic drugs that bind to ergosterol. As such, these drugs affect the cell membrane, like the azoles. However, it is still unclear how polyenes kill off cells. Either, ergosterol binding creates channels that allow cellular ions and other constituents to leak out of the cell or the polyenes act as a sponge and extract ergosterol from lipid bilayers (Anderson *et al.*, 2014; Perlin *et al.*, 2017).

Of the polyenes, only amphotericin B is used to treat invasive infections and it has the broadest spectrum activity of all antifungals (Roemer and Krysan, 2014). For several years, amphotericin B has been the primary therapy for invasive fungal infections. Due to the high toxicity and the discovery of safer drug classes, it has become second-line therapy (Perlin *et al.*, 2017). To counteract toxicity, lipid-complexed formulations of amphotericin B have been developed, which have safer profiles, *e.g.* because of more efficient distribution of the drug and altered pharmacokinetics, but are hampered in wide usage because of their high cost (Hamill, 2013; Perlin *et al.*, 2017). Next in line was the approval of the drug flucytosine, in the 1960s. It is a pyrimidine analogue, which interferes with DNA and RNA synthesis. It is generally used in combination with polyenes to treat cryptococcal meningitis. Monotherapy with flucytosine is rare, as drug resistance is rapidly developed (Perfect, 2017). Apart from the development of the triazoles in the 1980s, the latest breakthrough in antifungal therapy has been the introduction of the lipopeptide echinocandins to the market, around the beginning of the new millennium. These drugs target the fungal cell wall by inhibiting 1,3-β-glucan synthesis (Ostrosky-Zeichner *et al.*, 2010). Because mammals lack a cell wall, the echinocandins have little host toxicity. Three forms are used in the clinic: anidulafungin, caspofungin, and micafungin. They have become the recommended first-line treatment of invasive candidiasis and candidemia (Grau *et al.*, 2015; Perfect, 2017).

Apart from these three main drug classes and flucytosine, some other classes are used for the treatment of topical fungal infections. An example is terbinafine, which belongs to the class of the allylamines and inhibits the squalene epoxidase Erg1 in the process of sterol biosynthesis. It is used for the treatment of onychomycosis of the toenail or fingernail, caused by dermatophytes (Zane *et al.*, 2016).

In some cases, antifungal drugs are used in combination therapy to increase the antifungal activity, as already demonstrated by the combined use of amphotericin B and flucytosine in the treatment of cryptococcal meningitis. Furthermore, our lab has demonstrated the synergistic effect against *C. albicans in vitro* growth between the azole fluconazole (FLC) and doxycycline (DOX), as explained in paragraph 1.1 (Fiori and Van Dijck, 2012). The beneficial effect of DOX on FLC activity has been further validated *in vitro* with regard to antifungal activity on *C. albicans* biofilms and *C. glabrata* isolates (Gao *et al.*, 2013; Hooper *et al.*, 2018). Despite promising results obtained *in vitro* or *in vivo* on the antifungal activity of various (>200) drug combinations with diverse biological targets, combination therapy with compounds other than the four classes of antifungals has not been used for the treatment of fungal infections (Chen *et al.*, 2014; Spitzer *et al.*, 2017). The combination of drugs can nonetheless bring many advantages to antifungal therapy, such as reduced host toxicity by reduced amounts of drugs or shorter durations of treatment and delay or prevention of onset of resistance by a rapid reduction of colonizing pathogens and improved therapeutic activity. An increased antifungal effect during combination therapy can be caused by different mechanisms (Spitzer *et al.*, 2017). First, the effective concentration of an antifungal drug can be increased at the target site by the addition of a second bioactive compound. In this situation, the second drug

does not need to carry antifungal activity *in se*. Secondly, two antifungals can target different steps in the same biological pathway, leading to increased efficacy of the drugs, either in a synergistic or more frequently in an additive manner. Thirdly, the drugs can target different pathways that converge on the same essential biological function. Generally, a combination of these mechanisms rather than one of either three is responsible for the observed enhanced combinatorial effect.

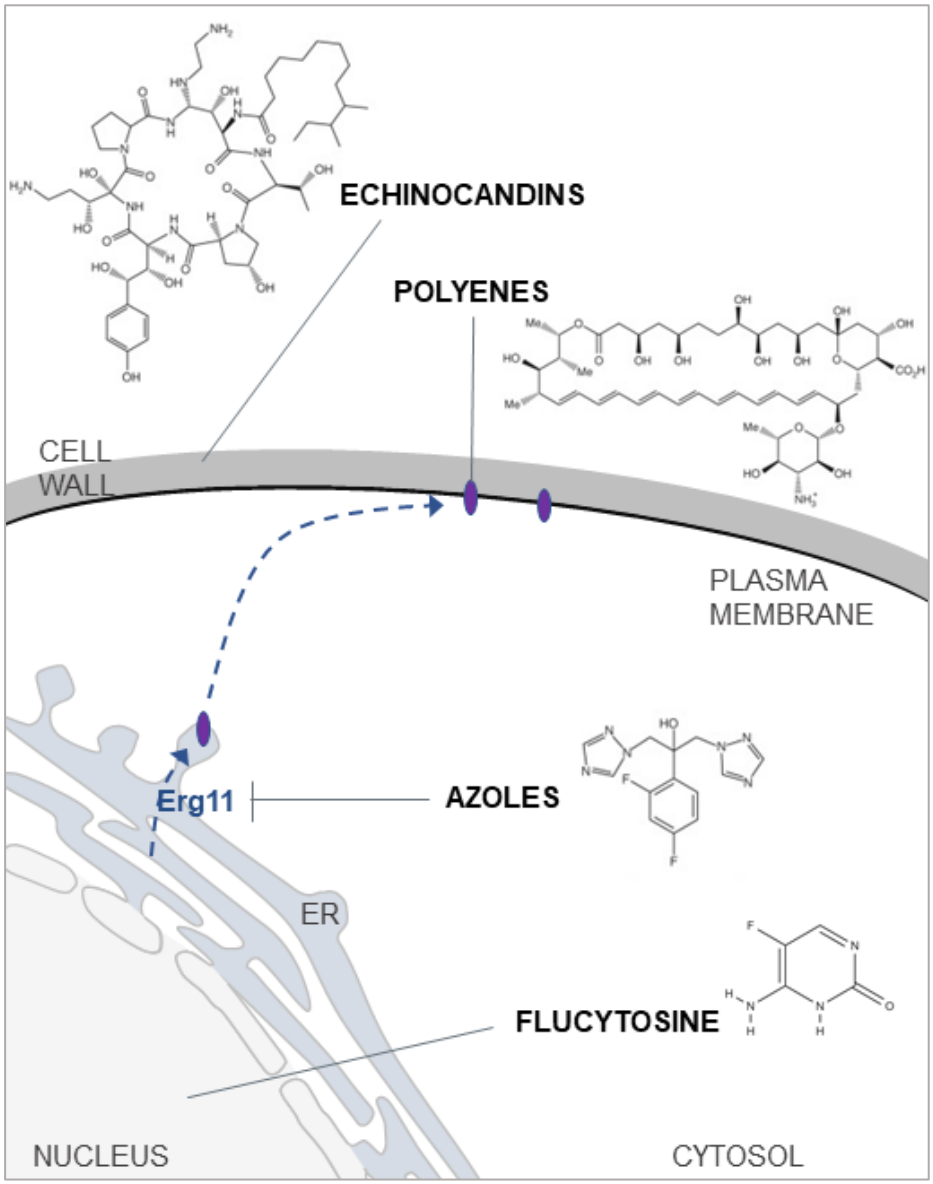


Fig. 1.1. Simplified schematic representation of the targets of the major antifungal drug classes. The azoles, represented here by fluconazole, inhibit Erg11, which is important for ergosterol biosynthesis (represented by oval structures). The polyenes, of which the amphotericin B structure is included, bind ergosterol in the plasma membrane. Flucytosine affects DNA and RNA synthesis in the nucleus. The echinocandins, for which caspofungin is depicted, target an enzyme important to the biosynthesis of the cell wall. The chemical structures were taken from Roemer and Krysan (2014) and MolView (http://molview.org/).

In conclusion, only a limited set of antifungal drugs or combination therapies is used in the clinic to treat fungal infections. It is necessary to expand the current set of antifungals to reduce the risk of the development of resistance and to increase the effectiveness of antifungal treatment. Some drugs affecting other steps in fungal biology are in clinical trials, such as APX001, which is an inhibitor of glycosyl phosphatidylinositol synthesis and MGCD290, which inhibits the fungal Hos2 histone deacetylase. Furthermore, the repurposing of existing drugs for the treatment of fungal infections is being considered. For example, the use of rifampin, which has been approved for the treatment of bacterial infections by inhibiting bacterial RNA polymerase, and the use of verapamil, which targets calcium channels and has been approved for the treatment of cardiac conditions, have both been shown to enhance the activity of existing antifungal drugs in combination therapy. In addition to ongoing improvements of the existing antifungal drug classes, *e.g.* by chemical modifications, this brings about some interesting prospects for future therapies (Perfect, 2017). Furthermore, promising antifungal therapies could result from immune-based therapies, which might become valuable adjuncts to existing antifungal treatments (Armstrong-James *et al.*, 2017). A problem here is that most people suffering from invasive fungal infections have an impaired immune system, which means that they are likely to mount a suboptimal response to vaccine therapy. Vaccination could however be considered as a prophylactic therapy in patients with a relatively intact immune system, *e.g.* patients who will undergo organ transplantation or people diagnosed with early HIV infection. It would also be interesting to vaccinate people who will travel to regions where endemic species like *C. gattii* can infect immunocompetent people (Armstrong-James *et al.*, 2017). Up to now, experimental data on therapeutic fungal vaccines is limited, although sufficient research has been performed in model systems to validate the potency of vaccine therapy against fungal infections (Perfect, 2017). The NDV-3A vaccine has recently been tested in phase 2 clinical trials for its impact on recurrent vulvovaginal candidiasis (RVVC). The outcome of the clinical trial is promising and supports further development of the vaccine. NDV-3A carries a *C. albicans* agglutinin-like sequence 3 (Als3) antigen. Als3 is a well-studied virulence factor, important for *e.g.* adhesion to and invasion of host cells (Edwards *et al.*, 2018). Whether any of these possibilities will effectively boost the antifungal collection remains an open question. The improvement of host defense mechanisms could also be an interesting approach. A deeper insight into the immune defects that underlie increased susceptibility to fungal infections creates opportunities to tune the immune responses where necessary. It has been reported that cytokines and growth factors are interesting classes of biologicals to enhance antifungal host defenses (Armstrong-James *et al.*, 2017).

1.2.3.2 Antifungal drug resistance and tolerance

Antifungal drug activity: determination of the MIC

Resistance to all classes of antifungals has been reported (Perlin *et al.*, 2017). Some species have an intrinsic lower susceptibility towards drugs (primary or innate resistance), while other acquire resistance mechanisms during treatment (secondary or acquired resistance). Primary resistance often involves the same mechanisms as secondary resistance, although these organisms have not been previously exposed to the drug (Perlin *et al.*, 2017). As an example, the intrinsic activities of some drugs of the major antifungal drug classes to a selection of human fungal pathogens is given in Table 1.2. The mechanisms of drug resistance will be discussed in the next paragraph.

Table 1.2. Examples of the activities of antifungal drugs on various fungal pathogens (adapted from Delarze and Sanglard (2015)).

	AmB	FLC	VOR	POS	ANI	CASP	MICA	5-FC
Aspergillus								
A. flavus	±	-	+	+	+	+	+	-
A. fumigatus	+	-	+	+	+	+	+	-
A. niger	+	-	+	+	+	+	+	-
Candida								
C. albicans	+	+	+	+	+	+	+	±
C. glabrata	+	±	±	±	+	+	+	±
C. krusei	+	-	+	+	+	+	+	-
Cryptococcus								
C. neoformans	+	+	+	+	-	-	-	+

'+' represents antifungal activity, '-' indicates no activity of the drug towards that species and '±' means that the drug activity on that species can vary (+ or -). AmB: amphotericin B; FLC: fluconazole; VOR: voriconazole; POS: posaconazole; ANI: anidulafungin; CASP: caspofungin; MICA: micafungin; 5-FC: flucytosine.

Antifungal drug activity is typically measured by *in vitro* broth dilution assays, with standardized protocols defined by The European Committee on Antimicrobial Susceptibility Testing (EUCAST) and the Clinical and Laboratory Standards Institute (CLSI). Although the methods differ in some technical aspects, the measured antifungal activities are usually in close agreement (Pfaller, 2012; Delarze and Sanglard, 2015). With these methods the minimal inhibitory concentration (MIC) of a drug is determined, which is the concentration necessary to inhibit the growth of a certain species to a certain extent. Alternatively, the MIC of a drug can be measured by the use of Etests, which are strips containing a gradient of drug concentrations. These strips are incubated on an agar plate in the presence of cells, which have been evenly streaked out on the plate. The MIC is determined by the intersection of the Etest strip with the zone of growth inhibition that is caused by the applied

drug. The MIC values can be compared to epidemiological cut-off values to verify whether a specific strain is resistant to the drug.

If an antifungal is active against a pathogen, it is classified as a fungicidal or fungistatic drug, suggesting that the cells can be killed off by the drug or are inhibited in growth, respectively. For example, the echinocandins in general have a fungicidal effect on *Candida* species but are fungistatic towards *Aspergillus* species and have no activity on *Cryptococcus* (Roemer and Krysan, 2014). These terms have been implemented for *in vitro* susceptibility testing and are based on the MIC and MFC of a drug for a species. The MFC stands for the minimal fungicidal concentration and is defined as the drug concentration that is necessary to kill off a certain percentage of the cells, standard 99.9%. A drug is termed fungicidal if the MFC to MIC ratio is lower or equal to four (MFC/MIC ≤ 4) and fungistatic if it is higher than four (MFC/MIC > 4). This implies that a drug that kills off cells at a concentration eight times higher than the MIC is considered static, although it possesses cidal activity (Wald-Dickler *et al.*, 2018). As such, the cidal or static character of a drug should be interpreted with caution in relation to the successful outcome of antimicrobial therapy. Other factors, such as the contribution of the host immune system and the effective drug concentrations that reach the site of infection are also important factors in the clearance of fungal infections (Lewis and Graybill, 2008; Kumar *et al.*, 2018; Wald-Dickler *et al.*, 2018).

Although drugs with higher *in vitro* antimicrobial activity compared to others, are more likely to result in effective therapy, MIC values should be considered carefully with regard to clinical outcome in general, as it seems that there is only a limited correlation between *in vitro* and *in vivo* antifungal efficacy, depending on the used antifungal drug and the infecting species (Doern and Brecher, 2011; Borman *et al.*, 2017; Perlin *et al.*, 2017). Gradual consensus is being reached on the importance of identifying the susceptible or resistant character of fungal species prior to antifungal treatment in order to successfully predict the outcome of antifungal therapy in patients. The identification of resistance mechanisms seems to be a predictive measure of possible treatment failure and could therefore be a useful addition to *in vitro* susceptibility testing. Therefore, antifungal resistance tests are currently being developed, *e.g.* by means of genotyping, which are expected to further improve the predictive value of *in vitro* tests to clinical outcome. These assays should be more time-efficient than antifungal susceptibility tests and are aimed to reliably predict treatment failure, so that certain drugs are excluded from therapy (Doern and Brecher, 2011; Sanguinetti and Posteraro, 2017). Furthermore, patients often suffer from polymicrobial infections or take in multiple drugs simultaneously, which are factors that can affect the outcome of the administered antifungal therapy. Therefore, it has been recognized that *in vitro* antifungal susceptibility testing only partly predicts the success of antifungal therapy and that various factors related to the host are also important contributing factors (Rex and Pfaller, 2002; Doern and Brecher, 2011).

Antifungal resistance mechanisms

Fungal infections often reside in niches inside the body. These can be difficult to reach by the antifungal compound, leading to the delivery of suboptimal doses that might be tolerated by the fungus so that resistance mechanisms can be acquired. The same principle is true in microbial biofilms, where the matrix and the complex structure of the biofilm shield inner cells from the administered doses of antifungal drugs. Moreover, biofilm cells often already express resistance mechanisms prior to antifungal administration, perhaps as a precaution to overcome attack of other microbes occupying the same niche. This makes them difficult to eradicate (Nobile and Johnson, 2015). Another problem is the fact that medically related antifungal drugs are used in agriculture. Azole-based fungicides represent the most widely used class for antifungal crop protection. As such, cross-resistance of clinical *C. albicans* isolates to agricultural azoles has been reported as well as the other way around in which environmental yeasts have been shown cross-resistant to medical azoles (Muller *et al.*, 2007). Exposure to these drugs has seeded environmental reservoirs of drug-resistant pathogens (Perlin *et al.*, 2017). Furthermore, prophylaxis with antifungal drugs and repeated or long-term therapy is associated with the emergence of resistance.

Several well-defined mechanisms underlie resistance to azole antifungals. These processes can occur separately or concurrently in a single isolate. Among these mechanisms, the induction of efflux pumps is the most common, decreasing the drug concentration inside the cell (Perlin *et al.*, 2017). Overexpression or alteration of the drug target, *i.e.* by introducing point mutations, is also a common mechanism. The latter can interfere with drug interactions, causing reduced affinity of the azole drug to the Erg11 target and thus reduced drug susceptibility of the strain. Furthermore, genome plasticity can increase the levels of drug target or efflux pumps by means of loss of heterozygosity (leading to the replacement of wild type alleles with mutant alleles), increased chromosomal copy numbers (aneuploidy) or isochromosome formation (two identical chromosome arms flanking a centromere) (Perlin *et al.*, 2017). Other factors affected by the drug-induced stress can also influence azole susceptibility, *e.g.* loss of function of the sterol Δ-5,6-desaturase gene *ERG3* inhibits the production of a toxic sterol in the presence of Erg11 inhibition by azoles, which further decreases the azole drug potency (Shapiro *et al.*, 2011; Perlin *et al.*, 2017). Resistance to the echinocandin drug class is primarily caused by mutations in hot spot regions in the catalytic subunits of glucan synthase, and not by means of drug efflux (Perlin *et al.*, 2017). Resistance to the polyenes often occurs through selection of intrinsically less susceptible species during therapy. Resistance to polyenes is rarely acquired, but if so, it occurs mainly through decreasing the ergosterol levels in the cell membrane (Perlin *et al.*, 2017). In this way, azole therapy lowering the production of ergosterol interferes with the susceptibility to polyenes and resistance mechanisms to azole treatment can confer cross-resistance to polyenes, *e.g.* defective Δ-5,6-desaturase accumulated during azole treatment leads to the depletion of ergosterol and thus reduced sensitivity to polyenes (Shapiro *et al.*, 2011; Perlin *et al.*, 2017). Flucytosine resistance is mediated

by the decreased uptake and transport or metabolism of the drug due to the accumulation of specific mutations or by an increased synthesis of pyrimidines to outcompete the administered drug (Vermes *et al.*, 2000).

Antifungal tolerance

Drug tolerance is described as the survival of an organism at supra-MIC concentrations. The difference with resistance is that resistance is acquired through the accumulation of permanent genetic changes that lead to an increase in the MIC, while tolerance is believed to be an epigenetic process that is reversible and does not alter the MIC of the drug for that strain (as illustrated in Fig. 1.2) (Delarze and Sanglard, 2015). It makes sense that fungal pathogens can be more tolerant to fungistatic drugs than to fungicidal drugs, as the higher the cidal character of the drug, the closer the MFC lies to the MIC, resulting in little cell growth at supra-MIC concentrations. On the other hand, pathogens treated with fungistatic drugs will only be killed off at concentrations at least four times higher than the MIC, giving cells a higher probability to thrive at supra-MIC concentrations. To *C. albicans* in specific, the echinocandins and amphotericin B are fungicidal, while azoles are fungistatic. *C. albicans* tolerance to azole drugs is therefore a common observation and also known as trailing growth. It could be hypothesized that tolerance paves a way to resistance, as the cells are able to thrive in high drug concentrations and have the time to develop genetic alterations. Accordingly, inhibitors of tolerance could increase drug efficacy and delay the onset of resistance (Delarze and Sanglard, 2015).

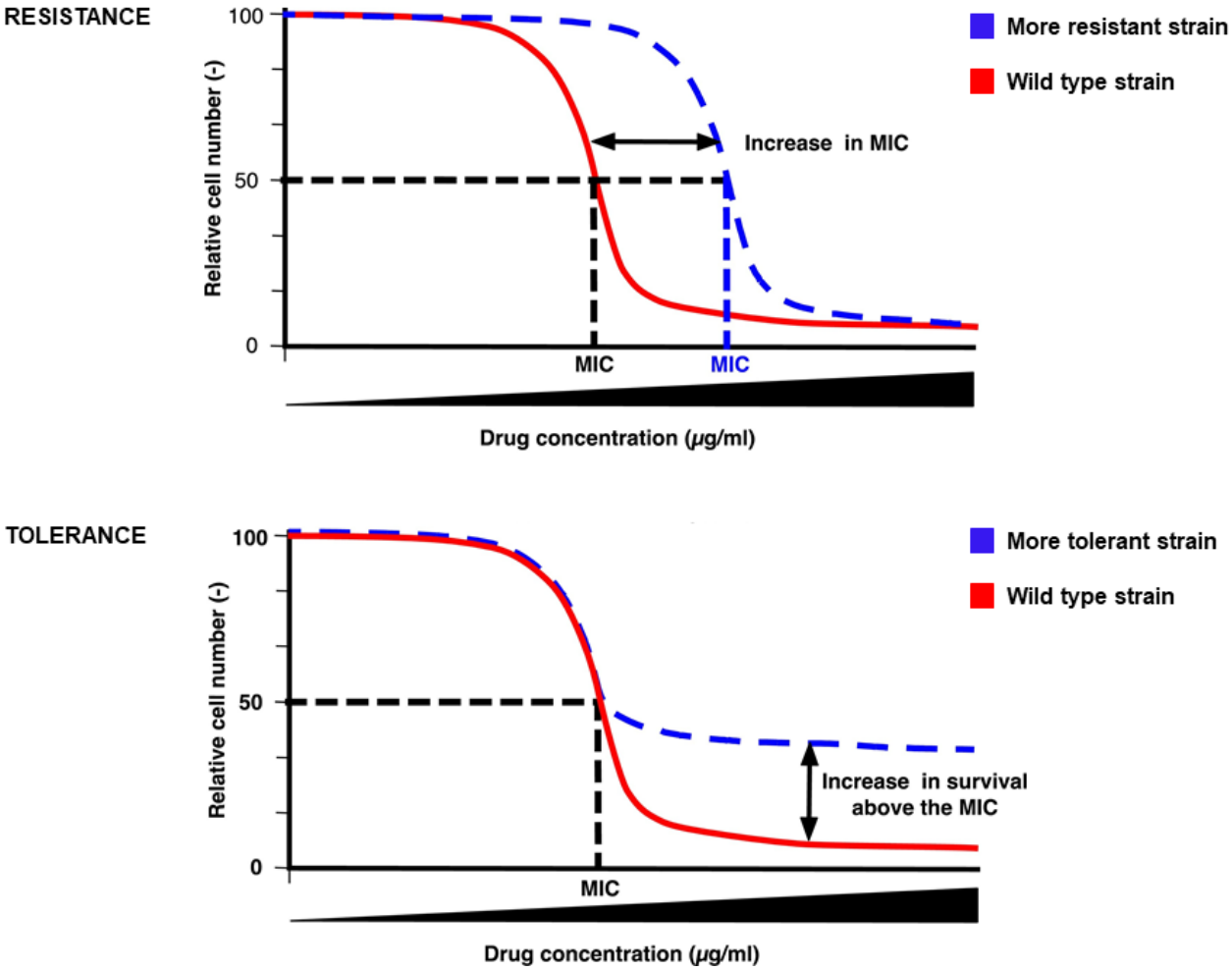


Fig. 1.2. Resistance versus tolerance. A strain that is more resistant towards a specific drug is characterized by an increased MIC value. This means that a higher dose of drug is required to inhibit the growth of the population to a certain percentage (*e.g.* 50%) than is necessary for the wild type strain. A strain that is more tolerant towards a specific drug grows better than the wild type at concentrations that are higher than the MIC, which is similar for both strains (the figure is taken from Delarze and Sanglard (2015) with permission).

The degree of tolerance can differ within a strain (Delarze and Sanglard, 2015). So far, the epigenetic programming and downstream molecular mechanisms that underlie antifungal tolerance remain largely unidentified. Although the involvement of calcineurin and the chaperone Hsp90 have been described in azole tolerance, detailed mechanisms have not been elucidated (Delarze and Sanglard, 2015). Furthermore, it has been discovered by our lab that the addition of DOX eliminates the tolerance of *C. albicans* to FLC (Fig. 1.3). The combination of FLC and DOX led to a synergistic effect that showed fungicidal activity towards *C. albicans* at high DOX concentrations and long incubation times and enhanced the fungistatic power of FLC during normal incubation periods (Fiori and Van Dijck, 2012).

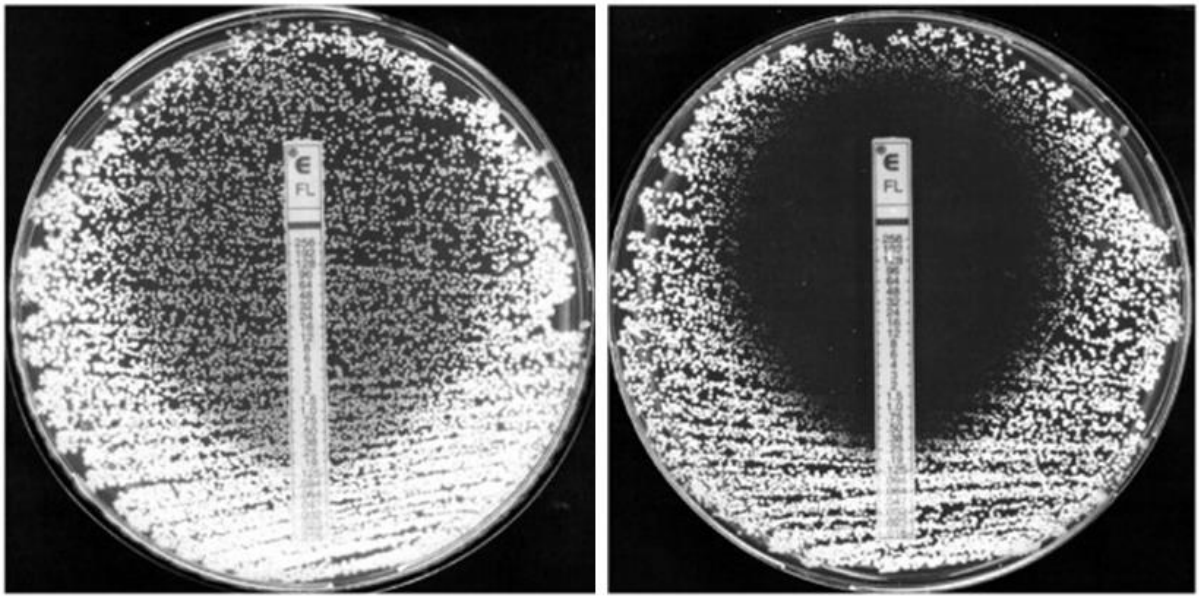


Fig. 1.3. Visualization of *C. albicans* tolerance to azoles by means of Etest susceptibility testing. Wild type *C. albicans* was spread out on an agar plate and incubated for two days in the presence of a FLC Etest strip. The intersection of the halo of growth inhibition with the Etest strip represents the MIC of the applied drug to the strain. While the MIC value is similar with or without the addition of DOX to the agar plate, the growth inside the halo, which represents the ability of the strain to grow at supra-MIC concentrations, is clearly absent when DOX is present, indicating that tolerance is lost (the figure is taken from Fiori and Van Dijck (2012) with permission).

1.3 The bimodal targeting of cytochrome P450s

1.3.1 What are cytochrome P450s?

The cytochrome P450 (CYP) superfamily comprises a group of monooxygenases that share specific characteristics, such as a prosthetic heme group, a cysteine that coordinates to the heme iron and a defined absorption peak at 450 nm when CYP is bound by carbon monoxide (hence the name) (Lamb and Waterman, 2013). The iron atom of the heme group is coordinated by six ligands, *i.e.* four nitrogen atoms of the heme group, the sulfur group of the conserved cysteine group and a weakly bound water molecule, which is displaced upon substrate binding (Lamb and Waterman, 2013). However, the enzymes are structurally and functionally diverse. Their catalytic functions include the biosynthesis of antibiotics, steroid hormones and membrane sterols, the biosynthesis and catabolism of signaling molecules and the metabolism of fatty acids and xenobiotics (Werck-Reichhart and Feyereisen, 2000). The CYP superfamily includes more than 15,000 genes across all biological kingdoms, which are grouped into families based on amino acid sequence similarity (Lamb and Waterman, 2013). In *S. cerevisiae*, three CYPs have been identified. In the *C. albicans* genome, nineteen putative CYP genes have been found (Lah *et al.*, 2008). However, these numbers are low compared to the high number of CYPs detected in filamentous fungi, where the largest amount can be found in *Aspergillus oryzae* with 155 CYPs. It has been hypothesized that filamentous growth might require a broad range of CYPs, to thrive in diverse ecological niches (Lah *et al.*, 2008). CYPs are found as soluble proteins in prokaryotes and as integral endoplasmic reticulum (ER) membrane or mitochondrial inner membrane proteins in eukaryotes (Werck-Reichhart and Feyereisen, 2000).

1.3.2 CYP51 alias Erg11 in yeast: a conserved lanosterol demethylase important for sterol biosynthesis

1.3.2.1 The conserved CYP51 protein

The first CYP51 to be purified was that of *S. cerevisiae*, in 1984. The CYP51 family is the most widely distributed member of the CYP superfamily, conserved in all biological kingdoms and found in over eighty organisms with an average amino acid sequence identity of about 30% (Lepesheva and Waterman, 2007). This percentage is lower than the accepted >40% identity within CYP families, however within the CYP51 family there is strict conservation of catalytic activity and high substrate specificity. CYP51 enzymes are sterol 14α-demethylases that remove the 14α-methyl group from sterol intermediates in a three-step reaction process during the biosynthetic pathway that leads to the formation of ergosterol in fungi, cholesterol in mammals and sitosterol in plants (Lepesheva and Waterman, 2011). This reaction is illustrated in Fig. 1.4, which depicts the

conversion of the substrate lanosterol to 4,4-dimethylergosta-8,14,24-trienol by the fungal CYP51 enzyme. Each of the three monooxygenase reactions in the catalytic CYP51 process requires oxygen and NADPH-derived reducing molecules. As CYPs generally cannot directly receive electrons from such cofactors, they need redox partners to shuttle the electrons to the heme iron (Lamb and Waterman, 2013). The eukaryotic CYP51s require cytochrome P450 reductase (CPR) as an electron donor partner. The CPR carries flavin adenine dinucleotide (FAD) and flavin mononucleotide (FMN) prosthetic groups, which are important for the electron transfer from the NADPH donor to the CYP protein (Wang *et al.*, 1997). Bacterial CYP51s can be reduced by flavodoxin/flavodoxin reductase and ferredoxin/ferredoxin reductase systems (Lepesheva and Waterman, 2007).

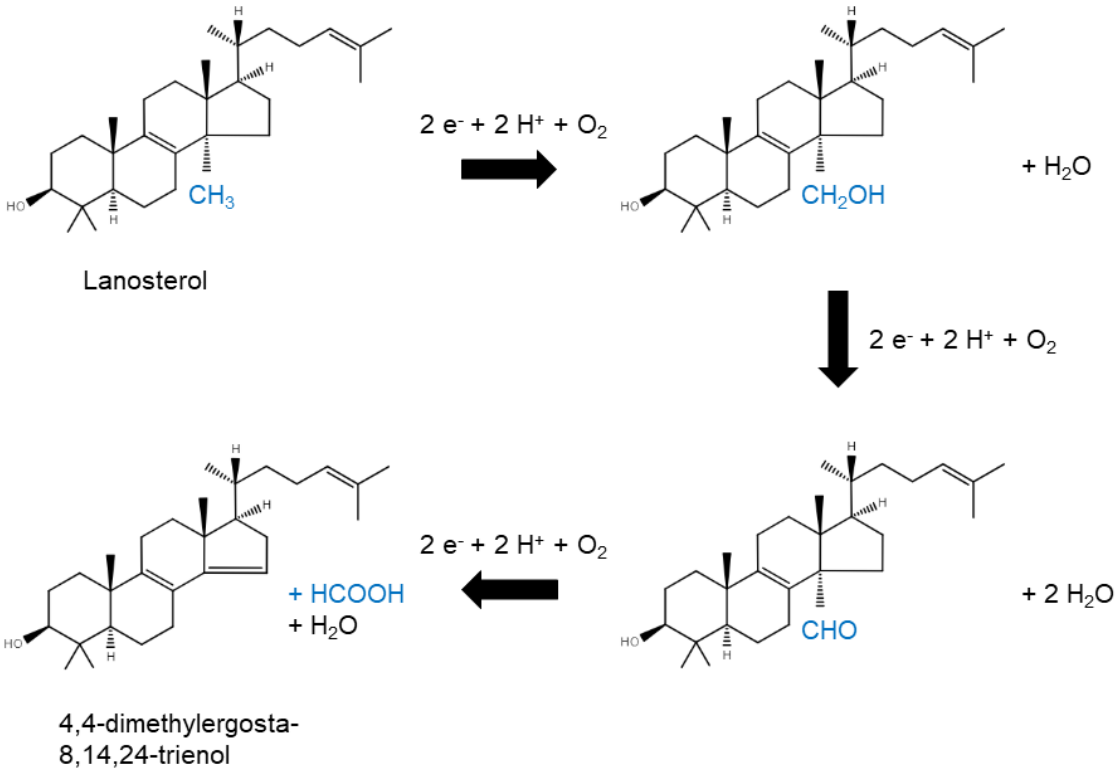


Fig. 1.4. Conversion of lanosterol to its 14α-demethylated product by three consecutive monooxygenase reactions, executed by the CYP51 enzyme. In the presence of oxygen, CYP51 demethylates its substrate. Fungal CYP51s convert lanosterol to 4,4-dimethylergosta-8,14,24-trienol. To exert its catalytic activity, the CYP51 enzyme requires two electrons from NADPH in each step, which are delivered to CYP51 through the CPR redox partner, and oxygen (adapted from Lepesheva and Waterman (2011)).

1.3.2.2 The CYP51 protein of yeast

The CYP51 sequences of *S. cerevisiae* and *C. albicans* share 62% identity and are encoded by the *ERG11* gene (Lepesheva and Waterman, 2011). Erg11 catalyzes a crucial step in the biosynthesis of the main yeast sterol ergosterol, by converting lanosterol to 4,4-dimethylergosta-8,14,24-trienol (as depicted in Fig. 1.4). Although *ERG11* has an essential function in *S. cerevisiae*, it is possible to work with *erg11* mutants under specific conditions. In an anaerobic environment, the Erg11 protein, amongst others, is not functional because of the lack of oxygen. However, if exogenous sterols are supplied through the medium, *S. cerevisiae* can grow anaerobically, whether the *ERG11* gene copy is present or not (Parks and Casey, 1995). Despite the metabolic cost of sterol production, *S. cerevisiae* is unable to take up sterols from the medium in aerobic conditions, even when *erg11* is deleted. This phenomenon is described as aerobic sterol exclusion, of which the molecular mechanisms are not well understood (Jacquier and Schneiter, 2012). Alternatively, *erg11* mutants can be grown aerobically when *ERG3* is deleted simultaneously (Bard *et al.*, 1993). As mentioned earlier (paragraph 1.2.3.2), Erg3 catalyzes the formation of a toxic sterol in *erg11* mutants (Bard *et al.*, 1993). Similar to *S. cerevisiae*, *C. albicans erg11* mutants have been obtained in an *erg3* mutant background, although it has been described that the toxic sterol produced by Erg3 is less of a problem to *C. albicans* than to *S. cerevisiae* (Bard *et al.*, 1993). Indeed, *C. albicans erg11* mutants have been reported to be viable in aerobic conditions, although they have a reduced growth rate (Sanglard *et al.*, 2003). Supplementation of sterols is thus not necessary for the growth of *C. albicans erg11* mutants. Nonetheless, the ability of *C. albicans* to take up sterols under aerobic conditions has been shown, which again underscores a notable dissimilarity between *S. cerevisiae* and *C. albicans* (Zavrel *et al.*, 2013).

The *S. cerevisiae* and *C. albicans* CPR is encoded by the *NCP1* gene. Contrary to *S. cerevisiae ERG11*, *NCP1* is not essential (Truan *et al.*, 1994). Although the cells suffer from the gene deletion, they still grow aerobically and do not need supplementation with ergosterol. This suggests that there is a redundancy in Erg11 redox partners. It has been demonstrated that the *S. cerevisiae* cytochrome b_5/NADH cytochrome b_5 reductase system can serve as a CPR to *C. albicans* Erg11 *in vitro* (Lamb *et al.*, 1999a). Furthermore, it has been shown that disruption of both the CPR and cytochrome b_5 redox systems is synthetically lethal in *S. cerevisiae* (Truan *et al.*, 1994). These findings suggest that the cytochrome b_5/NADH cytochrome b_5 reductase system could complement the action of *NCP1* in *S. cerevisiae*. Accordingly, this might also be true for *C. albicans*, although more direct evidence is missing.

1.3.2.3 The function of ergosterol and other sterols in yeast

The ergosterol biosynthesis pathway can be subdivided in an early or pre-squalene pathway that coincides with the isoprenoid pathway and a late or post-squalene pathway that is committed to sterol biosynthesis, as depicted in Fig. 1.5. The production of farnesyl diphosphate in the pre-

squalene part of ergosterol biosynthesis can also feed into other, non-sterol biosynthesis reactions, such as the production of dolichols and ubiquinones or prenylated proteins (Kuranda *et al.*, 2010). Sterols carry structural and regulatory functions that are of vital importance to the cell, *e.g.* to membrane permeability, activity of membrane-bound proteins and to the cellular growth rate (Bard *et al.*, 1993). In yeast, ergosterol is the main sterol incorporated in membranes and it determines their fluidity and integrity, similar to cholesterol in mammals. Next to these features which are described as the bulk functions of membrane sterols, ergosterol is also required for a process called sparking, which is elicited by micro-amounts of ergosterol. These, one might say hormonal amounts, are required to 'spark' growth. It has been found that other sterols can also satisfy the bulk function of the cell (in the range of 5 µg/mL) as long as micro-amounts of ergosterol or other sterols possessing C-5,6 unsaturated bonds are present (in the range of 10 ng/mL) to fulfill the sparking activity (Rodriguez and Parks, 1983). Ergosterol is mainly found in the plasma membrane, although small amounts can also be found in other compartments such as the mitochondrial inner membrane or the vacuolar membrane (Zinser *et al.*, 1993).

Any excess of precursor sterols and ergosterol are esterified to fatty acids and stored in lipid particles to maintain sterol homeostasis. Whenever the cell requires free sterols to be incorporated in the biosynthetic pathway or free ergosterol for membrane formation, the esterified sterols are cleaved by steryl ester hydrolases to free the sterols and fatty acids (Korber *et al.*, 2017).

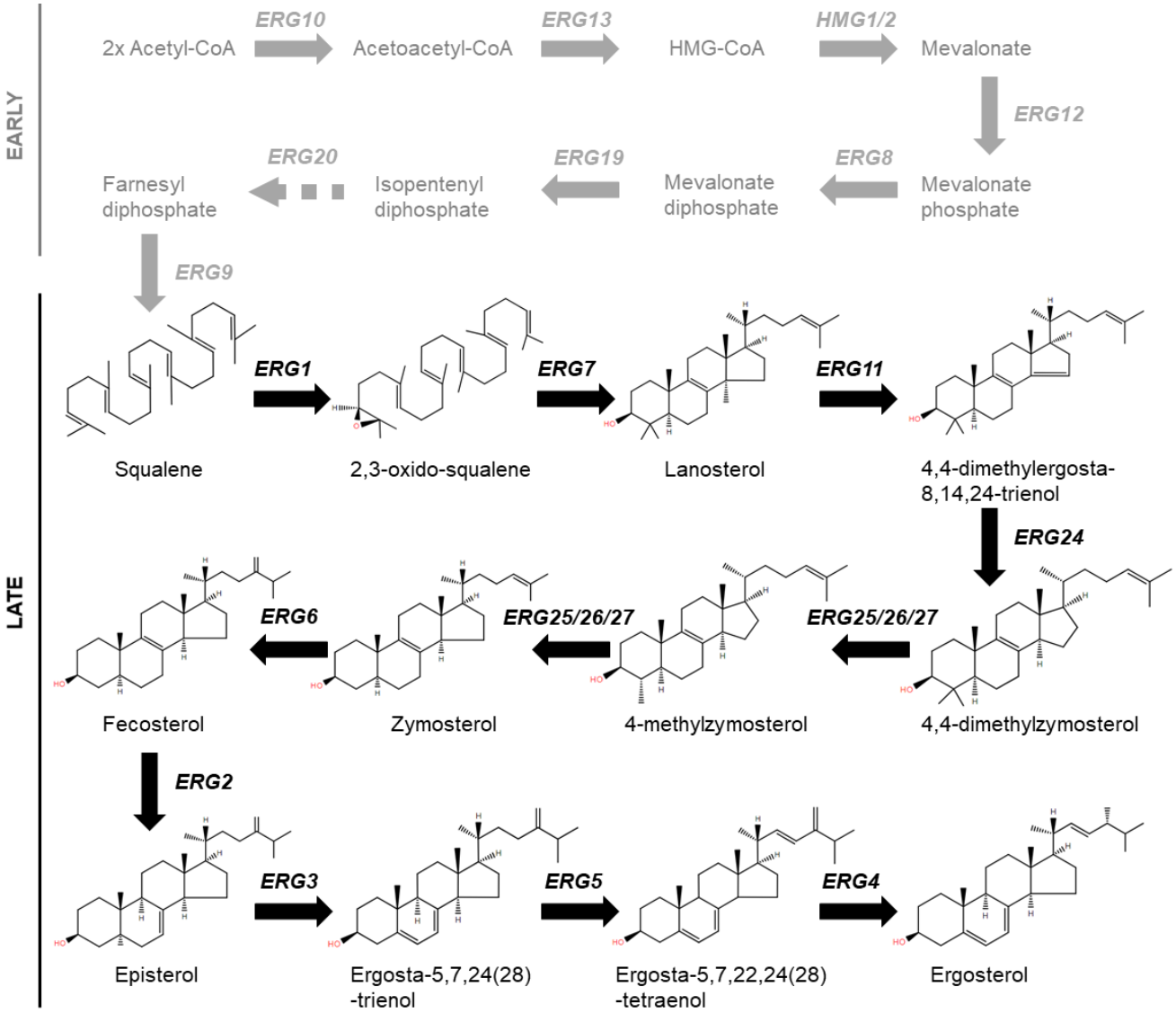


Fig. 1.5. Schematic representation of the ergosterol biosynthesis pathway. The early or pre-squalene pathway is common to the isoprenoid pathway and can lead to other products besides sterol production. The dotted line at *ERG20* represents a two-step reaction that includes the help of another enzyme encoded by *IDI1*. The production of squalene introduces the post-squalene part of the ergosterol biosynthesis pathway. Adapted from Cantu *et al.* (2011) and Kuranda *et al.* (2010). The lipid structures are downloaded from LIPID MAPS (http://www.lipidmaps.org).

1.3.2.4 Regulation of *ERG11* expression in *Saccharomyces cerevisiae* and *Candida albicans*

ERG11 expression is dependent on the carbon source and oxygen levels available to the cell (Karenlampi *et al.*, 1981; Turi and Loper, 1992). An early study concluded that *S. cerevisiae* CYP expression is high when cells are grown in the presence of fermentable hexose sugars but undetectable when cells are grown in the presence of nonfermentable carbon sources, such as

glycerol or ethanol (Karenlampi *et al.*, 1981). It had been stated that most of the CYP levels detected during vegetative growth in *S. cerevisiae* are produced by *ERG11* (Turi and Loper, 1992). Similarly, *C. albicans ERG11* expression is reduced when cells are grown in the presence of the nonfermentable carbon sources glycerol and acetate than when cells are grown in glucose (Lyons and White, 2000).

ERG11 transcript levels are inversely related to oxygen levels in *S. cerevisiae*, with higher *ERG11* expression in low oxygen conditions, although the enzyme is not functional in anaerobic conditions due to the lack of its heme cofactor and the requirement for oxygen during catalysis (Turi and Loper, 1992). Nevertheless, the cell will try to compensate for this lack of activity by increasing *ERG11* gene expression. The messenger RNA (mRNA) levels of the redox partner *NCP1* seem to be coordinately regulated with those of *ERG11* (Turi and Loper, 1992). In *S. cerevisiae*, two oxygen sensing mechanisms regulate the response to changes in the availability of molecular oxygen, dependent on heme synthesis or on the level of sterols in the cell (Fig. 1.6). Both mechanisms are important to the regulation of *ERG11* expression. In aerobic conditions, *ROX1* expression is activated by the heme-dependent Hap1 transcription factor. Rox1 is a transcriptional repressor that regulates gene expression in response to hypoxia. Under low oxygen levels, heme biosynthesis is limited, which results in reduced production of Rox1 and the consecutive derepression of its target genes (Kwast *et al.*, 2002). Both Erg11 and Ncp1 are hypoxia-controlled genes. On the other hand, adaptation to limited oxygen levels is also regulated by sterol levels. The production of sterols requires several oxygen-dependent reactions, *e.g.* the reaction catalyzed by Erg11 requires three O_2 molecules (Fig. 1.4). Upc2 serves as an ergosterol sensor. Its C-terminus binds ergosterol, which represses its activity. Dissociation of ergosterol and the Upc2 sensor leads to the translocation of Upc2 from the cytoplasm to the nucleus where it is involved in gene activation (Yang *et al.*, 2015). The transcription factor Upc2 shares substantive overlap with Rox1 in the regulation of heme and lipid biosynthesis genes, *e.g.* the *ERG11* and *NCP1* genes (Kwast *et al.*, 2002).

Azoles block the synthesis of ergosterol by inhibition of the Erg11 protein. By lowering the sterol levels, they induce the activity of Upc2 in a similar manner as hypoxic conditions (Grahl and Cramer, 2010). The transcriptional activity of *S. cerevisiae* Upc2 is more than twofold upregulated in the presence of FLC (Yang *et al.*, 2015). Upc2 has a paralog Ecm22 which shares partial overlap in the activation of genes important for azole resistance. It has been identified that, in contrast to a single *upc2Δ* deletion, the double *upc2Δ ecm22Δ* mutant cannot grow in the presence of FLC (Yang *et al.*, 2015). Similar to *S. cerevisiae*, *C. albicans ERG11* is upregulated when cells are treated with azoles, in a Upc2-dependent fashion (Henry *et al.*, 2002; Pierson *et al.*, 2004; Oliver *et al.*, 2007; Yang *et al.*, 2015). Also in *C. albicans*, *ERG11* expression is upregulated under hypoxia and this has been shown to be Upc2-dependent (Synnott *et al.*, 2010). A *C. albicans* homolog to Rox1, Rfg1, has been identified but does not seem to be involved in the regulation of hypoxic genes (Grahl

and Cramer, 2010). In general, it is hypothesized that conditions leading to the depletion of ergosterol induce the upregulation of *ERG11* (Song *et al.*, 2004).

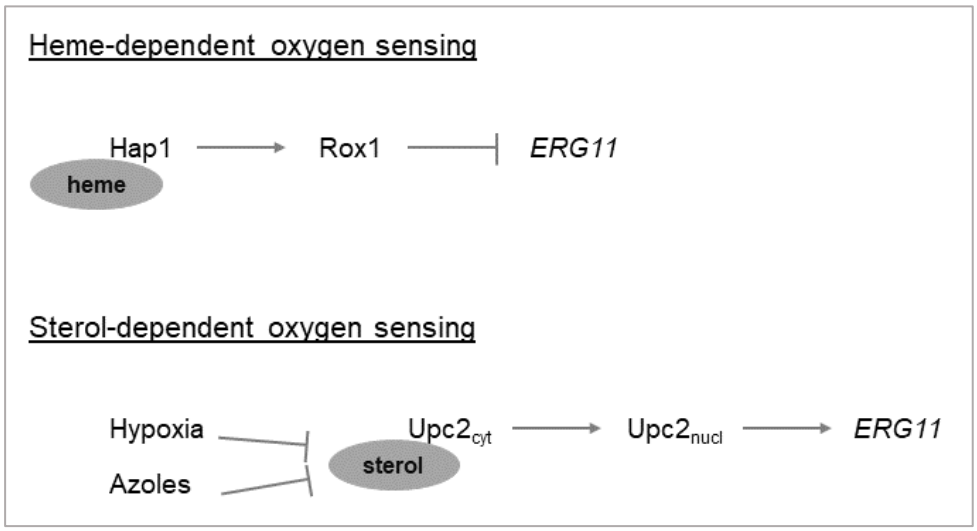


Fig. 1.6. Simplified scheme of oxygen-dependent mechanisms involved in the regulation of *ERG11* gene expression in *S. cerevisiae*. The heme-dependent oxygen sensing mechanism is dependent on the Hap1 transcriptional activator, which binds heme in an aerobic environment and activates the transcriptional repressor Rox1, which represses the expression of a set of genes important during hypoxia. *ERG11* is part of these hypoxia-controlled genes. A second mechanism that senses the oxygen levels in *S. cerevisiae* is based on the level of sterols in the cell. Depletion by low oxygen levels or inhibitors of sterol biosynthesis, such as the azoles, leads to the translocation of ergosterol-bound Upc2 from the cytoplasm to the nucleus, where unbound Upc2 will activate the expression of a set of genes, partly overlapping with those activated by Rox1, *e.g. ERG11*.

1.3.3 From mono to multi: protein targeting to subcellular compartments

The idea that proteins can be targeted to more than one location in the cell is generally accepted. In humans, about one quarter of all proteins localizes to multiple subcellular compartments. It has been found that these multiple localized proteins are typically part of a hub with many interaction partners (Ota *et al.*, 2016). For bi- or multimodal targeting, proteins need to contain different localization signals as the targeting signals to various organelles are generally different, as well as the mechanism of protein translocation across the organellar membranes. Several mechanisms could result in the localization of one protein to different subcellular compartments (Pino *et al.*, 2007; Yogev and Pines, 2011). For example, a single gene could result in multiple protein products with different targeting specificity through alternative transcription initiation, alternative splicing of the mRNA or translation initiation at alternative AUG codons or even non-AUG codons. The field of alternative transcription initiation is relatively unexplored in yeast. Only a few publications are found on the topic, yet it is hypothesized that many yeast genes contain not one but several

transcription start sites (TSS) (Zhang and Dietrich, 2005; Miura *et al.*, 2006). Two examples emphasize the significance of this phenomenon with regard to protein localization. Both the valyl-tRNA synthetase gene *VAS1* and the histidine-tRNA synthetase gene *HTS1* are transcribed as two mRNAs that differ in length, a long form that is translated to a mitochondrial protein and a shorter one that is translated to the cytosolic form of the protein (Natsoulis *et al.*, 1986; Chatton *et al.*, 1988). Alternative splicing in *S. cerevisiae* is rare, as only four percent of all genes contain introns, most of which with a simple structure of two exons and one intron (Schreiber *et al.*, 2015). Out of this limited pool, only one gene is known to result in two transcripts that are translated to proteins with different subcellular localizations, *i.e.* the mitochondria and the nuclear envelope. This is the serine/threonine phosphatase *PTC7* (Juneau *et al.*, 2009). Several examples exist of *S. cerevisiae* dually targeted proteins by means of alternative translation initiation, *e.g.* the targeting of glutaredoxin Grx2, glutathione reductase Glr1 and alanyl-tRNA synthetase Ala1 to the cytosol and mitochondria and of the fumarate reductase Osm1 to the ER and mitochondria (Outten and Culotta, 2004; Tang *et al.*, 2004; Porras *et al.*, 2006; Williams *et al.*, 2014). Alternatively, a single protein could be targeted to various subcellular sites if different parts of the protein are recognized by different organellar receptors or import machineries, a process referred to as bimodal targeting (Pino *et al.*, 2007). CYPs represent a primary example of bimodal targeting to ER and mitochondria. Additionally, if processes are considered beyond the products of a single gene, gene duplication could be considered as an event giving rise to similar proteins with different targeting information. However, for stable integration of most duplicates, functional divergence is a prerequisite, unless an increase in gene dosage is beneficial to the cells (Marques *et al.*, 2008; Qian and Zhang, 2009).

1.3.4 Bimodal targeting of cytochrome P450s to the endoplasmic reticulum and mitochondria in mammals

Mammalian CYPs of families 1, 2 and 3 are well-known for their multiple locations, especially the ER and mitochondria. The chimeric signals for bimodal targeting to ER and mitochondria typically consist of an N-terminal ER-targeting signal followed by a cryptic mitochondrial targeting signal (MTS), which contains two to five positively charged residues necessary for mitochondrial import (Avadhani *et al.*, 2011). This cryptic MTS differs from a canonical MTS in the sense that it is not located at the N-terminus of the protein and is not necessarily cleaved off upon import to mitochondria (Lemire *et al.*, 1989). Generally, an MTS is characterized as a region that is rich in positively charged and hydrophobic amino acids and is devoid of acidic amino acids. Usually, a regular alternation between basic and hydrophobic amino acids allows for a potential amphiphilic helix to form (Hurt and Schatz, 1987). It has been found that a cryptic MTS is more difficult to identify *in silico* by bioinformatical analysis, as it contains an overall weaker MTS with regard to basic and hydrophobic amino acids compared to a canonical MTS (Dinur-Mills *et al.*, 2008). Moreover, the tools to identify MTSs are trained with data sets of the more conventional N-terminal, cleavable signals. However, it is becoming evident that proteins can contain unconventional,

internal targeting signals. It seems that these are dynamic signals, which can be activated under specific conditions, depending on the needs of the cell (Vongsamphanh *et al.*, 2001; Karniely and Pines, 2005; Li *et al.*, 2010; Muhsain *et al.*, 2015; Opalinska and Meisinger, 2015). Once the bimodally targeted CYPs have reached the mitochondria, they associate with the inner membrane in a membrane-extrinsic orientation with the catalytic domain exposed to the mitochondrial matrix, similar to true mitochondrial CYP proteins (Avadhani *et al.*, 2011). The cryptic MTS of mammalian CYPs can be activated by two mechanisms, either cleavage by cytosolic proteases or phosphorylation by cytosolic kinases (Avadhani *et al.*, 2011).

The cleavage model of rat CYP1A1 includes a minor and major cleavage site, of which the resulting proteins are targeted with low respectively high abundance to mitochondria. The endoprotease responsible for cleavage of rat CYP1A1 is a serine protease that is homologous to human Ser protease 9 (Avadhani *et al.*, 2011). Alternatively, protein kinase A (PKA)-mediated phosphorylation activates the MTSs of CYP2B1, CYP2E1, and CYP2D6 resulting in the mitochondrial import of their full-length proteins in mammals (Avadhani *et al.*, 2011). Phosphorylation of CYPs results in decreased interaction with the signal recognition particle (SRP), which transports nascent chains or precursor proteins to the ER for co- or posttranslational import. This increases the potential of the cytosolic CYP polypeptide to interact with mitochondrial translocase proteins instead. There is no consensus on which of the translocation proteins are essential for the mitochondrial targeting of CYPs. It has been shown that mitochondrially targeted CYPs can be activated by mitochondrial adrenodoxin and adrenodoxin reductase (Avadhani *et al.*, 2011). Nonetheless, the physiological role of ER-mitochondrial targeting of mammalian CYPs remains obscure.

1.3.5 Bimodal targeting in yeast: exploring the possibility of mitochondrial Erg11

The bimodal targeting to the ER and mitochondria, where different parts of a protein are recognized for alternative localization, has not been demonstrated for yeast proteins, so far. It is interesting to speculate on a mitochondrial localization of Erg11, based on the various reports of ER-mitochondria bimodally targeted CYPs in mammals. Although the ergosterol biosynthesis process mainly takes place in the ER, several components have been localized to multiple organelles. For example, it is known that Erg1 is a component of the ER and of lipid droplets, while Erg6 has been reported to reside in the ER, lipid droplets and the mitochondrial outer membrane (Leber *et al.*, 1998; Pichler *et al.*, 2001; Sorger *et al.*, 2004; Zahedi *et al.*, 2006).

Over the years, great effort has been put into the defining of the yeast mitochondrial proteome. This has resulted in the most complete study so far, published in 2017, in which 3539 proteins of *S. cerevisiae* have been identified as mitochondrial proteins or proteins associated with mitochondria (Morgenstern *et al.*, 2017). This number has been focused to 901 proteins that make up the core mitochondrial proteome. Erg11 has been identified as one of the mitochondria-associated proteins, but not of the core mitochondrial proteome. Only one other study has localized

S. cerevisiae Erg11 to mitochondria (Prokisch *et al.*, 2004). All other enzymes of the ergosterol biosynthesis pathway have also been found to be associated with mitochondria, except for Erg19 and Erg20. Furthermore, both the Ncp1 and cytochrome b_5/cytochrome b_5 reductase have been identified as mitochondria-associated proteins (Morgenstern *et al.*, 2017). Mitochondrial proteome studies in *C. albicans* are limited and Erg11 has not been associated with a mitochondrial localization in the pathogen thus far.

As mentioned previously (paragraph 1.3.3), proteins with multiple subcellular localizations are often found to be part of hubs in protein interaction networks. Mo and Bard (2005) have identified Erg11 as one of the core proteins of such an interacting complex, which is referred to as the ergosome. It has been suggested that a multi-enzyme complex can support specific interactions between the enzymes of the ergosterol biosynthetic pathway. The core of the ergosome complex is made up of the Erg11, Erg25, Erg27 and Erg28 proteins, which have the greatest number of Erg protein interaction partners of all the ergosterol biosynthesis proteins. This finding combined with the identification of the mitochondrial association of Erg11 in *S. cerevisiae* might suggest that Erg11 could indeed have multiple cellular locations and could be bimodally targeted to the ER and mitochondria.

1.4 The degradation of cytochrome P450s[(1)]

In general, yeast cells contain two major degradation pathways, represented by the cytosolic ubiquitin-proteasome system (UPS) on one hand, presumed to degrade specific short-lived and damaged proteins and the vacuolar proteolytic system on the other hand, which is expected to degrade excess and senescent long-lived proteins. In mammals, there seems to be heterogeneity in the degradation of CYPs, as both the UPS and lysosomal proteolysis, the mammalian counterpart for vacuolar degradation, have been shown to break down specific CYP proteins (Murray *et al.*, 2002; Liao *et al.*, 2005). Heterologous expression of mammalian CYPs in *S. cerevisiae* similarly leads to the degradation of the CYPs by one of both mechanisms. The reason for this diversity in CYP degradation is unknown. As in this study the *S. cerevisiae* vacuolar proteases Pep4 and Prb1 are identified as important factors for Erg11 proteolysis, a short introduction on vacuolar degradation and autophagy is given.

1.4.1 The vacuolar proteases of *Saccharomyces cerevisiae*: seven actors on duty to preserve protein homeostasis

The primary function of the yeast vacuole is macromolecular degradation. However, the physiological relevance of yeast vacuoles stretches beyond this. In addition to a site of proteolysis, the vacuole serves as a reservoir of amino acids, ions and polyphosphates and it contributes to cellular ion and pH homeostasis (Van Den Hazel *et al.*, 1996; Li and Kane, 2009). The vacuolar proteases are responsible for a large fraction of the total cellular protein turnover, especially under nutritional stress conditions (Van Den Hazel *et al.*, 1996). The substrate range of the vacuolar proteases is wide and rather non-specific, assuring that the bulk of proteins gets degraded and constituents can be reused. So far, seven vacuolar proteases have been characterized in *S. cerevisiae*. They consist of two endoproteases called proteinase A and B encoded by *PEP4* and *PRB1*, two carboxypeptidases Y and S encoded by *PRC1* and *CPS1*, two aminopeptidases I and Y encoded by *APE1* and *APE3* and a dipeptidylaminopeptidase encoded by *DAP2*. The group of Brodsky has reported on an eighth vacuolar protease, encoded by *PFF1*, although its protease activity still needs to be demonstrated experimentally (Hecht *et al.*, 2014).

The activity of proteinase A (PrA) and proteinase B (PrB) has already been documented over 60 years ago (Lenney, 1956). PrA or Pep4 is an aspartic protease, while PrB or Prb1 is a subtilisin-like serine protease. Both Pep4 and Prb1 are produced as zymogens. They are delivered to the vacuole through the secretory pathway, in which they transit through the ER and Golgi for the addition of sugar residues. Upon entry into the vacuole, a redundant mechanism of autocatalytic and mature Pep4- and Prb1-dependent proteolytic activation steps is present to enable maturation of the Pep4 and Prb1 precursors to active isoforms (Van Den Hazel *et al.*, 1996; Hecht *et al.*, 2014).

[(1)] Adapted from “A Cinderella story: how the vacuolar proteases Pep4 and Prb1 do more than cleaning up the cell’s mass degradation processes. Kerstens and Van Dijck (2018), *Microb cell* **5**, p438-443”.

With the exclusion of Dap2, all vacuolar proteases are synthesized as precursor proteins (Hecht *et al.*, 2014). They are proteolytically matured in the vacuole by the action of Pep4 and Prb1, who stand at the top of the activation cascade. Importantly, Pep4 initiates the proteolytic cascade, as its activity is necessary for the production of active Prb1 and *pep4* mutants accumulate precursors of several vacuolar proteases with little biochemical activity (Woolford *et al.*, 1986; Rupp and Wolf, 1995). Once Prb1 is activated, it is the main actor for the proteolytic processing of the precursors, but Pep4 can do so as well, if necessary. In all, there is great redundancy built into the maturation process of vacuolar proteases (Woolford *et al.*, 1993).

1.4.2 The vacuolar proteases Pep4 and Prb1 are important for autophagic breakdown in *Saccharomyces cerevisiae*

1.4.2.1 A general introduction to autophagy in *Saccharomyces cerevisiae*

Generally, proteins destined for degradation reach the vacuole through endocytosis and autophagocytosis (Muller *et al.*, 2015; Galluzzi *et al.*, 2017). The endocytic process overlaps at multiple levels with the molecular machinery of the autophagic pathway. The past two decades have seen the revelation of many of the molecular mechanisms that govern autophagic processes. This culminated in awarding the Nobel Prize in Physiology or Medicine of 2016 to Prof. Dr. Yoshinori Ohsumi for his contribution to the identification of mechanisms of autophagy in yeast. Moreover, it was by the use of *pep4* and *prb1* mutants that autophagy has been demonstrated in yeast for the first time (Takeshige *et al.*, 1992). It has been found that autophagic processes are greatly conserved from yeast to mammals (Galluzzi *et al.*, 2017).

In *S. cerevisiae*, autophagic processes can be divided in macro- and microautophagy and concern all processes that involve the degradation of intracellular material by the vacuolar hydrolases (Galluzzi *et al.*, 2017). This ranges from cytoplasmic material to organelles such as damaged mitochondria or portions of the nucleus. While microautophagy is characterized by direct uptake of cargo by the vacuole by means of membrane invagination, macroautophagy depends on the formation of cytosolic double-membraned autophagosomes that fuse with the vacuole for the delivery of its cargo. Autophagy can be induced by various triggers, these can be either external factors such as nutrient deprivation, or internal factors such as the accumulation of damaged organelles (Palmer *et al.*, 2008; Reggiori and Klionsky, 2013). Otherwise, autophagy operates at a basal level. In *C. albicans*, the molecular machinery of autophagy is still largely unidentified (Palmer *et al.*, 2007; Palmer *et al.*, 2008).

1.4.2.2 The role of Pep4 and Prb1 in *Saccharomyces cerevisiae* autophagy

Prb1 is crucial in the breakdown of autophagic bodies in the vacuole (Takeshige *et al.*, 1992). Autophagic processes increase under nutrient deficient conditions, as do the levels of Pep4 and

Prb1. It has been estimated that under these conditions >80% of protein degradation is under control of Pep4 and Prb1, while this reduces to about half of it in vegetative growth conditions (Teichert *et al.*, 1989). Similar to nutritional stress, the protease activities rise substantially when cells transit from exponential to stationary phase. It has been described that Pep4, and not Prb1 is essential under nutrient starvation conditions. Likely, the explanation resides in the fact that Pep4 stands at the top of the proteolytic activation cascade (Teichert *et al.*, 1989). While a *prb1Δ* mutant only lacks Prb1 activity, a *pep4Δ* mutant is defective in maturation of most vacuolar proteases.

1.4.2.3 Non-vacuolar, autophagy-independent activities of *Saccharomyces cerevisiae* Pep4 and Prb1

In addition to the prominent role of Pep and Prb1 in the vacuolar proteolytic activation cascade and protein turnover, it should be noted that several non-vacuolar functions have been ascribed to Pep4 and Prb1 (reviewed in Kerstens and Van Dijck (2018)). These non-vacuolar activities seem to be stress-induced and seem to operate in an autophagy-independent manner. It has been described that proteases can be released from the vacuole by permeabilization of the membrane under stress conditions (Mason *et al.*, 2005). A similar phenomenon has been described in mammals and is known as lysosomal membrane permeabilization (LMP). It is hypothesized that this process is involved in the initiation of cell death pathways, but the molecular mechanisms have not been defined. The non-vacuolar functions of the Pep4 and Prb1 proteases range from the involvement of Pep4 in programmed cell death, to a role for both proteases in gene regulation and protection to hazardous protein forms, such as prions.

1.4.2.4 ER-phagy: a specific type of autophagy that sequesters and degrades excess proteins of the endoplasmic reticulum

The ER-associated degradation (ERAD) pathway is a continuous quality control process that supervises the proper folding of ER proteins by retrotranslocating misfolded proteins from the ER lumen to the cytosol, where they are ubiquitylated and sent for proteasomal degradation (Vembar and Brodsky, 2008). When the load of misfolded proteins becomes too high, cells are stressed and the unfolded protein response (UPR) is activated. The UPR induces ER membrane expansion and increases the folding capacity of the ER, while at the same time stimulating ERAD so that ER homeostasis can be reached again. The excess of ER that has been created can be eliminated by autophagic processes, so that the organelle size is readjusted to the needs of the cell (Schuck, 2016). Reticulophagy is the autophagic breakdown of parts of the ER and is also called ER-phagy. Both micro- and macroautophagic processes have been described for ER-phagy and it is unclear whether these occur independently of one another (Schuck *et al.*, 2014; Lipatova and Segev, 2015; Schuck, 2016; Galluzzi *et al.*, 2017). During ER-phagy, whorls can be observed, which are circular multilayered ER membrane structures that can vary in size from 200 to 800 nanometers as shown in Fig. 1.7 A (Schuck *et al.*, 2014). They are taken up by the vacuole by invagination of the vacuolar

membrane and as such resemble the process of microautophagy. In addition, ER stress activates macroautophagy and it has been shown that macroautophagy and autophagy of ER whorls can occur in the same cell, which is schematically depicted in Fig. 1.7 B (Schuck *et al.*, 2014). Interestingly, it has recently been discovered by quantitative mass spectrometry (MS) analysis in mammalian cells that autophagosomes clearing excess ER are mainly enriched in components of the folding machinery, such as chaperones and protein disulfide isomerases, while levels of ERAD factors are not significantly enriched (Fumagalli *et al.*, 2016). How ER macroautophagic processes can discriminate between these ER proteins remains unknown. From these observations, we can assume that ERAD and autophagy represent two complementary ways to clear excess ER proteins.

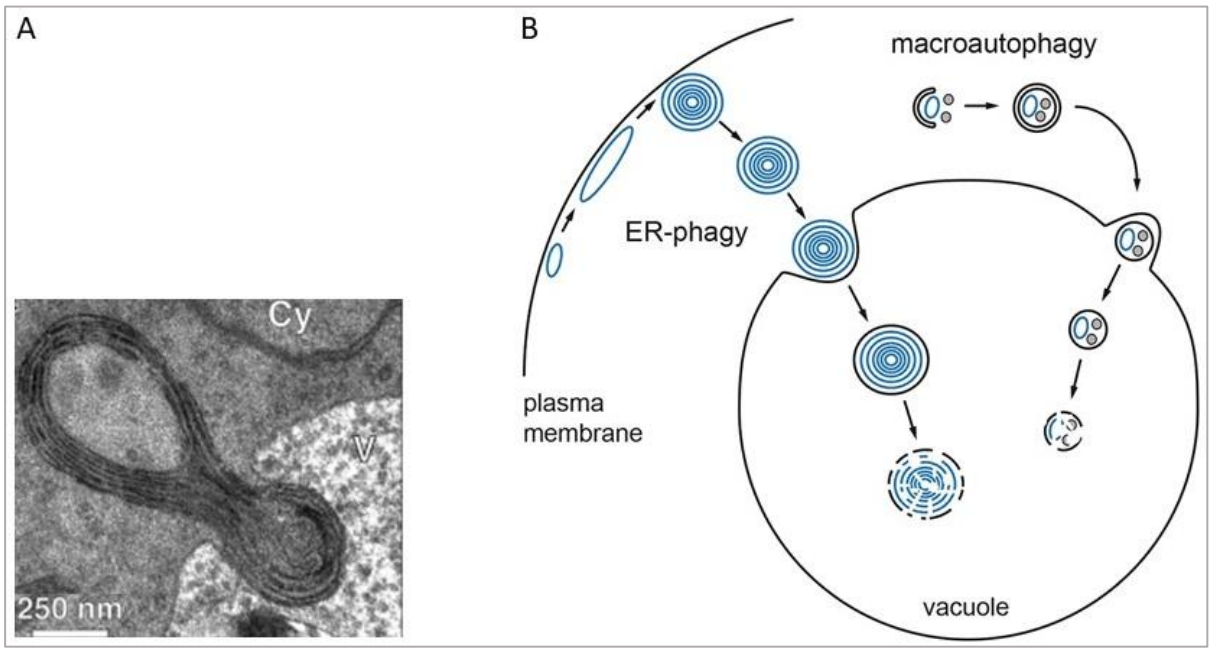


Fig. 1.7. The process of ER-phagy is dependent on micro- and macroautophagic processes. (A) Microautophagy of the ER occurs through the formation of whorls, which are taken up by the vacuole for degradation. It is clear from this electron micrograph that the vacuolar membrane is invaginated during the uptake of the ER whorl (Cy: cytosol; V: vacuole). (B) Schematic representation of micro- and macroautophagic processes eliminating excess ER during ER-phagy, which can occur simultaneously in one cell (the figures are taken from Schuck *et al.* (2014) with permission).

Aim of this study

The azole target Erg11 has been detected as multiple bands on western blot in the opportunistic human pathogen *C. albicans* and in the model organism *S. cerevisiae*, when cells have been treated with FLC. Untreated cells, on the other hand, display only a single Erg11 protein band on western blot with a molecular mass of about 60 kilodalton (kDa). As the truncated Erg11 products are specifically observed during azole therapy, it has been hypothesized that they might be important to the response of yeast cells to these antifungal drugs.

As certain mammalian CYPs have been reported to undergo ER-mitochondria bimodal targeting upon drug treatment, it has been hypothesized that the azole-induced shorter forms of Erg11 might also be mitochondrially targeted products. So far, no clear function has been ascribed to the mitochondrial targeting of mammalian ER CYPs (Avadhani *et al.*, 2011). The potentially conserved process in yeast opens new perspectives to the elucidation of the physiological significance of this process, as well as to the identification of the molecular mechanism involved.

Therefore, in this study, the bimodal targeting of Erg11 to the ER and mitochondria has been investigated as well as the effect of the truncated Erg11 products on azole therapy in *S. cerevisiae* and through homologous studies also partly in *C. albicans*. The generation process of the additional Erg11 products has been examined as well as their localization and function.

Azoles are the most used class of antifungals. If the Erg11 products are indeed mitochondrially localized, it might be reasoned that they could be shielded from azole drug treatment by the mitochondrial membrane barrier. The low levels of mitochondrial Erg11, if existent and if functional, could sustain viability and enable cells to survive antifungal drug therapy. Alternatively, the truncated, mitochondrial Erg11 products could bind FLC, functioning as a sponge and shielding ER Erg11 from adverse drug effects. If either of these hypotheses would be true, the absence of the additional Erg11 protein products could increase the potency of azole drugs, resulting in a reduced MIC value or in decreased tolerance levels. Enhanced activity of FLC, or azoles in general, on the growth of *C. albicans* and potentially on that of other fungal pathogens could have important, beneficial consequences to the treatment of fungal infections in the clinic. Such a finding would be the ultimate end goal of this research.

CHAPTER 2

SACCHAROMYCES CEREVISIAE ERG11 IS DETECTED AS MULTIPLE BANDS ON WESTERN BLOT

Parts of this chapter are based on the manuscript: “On the whereabouts of yeast Erg11: a report on localization and degradation”, which is in preparation. All the experiments described in this chapter have been designed and performed by Winnie Kerstens, with technical assistance by Ilse Palmans, except for the MS analysis, which has been performed by the VIB Proteomics Expertise Center in Ghent.

2.1 Defining the conditions of Erg11 detection on western blot

Preliminary, unpublished results on the characterization of the synergistic effect between fluconazole and doxycycline have demonstrated that the target of azole antifungals, Erg11 is detected as multiple bands on western blot when cells are grown in the presence of FLC. This is observed both in the opportunistic human pathogen *Candida albicans* and in the model organism *Saccharomyces cerevisiae*. The conditions under which the multiple Erg11 bands are detected on western blot have been further defined in *S. cerevisiae*.

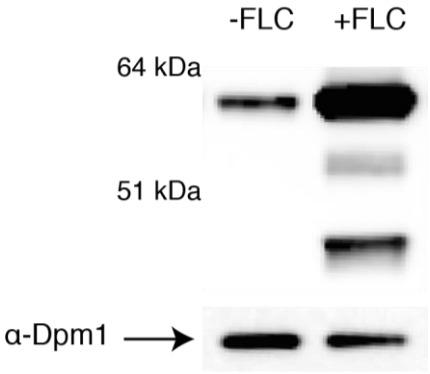


Fig. 2.1. Western blot of protein extracts isolated from wild type *S. cerevisiae* expressing endogenously HA-tagged Erg11 in the absence or presence of FLC shows additional Erg11 products in the presence of the drug. Cells are grown overnight in the absence or presence of 20 µg/mL FLC in rich medium. Protein extracts have been isolated from AFC202 and loaded on gel. The corresponding western blot has been probed with the anti-HA antibody. Under azole treatment, multiple Erg11 bands are detected on western blot, in addition to the full-length form of the protein, which is upregulated compared to the untreated condition. The blot is incubated with α-Dpm1 as a loading control.

To visualize Erg11 on western blot, the protein has been tagged at its C-terminus with a triple HA-epitope tag (3x YPYDVPDYA), to which commercial antibodies are available. The tag has been introduced at the endogenous *ERG11* locus in the wild type *S. cerevisiae* strain BY4742, creating strain AFC202. Untreated cells display a single Erg11 band, when detected on western blot, with a size of about 60 kDa. As mentioned in paragraph 1.3.2.4, it has been described that *ERG11* is upregulated under FLC treatment, both in *S. cerevisiae* and in *C. albicans*. Indeed, the amount of

Erg11 protein from AFC202 grown in the presence of FLC is upregulated compared to non-treated cells (Fig. 2.1). Furthermore, multiple Erg11 bands with different molecular weights (M_W) are detected in protein extracts of cells treated with FLC. Although Anti-Dpm1 has been included as a loading control, it has been merely added for visual inspection of equal loading but not for quantification purposes, as the optimal visualization of the additional bands requires overexposure of the full-length protein. This could have been resolved, however, by including serial dilutions of the FLC-treated sample on the blot. In general, western blot analysis has mainly been used throughout this study to determine the presence of additional Erg11 products but not to quantify Erg11 amounts.

As the HA-tag is located at the C-terminus of the Erg11 protein, the shorter bands must be devoid of their N-terminus. It can however not be excluded that additional Erg11 products are also formed at the N-terminus, but this cannot be detected in this analysis. To exclude the hypothesis that the observed Erg11 pattern is dependent on the tag placed on Erg11, an anti-Erg11 antibody has been developed by GenScript against the internal Erg11 peptide 'STYKDGVKMTDQEI'. Unfortunately, it has been found to have a low affinity for the Erg11 target and requires plasmid-born overexpressed Erg11 for a clear signal. Nonetheless, overexpression of *ERG11* leads to the detection of a similar Erg11 pattern on western blot, even in the absence of FLC, suggesting that the additional Erg11 forms are generated independent of the tag placed at the C-terminus of Erg11 and independent of treatment with FLC (Fig. 2.2 A). A similar Erg11 pattern has been detected on western blot for cells grown in the presence of FLC. A semi-quantitative interpretation of the results has been included, where the intensities of the full-length and additional Erg11 bands have been compared between the untreated and FLC-treated samples (Fig. 2.2 B). There seems to be a trend towards induction of both full-length and truncated Erg11 products for FLC-treated samples. Furthermore, the increase in additional products tends to be higher in treated cells compared to the induction of full-length Erg11. However, the observed trends in band intensities are minor.

The detection of Erg11 with commercial antibodies is preferred over the low affinity anti-Erg11, as it allows the detection of Erg11 at endogenous expression levels. Therefore, C-terminally tagged versions of Erg11 are used throughout this study. Overall, the results from Fig. 2.1 and 2.2 show that the additional Erg11 bands can be detected on western blot whether the protein is plasmid-born or endogenously expressed and whether it is tagged or not. It seems that upregulation of the Erg11 protein, be it by FLC treatment or by plasmid-based overexpression of *ERG11* is sufficient for the detection of additional Erg11 bands on western blot.

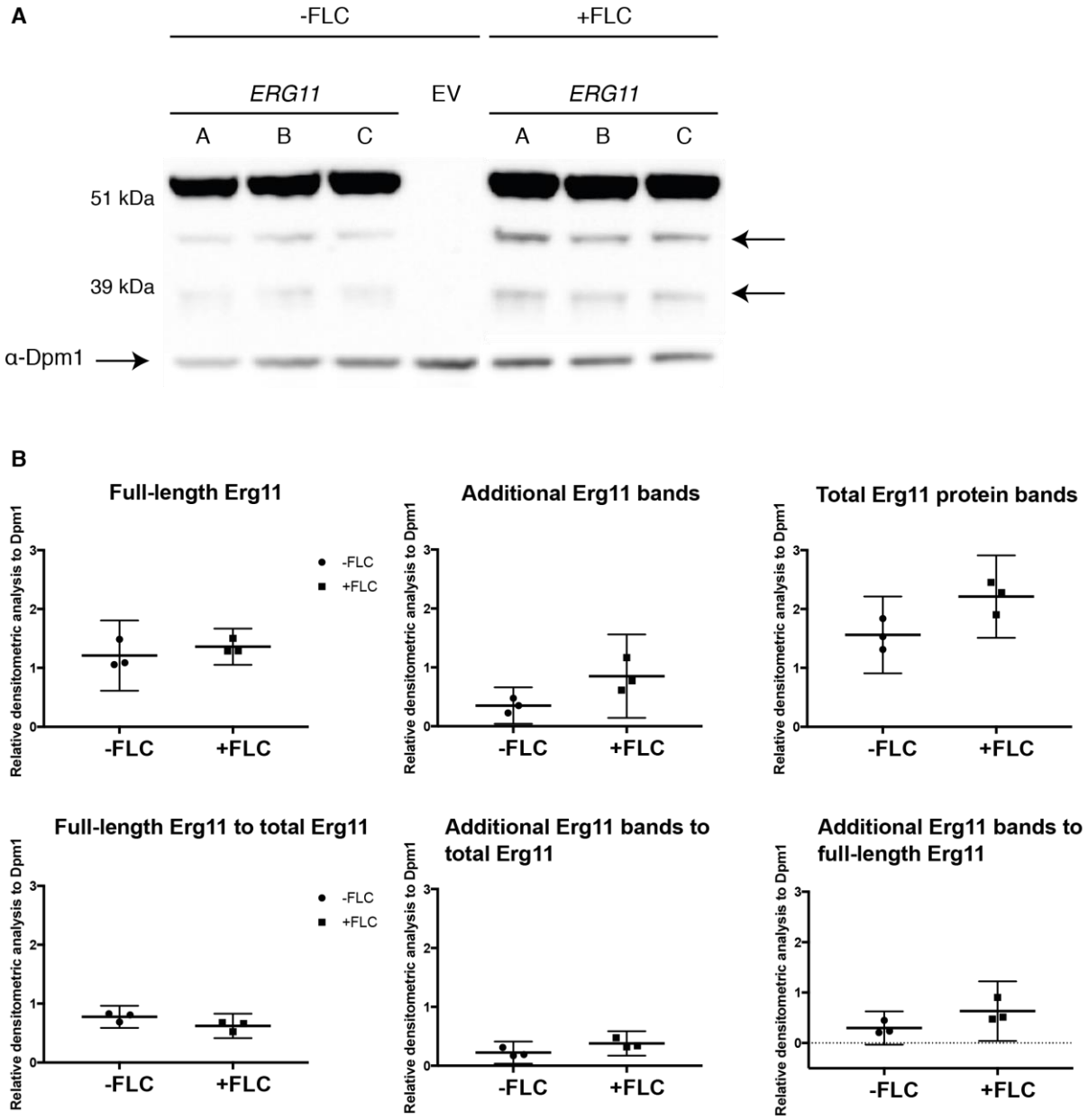


Fig. 2.2. Western blot probed with a custom-made anti-Erg11 antibody proves that additional Erg11 products are generated independent of a C-terminal tag and independent of FLC treatment. (A) Plasmid-born and untagged *ERG11* from pAFC88 has been overexpressed in the BY4742 wild type strain. The empty vector (EV) has been introduced into BY4742 as a negative control. Three individual transformants have been grown in -Leu drop out medium in the presence or absence of FLC. Additional Erg11 bands can be detected both in the untreated and FLC-treated cells transformed with the pAFC88 plasmid. Anti-Dpm1 has been used as a loading control. (B) A semi-quantitative analysis of the intensities of the full-length and additional Erg11 bands (indicated by the arrows) shows a trend towards increasing amounts of Erg11 bands in the presence of FLC treatment, both for full-length, truncated forms or total levels of Erg11. The Erg11 bands have been quantified relative to the densitometric values of the corresponding Dpm1 loading control bands. The results of the full-length and additional Erg11 bands have also been plotted relative to the total levels of Erg11 per lane or relative to one another, indicating that a slight increase in additional bands compared to full-length Erg11 might be present under FLC treatment compared to untreated cells. Mean and individual data points of the three biological replicates are shown with 95% confidence intervals.

In a next experiment, it has been investigated whether additional bands of Erg11 can be detected in the absence of FLC, at endogenous expression levels. For this, increasing amounts of total extracted proteins have been loaded on western blot, isolated from cells grown in the absence or presence of FLC, in rich YPD medium or in minimal synthetic defined (SD) medium supplemented with the necessary amino acids to complement the auxotrophies of AFC202 (Fig. 2.3). It has been found that additional Erg11 bands can be observed in untreated *S. cerevisiae* cells expressing endogenous Erg11-HA, if high enough amounts of protein are loaded. However, detection is improved in rich medium over minimal medium. Furthermore, the molecular weights of the Erg11 bands on western blot are similar for cells grown in rich medium or in minimal medium. Overall, these results seem to indicate that the Erg11 products are always present in a cell, presumably at basal levels and are upregulated under the influence of Erg11 overproduction, *e.g.* by FLC addition. Ideally, a quantitative analysis of the Erg11 bands would have been included, to further validate this idea. However, no loading control has been included in this experiment, as the increasing amounts of full-length Erg11 have been used as an indication that increasing amounts of total protein have been loaded on gel. The aim of this experiment has been to demonstrate that the additional bands of Erg11 are not exclusive to FLC-treated cells and overexpressed Erg11 and that the molecular weights of these extra Erg11 products are similar for untreated and treated cells.

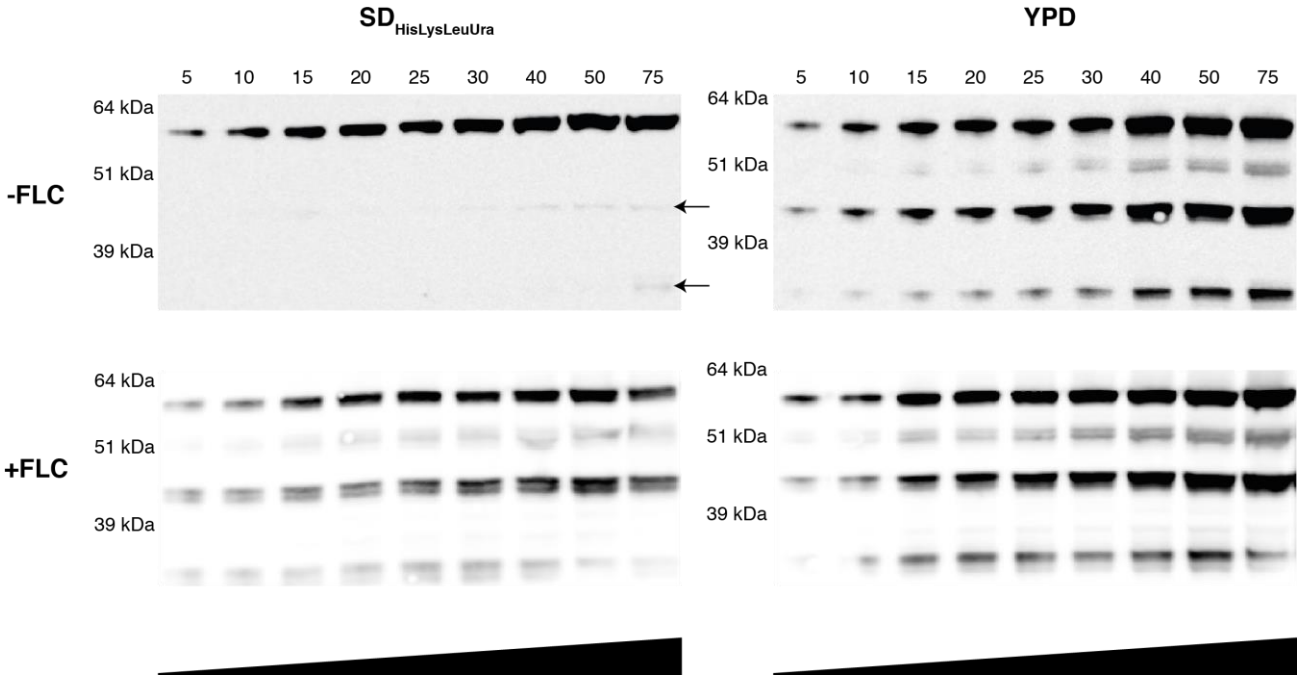


Fig. 2.3. Western blot with increasing amounts of total protein indicates that the additional Erg11 bands can be detected in all tested growth conditions. Proteins have been extracted from AFC202 grown in rich or minimal medium in the absence or presence of FLC. Increasing amounts of total protein (ranging from 5 to 75 µg) have been loaded on gel, as indicated. The additional Erg11 products have been found to have a similar molecular weight in all growth conditions and can be best detected when cells are grown in rich medium or in the presence of FLC (the additional Erg11 bands on the blot of minimal medium minus FLC have been indicated by arrows).

The concentration of FLC that is necessary for optimal visualization of the additional Erg11 forms on western blot has been determined by growing cells in various concentrations of the drug, ranging from 0 µg/mL to 30 µg/mL in minimal medium. It has been found that the shorter bands of Erg11 are best detected at FLC concentrations higher than the MIC, which is 8 µg/mL for AFC202, as determined by Etest (Fig. 2.4). It has been decided to use a concentration of 20 µg/mL of FLC as an easy read-out system for the detection of Erg11 bands on western blot. From this Etest, it is also clear that tolerance in *S. cerevisiae* cannot be visualized by growth inside the halo, as is the case for *C. albicans* strains. The reason for this is unclear.

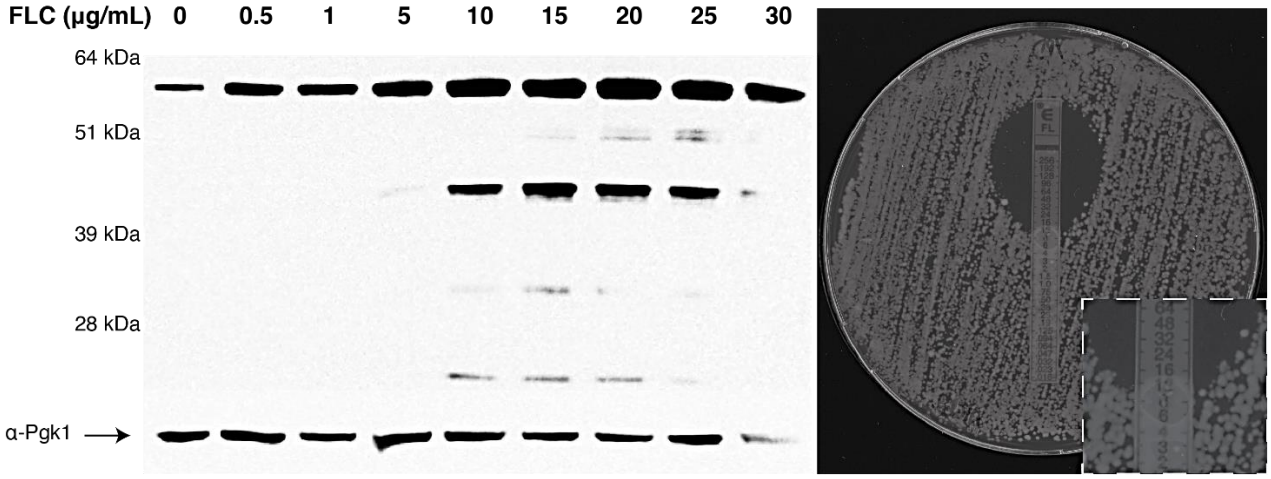


Fig. 2.4. Erg11 bands are best detected on western blot at supra-MIC values of FLC. AFC202 is grown in minimal medium in the presence of a range of FLC concentrations (from 0 to 30 µg/mL) to test the optimal concentration for the detection of additional Erg11 bands on western blot. Anti-Pgk1 has been used as a loading control. The MIC of AFC202 to FLC has been tested via Etest and is found to be 8 µg/mL, as can be seen from the inset. Additional bands of Erg11 are best detected on western blot at concentrations higher than the MIC.

The multiple bands of Erg11 are best detected on western blot after a growth period of 12 up to 24 hours in the presence of FLC, but already after 4 to 8 hours in the absence of drugs (Fig. 2.5 A). Therefore, it has been decided to consistently grow cells for 16 hours under FLC treatment, to analyze Erg11 on western blot. In addition, the growth of the AFC202 strain has been measured spectrophotometrically by determining the optical density of the culture at 600 nm in the absence or presence of FLC over a period of 72 hours in a microtiter plate. As can be seen from the growth curve, at the time points where the additional Erg11 bands are observed, the cells are still in the lag phase or in early exponential phase (Fig. 2.5 B). It is not unreasonable that *ERG11* would be upregulated in the lag phase, as it would ensure ergosterol production and robust cell growth in this early stage. Unfortunately, no other data could be found in the literature to support this idea. A previous study however, has identified that CYP expression, most of which is assumed to be produced by *ERG11*, is highest at the beginning of stationary phase, although no CYP protein

concentrations have been measured during the lag phase (Karenlampi *et al.*, 1981; Turi and Loper, 1992).

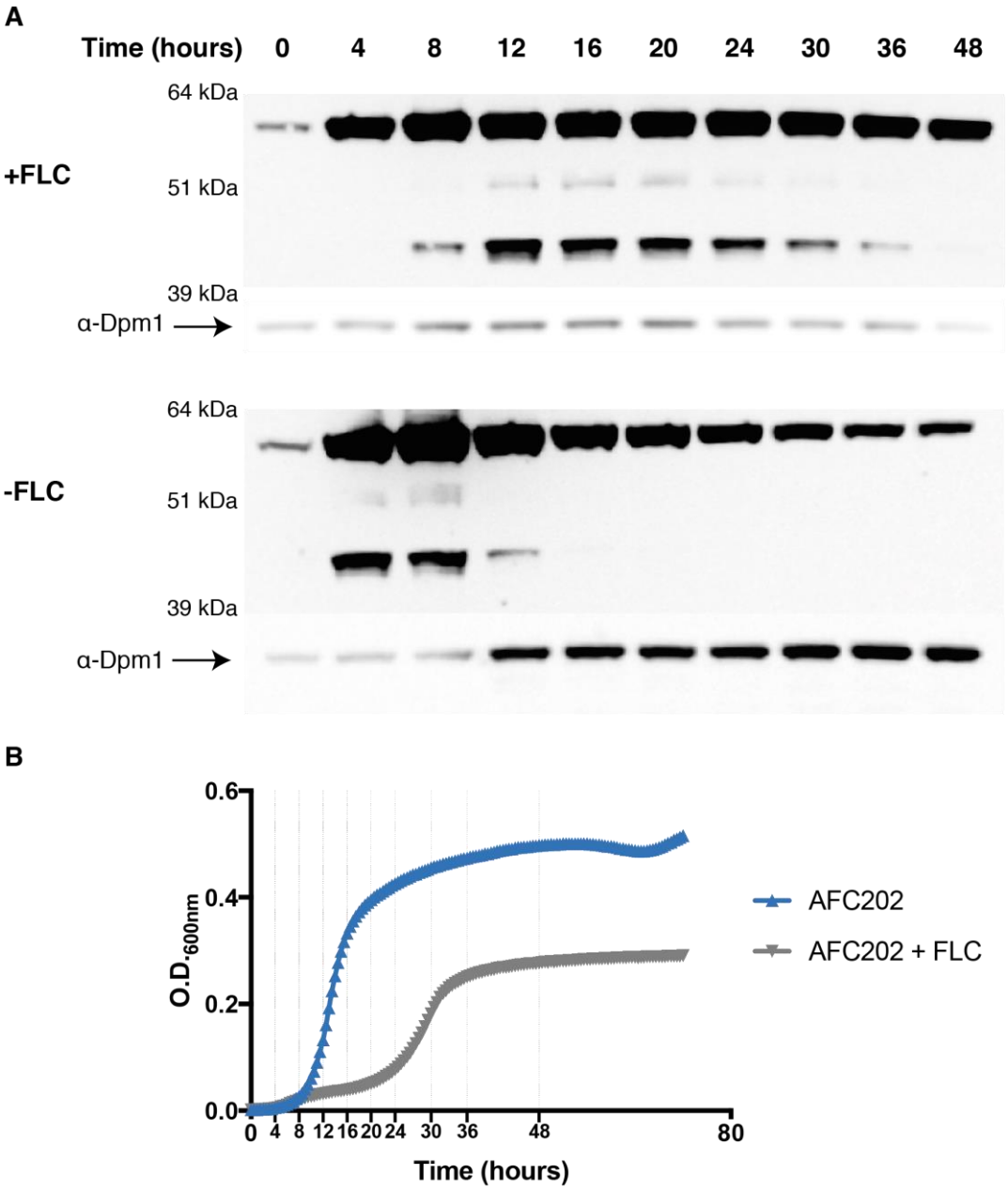


Fig. 2.5. A time-course study of Erg11-HA detection on western blot indicates that Erg11 bands are best detected in the lag to early exponential phase. (A) AFC202 has been grown in minimal medium in the presence or absence of FLC. At the indicated time points, cells have been isolated to study the corresponding Erg11 pattern on western blot. 10 µg of total protein has been loaded of the extracts of FLC-treated cells and 35 µg of those of non-stressed cells. This higher amount of total protein is necessary to detect the additional Erg11 bands in the absence of FLC. Anti-Dpm1 has been used as a loading control, however Dpm1 expression is not stable during the lag phase in non-stressed cells and is therefore not an appropriate control for quantification of the western blot results. (B) The growth curve of AFC202 in minimal medium with or without FLC indicates that Erg11 bands are best detected in lag to early exponential phase.

2.2 Identification of the truncated Erg11 forms detected on western blot

Several attempts have been made to identify the sequences of the truncated Erg11 bands detected on western blot. Previously, attempts have been made in our lab to purify the Erg11 forms for Edman degradation sequencing, but this method was unsuccessful. This could be attributed to an unknown chemical modification of the Erg11 N-termini of the shorter forms, which would block the chemical reaction necessary for identification of the first amino acids, or to the minute amounts of the Erg11 truncated forms, which could be too low for detection by Edman sequencing. Therefore, an MS-based approach has been used for the identification of the sequences of the truncated Erg11 forms.

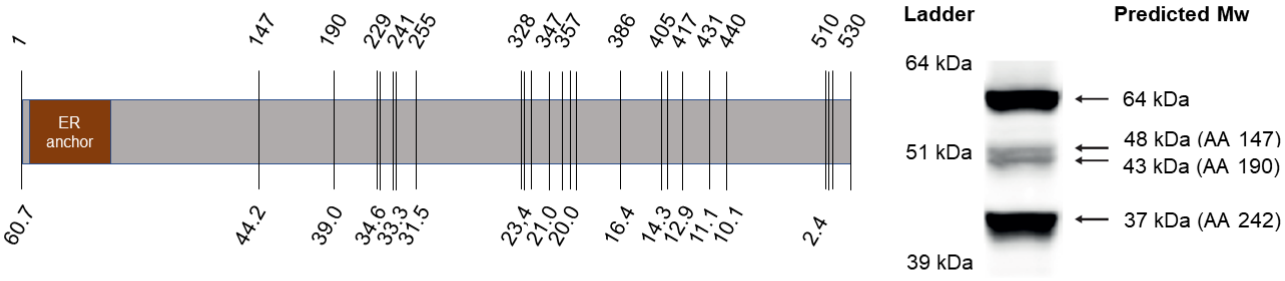
The wild type BY4742 *S. cerevisiae* strain has been transformed with an *ERG11-HA* overexpressing plasmid or the empty vector, as a negative control. Proteins have been extracted from the cells and Erg11 has been purified from these extracts based on its HA-tag, by magnetic anti-HA beads. Triplicates of purified Erg11 samples and negative control samples have been sent to the VIB Proteomics Expertise Center (PEC) in Ghent for MS analysis. With the used technique, all free N-termini (and ε-amines of lysines) have been heavily labelled with an N-hydroxysuccinimide ester of trideutero-acetate (AcD_3-NHS). It has been calculated that at least 94% of the lysine residues have been labeled, indicating that the chemical reaction was successful. This approach has resulted in the identification of 23 possible Erg11 N-termini, representing various (non-methionine) residues as the starting amino acid (Fig. 2.6 A).

The AcD_3-labelled Erg11 peptides identified in the MS spectra likely correspond to the additional Erg11 bands observed on western blot. However, the relevance of each identified residue should be validated, *i.e.* by mutational analysis. On the other hand, some N-termini might have been overlooked during this analysis, *e.g.* because of a suboptimal length of Erg11 peptides generated by tryptic digestion for detection with MS. In the MS data, the integrated peak areas of the identified MS1 Erg11 peptides and the MS2 peptide spectrum match (PSM) counts have been included (Fig. 2.6 B and Appendix I). These data might give an indication of the abundances with which the Erg11 N-termini have been identified, however factors such as the ionization efficiency of the generated peptides influences these results. Those factors have not been accounted for in the data and therefore this is not a true quantitative analysis. So, although these data indicate that the most likely cleavage sites are at positions 242, 386, 510 and 511 and possibly at 347, although there is a large technical variability, other identified residues are also expected to be true cleavage sites, as they would produce Erg11 products with molecular weights roughly corresponding to those observed on western blot, *i.e.* residues 147 and 190, as suggested in Fig. 2.6 A. This could be investigated further by examining the Erg11 pattern of corresponding mutants on western blot. Additional data from the MS analysis can be found in Appendix I.

Because of the high number of Erg11 N-termini that have been identified, it is unlikely that these are generated by a process other than cleavage reactions. Indeed, the proteases Pep4 and Prb1 have been identified for their involvement in the generation of the Erg11 products (as explained in Chapter 4). This supports the hypothesis that a cleavage process is responsible for the detection of the additional Erg11 bands on western blot.

A

N-term	1	147	190	229	230	241	242	255	328	329	331	347	357	360	362	386	405	408	417	431	440	510	511	512
Mw	60.7	44.2	39.0	34.6	34.5	33.3	33.1	31.5	23.4	23.3	23.0	21.0	20.0	19.6	19.3	16.4	14.3	13.9	12.9	11.1	10.1	2.4	2.3	2.2



B

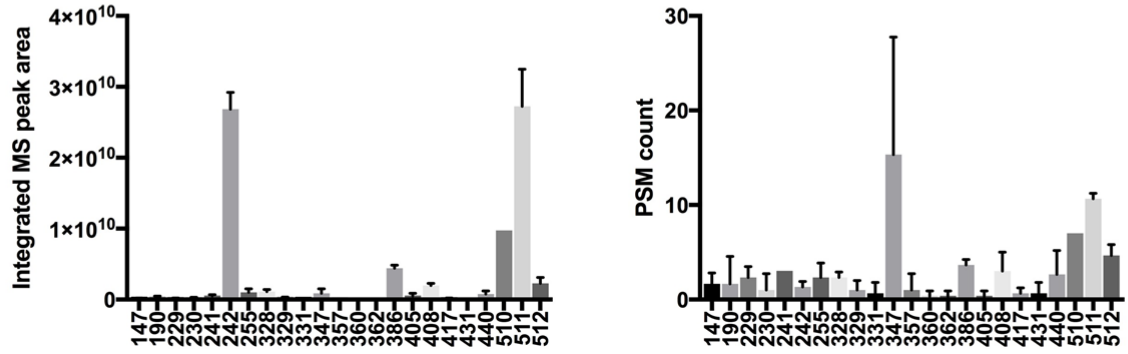


Fig. 2.6. Results of the MS analysis, identifying putative additional Erg11 products. (A) The 23 possible N-termini that have been identified in this MS analysis are indicated, together with the predicted molecular weight (in kDa) of the Erg11 products corresponding to that N-terminus. The molecular weights of the Erg11 products have been estimated with an ExPASy program (https://web.expasy.org/compute_pi/). As a suggestion, the Erg11 bands detected on western blot have been associated with certain identified residues (these Erg11 products are tagged with the HA-tag, which is about 4.4 kDa). It should be noted that the ladder included on the western blot does not fully correspond to the predicted molecular weights of the online tool, not even for the full-length protein. The importance of the identified residues to the observed Erg11 products should be further validated by mutational analysis. (B) The integrated MS1 peak areas of all peptides corresponding to the same N-terminus have been added up and the average value for the three technical replicates is shown. Similarly, the average PSM count for each N-termini is depicted. Mean values are shown with standard deviation, representing the technical variation.

2.3 Discussion

Previous unpublished studies in our lab have indicated the presence of multiple Erg11 bands on western blot when cells are treated with the antifungal drug fluconazole, in the opportunistic pathogen *C. albicans* and in the model organism *S. cerevisiae*. In this chapter, these findings have been investigated in more detail in *S. cerevisiae*. In conclusion, it has been found that the Erg11 pattern detected on western blot is independent of FLC treatment and of the culture medium used. However, the detection of the additional bands improves when Erg11 levels are induced (*e.g.* by azole treatment or by plasmid-based overexpression of the *ERG11* gene). The Erg11 forms can be detected by commercial antibodies directed at a C-terminal epitope tag or by a custom-made polyclonal anti-Erg11 antibody, eliminating the hypothesis that the Erg11 forms are artefacts due to protein tagging. For the optimal detection of the Erg11 bands on western blot, it has been decided to extract proteins at the time point of 16 hours, after overnight growth of the *S. cerevisiae* cultures with supra-MIC concentrations of fluconazole (20 µg/mL). Although a quantitative interpretation of western bot data has not been included for most blots throughout this study, a semi-quantitative analysis of overexpressed Erg11 levels detected by the anti-Erg11 antibody indicates a slight trend towards increased levels of Erg11 in the presence of FLC treatment, of which the additional Erg11 products might be more upregulated than the full-length Erg11 protein.

The sequences of the truncated Erg11 forms have been examined by MS analysis, which has led to the identification of 23 possible Erg11 N-termini. A mutational analysis of the identified residues could further confirm their significance as putative cleavage sites. Indeed, this high number of N-termini suggests that the Erg11 bands are generated by a proteolytic process, rather than by means of alternative transcription or translation start sites. Furthermore, the *ERG11* sequence has not been associated with the presence of introns, so the mechanism of alternative splicing can be excluded. Furthermore, this high number suggests that the additional Erg11 bands might be degradation products, rather than specific cleavage products, as observed with the mammalian model of CYP cleavage and the process of bimodal targeting, where at most two cleavage products are generated in addition to the full-length protein form. The likelihood of Erg11 degradation will be discussed further in Chapter 4.

CHAPTER 3

ERG11 CONTAINS A MITOCHONDRIAL TARGETING SIGNAL IN *SACCHAROMYCES CEREVISIAE*

Parts of this results section are based on and contain text from “Visualization of Erg11 in *Saccharomyces cerevisiae* using focused ion beam scanning electron microscopy”, which will be submitted to mSphere and the manuscript “On the whereabouts of yeast Erg11: a report on localization and degradation”, which is in preparation. All the experiments described in this chapter have been designed and performed by Winnie Kerstens, with technical assistance by Ilse Palmans, except for part of the sample preparation and imaging of the FIB-SEM samples, performed by the VIB BioImaging Core in Ghent and for the *in silico* analysis of protein structures by Prof. A. Voet.

3.1 Construction of truncated Erg11 products in *Saccharomyces cerevisiae*

The observation that Erg11 is detected as multiple forms on western blot during FLC therapy has initially led to the hypothesis that Erg11 could be bimodally targeted to the ER and mitochondria, in analogy to mammalian drug-induced CYPs. Hence, Dr. A. Fiori started to investigate whether Erg11 possesses a cryptic MTS, similar to mammalian CYPs. As explained in paragraph 1.3.4, it is difficult to identify a cryptic MTS based on bioinformatical analysis, as these programs are intended to be used for the recognition of canonical MTSs. Nonetheless, previous analysis by Dr. A Fiori has revealed that the removal of the first 150 amino acids of Erg11 increases the mitochondrial targeting potential of Erg11 from 0.25 for the full-length form to 0.59 for the N-terminal Erg11$^{\Delta 150}$ truncated form in MitoProt, an online tool for the prediction of MTSs (Claros and Vincens, 1996). Accordingly, a plasmid-based V5-tagged Erg11 construct has been made that lacks its N-terminal 150 amino acids (Fig. 3.1 A). Interestingly, its size roughly matches that of the ±50 kDa additional forms of wild type Erg11, when detected on western blot (Fig. 3.1 B). Moreover, this truncation exposes a stretch of charged and polar amino acids, which could constitute an MTS. It should be noted that, at that time, the MS analysis of purified Erg11 (described in Chapter 2) had not been performed. In the MS analysis, an N-terminus has been identified at position 147. In analogy to the Erg11$^{\Delta 150}$ construct, the putative Erg11 product starting at position 147 would also roughly correspond to the highest molecular weight additional bands of wild type cells on western blot.

The idea that Erg11 carries a cryptic MTS around amino acid 150 has been tested. Additional Erg11 constructs have been made, in which four lysine to alanine substitutions have been introduced to disrupt the putative MTS, both in the full-length Erg11 construct and in the truncated Erg11 construct, creating Erg11****-V5 and Erg11$^{\Delta 150****}$-V5, respectively (Fig. 3.1 A). The conversion of lysines 151, 152, 155 and 160 into alanines should decrease the mitochondrial targeting potential of the sequence because of the loss of the positively charged residues, which are crucial to an MTS (Lemire *et al.*, 1989). This is validated by a MitoProt score of 0.05 for Erg11$^{\Delta 150****}$. As an additional control, an Erg11 construct lacking its ER membrane anchor has been included (Erg11$^{\Delta 74}$-V5). As Erg11 is anchored in the ER membrane with its N-terminus, exposing its catalytic

site to the cytosol, this would generate a soluble, cytosolic Erg11 protein. The expression of all these Erg11 constructs has been analyzed on western blot (Fig. 3.1 B).

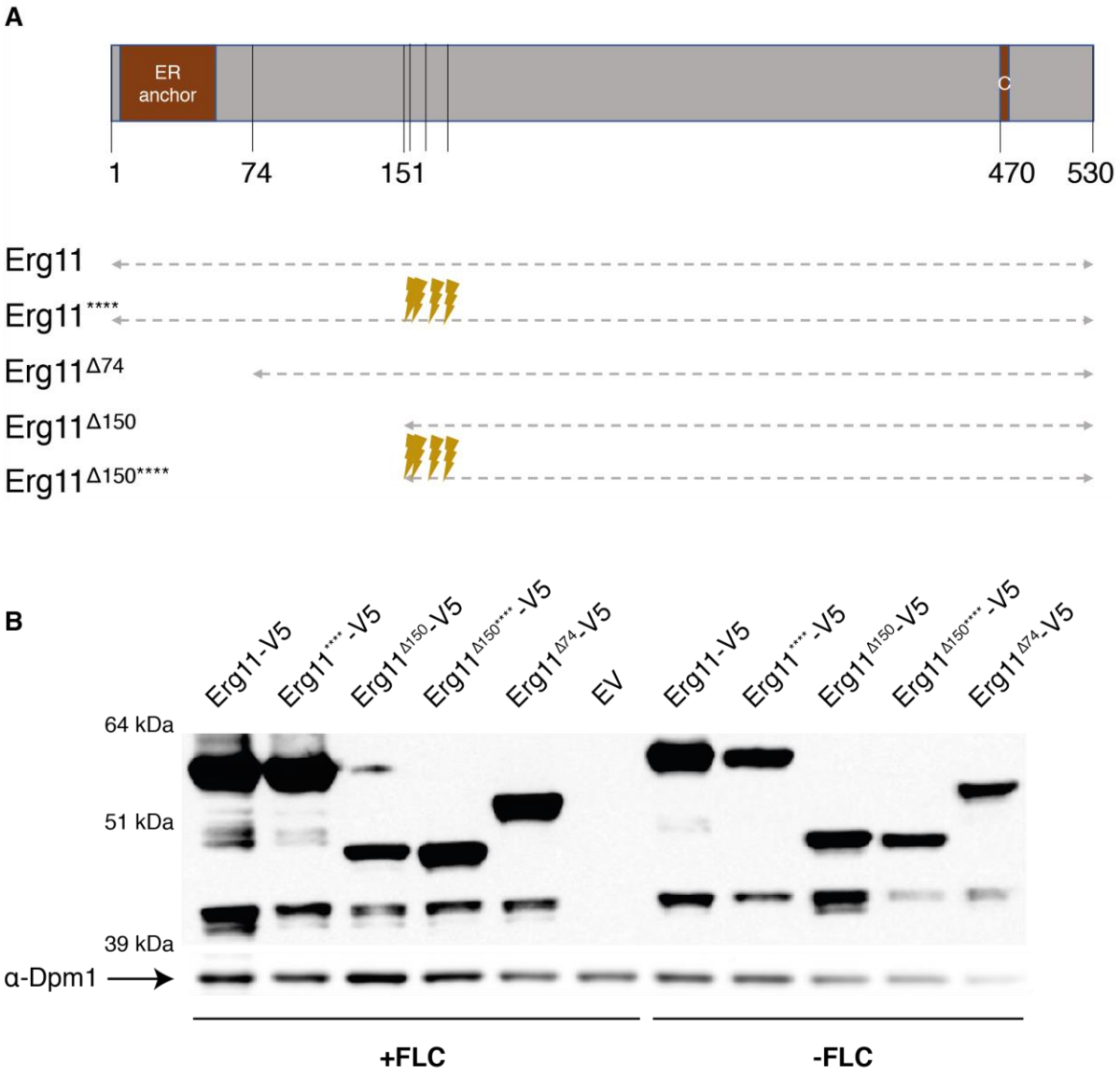


Fig. 3.1. The expression of plasmid-born, V5-tagged full-length Erg11 and Erg11 truncated constructs has been investigated on western blot. (A) Erg11 constructs have been generated, lacking an N-terminal part of the protein by deleting the first 74 or 150 amino acids. The putative, cryptic MTS has been altered by introducing four lysine to alanine substitutions at positions 151, 152, 155 and 160 (indicated by marks), either in the full-length Erg11 protein or in the truncated form that lacks the N-terminal 150 amino acids. The ER anchor region and the conserved cysteine that coordinates to the heme group have also been indicated in this schematic representation of the *S. cerevisiae* Erg11 constructs. (B) Proteins have been extracted from cells expressing *ERG11-V5*, *ERG11****-V5*, *ERG11$^{\Delta 150}$-V5*, *ERG11$^{\Delta 150****}$-V5*, *ERG11$^{\Delta 74}$-V5* or the empty vector (EV), after overnight growth in adenine supplemented -Trp drop out medium in the presence of 3 µg/mL anhydrotetracycline (ATC) to induce the expression of the constructs and in the presence or absence of FLC (20 µg/mL). Anti-V5-HRP has been used to detect the V5-tagged Erg11 proteins. Anti-Dpm1 has been used as a loading control.

3.2 Is Erg11 bimodally targeted to ER and mitochondria in *Saccharomyces cerevisiae*?

3.2.1 Restoration of arginine auxotrophy by mitochondrial targeting of Erg11-Arg8$^{\Delta 13}$ chimeras

The Erg11 constructs (Erg11, Erg11****, Erg11$^{\Delta 150}$, Erg11$^{\Delta 150****}$ and Erg11$^{\Delta 74}$) have subsequently been adapted to examine the possibility of Erg11 localization to yeast mitochondria. Arg8, a protein involved in arginine biosynthesis, requires localization to the mitochondrial matrix to exert its function. If Arg8 cannot reach the mitochondria, cells become auxotrophic for arginine (Steele *et al.*, 1996; He and Fox, 1999). Arg8$^{\Delta 13}$, devoid of its N-terminal 13 amino acids MTS, has been fused to the C-terminus of all described Erg11 constructs and transformed into an *arg8*Δ strain. Only if the resulting chimeric protein is shuttled to the mitochondria, the Arg8$^{\Delta 13}$ moiety can restore the arginine auxotrophy of the *arg8*Δ cells (Fig. 3.2 A). *arg8*Δ cells expressing the full-length Erg11-Arg8$^{\Delta 13}$ or Erg11****-Arg8$^{\Delta 13}$ constructs show, similar to Arg8$^{\Delta 13}$, poor growth on minus arginine medium. The Erg11$^{\Delta 150}$-Arg8$^{\Delta 13}$ construct, exposing the putative MTS on the other hand shows robust growth on arginine limiting medium. When the putative MTS is perturbed by lysine to alanine substitutions, the growth of the resulting construct (Erg11$^{\Delta 150****}$-Arg8$^{\Delta 13}$) is weakened, indicating a loss of mitochondrial targeting. Furthermore, Erg11$^{\Delta 74}$-Arg8$^{\Delta 13}$ shows little to no growth as expected, as this is not a mitochondrially localized protein. As a negative control, Arg8$^{\Delta 13}$ has been fused to another ER-resident protein, Sec61, which did not restore arginine prototrophy. Furthermore, grafting 50 amino acids of the putative Erg11 MTS (AA 148 to 197) to the N-terminus of Arg8$^{\Delta 13}$ results in efficient targeting of the construct to the mitochondria, indicated by the robust growth on arginine restricted medium (Fig. 3.2 B). However, if the putative Erg11 MTS segment is mutated by interchanging the four lysine residues to alanines (MTS****-Arg8$^{\Delta 13}$), the arginine auxotrophy is not restored. Altogether, these results clearly indicate that Erg11 encompasses a cryptic internal MTS, for which the positively charged lysine residues are important.

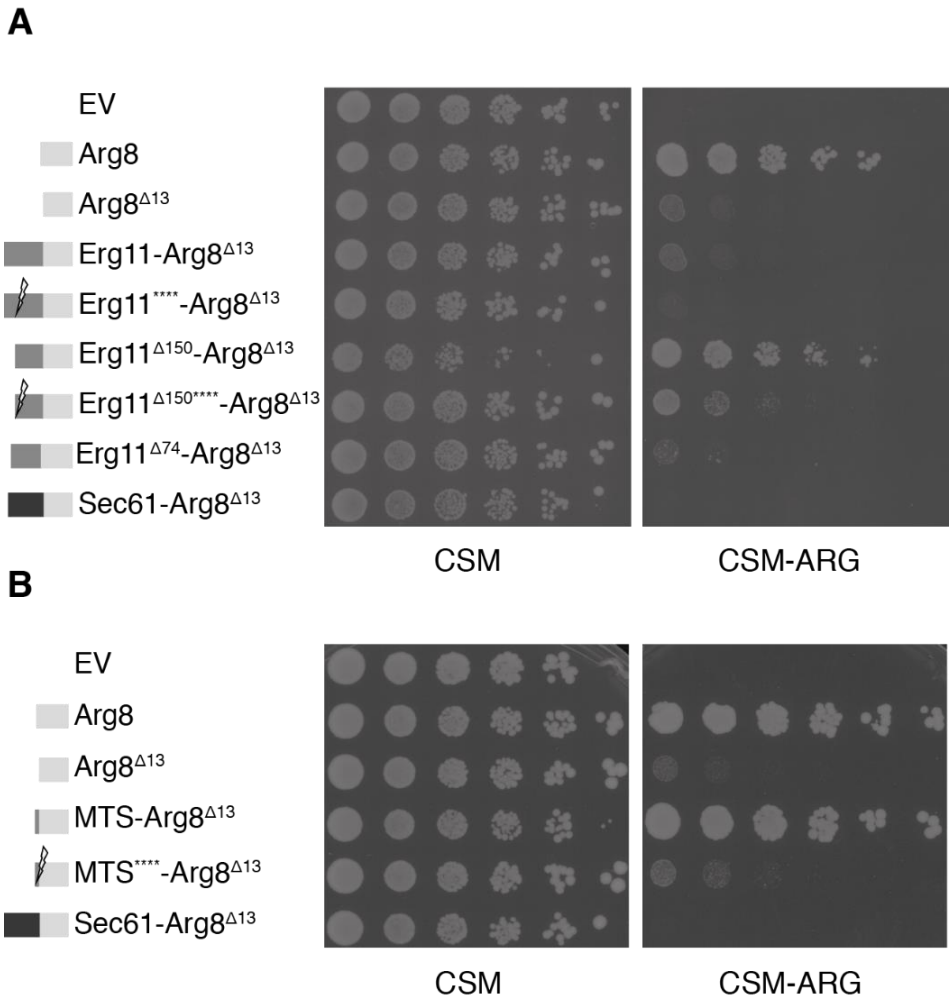


Fig. 3.2. Spot assay of plasmid-born Erg11-Arg8$^{\Delta 13}$ chimeric proteins in an *arg8Δ* background strain on complete synthetic medium (CSM) or CSM depleted of arginine (CSM-ARG). (A) Arginine auxotrophy of the *arg8Δ* cells is restored when full-length Arg8 is introduced, but not when Arg8$^{\Delta 13}$ is expressed, which lacks the MTS. Fusing full-length Erg11 at the N-terminus of Arg8$^{\Delta 13}$ does not restore growth, however fusing Erg11$^{\Delta 150}$ N-terminally to Arg8$^{\Delta 13}$ does restore growth on arginine limiting medium, indicating that this construct exposes an MTS. Decreasing the MTS potential of the Erg11$^{\Delta 150}$-Arg8$^{\Delta 13}$ construct by lysine to alanine substitutions (****) clearly decreases growth on minus arginine medium. Loss of the ER membrane anchor is not sufficient for mitochondrial targeting, as Erg11$^{\Delta 74}$-Arg8$^{\Delta 13}$ cannot grow on arginine deficient medium. Fusion of a random ER membrane protein, Sec61 to Arg8$^{\Delta 13}$ does not restore growth of the *arg8Δ* cells. (B) Grafting 50 amino acids of the putative MTS region of Erg11 to the N-terminus of Arg8$^{\Delta 13}$ is sufficient to restore growth on arginine restricted medium. However, growth is severely diminished if the four lysine residues in the MTS are mutated to alanine residues. Results are shown after three days of growth.

3.2.2 Analysis of the subcellular localization of the Erg11 variants by microscopy

To further confirm the mitochondrial targeting of Erg11$^{\Delta 150}$ and to investigate the bimodal targeting of the full-length Erg11 construct to ER and mitochondria, two different microscopy techniques have been used, *i.e.* fluorescence microscopy and focused ion beam scanning electron microscopy (FIB-SEM).

3.2.2.1 Fluorescence microscopy

In this approach, plasmid-based truncated and full-length forms of Erg11 have been C-terminally tagged with the fluorophore mCherry and transformed to *S. cerevisiae* (Fig. 3.3). At the same time, a plasmid has been introduced carrying a GFP-tagged (green fluorescent protein) marker protein, to confirm the localization of the Erg11-mCherry constructs, *i.e.* Sec63-GFP for ER localization, GFP-tagged carboxypeptidase S (CPS) for vacuolar localization and GFP fused to the mitochondrial presequence of *Neurospora crassa* F_0-ATPase subunit 9 as a mitochondrial marker (mtGFP). Fluorescence microscopy shows that full-length Erg11-mCherry localizes to the ER, as described before (Ott *et al.*, 2005). The ER localization of full-length Erg11 is independent of the MTS mutation, as Erg11****-mCherry also localizes to the ER, corresponding with the Sec63-GFP signal. However, when Erg11****-mCherry is expressed, the ER structure seems to be less well formed, with less clear perinuclear and cortical ER signals for both the GFP-control and the mCherry-signal, compared to wild type Erg11-mCherry cells. Furthermore, confocal microscopy confirms the mitochondrial localization of the Erg11$^{\Delta 150}$-mCherry construct, as it co-localizes with the mtGFP marker. Perturbation of the MTS clearly affects mitochondrial targeting, as Erg11$^{\Delta 150****}$-mCherry localizes to the cytoplasm instead of mitochondria. Moreover, some Erg11$^{\Delta 150****}$-mCherry signal can be observed inside the CPS-GFP marked vacuole, where it is possibly delivered for degradation. Remarkably, the Erg11$^{\Delta 74}$-mCherry construct does not localize to the cytosol. Instead the Erg11 protein devoid of its ER-anchor localizes to a specific compartment adjacent to the vacuole, which could be a prevacuolar structure. There is no obvious explanation as to why Erg11$^{\Delta 74}$-mCherry localizes to this structure, while the Erg11$^{\Delta 150****}$-mCherry construct does localize to the cytosol, as both are expected to be cytosolic proteins. The use of additional marker proteins could further identify the nature of the compartment to which Erg11$^{\Delta 74}$-mCherry localizes.

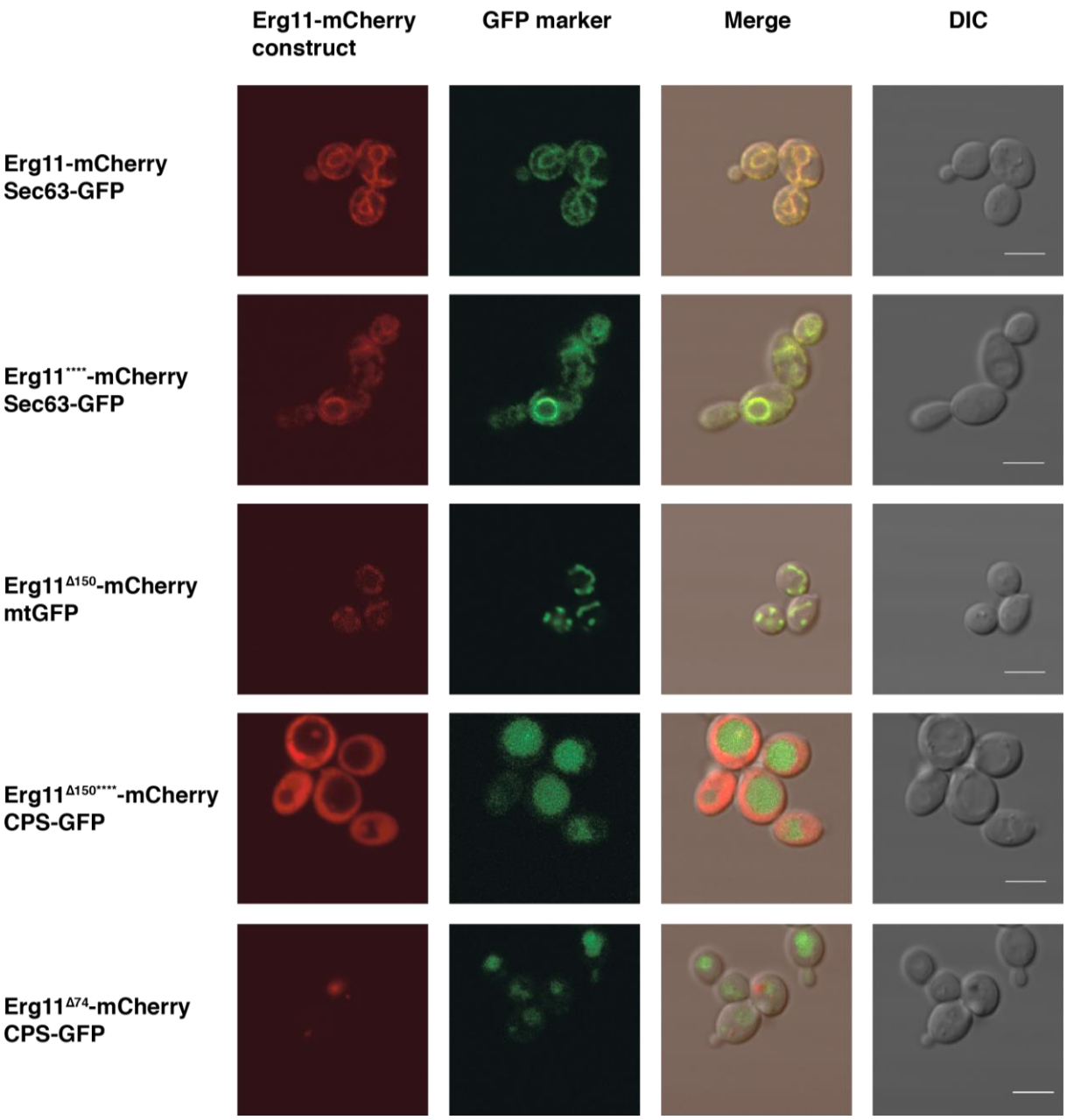


Fig. 3.3. Fluorescence microscopy of mCherry-tagged Erg11 variants in the presence of GFP marker proteins. The full-length Erg11-mCherry constructs (Erg11 and Erg11****) both localize to the ER, as confirmed by their colocalization with Sec63-GFP. The Erg11$^{\Delta 150}$-mCherry construct clearly colocalizes with the mtGFP marker. The Erg11$^{\Delta 150****}$-mCherry carries a disrupted MTS and therefore cannot reach the mitochondria. Instead, it localizes to the cytoplasm. Erg11$^{\Delta 74}$-mCherry possibly localizes to a prevacuolar compartment. The scale bar represents 5 µm.

These results clearly indicate that Erg11 can be targeted to mitochondria, when its MTS is exposed. However, if bimodal targeting of Erg11 is occurring in the wild type construct, we would expect to see both ER and mitochondrial localization of the Erg11-mCherry construct. Therefore, yeast cells transformed with the full-length Erg11-mCherry construct have also been transformed with the

mitochondrial GFP marker. Unfortunately, with magnifications limited to 60x, it is impossible to be conclusive on the potential bimodal targeting of Erg11. There is little overlap visible between the Erg11 construct and mitochondria but here and there some yellow signal seems to be present (Fig. 3.4). This indicates overlay of GFP-tagged mitochondria and red-fluorescent Erg11. It could be possible that a fraction of Erg11 is truly targeted to mitochondria. Alternatively, the yellow fluorescence possibly represents sites of contact between the ER and mitochondria, where Erg11 could be part of an ER-mitochondria membrane interface. Close contacts between the ER and mitochondria (and also between other organelles) have been described in yeast and mammals. Two protein complexes that tether both organelles together in *S. cerevisiae* have been characterized as the ER-mitochondria encounter structure (ERMES) and the ER membrane protein complex (EMC) (Kornmann *et al.*, 2009; Lahiri *et al.*, 2014). It would be interesting to visualize the cells with greater magnification (*e.g.* 100x) to exclude one of both possibilities. It has been tried to increase the yellow fluorescent signal by treating the cells with FLC, which might increase the production of Erg11 forms and thus potentially increases the mitochondrial targeting of Erg11. However, no clear enhancement of yellow fluorescent signal has been observed, although no quantitative measurements have been taken. Moreover, the Erg11 constructs are already overexpressed, which similarly leads to the detection of additional Erg11 forms on western blot.

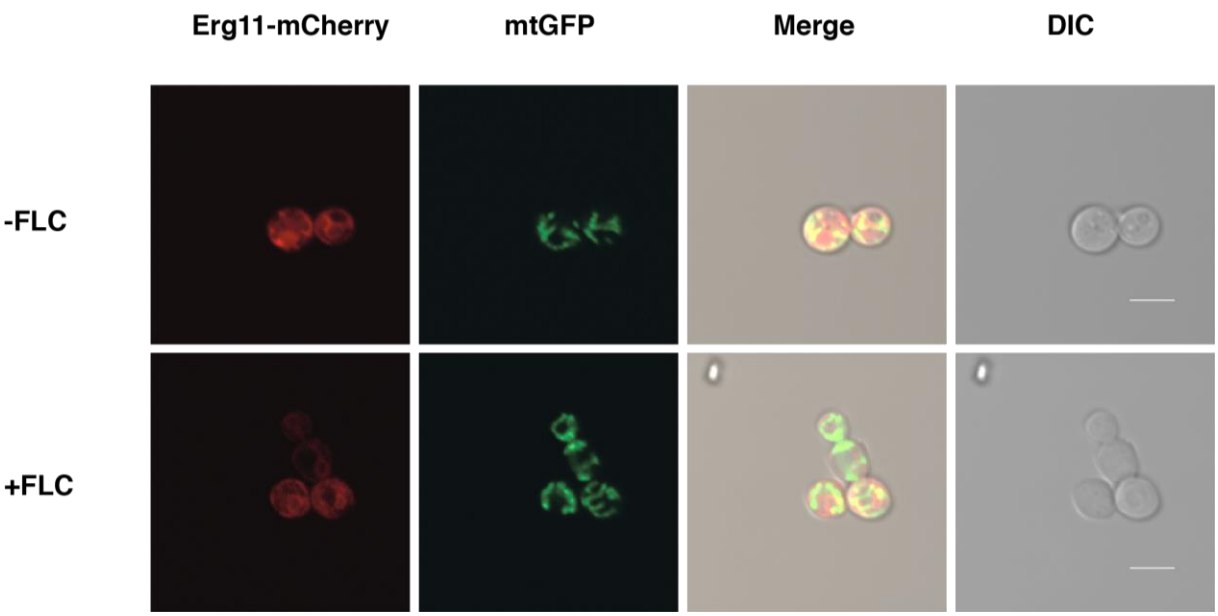


Fig. 3.4. Examining the possibility of bimodal targeting of full-length Erg11 by means of fluorescence microscopy. Some yellow fluorescent signal can be detected, which represents colocalization of full-length Erg11-mCherry and the mtGFP marker. This suggests that Erg11 is associated with mitochondria at some sites. Fluorescence microscopy has also been performed in the presence of FLC, to potentially enhance the detection of yellow fluorescence, however no enhancement has been observed by visual inspection. The scale bar represents 5 µm.

3.2.2.2 Focused ion beam scanning electron microscopy

In a second approach, a different, novel and sensitive technique has been used to study the localization of Erg11 in *S. cerevisiae*. Similar to transmission electron microscopy (TEM) tomography, FIB-SEM can generate three dimensional (3D) images of the internal structure of samples, which is different from standard SEM, imaging sample surfaces. The technique of FIB-SEM depends on two different kinds of beams: an ion beam (typically gallium, Ga^+) and an electron beam (Kizilyaprak *et al.*, 2014). The destructive ion beam is placed under an angle of 45 to 55 degrees with respect to the electron beam and mills away tranches of a sample, the thickness of which can be fixed and is usually a few nanometers. The electron beam of the scanning electron microscope is focused on the same point and is responsible for the imaging of the newly created surfaces. As such, FIB-SEM allows sample preparation and 3D-imaging resolution at the nanoscopic scale.

To obtain an electron-dense signal, the Erg11 variants have been fused to APEX2, which is an engineered peroxidase that catalyzes the polymerization of diaminobenzidine (DAB) (Lam *et al.*, 2015). DAB has a high affinity for osmium tetroxide, which intensifies the electron density of the tagged protein, rendering a clear EM-signal. Furthermore, a negative control has been included, carrying wild type Erg11 without the APEX2-tag. It has been found that the detection of APEX2-tagged Erg11 is strongly enhanced when the yeast cell wall is lysed and spheroplasts are formed. Most likely, this enhances the uptake of DAB into the cells. This is the first time this technique has been described in *S. cerevisiae*. The study has been performed in collaboration with the VIB BioImaging Core in Ghent.

Cells expressing the control construct have been grown in the absence or presence of FLC. In both cases, internal structures have been clearly observed, such as the nucleus and mitochondria (Fig. 3.5). FIB-SEM imaging of C-terminally APEX2-tagged full-length Erg11 shows a bright ER localization signal. Additionally, it has been observed that the ER produces some aberrant, multilayered ER membrane structures, termed ER whorls, which will be discussed in more detail in Chapter 4. Unfortunately, the FIB-SEM sample of FLC-treated cells with APEX2-tagged full-length Erg11 is not of the best quality and contains little Erg11 signal. Interestingly, the detected signal, present as multilayered ER membrane structures, is often in close contact and surrounded by high amounts of mitochondria, indicated by the arrows in Fig. 3.5. Such a localization corresponds to the fluorescence microscopy data of full-length Erg11, which has already hinted towards a close apposition of Erg11 and mitochondria, or even to the presence of Erg11 inside mitochondria. Unfortunately, mitochondria are difficult to visualize in the FIB-SEM sample without FLC, excluding the possibility to examine the localization of full-length Erg11 in relation to mitochondria. Yet, it seems that no true mitochondrial localization is observed for full-length Erg11, either in the absence or presence of FLC. This suggests that Erg11 is not bimodally targeted to ER and mitochondria. Rather, Erg11 could be targeted to ER-mitochondria contact sites.

The Erg11$^{\Delta 150}$-APEX2 construct clearly localizes to the mitochondria, with a signal present throughout the organelles, suggesting that this truncated version of Erg11 is not present in the outer mitochondrial membrane (OM), but rather internally, with possible localizations to the inner membrane (IM), the intermembrane space (IMS) or the matrix. It has been tried to further define the localization of this construct by staining the spheroplasts with a shorter incubation period of DAB, which would result in a less intense signal, but this has not resulted in successful data, as no signal at all has been observed. However, combined with the results of the *ARG8* assay, where the C-terminal Arg8$^{\Delta 13}$ moiety needs to reach the matrix to be functional, these results suggest that the Erg11$^{\Delta 150}$ construct is most likely present as an inner membrane protein exposing its C-terminus to the matrix or as a soluble matrix protein.

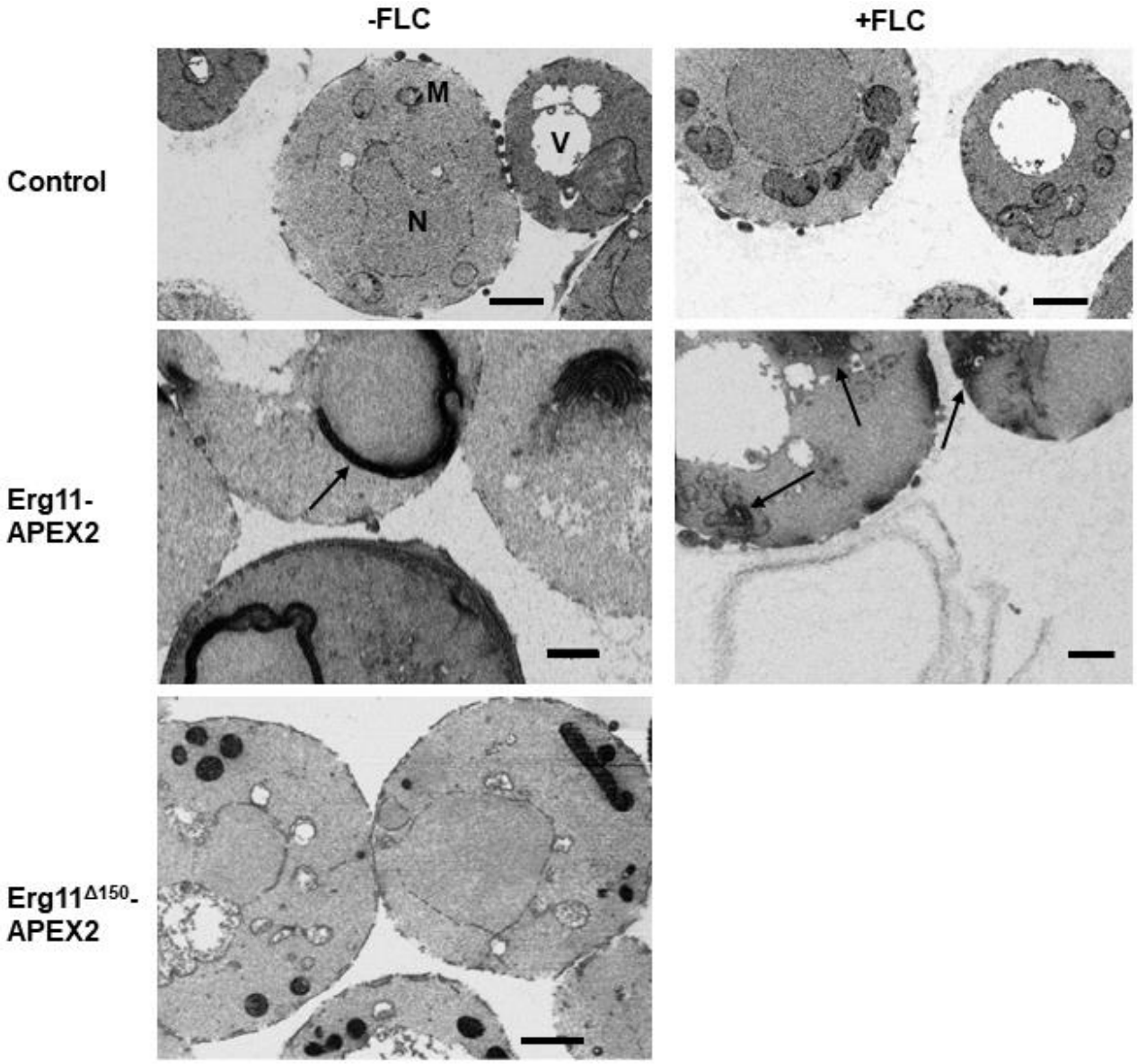


Fig. 3.5. FIB-SEM imaging of APEX2-tagged full-length and truncated Erg11 protein and control cells. Wild type *S. cerevisiae* AFC202 cells have been transformed with a vector overproducing Erg11-APEX2, Erg11$^{\Delta 150}$-APEX2 or untagged Erg11 as a negative control. Spheroplast formation is induced to enhance the DAB staining of the APEX2-tagged proteins. In the negative control cells, the nucleus (N), vacuoles (V) and mitochondria (M) are clearly visible. Moreover, compared to the -FLC samples, it seems that the number of mitochondria is enriched in FLC-treated cells. In the absence of FLC, the full-length Erg11-APEX2 signal is clearly observed in the ER (as indicated by the arrow), where also multilayered, concentric structures are featured, termed ER whorls. In the presence of FLC, Erg11 is observed in multilayered ER structures, which are in close association with mitochondria (indicated by the arrows). The Erg11$^{\Delta 150}$-APEX2 signal localizes to mitochondria, where it fills the inner structure. The black scale bar on each micrograph represents 1 µm.

3.3 Is mitochondrially localized, truncated Erg11 functional?

Previous results could not confirm the bimodal targeting of full-length Erg11 to the ER and mitochondria. Nevertheless, it is clear that Erg11 possesses a cryptic MTS that targets the Erg11$^{\Delta150}$ construct to mitochondria upon its exposure. In this section, it has been examined whether the mitochondrial Erg11$^{\Delta150}$ construct represents a functional lanosterol demethylase. As *ERG11* is essential in *S. cerevisiae*, only spores carrying a functional copy should be viable. Based on this assumption, diploid strains have been generated carrying a HA-tagged *ERG11* construct (*ERG11-HA*, *ERG11****-HA*, *ERG11$^{\Delta150}$-HA*, *ERG11$^{\Delta150****}$-HA*, *ERG11$^{\Delta74}$-HA*) in one of the two *ERG11* alleles of the diploid wild type strain BY4743, creating heterozygous strains. As a negative control, solely the HA-tag has been introduced at one of the two *ERG11* alleles. The diploids have been induced to sporulate and subsequently subjected to tetrad dissection to examine the functionality of the *ERG11-HA* constructs. This is schematically represented in Fig. 3.6 A.

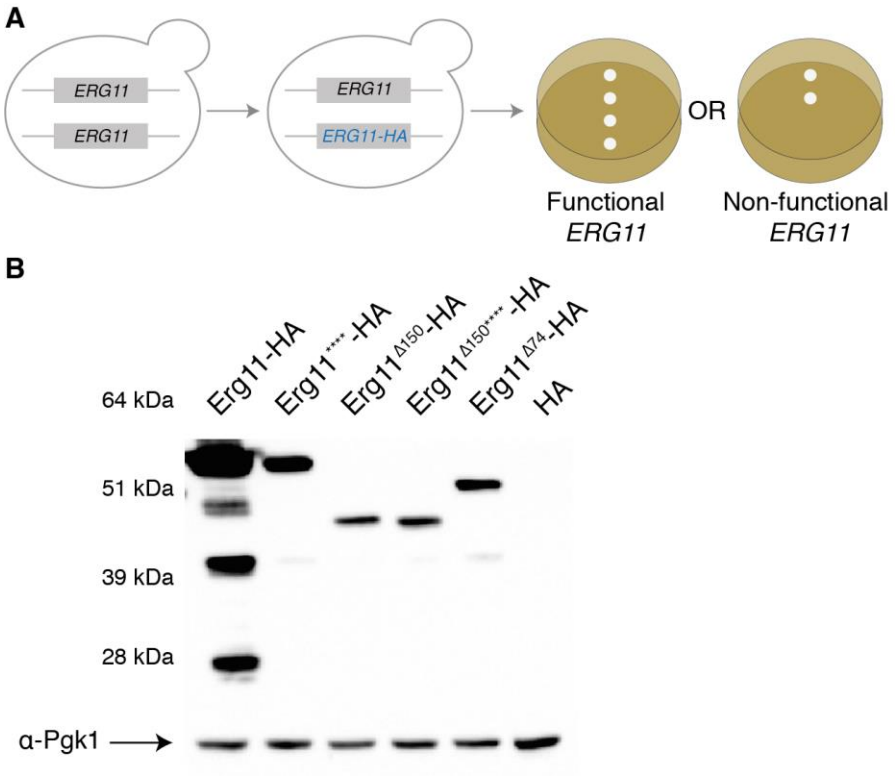


Fig. 3.6. Diploid strains carrying a HA-tagged *ERG11* variant in one of two *ERG11* alleles are subjected to tetrad dissection. (A) Schematic representation of the aim of this experiment. Diploid strains carrying HA-tagged full-length or truncated *ERG11* or solely the HA-tag in one of both *ERG11* alleles of the BY4743 wild type strain have been constructed, induced to sporulate and subjected to tetrad dissection. If all four spores grow, a functional HA-tagged variant of *ERG11* is present, as this gene is essential. Otherwise, only the wild type *ERG11* copies will result in viable spores. (B) Anti-HA probed western blot of protein extracts of the diploid strains, grown in rich medium with FLC, confirms that the strains produce HA-tagged Erg11 proteins. The HA-tag only is small and runs off the gel prior to western blotting. Anti-Pgk1 is used as a loading control.

First, the expression of the HA-tagged *ERG11* constructs has been verified in the diploid strains via western blot (Fig. 3.6 B). Next, the diploids have been induced to sporulate and have been subjected to tetrad dissection on rich medium. Only the full-length HA-tagged *ERG11* constructs (*ERG11* and *ERG11*****) have shown able to germinate, albeit at different rates, as can be seen in Fig. 3.7 A. To overcome the slow germination of the *ERG11******-HA* spores and to exclude possible inhibitory effects of YPD medium on the germination of *erg* mutants, as indicated by Crowley *et al.* (1996) for *erg24* mutants, tetrads have been dissected on defined media supplemented with succinate, similarly to their experiments (Fig. 3.7 B). Indeed, the rate of germination improves for the *ERG11******-HA* spores on minimal medium, supplemented with the necessary amino acids to complement the auxotrophies of the strain. However, under these conditions, all constructs are able to germinate, including the negative control containing only the HA-tag at the *ERG11* locus. Remarkably, this indicates that *ERG11* is not essential under these growth conditions. In contrast, when the diploids have been dissected on complete synthetic medium (CSM), only spores carrying the wild type, full-length copy of *ERG11* germinate. In a next step, it has been tested whether the ability of *erg11* cells to germinate on minimal medium is dependent on the addition of succinate to the medium. This could form a possible explanation because of its twofold link with heme biosynthesis: i) succinyl-CoA is required in the first step of heme biosynthesis and ii) succinylacetone is a known inhibitor of heme synthesis (Kursu *et al.*, 2013; Hanna *et al.*, 2018). Either way, the addition of succinate could affect heme levels, be it in a stimulatory or an inhibitory manner and as such influence ergosterol biosynthesis or any other heme-related process that is important to cell viability. However, it has been found that spores also germinate on minimal medium without the supplementation of succinate. In fact, *ERG11***** spores grow even better in the absence of succinate (Fig. 3.7 C). A list of the tested media can be found in Table 3.1.

Table 3.1. Used media during tetrad dissection.

Yeast Peptone Dextrose YPD	**Complete Synthetic Medium CSM**	**Synthetic Defined Medium SD**
Yeast extract	Amino acids	-
Bacto Peptone	Nitrogen Base	Nitrogen Base
2% glucose	Ammonium Sulfate	Ammonium Sulfate
	2% glucose	2% glucose

The obtained *erg11* mutants have been repeatedly streaked on fresh agar, for two to three times, to assess their viability. Preliminary results have shown that only some of the *erg11* spores retain viability. As the BY4743 diploid strain is heterozygous for lysine and methionine auxotrophy, it has been tested whether the presence of auxotrophies could be linked to the viability of the spores. However, analysis of the few obtained spores indicates that this is not the case. Higher amounts of

spores should be tested to confirm this finding. As the germination of *erg11* mutants is inhibited when tetrads are dissected on complete synthetic medium or on rich YPD medium, it has been hypothesized that the availability of amino acids could have an inhibitory effect on the growth of *erg11* spores. In all, to come up with a conclusive explanation, the conditions that allow germination and viability of the *erg11* spores should be examined in more detail, *e.g.* the contributions of individual amino acids to the germination of *erg11* spores could be studied by adding these to the SD medium. Moreover, the genotypes of the surviving spores should be examined to eliminate the hypothesis that certain mutations might be responsible for this phenotype, *e.g.* loss of *ERG3* function. Lastly, it will be informative to introduce the *erg11* deletion in different reference wild type strains and examine whether the phenotype is conserved.

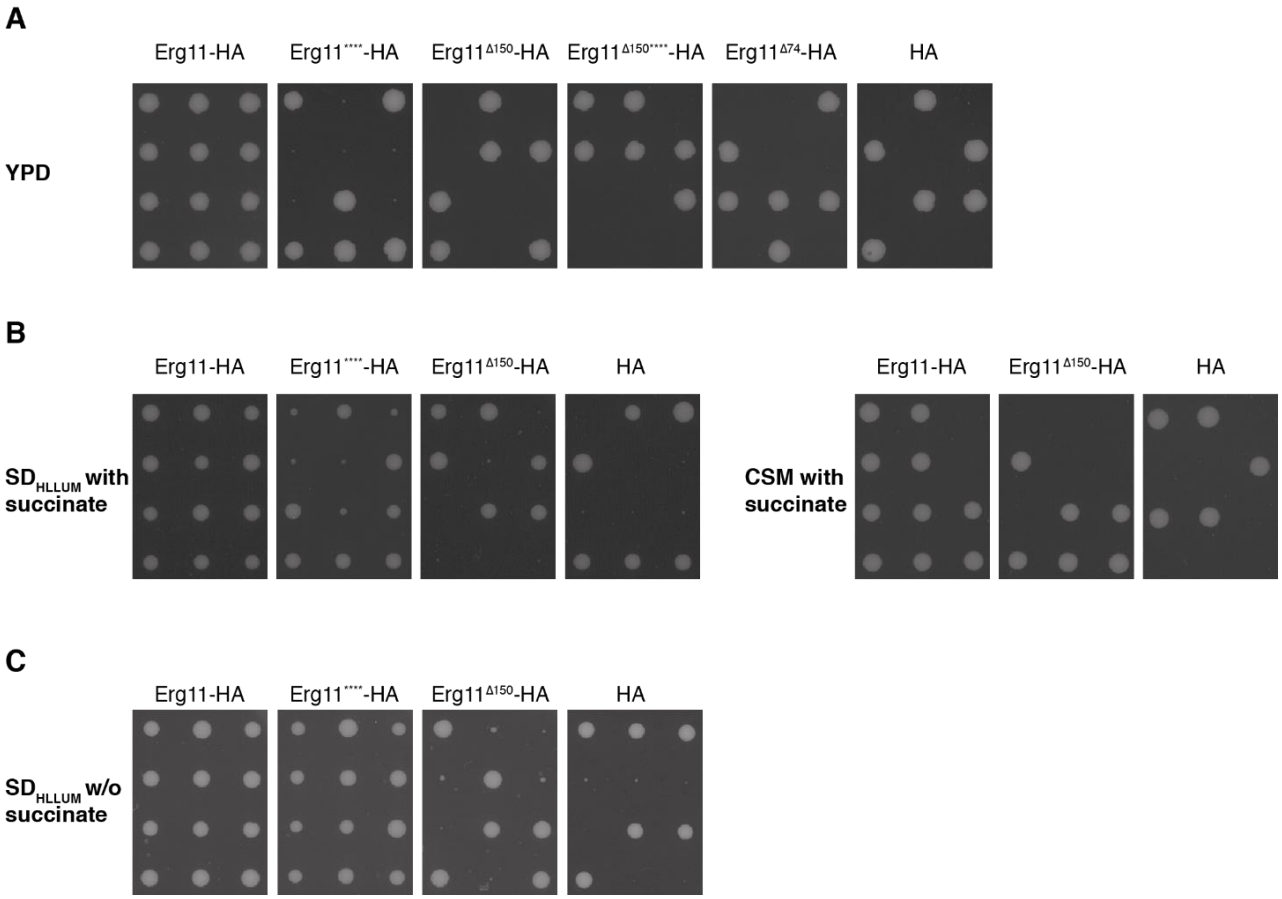


Fig. 3.7. Tetrad dissection of diploids expressing HA-tagged *ERG11* variants on different media. (A) The generated diploids containing one wild type copy of *ERG11* and one HA-tagged variant are induced to sporulate and subjected to tetrad dissection on rich medium. Only spores expressing full-length *ERG11* are able to germinate. (B) Tetrads have been dissected on minimal synthetic defined medium or on complete synthetic medium, supplemented with succinate to overcome possible inhibitory effects of YPD. All spores are able to germinate, even those expressing the negative control. (C) To investigate a possible contribution of succinate to the results observed in (B), tetrads have been dissected on minimal medium without the addition of succinate. Also in this condition, all spores are able to germinate. They grow even better than in the presence of succinate. The pictures have been taken after three days.

From these results, it has been concluded that mitochondrial Erg11 does not retain its lanosterol demethylase function, as the *ERG11*$^{\Delta 150}$ spores do not germinate on rich medium. On minimal medium, the spores do germinate, however, at a similar rate as the spores carrying only the HA-tag at the *ERG11* locus. Nonetheless, Erg11$^{\Delta 150}$ might have a different function within mitochondria, independent of Erg11 lanosterol demethylase activity.

Therefore, in a next step, the generated diploid strains have been examined in more detail. As all the diploid strains contain one wild type copy of *ERG11* and one truncated copy, they represent good models to study a possible beneficial effect of the presence of mitochondrial Erg11. To examine this, firstly, their growth rates have been tested. These are found to be similar for the different strains, when tested in minimal medium supplemented with essential amino acids or in rich medium (Fig. 3.8 A). Some differences have been observed if the diploids are grown in the presence of FLC in rich YPD medium. These differences are most likely explained by the presence or absence of the additional HA-tagged Erg11 copy, of which the full-length forms (Erg11 and Erg11****) can efficiently bind FLC and decrease the total number of drug molecules available to inhibit functional Erg11, while the Erg11$^{\Delta 150}$, Erg11$^{\Delta 150****}$ and Erg11$^{\Delta 74}$ forms might have reduced binding with FLC, leading to increased inhibition of the functional non-tagged wild type copy of Erg11. The absence of such a difference in minimal medium could have several reasons, one of which might be the non-essential nature of *ERG11* in this medium.

The sensitivity of the diploid strains to FLC has also been tested by Etest. Again, no significant differences between the strains have been observed. A similar explanation can be given to the interpretation of the Etest results, where the strains expressing the full-length HA-tagged Erg11 proteins have a slightly higher MIC value to FLC (4 µg/mL) than those expressing the truncated Erg11 forms or the negative control (2-3 µg/mL) (Fig. 3.8 B).

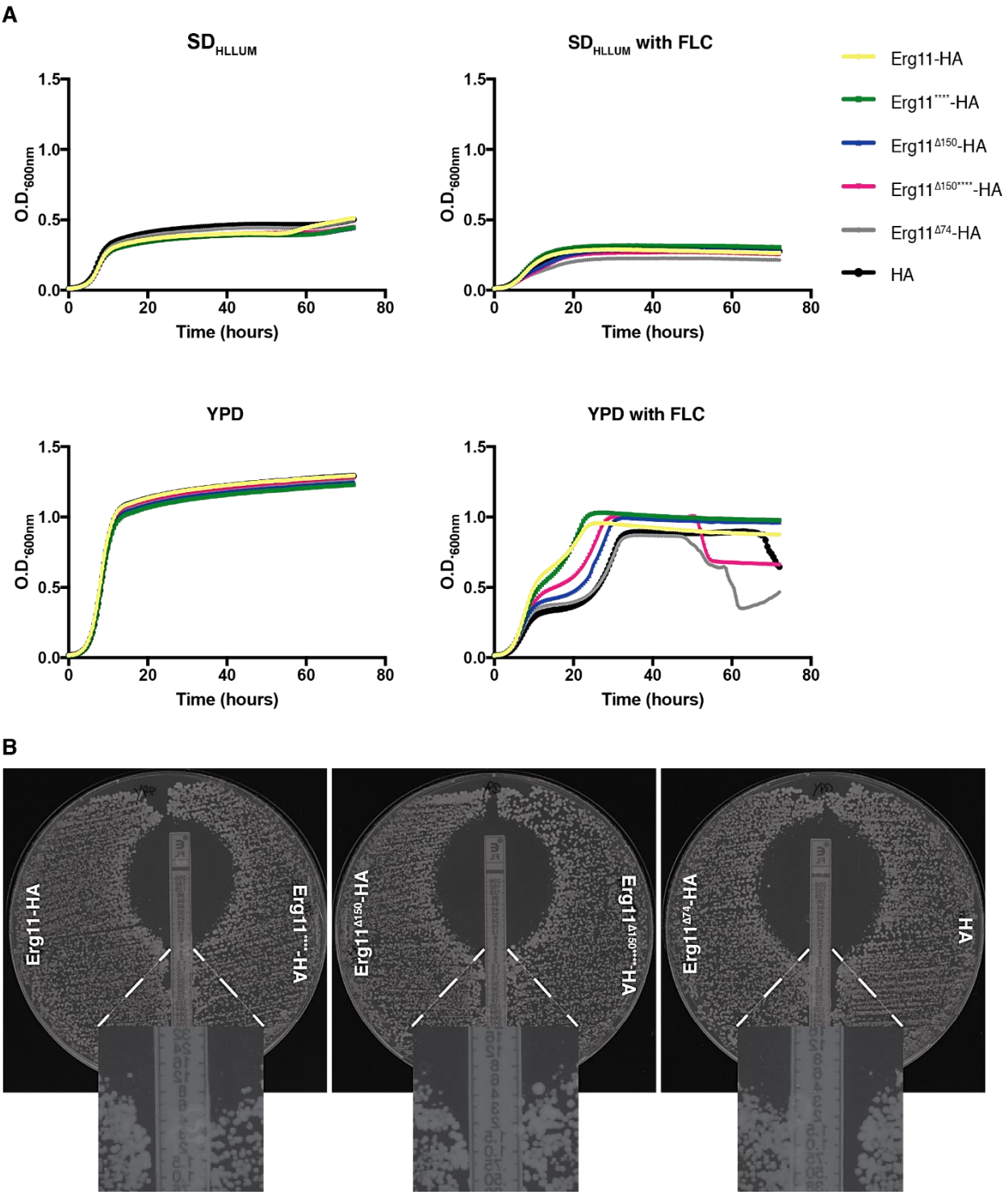


Fig. 3.8. No notable differences have been observed for the growth of the diploid strains in minimal and in rich medium or for their FLC susceptibility examined by Etest. (A) The average growth curves of three technical repeats of the diploid strains in rich and minimal medium are shown, in the absence or presence of FLC (20 μg/mL). (B) FLC Etests have been performed with the diploid strains on YPD. Diploids expressing full-length Erg11 proteins have a slightly higher MIC (4 μg/mL) than diploids expressing truncated Erg11 forms or the negative control (2-3 μg/mL).

Several research labs have indicated a tight connection between ergosterol formation and mitochondrial DNA (mtDNA) or in general between mitochondrial membrane composition and mitochondrial function (Parks and Casey, 1995; Schneiter, 2007). Therefore, the mitochondrial function of the diploids has been assessed by spotting the strains onto agar plates containing ethanol and glycerol as carbon source (YPEG). On this medium, the cells are obliged to respire for survival instead of fermenting the sugars in the medium (Fig. 3.9 A). No differences have been observed between the diploids. Additionally, the mitochondrial copy numbers of the diploids have been assessed from cells grown in minimal medium in absence or presence of FLC (Fig. 3.9 B). This method is based on quantitative PCR (qPCR) amplification of the mitochondrial gene *COX1* relative to the household gene *ACT1*. It has been described that a small alteration, *e.g.* a doubling in mitochondrial copy number, represents a significant change, as the 20 to 50 mtDNA copies per cell make up 10% to 20% of the total cellular DNA (Taylor *et al.*, 2005). However, no notable differences have been observed between the diploids in the same growth condition. When samples are compared with and without FLC addition, there is a remarkable increase in mtDNA copy number in the presence of FLC, for all samples (Fig. 3.9 C). Although several links between mitochondrial function and azole susceptibility have been described in *S. cerevisiae* and in pathogenic *Candida* species, *e.g.* the correlation of mtDNA loss and drug resistance, no data has been found in the literature on the upregulation of mtDNA in the presence of FLC or azoles in general (Shingu-Vazquez and Traven, 2011; Qu *et al.*, 2012). Nonetheless, this effect seems to be independent of *ERG11*, at least when studied in the diploid strains, as all strains show a similar level of upregulation. This experiment has only been performed once, so it is not useful to do a statistical analysis and the results should be considered as preliminary data.

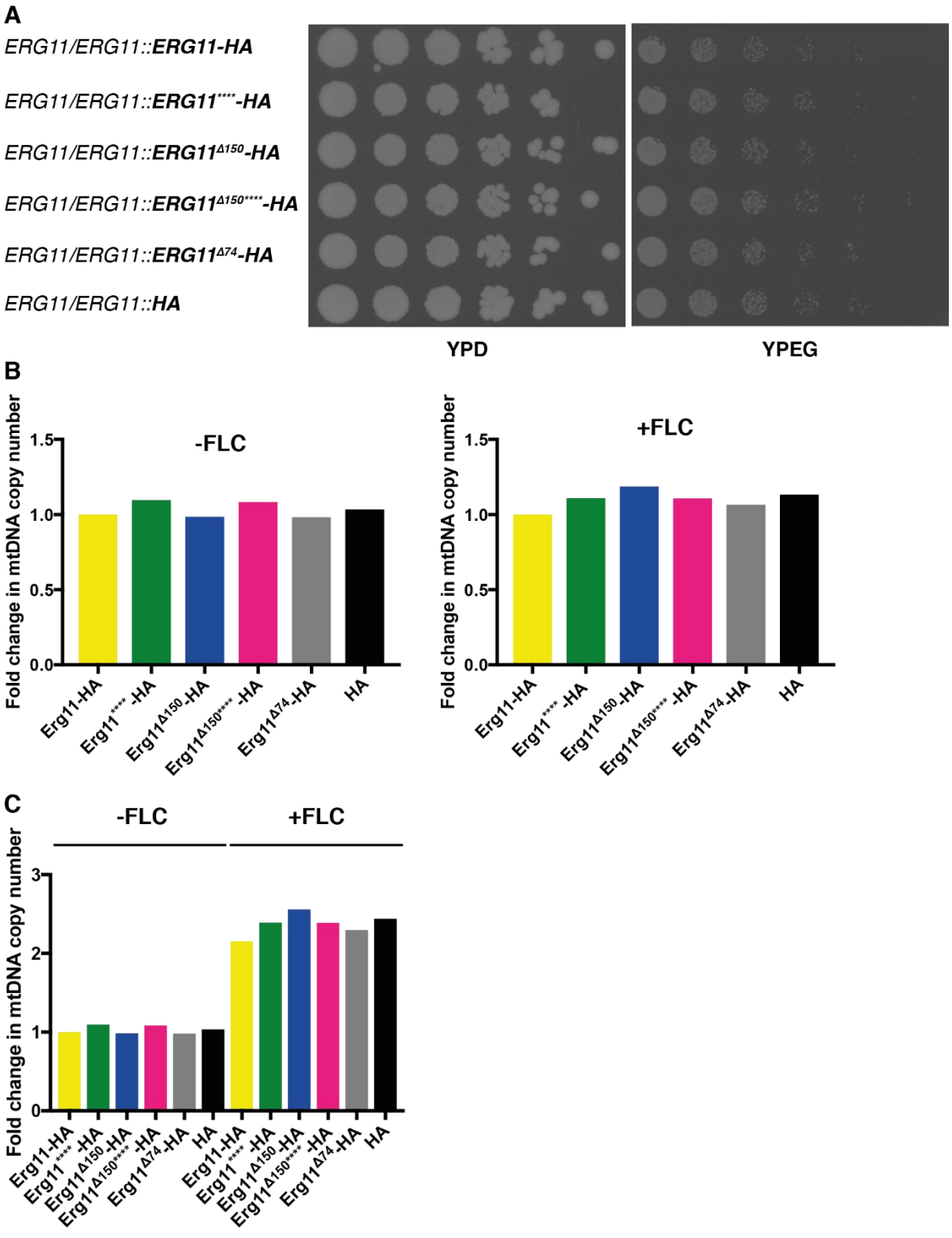


Fig. 3.9. Assessment of mitochondrial respiration and mtDNA copy number in the diploid strains. (A) The diploids have a similar ability to respire, as tested by growth on YPEG. (B) The fold change in mtDNA copy number of the diploid strains is also similar for cells grown in the absence or presence of FLC, as determined relatively to the wild type, expressing full-length *ERG11-HA*. (C) When all strains are compared in the same graph and normalized to the untreated full-length *ERG11-HA* wild type strain, it is clear that mtDNA is upregulated in the presence of FLC to a similar level in all the tested strains. No statistical analysis is included, as all measurements are n=1. Therefore, these results should be considered as preliminary data.

Finally, it has been tested whether the mitochondrial targeting of the Erg11$^{\Delta 150}$ construct results in an altered susceptibility towards FLC. The wild type strain AFC202 has been transformed with a plasmid expressing full-length *ERG11* or *ERG11*$^{\Delta 150}$ from a strong promoter or with the empty vector. A broth microdilution assay has been performed in -Leu drop out medium, in which the cells have been incubated with increasing, twofold concentrations of FLC (from 0 µg/mL to 1 µg/mL to 64 µg/mL). After 48 hours of incubation, the MIC has been determined by visual inspection of the microtiter plates and by measuring the optical densities of the wells. The MIC_{90} of the wild type strain carrying *ERG11* has been determined as 64 µg/mL, which indicates that this strain has low susceptibility to FLC treatment. This is in agreement with previous results from our lab, which have identified *ERG11* as a multicopy suppressor of FLC susceptibility in *S. cerevisiae* (Demuyser *et al.*, 2017). The MIC of AFC202 expressing *ERG11*$^{\Delta 150}$ is 32 µg/mL, while that of AFC202 carrying the empty vector is 16 µg/mL. These differences could again be explained by the presence or absence of additional Erg11, of which the full-length form is functional and binds the FLC molecules, reducing the total number that can inhibit functional Erg11, while the Erg11$^{\Delta 150}$ protein is not functional and possibly binds FLC with less affinity than wild type Erg11.

Additionally, the tolerance of the strains can be measured quantitatively with this experiment, in contrast to a visual impression on Etest. To measure tolerance to the administered drug, the cells are transferred from all wells of the broth microdilution assay after 48 hours of incubation to a new microtiter plate and serially diluted to an optimal concentration to perform colony forming unit (CFU) counts, after the cells have been plated on rich, non-selective medium. As such, the number of cells that have survived the treatment can be assessed. Interestingly, the tolerance level of the AFC202 strain overexpressing the *ERG11*$^{\Delta 150}$ construct is lower than that of AFC202 with the empty vector, disproving the initial hypothesis that mitochondrial, truncated Erg11 could enhance tolerance to FLC (Fig. 3.10). However, this experiment has been performed only once and should therefore be considered as preliminary data.

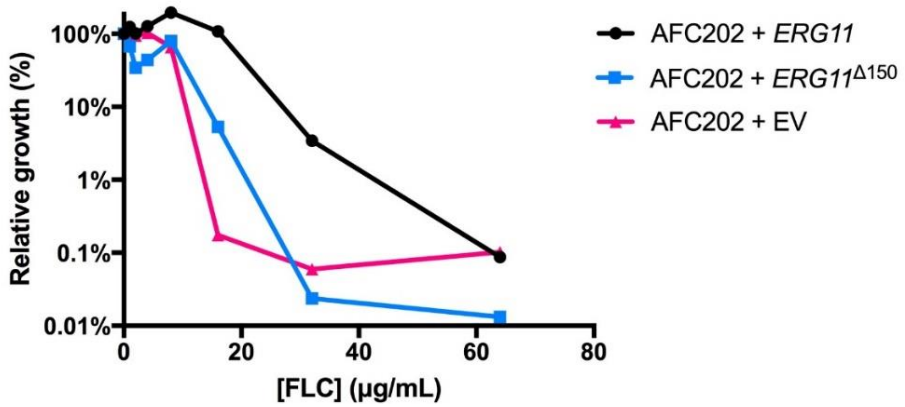


Fig. 3.10. Survival assay to FLC treatment of AFC202 carrying additional *ERG11*. The ability of cells to survive a range of FLC concentrations has been tested. The cells, expressing *ERG11* or *ERG11*$^{\Delta 150}$ from a strong promoter or carrying the empty vector, have been diluted and plated on non-selective medium for CFU counts, after 48 hours of incubation in FLC-containing wells. The CFU counts for each strain have been normalized to the untreated condition, which represents 100% of growth. All measurements are n=1. Therefore, these results should be considered as preliminary data. The tolerance level of AFC202 overexpressing *ERG11*$^{\Delta 150}$ is lower than that of AFC202 with the empty vector, contradicting the initial hypothesis that mitochondrial, truncated Erg11 might enhance tolerance to FLC.

Additionally, analysis of the Erg11$^{\Delta 150}$ protein based on a full-length *S. cerevisiae* Erg11 crystal structure retrieved from the Protein Database (PDB entry 4WMZ, Sagatova *et al.* (2015)), indicates that the Erg11 structure is strongly affected by the deletion of the first 150 amino acids (Fig. 3.11 A). This is expected, as almost 30% of the protein is deleted. The full-length protein consists of an ER-anchor and a bulk, cytosolic part of the protein. Upon removal of the first 150 amino acids, the ER-anchor is lost. Additionally, it is predicted that the inner heme group and the substrate cavity become accessible to the surroundings. These predictions further support the hypothesis that the Erg11$^{\Delta 150}$ construct is a catalytically inactive variant of Erg11. Furthermore, an electrostatic potential profile of the Erg11 protein suggests that the removal of the first 150 amino acids exposes a large hydrophobic region to the hydrophilic environment, which is an unstable condition (Fig. 3.11 B). In conclusion, the deletion of the first 150 amino acids most likely leads to refolding and eventual degradation of the Erg11$^{\Delta 150}$ protein. However, only crystallization data of the full-length Erg11 protein are available and not of the Erg11$^{\Delta 150}$ construct, so no definite conclusions can be made on its protein structure.

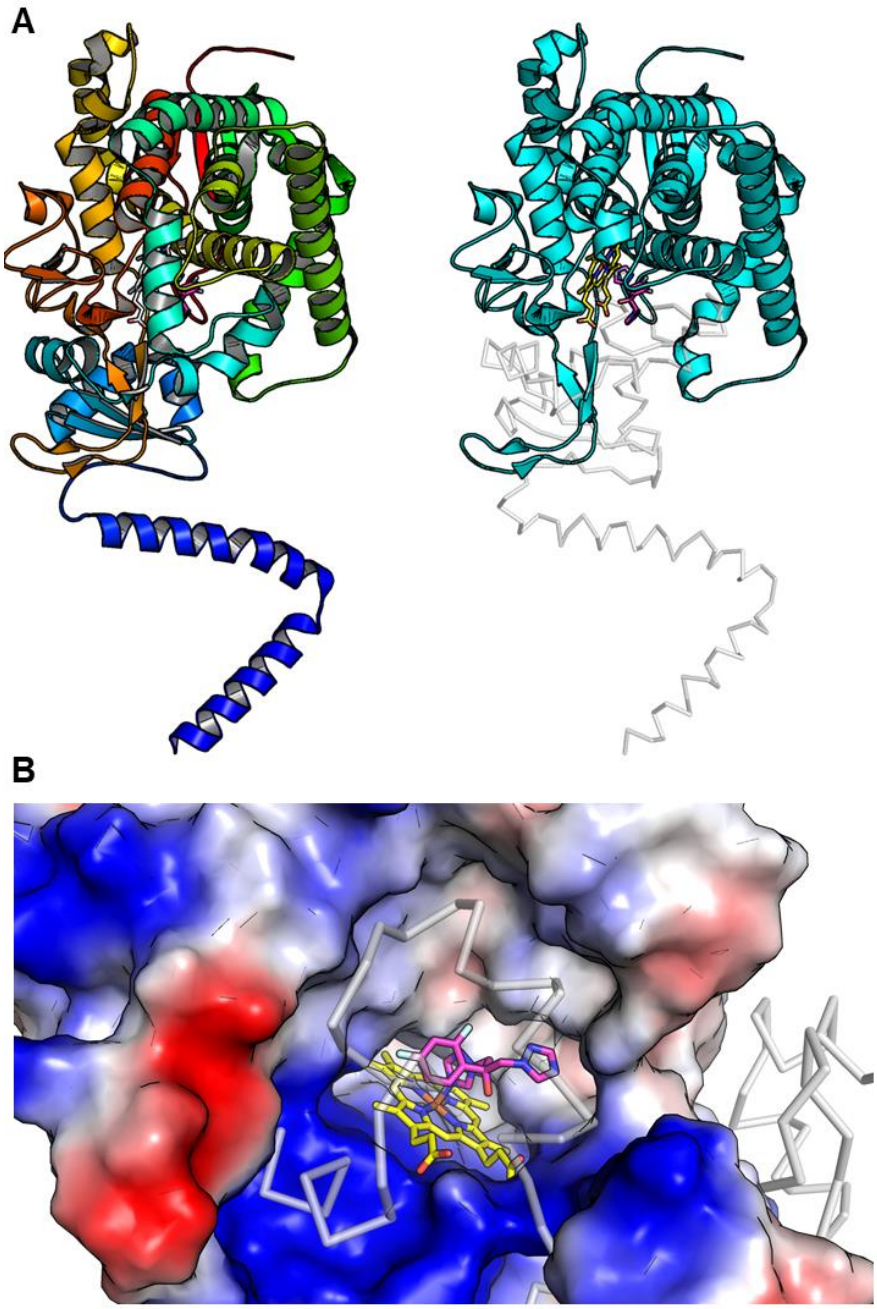


Fig. 3.11. Analysis of the *S. cerevisiae* Erg11 protein based on crystallization data (PDB entry 4WMZ Sagatova *et al.* (2015)) indicates that deletion of the N-terminal 150 amino acids leads to an unstable protein, which will most likely be degraded. (A) The Erg11 structure is shown in the left panel, with a color gradient from blue at the N-terminus to red at the C-terminus. The structure consists of an ER-anchor, separated from the bulk of the protein. The heme cofactor is depicted in yellow and FLC is shown in magenta. In the right panel, the same Erg11 structure has been deleted of its 150 N-terminal amino acids (in white). The remaining part of the protein is in cyan. By deleting the N-terminal 150 amino acids, the heme group and the substrate channel are predicted to become exposed to the surroundings. (B) An electrostatic potential map of the Erg11 protein, with regions of negative potential colored in red and of positive potential in blue, shows that upon removal of the first 150 amino acids, a large hydrophobic region (white) becomes exposed to the environment, which is an unstable condition.

3.4 Does the mitochondrial targeting signal have a function in full-length Erg11?

So far, it remains unclear why Erg11 contains an MTS and whether it is associated with mitochondrial targeting *in vivo*. To further analyze the role of the cryptic MTS in full-length Erg11, endogenous, isogenic *ERG11-HA* and *ERG11****-HA* strains, obtained during tetrad dissection, have been studied further. First, their growth has been analyzed in the absence or presence of FLC in minimal medium. Fig. 3.12 (A) shows that The *ERG11****-HA* strain grows slower than the wild type strain. The addition of FLC affects the growth rate of both strains but this seems more pronounced in the *ERG11****-HA* strain. Moreover, the MIC of *ERG11****-HA* cells to FLC reduces to 1 µg/mL (Fig. 3.12 B). The MIC of the wild type *ERG11-HA* strain in minimal medium is 8 µg/mL, similar to the MIC in rich medium, defined by Etest (Fig. 2.4). Furthermore, the growth of the strains on YPEG medium has been tested, to examine their ability to respire. No differences have been observed between the *ERG11-HA* and the *ERG11****-HA* strains (Fig. 3.12 C).

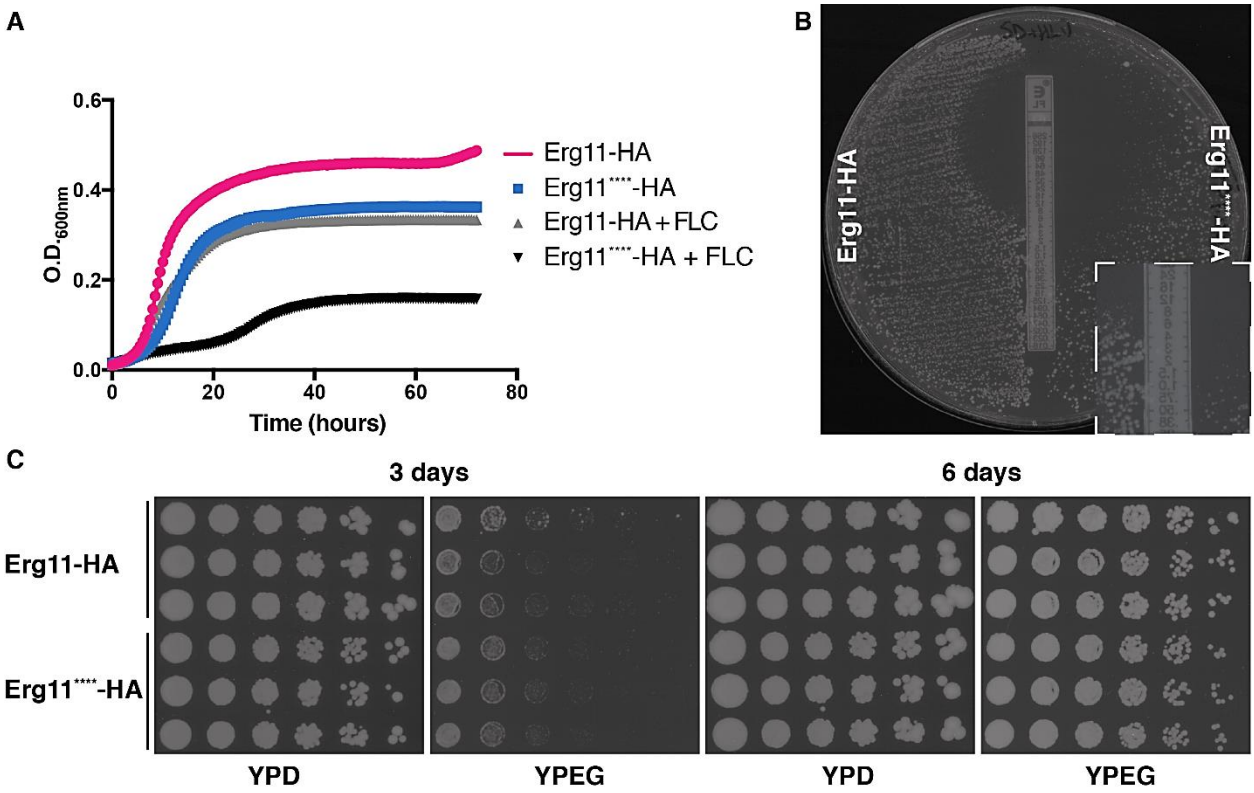


Fig. 3.12. Analysis of the growth and FLC susceptibility of strains expressing *ERG11-HA* or *ERG11****-HA* endogenously. (A) The growth of *ERG11****-HA* cells is reduced compared to wild type cells, as measured in minimal medium in the absence or presence of FLC (20 µg/mL). (B) A FLC Etest has been performed on minimal medium. The MIC of the wild type strain is 8 µg/mL while that of the *ERG11****-HA* strain is 1 µg/mL. (C) The growth of the strains has been examined on YPEG medium but no differences in their ability to respire have been observed. Pictures are shown after three or six days of growth.

Interestingly, *ERG11****-HA* cells already display additional bands on western blot in the absence of FLC. It has been tried to analyze whether the full-length band is upregulated in *ERG11****-HA* cells compared to *ERG11-HA* cells in the absence of FLC. Although the absolute densitometric values do indicate this, the inconsistencies of the anti-Pgk1 loading control in the Erg11-HA samples exclude a comparable analysis for values relative to the loading control. In the presence of FLC, it is clear from the blot that the mutant cells show no obvious upregulation of Erg11 protein levels as do wild type cells (Fig. 3.13). These results might indicate that the Erg11**** protein is less functional than the wild type form and is more rapidly degraded, under the assumption that the additional bands represent degradation products.

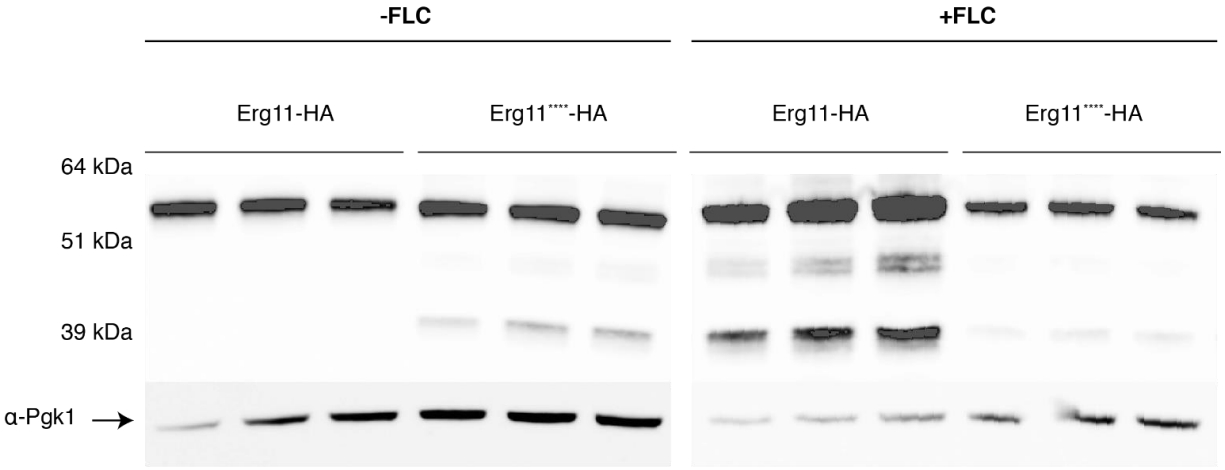


Fig. 3.13. Western blot of strains expressing *ERG11-HA* or *ERG11****-HA* endogenously. Cells have been grown in minimal medium in the absence or presence of FLC in triplicate. Already in the absence of FLC, additional bands of Erg11****-HA are observed on western blot, although the protein is expressed at endogenous levels. In the presence of FLC, the Erg11****-HA protein is not upregulated and the presence of additional bands is not induced, in contrast to the wild type strain. Anti-Pgk1 is used as a loading control.

As discussed in paragraph 1.3.2.4 and in Song *et al.* (2004), the transcriptional regulation of *ERG11* and other genes involved in sterol metabolism has been associated with intracellular sterol levels, both in yeast and in mammals. It has been suggested that conditions leading to reduced ergosterol levels lead to increased transcription of *ERG11*. Therefore, it could be hypothesized that *ERG11* expression will be upregulated when the activity of the Erg11 protein is lost or reduced. To further validate the idea that the Erg11****-HA protein is less functional than wild type Erg11, the expression levels of *ERG11* have been measured by real-time quantitative reverse transcription PCR (qRT-PCR). As anticipated, *ERG11* expression is upregulated in the *ERG11****-HA* strain compared to the wild type strain, both in absence and presence of FLC treatment (p-value <0.0001 for -FLC and 0.0171 for +FLC), suggesting that the cell tries to compensate for the less functional form of Erg11 (Fig. 3.14 A). However, as can be seen from Fig. 3.13, the upregulation of *ERG11****-HA* does not result in a similar increase in Erg11****-HA protein levels. A possible explanation will be provided in

Chapter 4, where the degradation of Erg11 is further discussed. Furthermore, this assay indicates that *ERG11* expression increases in the presence of FLC for the wild type strain, as described in literature, but not for the mutant strain (Pierson *et al.*, 2004). This result explains why the additional bands of Erg11****-HA are not more pronounced in the presence of FLC.

In a different assay, the ergosterol levels of both strains have been measured. In agreement with the hypothesis that the Erg11****-HA protein is less functional, cells expressing the MTS-mutation produce significantly less ergosterol than the wild type strain, in the absence and presence of FLC (p-values <0.0001, Fig. 3.14 B). The reduced ergosterol levels could explain the slower growth of the *ERG11****-HA* spores after tetrad dissection (Fig. 3.7). It could also explain the higher sensitivity of the *ERG11****-HA* strain towards FLC, as the cell is overall weaker and the low levels of ergosterol present will be further depleted by the action of FLC. Perhaps, the amount of ergosterol that is produced by the Erg11**** strain is sufficient to fulfill the sparking function of ergosterol, while other sterols can perform the bulk function.

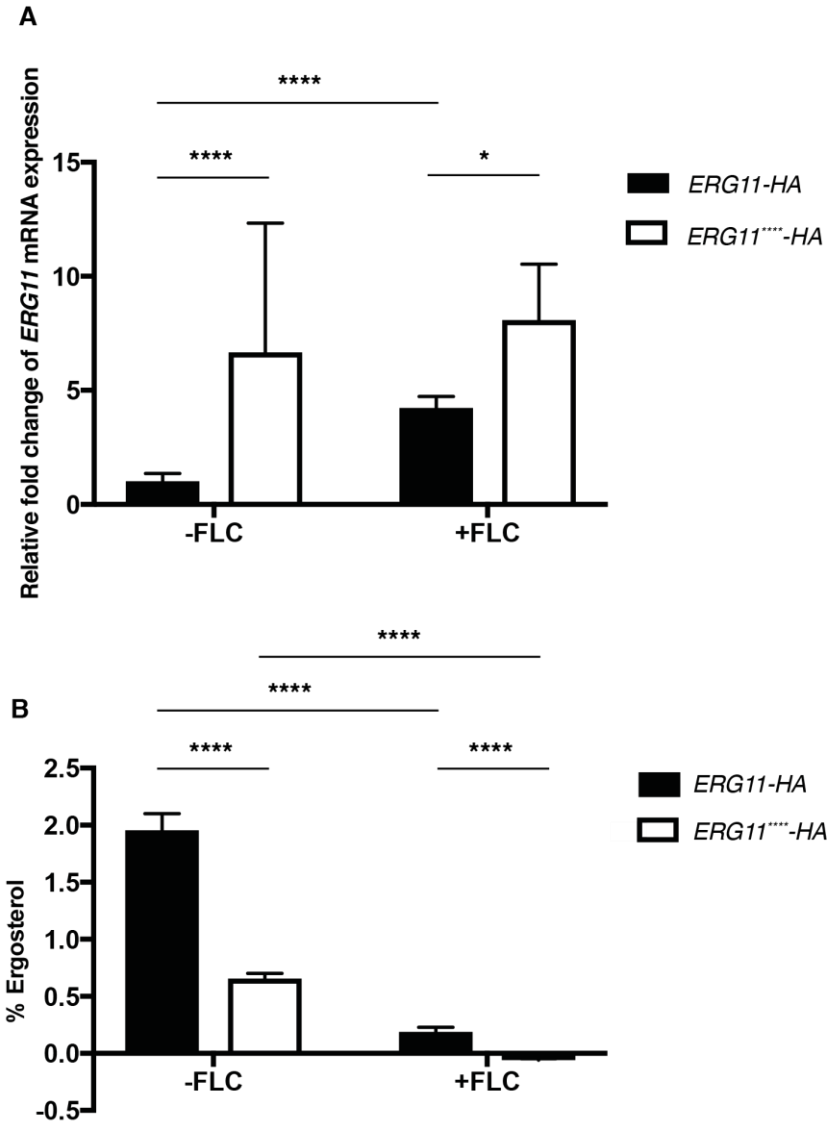


Fig. 3.14. Analysis of *ERG11* mRNA levels and ergosterol production of the strains expressing *ERG11-HA* or *ERG11**-HA* endogenously**. (A) qRT-PCR analysis of *ERG11* mRNA levels of cells grown in the absence or presence of FLC. Mean values with 95% confidence intervals are shown. The mRNA is significantly upregulated between the -FLC and +FLC condition for the wild type strain with a p-value <0.0001. The mRNA levels are also significantly upregulated in the *ERG11****-HA* strain compared to the wild type strain, in the absence or presence of FLC treatment (p-value <0.0001 for -FLC and 0.0171 for +FLC). (B) Quantification of ergosterol in *ERG11-HA* and *ERG11****-HA* cells. Mean values with 95% confidence intervals are shown. The ergosterol content is significantly different between treated and untreated cells of the same strain and between strains in the same condition, with p-values <0.0001. Statistical analysis has been performed by two-way ANOVA (analysis of variance) with correction for multiple comparisons by the Bonferroni post-hoc test.

These results underscore the importance of the four lysine residues in the Erg11 MTS to the functionality of the full-length protein. However, the exact role of these residues remains unclear. They could be important to the overall stability of the protein, to the interaction of Erg11 with its redox partner, with other biosynthesis proteins in the ergosome or with its substrate or to the targeting of Erg11 to mitochondria or mitochondria-associated subdomains in the ER, which could be important for the optimal functionality of the protein. *In silico* analysis based on crystallization data of *S. cerevisiae* Erg11 (PDB entry 4WMZ, Sagatova *et al.* (2015)) shows that the lysine residues are all predicted to be on one side of the protein (Fig. 3.15 A). To test the hypothesis that the lysine residues could be important for the interaction with the redox partner of Erg11 and more specifically to the transfer of electrons from the donor to the heme group, possible interactions between the crystal structure of the FMN binding domain of *Bacillus megaterium* cytochrome P450BM-3 (PDB entry 1BVY (Sevrioukova *et al.*, 1999)) and *S. cerevisiae* Erg11 have been modeled. Indeed, based on these crystallization data, it can be predicted that the lysine residues of Erg11 are important for the interaction with the redox partner and the corresponding electron flow to the Erg11 heme group, as the predicted interaction of Erg11 with the FMN-binding domain is situated around the lysine residues, as can be seen in Fig. 3.15 A. Furthermore, it has been described that the K151 residue and its coordination around the heme group are highly conserved in the fungal lineage (Monk *et al.*, 2014). The predicted interaction of the lysine residue with the carboxylate group of the heme cofactor, as depicted in Fig. 3.15 B, could also partly explain the reduced function of the Erg11**** protein (Sagatova *et al.*, 2015). The substitution of the lysine residue to an alanine could have profound effects on the structure and function of the Erg11 protein, possibly causing reduced ergosterol production.

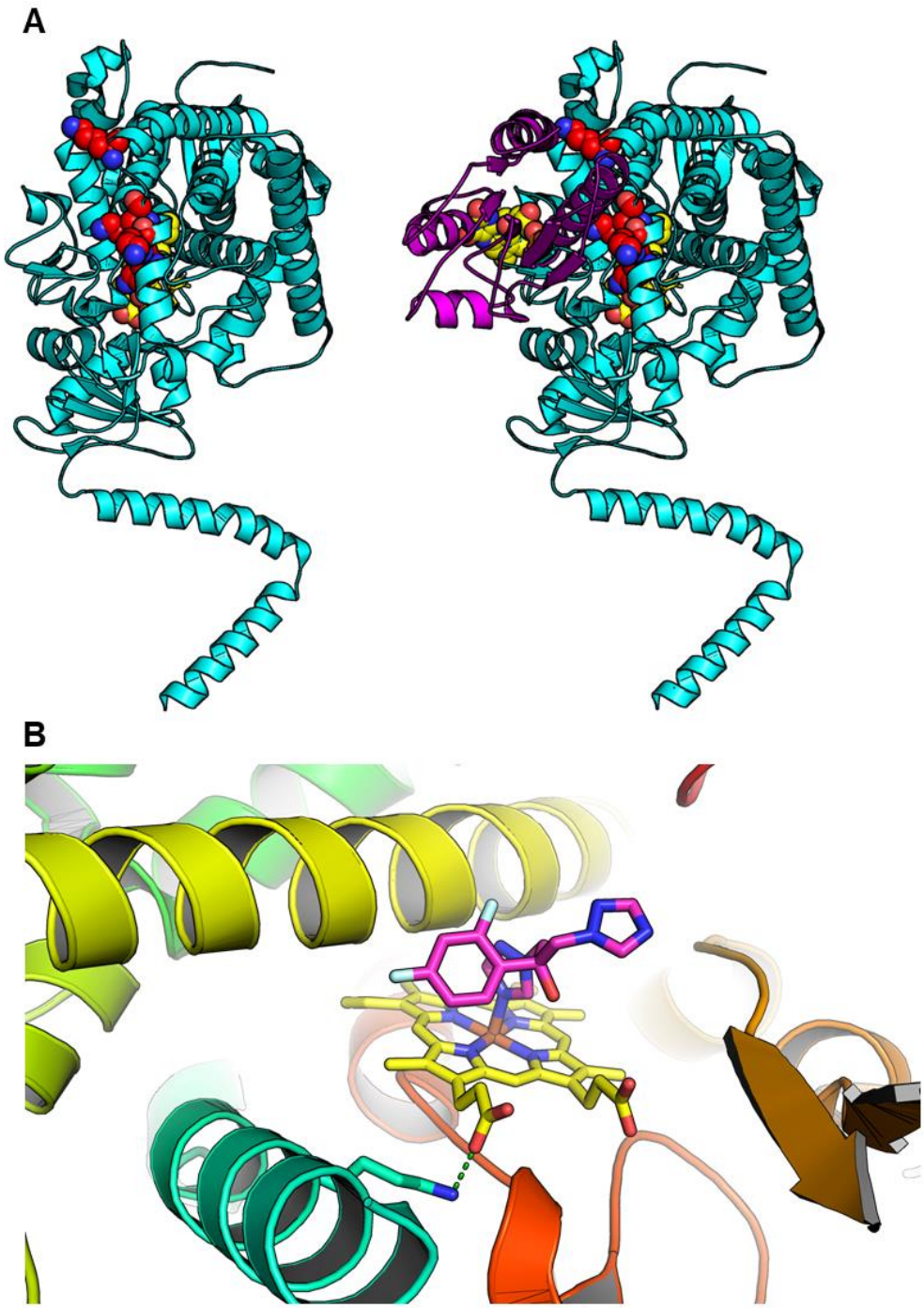


Fig. 3.15. The lysine residues in the Erg11 MTS are predicted to be important for the coordination of the Erg11 redox partner and the heme group. (A) The Erg11 structure based on PDB entry 4WMZ (Sagatova *et al.*, 2015) is shown in the left panel, with the carbon atoms of the four lysine residues (K151, K152, K155 and K160) indicated as red spheres and their nitrogen atoms in blue. The heme group is colored yellow. In the right panel, the interaction of the FMN binding domain of *B. megaterium* cytochrome P450BM-3 (PDB entry 1BVY (Sevrioukova *et al.*, 1999)) to Erg11 has been modeled. The FMN binding domain has been colored purple and contains a yellow-colored FMN group. Based on this model, it is hypothesized that the lysine residues of Erg11 are important to the interaction with its redox partner. (B) The predicted interaction of the Erg11 lysine residue K151 with the heme group (depicted by the dotted line), described by Sagatova *et al.* (2015), is shown.

3.5 Discussion

In this chapter, it has been shown that Erg11 possesses a cryptic MTS, which is exposed if the N-terminal 150 amino acids of the protein are deleted, resulting in efficient targeting of Erg11$^{\Delta 150}$ to the mitochondria. The observation that the size of the Erg11$^{\Delta 150}$ truncated protein roughly corresponds to the largest additional Erg11 bands of wild type cells on western blot has driven the hypotheses that the additional Erg11 products could indeed be mitochondrially targeted. Therefore, the hypothesis of bimodal targeting of Erg11 to ER and mitochondria has been investigated further by microscopic analysis. During fluorescence microscopy, some overlapping signal has been observed between Erg11-mCherry and the mitochondrial GFP-marker, yet the magnification limit of the lens has prevented a detailed analysis of this colocalization. FIB-SEM offers an alternative method to study the localization of Erg11. In absence of FLC, the Erg11 protein localizes to the ER. Additionally, electron-dense signal has been observed in the vacuole (further discussed in Chapter 4). The FIB-SEM sample with FLC treatment shows little Erg11 signal. However, the observed signal seems to be present in multilayered ER structures that are in close apposition to mitochondria. Overall, these results suggest that Erg11 is not bimodally targeted to the ER and mitochondria but that it might localize to ER subdomains that are in close contact with mitochondria. Furthermore, as vacuolar Erg11 signal has been observed in the FIB-SEM sample of full-length Erg11 without FLC, the truncated Erg11 fragments are more likely to be present in the vacuole than in the mitochondria. Indeed, although MS analysis has identified a possible N-terminus at amino acid 147, of which the corresponding Erg11 fragment would expose its cryptic MTS, also 22 other possible Erg11 N-termini have been identified, of which the corresponding Erg11 products would lack the cryptic MTS (Chapter 2). The high number of possible Erg11 fragments further suggests that the additional bands observed on western blot are degradation products.

The cryptic MTS of Erg11 spans the region from amino acids 148 to 197. Fusion of only this region to Arg8 devoid of its MTS results in efficient targeting of the protein to mitochondria. Furthermore, exposing the MTS of Erg11 (Erg11$^{\Delta 150}$) clearly targets the protein to mitochondria, as proven by the *ARG8* assay and microscopic analysis. The lysine residues 151, 152, 155 and 160 are crucial to the MTS, as substitution of these residues to alanines in the Erg11$^{\Delta 150}$ construct (Erg11$^{\Delta 150****}$) results in loss of mitochondrial targeting. To assess whether all of these residues are important to mitochondrial targeting, or whether some lysine residues are more important than others, it has been attempted to examine the subcellular localization of Erg11$^{\Delta 150}$-mCherry constructs carrying single lysine to alanine substitutions. Unfortunately, there have been some problems with the constructs, as no clear red fluorescent signal could be detected. Solving this issue will be informative on the further characterization of the Erg11 MTS. Furthermore, it has been tried to define the submitochondrial localization of the Erg11$^{\Delta 150}$ construct with FIB-SEM, but this has been unsuccessful. However, the combination of FIB-SEM imaging of Erg11$^{\Delta 150}$ together with the results

obtained in the *ARG8* assay, suggest that Erg11$^{\Delta 150}$ localizes to the mitochondrial matrix or to the IM, exposing its C-terminus to the matrix. The latter conformation would be similar to mitochondrially localized mammalian CYPs (Avadhani *et al.*, 2011). Interestingly, Lamb *et al.* (1999b) have reported on an engineered soluble *C. albicans* Erg11, that has shown full catalytic activity *in vitro*, indicating that a soluble version of Erg11 can be functional in specific environments and that activity is independent of the presence or absence of the membrane anchor. This indicates that potentially matrix-localized Erg11 could be active.

The functionality of the truncated, mitochondrially targeted Erg11$^{\Delta 150}$ construct has been evaluated. Most likely, this protein is not a functional lanosterol demethylase, as spores carrying the *ERG11$^{\Delta 150}$* construct do not germinate on rich medium. Additionally, it has been tested whether truncated, mitochondrial Erg11 could have another function in mitochondria, by studying diploids that carry one wild type copy and one HA-tagged wild type or mutant version of *ERG11* at the endogenous *ERG11* alleles. No notable differences have been observed between diploids carrying wild type *ERG11-HA*, *ERG11$^{\Delta 150}$-HA* or any other construct concerning growth or FLC susceptibility. Also, the mtDNA copy number and respiration ability, tested by growth on YPEG, are similar for all the diploid strains, although these are only preliminary results. Furthermore, no increase in azole tolerance has been observed for wild type cells overexpressing mitochondrial Erg11$^{\Delta 150}$, as initially hypothesized, compared to a strain carrying the empty vector. Overexpression of Erg11$^{\Delta 150}$ in a wild type strain does seem to increase the MIC twofold compared to a strain carrying the empty vector, which might be explained by the possibility that the truncated form of Erg11 can bind FLC and as such lower the levels of the drug inside the cell available to inhibit wild type Erg11. The overexpression of full-length Erg11 in a wild type strain results in a fourfold increase of the MIC compared to the empty vector. These preliminary results suggest that the effect of Erg11$^{\Delta 150}$ on FLC susceptibility is not dependent on its mitochondrial localization and is not specific to the truncated version, as full-length ER Erg11 elicits a similar but stronger effect on the MIC. In conclusion, as Erg11$^{\Delta 150}$ has not been associated with a function inside mitochondria, it is hypothesized that the Erg11$^{\Delta 150}$ protein might not be a functional protein, possibly because the first 150 amino acids are crucial to the protein's stability and functionality, as suggested based on crystallization data of the full-length protein. The deletion of these residues most likely exposes the heme group and substrate channel to the surroundings. Alternatively, the localization inside mitochondria could prohibit the functioning of the Erg11$^{\Delta 150}$ protein. Mitochondrially localized mammalian CYPs are activated by the adrenodoxin/adrenodoxin reductase system (Avadhani *et al.*, 2011; Ewen *et al.*, 2012). Yeast homologs to these redox proteins have been identified as ferredoxin and ferredoxin reductase, which are important to the biogenesis of iron-sulfur proteins in yeast mitochondria (Lange *et al.*, 2000). Furthermore, yeast mitochondria also contain a cytochrome b_5 reductase and mitochondrial proteomics have indicated that cytochrome b_5 could be targeted to mitochondria (Morgenstern *et al.*, 2017). The latter redox system is sufficient to the functionality of *C. albicans* Erg11 *in vitro* (Lamb *et al.*, 1999a). Therefore, the hypothesis that the

mitochondrial localization of Erg11$^{\Delta 150}$ could inhibit its function is unlikely, as these redox systems could provide Erg11 with the necessary electrons. In addition, the analysis of sterol contents of various organelles has led to the finding that lanosterol is present in mitochondrial membranes, suggesting that mitochondrial Erg11$^{\Delta 150}$ could access its substrate (Zinser *et al.*, 1993).

Taken together, the function of the Erg11 MTS *in vivo* is not clear. If bimodal targeting of Erg11 does not occur in *S. cerevisiae*, the function of the MTS could be to target the Erg11 protein to specific ER membrane domains that are in close apposition to mitochondrial membranes. This kind of localization strategy has been observed for mammalian acyl-CoA:diacylglycerol acyltransferase 2 (DGAT2) and for the *S. cerevisiae* proteins phosphatidylserine and phosphatidylinositol synthases. These proteins are enriched in an ER subdomain, called the mitochondria-associated membrane (MAM) or originally described as 'microsomal fraction associated with mitochondria' (Gaigg *et al.*, 1995; Stone *et al.*, 2009). MAMs are known to be enriched for lipid biosynthesis enzymes. Although the authors have identified a true MTS in DGAT2, capable of targeting red fluorescent protein (RFP) to mitochondria, they suggest that the protein merely associates with mitochondria through its specific sublocalization to the MAM ER domain, where it may act as a bridge to promote lipid exchange between ER and mitochondria (Stone *et al.*, 2009). The association of DGAT2 with MAMs is especially upregulated when the cells are treated with oleate, an inducer of lipid biosynthesis. Similarly, we have tried to enhance the visualization of Erg11 localization to mitochondria or mitochondria-associated membranes during microscopy studies by inducing *ERG11* expression with FLC treatment (even though azole treatment does not result in increased ergosterol production). Also other ER-mitochondria contact sites, such as the ERMES and EMC tether complexes and their components have been identified in *S. cerevisiae*. The importance of these organelle contact sites to the biology of the cell is underscored by the finding that the simultaneous deletion of both complexes is lethal to *S. cerevisiae* (Kornmann *et al.*, 2009; Lahiri *et al.*, 2014). Based on the results described in this chapter, it is interesting to speculate on a localization of Erg11 to such ER-mitochondria contact sites.

It has been demonstrated that the characterized lysine residues in the Erg11 MTS are important to the function of the protein, as substitution of these residues to alanines in full-length Erg11 (Erg11****) results in cells with reduced ergosterol production. This could be explained by a possible mislocalization of the Erg11**** protein. However, it is more likely explained by the predicted role of these lysines to the interaction of Erg11 with Ncp1, based on crystallization data of Erg11 and redox partners. Lessening this interaction will lead to a reduced electron flow from the NADPH donor to the Erg11 heme cofactor, which will inhibit the activity of Erg11 and lead to reduced ergosterol biosynthesis. This hypothesis could be examined further, *e.g.* by interaction experiments between Erg11 and Ncp1, by fusing both wild type Erg11 and Erg11 mutants, with the characterized lysine residues altered to alanines, and Ncp1 to epitope tags for immunoprecipitation experiments. The role of each of the four lysine residues to the interaction with the redox partner could be examined. A similar study could also be performed with possible mitochondrial interaction partners. As such,

the importance of the Erg11 MTS *in vivo* could be investigated further. Additionally, Sagatova *et al.* (2015) have predicted that the Erg11 K151 residue interacts with the carboxylate group of the heme cofactor. Therefore, the K151A substitution will also interfere with this coordination, which could affect the activity of Erg11.

Lastly and unexpectedly, it has been discovered that *erg11* null mutants can germinate on minimal medium. The details of this process have not been clarified. Possibly, the level of amino acids present in the used media can be linked to this finding, as the germination of *erg11* mutants on YPD and CSM is inhibited, which are growth sources rich in amino acids, in contrast to minimal medium. This could be examined further by dissecting the tetrads on minimal media, supplemented with individual amino acids or groups of amino acids with similar properties and investigate whether the ability to germinate is lost on certain media.

CHAPTER 4

THE VACUOLAR PROTEASES PEP4 AND PRB1 ARE IMPORTANT FOR THE GENERATION OF MULTIPLE ERG11 BANDS ON WESTERN BLOT

Parts of this results section are based on the manuscript: “On the whereabouts of yeast Erg11: a report on localization and degradation”, which is in preparation. All the experiments described in this chapter have been designed and performed by Winnie Kerstens, with technical assistance by Ilse Palmans.

4.1 Testing the cleavage hypothesis: is a protease responsible for the generation of multiple Erg11 bands on western blot?

Several mechanisms could be responsible for the formation of the additional Erg11 bands observed on western blot, as briefly outlined in paragraph 1.3.3. However, the high amounts of protein bands suggest that a proteolytic mechanism is the most likely process for their generation. Therefore, the hypothesis that the Erg11 forms are produced in a cleavage process has been tested. For this, a genome-wide search for all non-essential genes annotated with a protease or peptidase function has been performed in *S. cerevisiae*, using the Generic Genome Browser tool (GBrowse), which is integrated into the *Saccharomyces* Genome Database (http://www.yeastgenome.org, consulted on 2015-04-20). In total, 99 genes have been found. Accordingly, 96 strains from the haploid *S. cerevisiae* deletion collection deleted for a protease or peptidase have been transformed with a multicopy plasmid expressing *ERG11-V5*, so that their Erg11 pattern could be examined on western blot. In addition, three deletion strains, which are absent from the deletion collection, have been constructed in the endogenous *ERG11-HA* tagged AFC202 background. Out of the 99 mutants that have been tested (a list of the tested deletions can be found in Appendix II), two protease deletion strains lack all additional Erg11 forms apart from full-length Erg11. These strains carry a deletion in *PEP4* (ORF *YPL154C*) or *PRB1* (ORF *YEL060C*), encoding vacuolar proteinases A or B, respectively. These results have been verified by introducing the corresponding single and double deletions into the wild type strain AFC202, confirming that the Erg11 forms are generated in a cleavage-dependent process (Fig. 4.1). As explained in paragraph 1.4.1, ***pep4Δ*** mutants are devoid of several active proteases including Prb1, while ***prb1Δ*** only lacks active Prb1. If Pep4 would be the responsible protease cleaving Erg11, a ***prb1Δ*** mutant would have little defect in the generation of Erg11 truncated forms. However, as the absence of Erg11 truncations is observed in both protease mutants, it is hypothesized that Prb1 is the actual cleaver of Erg11. It can be observed on the highly overexposed blot that the ***prb1Δ*** mutant does exhibit faint additional Erg11 bands with shifted molecular weights compared to the wild type. This suggests that Pep4 or another protease could partly take over the cleavage of Erg11 in its absence, although in very low quantities. In ***pep4Δ*** strains, faint additional bands of molecular weights similar to those of wild type cells are observed, which could be generated by very low levels of a catalytically active variant of Prb1 (Mechler *et al.*, 1988). In the ***pep4Δ prb1Δ*** double mutant, no additional bands of Erg11 are observed, even when the blot is highly overexposed.

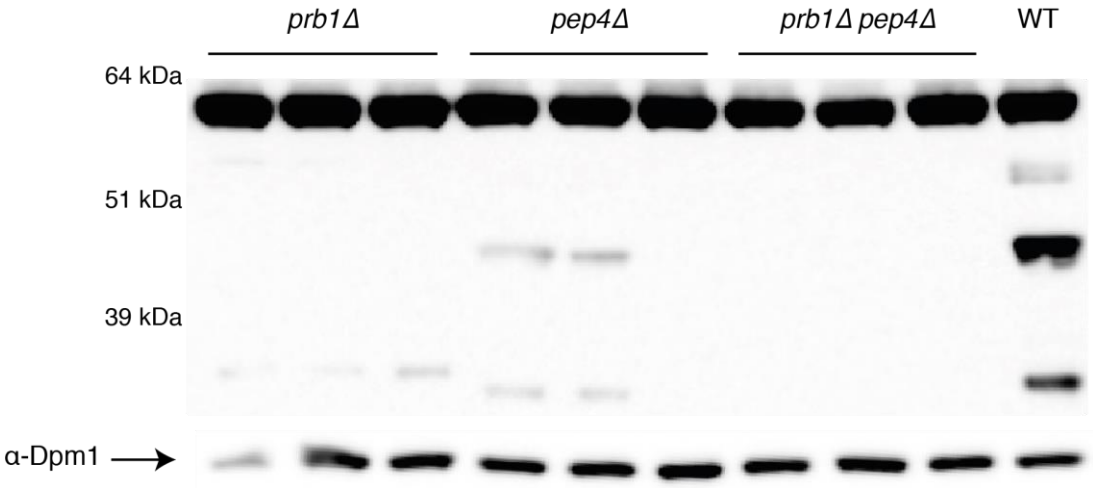


Fig. 4.1. Anti-HA immune-decorated western blot, showing the Erg11-HA protein of three different transformants of a *prb1Δ*, a *pep4Δ* or a *prb1Δ pep4Δ* deletion strain or of the wild type AFC202 strain. Proteins have been extracted from cells grown in YPD medium in the presence of FLC. Very faint Erg11 bands are observed in the single deletion mutants, while no additional bands are detected in the double *prb1Δ pep4Δ* deletion strain. Anti-Dpm1 is used as a loading control.

Furthermore, the reintegration of plasmid-born *PEP4* and *PRB1* to *pep4Δ* and *prb1Δ* deficient strains respectively, results in the reappearance of the Erg11 pattern on western blot (Fig. 4.2). In the *prb1Δ* strain and in the *prb1Δ pep4Δ* deletion strain transformed with *PEP4*, additional Erg11 bands can be observed of aberrant molecular weights compared to the wild type strain, again suggesting that these are produced by Pep4 or another protease that cleaves at alternative sites than Prb1. On the other hand, the faintly observed bands in the *PRB1*-transformed double deletion strain have the expected molecular weights, in agreement with the hypothesis that Prb1 is the actual cleaver of Erg11. The introduction of additional levels of *PEP4* or *PRB1* to the wild type strain does not lead to observable effects on the detection of Erg11.

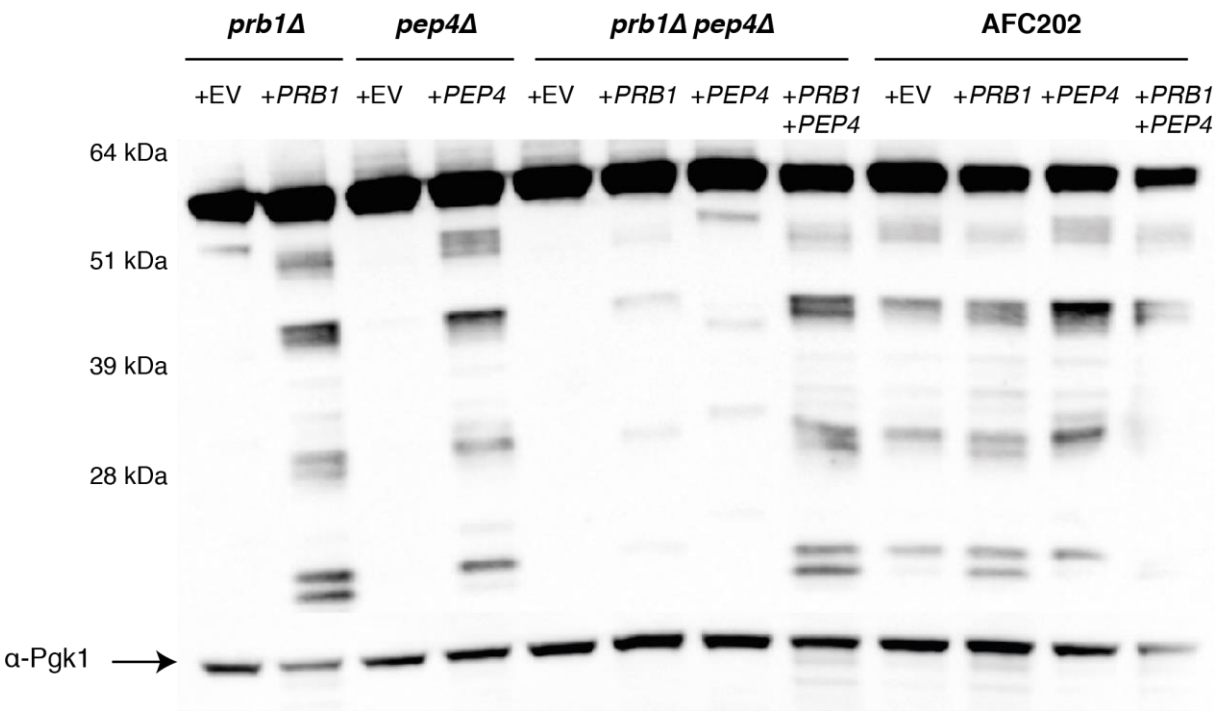


Fig. 4.2. *PEP4* and *PRB1* have been introduced to the *prb1Δ*, the *pep4Δ* and the *prb1Δ pep4Δ* deletion strains and to the wild type strain AFC202 on a centromeric plasmid. Proteins have been extracted from cells grown in -Leu drop out medium in the presence of FLC. It is clear that the introduction of the deleted gene results in the reappearance of additional Erg11 products in *prb1Δ* and *pep4Δ* cells. In cells carrying the double deletion, the introduction of *PRB1* leads to the detection of a faint but expected pattern of additional Erg11 bands, while the introduction of *PEP4* leads to the detection of faint bands of aberrant molecular weights. The absence of some additional Erg11 bands in the last lane is probably an artefact from incomplete blotting. Anti-Pgk1 is used as a loading control.

Next, it has been examined whether the absence of the Erg11 additional products has any effect on the overall performance of the protease deletion strains. However, the *pep4Δ* and *prb1Δ* single and double deletion strains show no growth defect in or on YPD medium and on YPEG medium and show no altered susceptibility or tolerance to FLC (Fig. 4.3). The MIC of the wild type and the mutant strains in YPD medium is 16 µg/mL by broth microdilution assay. Overall, these results indicate that the presence of additional Erg11 truncated products is not essential to cells and has no observable effect on general performances related to mitochondrial respiration or azole susceptibility. It has been kept in mind that, if a difference would have been observed, this could also be caused by the loss of function of the deleted gene(s) instead of by the absence of the additional Erg11 forms. These results further suggest that the additional bands of Erg11 are degradation products and do not have a functional role in the cell.

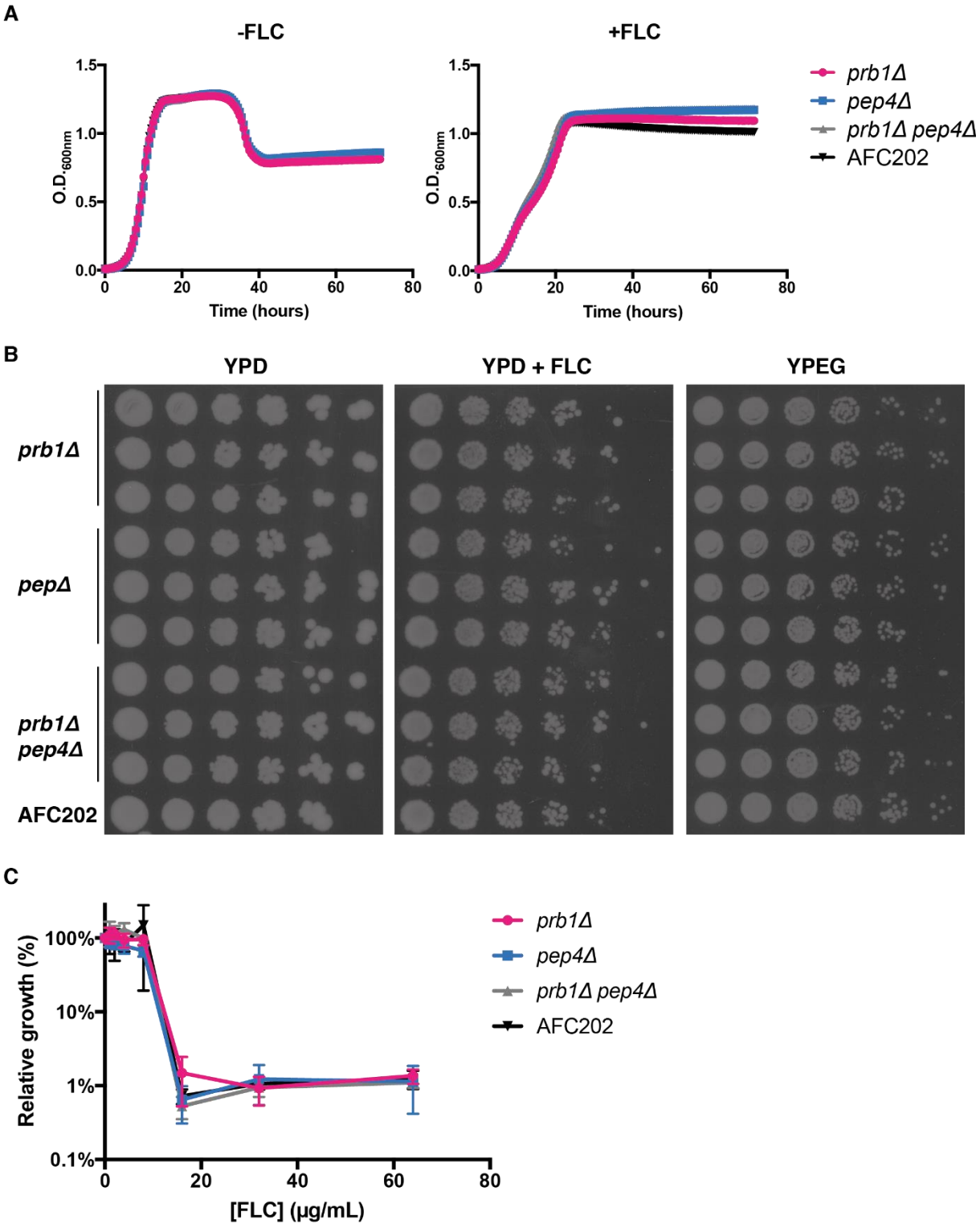


Fig. 4.3. General examination of the *prb1Δ*, the *pep4Δ* and the *prb1Δ pep4Δ* strains. (A) The average growth curves of three biological repeats of the wild type, single and double deletion strains in rich YPD medium in the absence or presence of FLC are found to be similar. (B) A spot assay of the strains on YPD with or without 20 µg/mL FLC treatment (results shown after 3 days of growth) and on YPEG (results shown after 4 days of growth) shows no observable differences between the strains. (C) A survival assay of the wild type and the deletion strains to FLC treatment in YPD medium shows no significant differences. The mean values of three biological repeats are shown with the standard deviation.

It has been examined whether FLC treatment results in the upregulation of *PRB1* and *PEP4* expression levels, in addition to upregulation of *ERG11*, to test whether the observation of the additional Erg11 bands on western blot is solely caused by the increased Erg11 protein levels or could also be caused by the upregulation of degradation processes. qRT-PCR analysis of *PEP4* and *PRB1* expression has been performed on cells grown in the presence or absence of FLC (Fig. 4.4). It has been found that *PRB1* expression is about twofold upregulated in wild type cells, when these are treated with FLC. *PEP4* expression, on the other hand is not significantly different between treated and untreated conditions. The increased expression of *PRB1* could contribute to the increased detection of the Erg11 forms on western blot in the presence of FLC, besides the higher expression of *ERG11* itself.

It has also been tested whether the Erg11**** mutant carries increased levels of Prb1 compared to the wild type strain, as in this mutant additional Erg11 bands are already observed in the absence of FLC treatment (Fig. 3.13). However, both in the absence or presence of FLC, no significant differences have been observed in the *PEP4* and *PRB1* levels of the Erg11**** strain compared to the wild type strain. This excludes the upregulation of protease gene expression levels as a possible explanation to the observed Erg11**** bands in the absence of FLC. However, other processes might be the causative factors for this observation. i) In the Erg11**** strain, the full-length Erg11**** mutant protein itself might be upregulated, which would enhance the detection of the smaller bands. ii) In contrast to the mRNA levels, the amount of active proteases could be upregulated. It has been reported that there is no correlation over time between the mRNA and protein levels of Prb1, partly caused by a retardation of Pep4-dependent maturation of the Prb1 protein (Moehle and Jones, 1990). iii) Lastly, under several conditions, non-vacuolar activity of the Pep4 and Prb1 proteases has been reported, as reviewed in Kerstens and Van Dijck (2018) and briefly described in paragraph 1.4.2.3. This has been ascribed to the permeabilization of the vacuolar membrane, known as LMP in mammals. It has been suggested that LMP is dependent on the cholesterol content of its membrane under oxidizing conditions in a murine model (Reiners *et al.*, 2011). In a similar concept, the reduced levels of ergosterol production in the Erg11**** cells could be responsible for the release of vacuolar proteases, which could result in concomitant enhanced degradation of Erg11****.

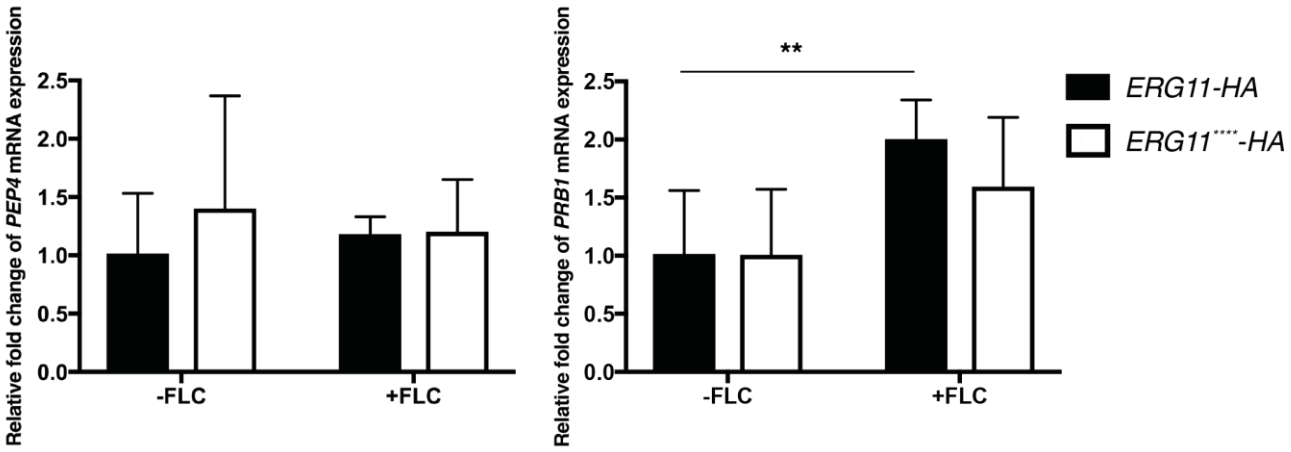


Fig. 4.4. qRT-PCR analysis of *PEP4* (left) and *PRB1* (right) mRNA levels of cells expressing *ERG11-HA* or *ERG11**-HA* endogenously.** Cells have been grown in the absence or presence of FLC in minimal medium. Mean values of three biological repeats are shown with 95% confidence intervals. A significant upregulation of *PRB1* mRNA levels is detected for wild type cells grown in the presence of FLC (p-value of 0.0071). No other significant differences have been identified. Statistical analysis has been performed by two-way ANOVA and has been corrected for multiple comparisons by the Bonferroni post-hoc test.

4.2 *ERG11* overexpression triggers ER stress in *Saccharomyces cerevisiae*

For several CYPs, it has been shown that their overexpression induces ER stress, as the ER needs to accommodate for the increased synthesis rates of the proteins (Sandig *et al.*, 1999). As explained in paragraph 1.4.2.4, the surplus of ER membrane that has been generated, will subsequently be degraded by autophagy. FIB-SEM results have shown for the first time that overexpression of *S. cerevisiae ERG11* also leads to ER stress. The electron-dense signal can be observed in stacks of paired ER membranes at perinuclear sites or elsewhere in the cell, termed karmellae respectively lamellae or collectively described here as ER whorls (Fig. 4.5). Moreover, the Erg11-APEX2 signal is observed in the vacuole, indicating that the excess of ER is sent there to be degraded. As FLC induces the overexpression of *ERG11*, it could be suggested to be an ER stress inducing agent, as also described by others (Dudgeon *et al.*, 2008; Kim *et al.*, 2012).

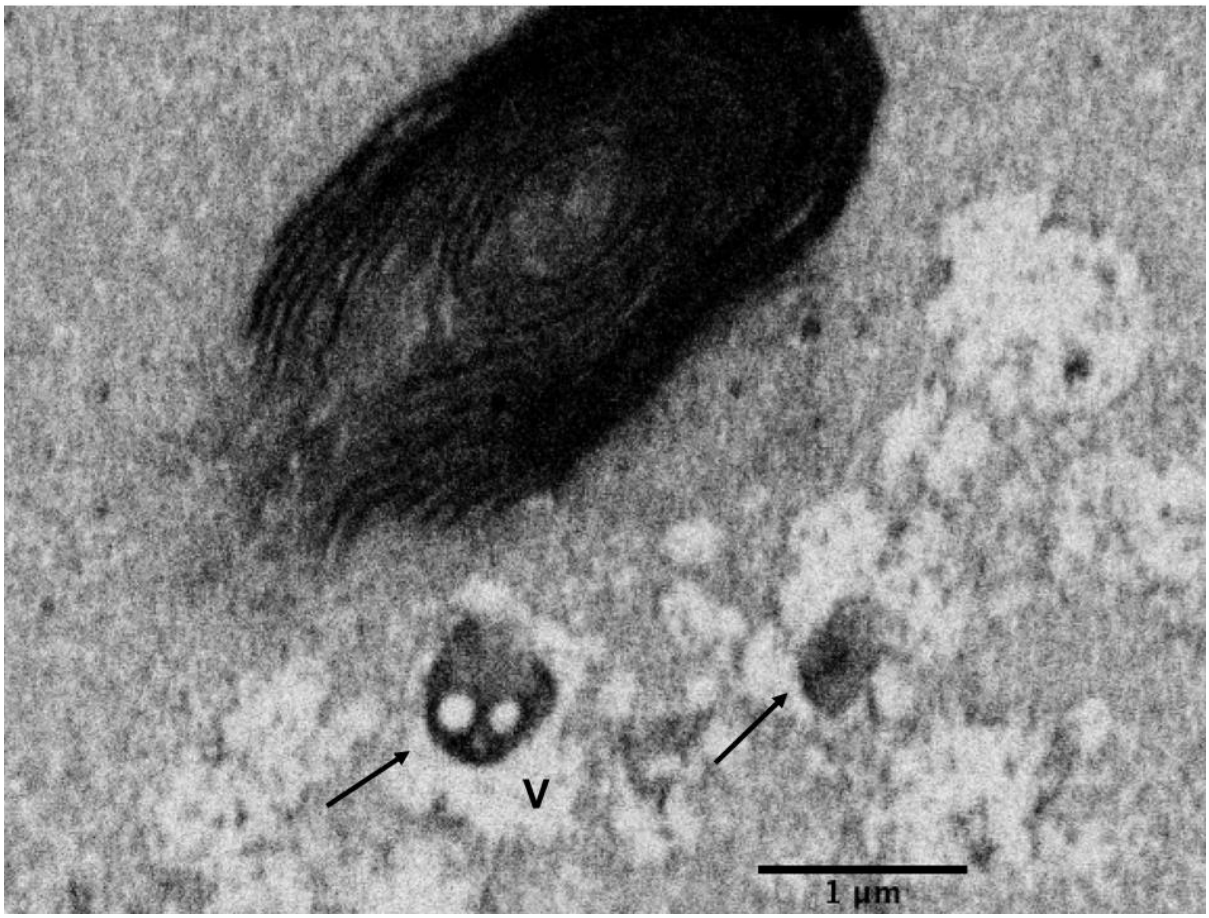


Fig. 4.5. FIB-SEM imaging of full-length Erg11-APEX2, showing concentric, multi-layered ER structures or whorls. Whorls are taken up by the vacuole (as indicated by the arrows) through microautophagy, for their degradation. The 'skull' signal observed in the vacuole is typical for the degradation of whorls. This is the first report of whorl formation due to overproduction of *S. cerevisiae* Erg11. The scale bar represents 1 µm (V: vacuole).

Taken together, these findings suggest that the additional Erg11 forms are degradation products that are generated by the vacuolar proteases Pep4 and Prb1 and are delivered to the vacuole by the process of ER-phagy. This process is stimulated by treating cells with FLC, which leads to upregulation of the Erg11 protein and thus ER stress. This hypothesis has been tested further, by the use of another ER stress inducing chemical, tunicamycin (TUN). TUN inhibits protein N-glycosylation, which interferes with proper protein folding in the ER (Oslowski and Urano, 2011). TUN-treated AFC202 cells also display upregulated full-length Erg11 and shorter Erg11 bands on western blot, although less abundant than FLC-treated cells, based on the concentrations tested here (Fig. 4.6). Higher overexposure of the blot in Fig. 4.6 leads to better detection of additional Erg11 bands in the TUN-samples but makes the FLC-sample become bad-looking, which would hinder comparison between the two conditions. Higher concentrations of TUN had to be used to indirectly detect ER stress on western blot by enhanced Erg11 protein degradation than has been described in literature for other proteins. These results suggest that the ER stress elicited by FLC is different from that produced by TUN, regarding Erg11 detection on western blot, which corresponds to the different molecular effects they provoke, *i.e.* Erg11 inhibition and consequent upregulation versus inhibition of protein glycosylation.

Moreover, the effect of the azole stressors voriconazole (VOR) and ketoconazole (KETO), of the polyene amphotericin B (AmB) and of the echinocandin caspofungin (CASP) on the additional Erg11 bands has been tested in wild type AFC202. All but AmB treatment result in upregulation of full-length Erg11 and detection of additional Erg11 forms on western blot. These results indicate that the detection of Erg11 forms on western blot is not restricted to azole-treated cells and can be observed under various kinds of stresses.

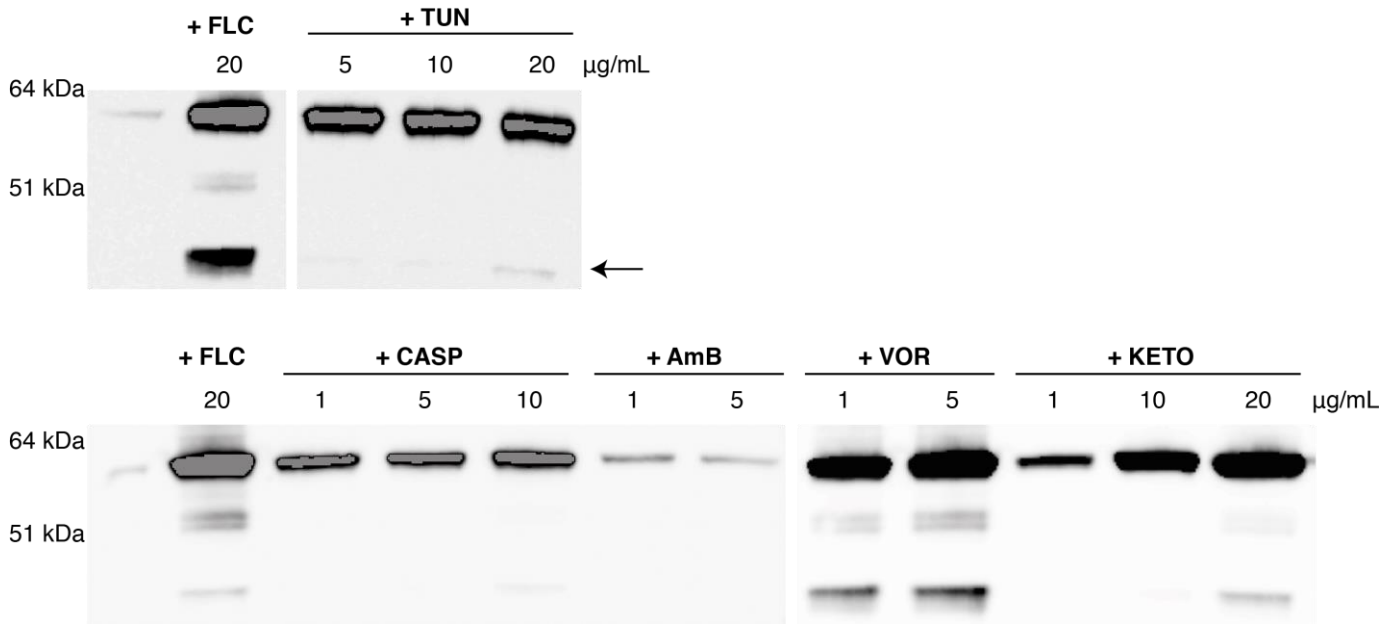


Fig. 4.6. Erg11 detection on western blots of cells treated with various stressors. The wild type strain AFC202 has been grown in minimal medium in the presence of the ER stressors FLC and various concentrations of TUN. The Erg11 protein products are from the same blot but a part has been left out for optimal visualization. Although less abundantly, TUN-treated cells display additional Erg11 bands (indicated by the arrow). Additionally, AFC202 cells have been grown in the presence of several antifungals, for which different concentrations have been tested. In the presence of other azoles or of the echinocandin CASP, additional Erg11 bands are detected. This is not true for AmB treatment. The protein bands are colored grey because of an altered setting at the detector for western blotting (which was unclear how to change at the time). This indicates that the bands are overexposed, which is necessary for optimal detection of the additional Erg11 forms. No loading controls have been included for these blots.

4.3 Discussion

A screening has been set up in which all non-essential *S. cerevisiae* gene products annotated with a protease or peptidase function have been assessed for their potential to cleave Erg11. This has been done by transforming the corresponding deletion strains from the *S. cerevisiae* haploid deletion collection with an *ERG11-V5* overexpressing plasmid followed by visualization of the Erg11 pattern on western blot. This experiment has led to the identification of the vacuolar proteases Pep4 and Prb1 as potential cleavers of Erg11. Because Pep4 acts upstream of the other vacuolar proteases and is necessary for the activation of Prb1, it is hypothesized that Prb1 is the actual protease cleaving Erg11. This idea is supported by two findings. i) The *pep4Δ* and *prb1Δ* deletion strains display a similar Erg11 phenotype on western blot, whereas the *prb1Δ* strain has been described to retain Pep4 activity (Rupp and Wolf, 1995). ii) Secondly, *PRB1* expression is upregulated under FLC treatment, whereas *PEP4* expression is not. However, no direct evidence has been generated for the cleavage reaction of Erg11 by Prb1. Though unlikely, it could be possible that Prb1 catalyzes another reaction that initiates the formation of Erg11 truncations, possibly in a non-protease manner, as all non-essential proteases and peptidases have been tested during this screening. To examine the direct or indirect effect of Prb1, the protease could *e.g.* be purified to investigate whether it can cleave purified Erg11 *in vitro*.

As the proteases Pep4 and Prb1 are involved in degradation processes in the vacuole, it is assumed that the Erg11 bands observed on western blot are degradation products. In further support of this hypothesis, similar patterns of protein products on western blot have been observed for other proteins and have been ascribed to degradation by Pep4 and Prb1 (Ziegler and Schwartz, 1991; Onodera and Ohsumi, 2004; Schuck *et al.*, 2014). Furthermore, it is known that Pep4 and Prb1 degrade their substrates to peptides, which are further degraded to single amino acids by carboxypeptidases and aminopeptidases. Such a cleavage process could explain the observed Erg11 bands on western blot (Teichert *et al.*, 1989; Shen *et al.*, 2008). Moreover, the *pep4Δ prb1Δ* double mutant, which lacks all other forms of Erg11 but the full-length form, does not show any defect in growth. This means that the truncated forms of Erg11 are not essential under the tested conditions. Furthermore, the absence of additional Erg11 forms does not affect the susceptibility and tolerance to FLC, nor does it affect mitochondrial respiration. The combination of these results leads to the conclusion that the observed Erg11 forms on western blot are degradation bands and do not carry functional significance.

Furthermore, FIB-SEM analysis has indicated that the upregulation of Erg11 expression induces ER stress, in agreement with other reported examples of CYP-induced ER stress and the described function of azoles as ER stressors (Sandig *et al.*, 1999; Dudgeon *et al.*, 2008; Kim *et al.*, 2012). ER stress is alleviated by autophagic processes, as also observed for the Erg11-APEX2 signal

detected in the vacuole. These results suggest that the additional bands of Erg11 are generated by the mechanism of ER-phagy, by targeting Erg11-containing ER to the vacuole for degradation by Pep4 and Prb1. The classic ER-stressor TUN is also able to induce Erg11 overproduction and degradation, but to a lesser extent than the Erg11-targeted azole drugs. Remarkably, the echinocandin antifungal class, represented by CASP, also induces Erg11 expression, indicative of ER stress under this condition. It is unclear whether the increased levels of Erg11 are a direct effect of CASP treatment or an indirect consequence of a general increase in ER membranes.

Mammalian CYPs can be degraded by the cytosolic proteasome or by proteases in the lysozyme, which is functionally similar to the fungal vacuole with respect to protein degradation. The expression of mammalian CYPs in *S. cerevisiae* also results in the degradation of the proteins by the proteasome or by vacuolar proteases, depending on the CYP protein (Murray *et al.*, 2002; Liao *et al.*, 2005). Here, it has been shown that Erg11 is most likely degraded by vacuolar proteolysis. However, Erg11 degradation has also been demonstrated by a side branch of ERAD, where the Asi complex delivers the Erg11 protein to the proteasome. The Asi complex is located in the inner nuclear membrane, an ER subdomain that is connected to the rest of the ER membrane at nuclear pores. It provides a quality control to assure that Erg11 is excluded from this domain and is restricted to appropriate ER subdomains for sterol synthesis (Foresti *et al.*, 2014). The fact that both proteasomal and vacuolar degradation systems are available for Erg11 degradation could explain the results obtained in Chapter 3 on the Erg11****-HA protein. Although the *ERG11******-HA* mRNA levels are upregulated compared to *ERG11-HA* levels, no similar increase in Erg11****-HA protein levels has been detected on western blot. Some truncated Erg11 bands are detected in the absence of FLC, suggesting that the protein is partly degraded in the vacuole. However, these bands are not as abundant as those of wild type Erg11 upregulated by the presence of FLC, suggesting that parts of the Erg11**** protein pool might already be degraded at an earlier time point, possibly by another mechanism. It could be hypothesized that most of the upregulated, less functional Erg11****-HA protein is degraded immediately after its synthesis, by ERAD and the proteasome, both in the absence and presence of FLC treatment. However, some ‘wild type’ levels of the Erg11****-HA protein seem to be retained by the cells, possibly to ensure low amounts of ergosterol production. These are eventually degraded by vacuolar proteolysis.

CHAPTER 5

TRANSLATING THE RESULTS TO THE OPPORTUNISTIC HUMAN PATHOGEN *CANDIDA ALBICANS*

5.1 *Candida albicans* Erg11 is detected as multiple bands on western blot

All the experiments described in this chapter have been designed and performed by Winnie Kerstens, with technical assistance by Ilse Palmans.

The results that have been obtained in *S. cerevisiae* concerning the conditions under which additional Erg11 products can be detected on western blot, the identification of the cryptic MTS and the process by which the truncated Erg11 products are generated, have been used to investigate whether similar processes also occur in *C. albicans*. Furthermore, it has been examined whether the additional Erg11 products affect azole therapy in this pathogenic fungus, despite the negative results obtained in *S. cerevisiae*.

Similar to the detection of *S. cerevisiae* Erg11 on western blot, the Erg11 protein of the endogenously *ERG11-HA* tagged wild type *C. albicans* strain AFA79a can be detected on western blot as multiple bands when cells are treated with FLC, in addition to induced levels of the full-length protein (Fig. 5.1 A). However, the pattern of *C. albicans* Erg11 bands is distinct from that of *S. cerevisiae*. The susceptibility of *C. albicans* to FLC is remarkably higher compared to *S. cerevisiae*, with an MIC of 0.125 µg/mL for AFA79a, as determined by Etest on RPMI agar (Fig. 5.1 B). RPMI medium is typically used to culture various mammalian cells and is recommended by CLSI and EUCAST as a suitable medium for MIC measurements of fungal pathogens. It has been decided to add a supra-MIC FLC concentration of 10 µg/mL to *C. albicans* cultures, for a clear detection of Erg11 protein bands on western blot. Furthermore, as mentioned in Chapter 2, it is clear from the Etest that tolerance to azoles is more pronounced on Etests with *C. albicans* cells than with *S. cerevisiae* cells. The reason for this is not clear.

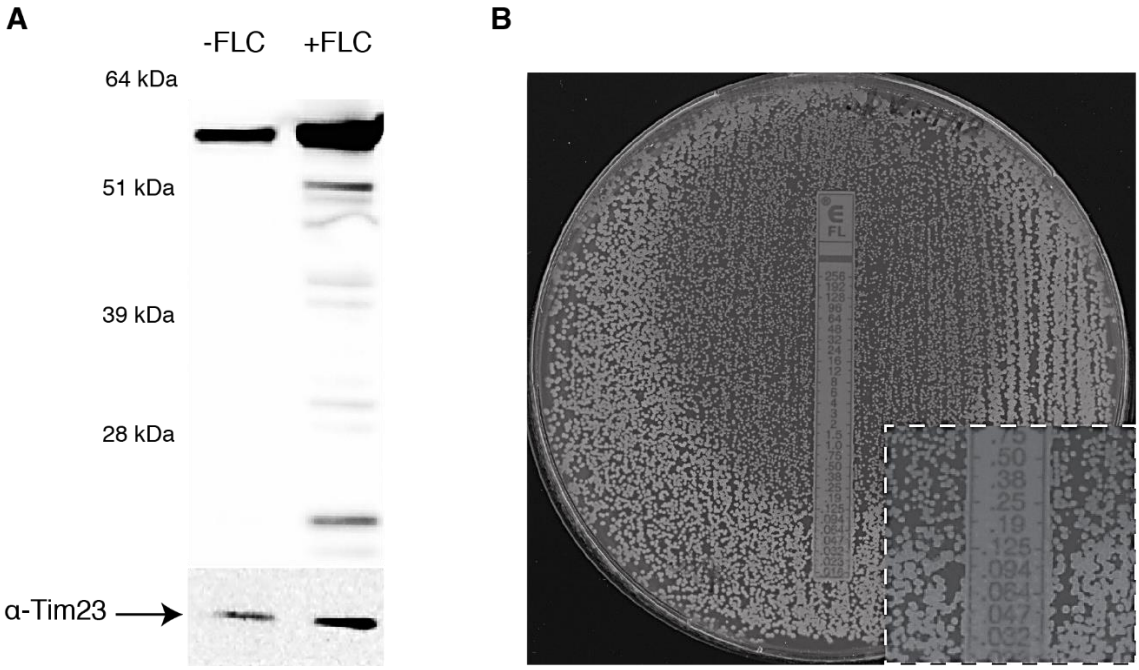


Fig. 5.1. The Erg11 protein pattern of the endogenously *ERG11-HA* tagged wild type strain AFA79a has been examined on western blot as well as its FLC susceptibility by Etest. (A) Western blot detection of Erg11-HA from cells grown overnight in rich medium in the absence or presence of 10 µg/mL FLC shows additional Erg11 bands in the presence of FLC. Anti-Tim23 has been included as a loading control. (B) The Etest of AFA79a to FLC defines the MIC as 0.125 µg/mL (the region around the MIC value is enlarged in the inset) and clearly shows the tolerance of the strain to FLC, as growth inside the halo.

Similar to *S. cerevisiae*, the pattern of Erg11 is comparable between cells grown in minimal or in rich medium. Furthermore, if high enough amounts of total protein are loaded, the additional bands of Erg11 can be observed in the absence of azole treatment, especially in rich medium (Fig. 5.2 A). The additional Erg11 bands appear on western blot between 4 and 8 hours of growth in minimal medium in the absence of FLC, corresponding to late lag or early exponential phase (Fig. 5.2 B). When cells are treated with FLC, the bands are detected at later time points (most clearly from 12 to 30 hours after inoculation). It can be seen from Fig. 5.2 C that *C. albicans* cells have a hard time growing in minimal medium in the presence of FLC, as no defined growth stages can be observed in the growth curve. This severe growth problem is not observed in rich medium.

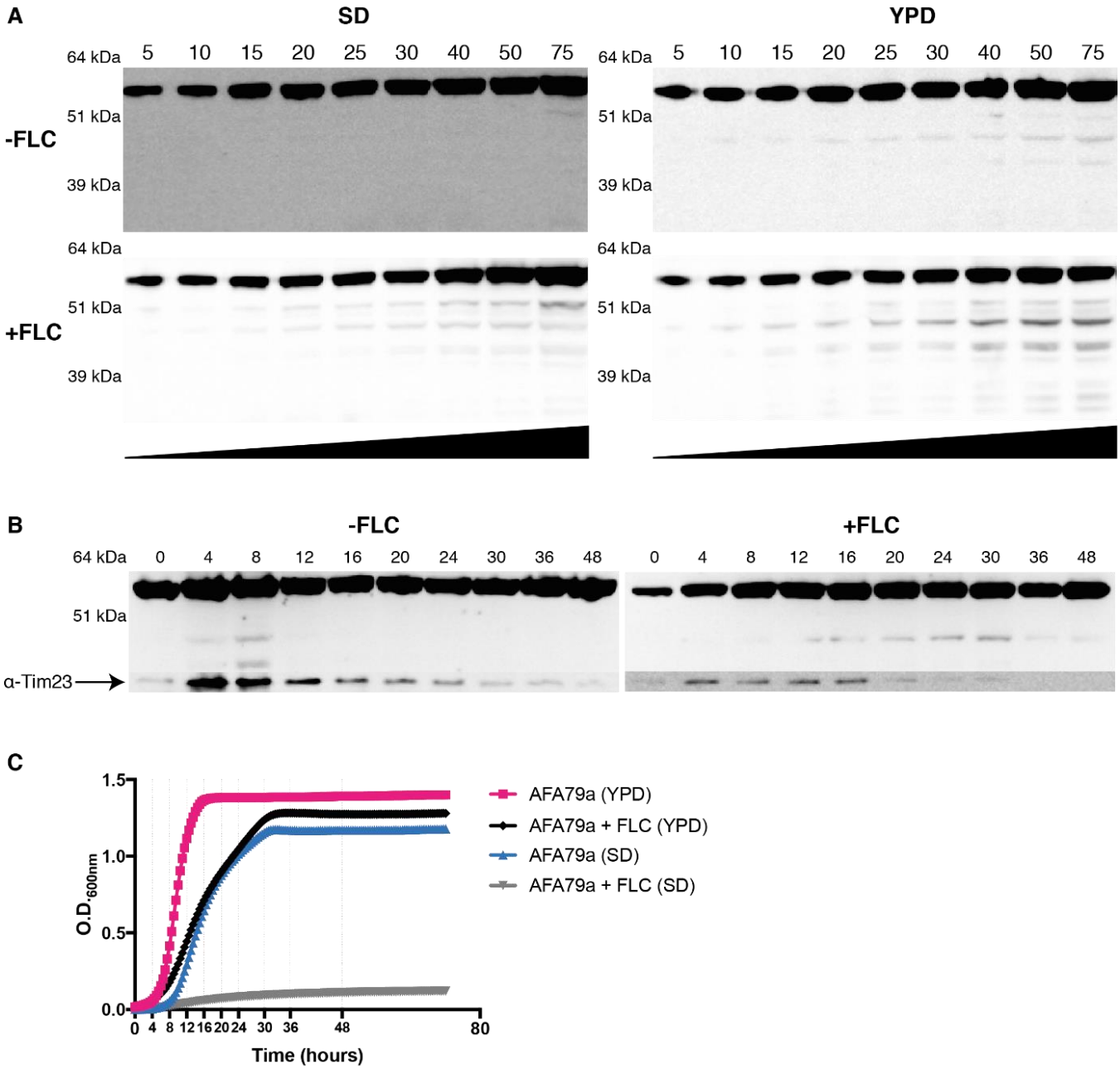


Fig. 5.2. Examination of optimal conditions for the detection of additional *C. albicans* Erg11 bands on western blot. (A) A western blot of increasing amounts of total protein (ranging between 5 and 75 µg) shows that additional bands of Erg11 have comparable molecular weights whether cells are grown in minimal or in rich medium and in the absence or presence of FLC. (B) A time-course study of AFA79a cells grown in minimal medium in the absence or presence of FLC has been performed on western blot. 10 µg of total protein extract has been loaded for FLC-treated cells and 35 µg of non-stressed cells. While additional bands of Erg11-HA are already observed after four to eight hours of growth in the absence of FLC, these only appear after about twelve hours in the presence of FLC. Anti-Tim23 has been used as a loading control but it is not very suited. (C) Growth curve of AFA79a in minimal and rich medium, in the absence and presence of FLC. It can be seen that *C. albicans* grows efficiently in the presence of FLC in rich medium but not in minimal medium.

5.2 *In silico* analysis of a putative MTS of *Candida albicans* Erg11

We have shown that the detection of additional Erg11 forms is conserved between *S. cerevisiae* and *C. albicans*. Subsequently, it has been examined whether the MTS of *S. cerevisiae* Erg11 is also conserved. Indeed, it has been found that this region (*S. cerevisiae* Erg11 AA 148 to 197, the region that has been fused N-terminally to Arg8$^{\Delta 13}$ in Fig. 3.2) is well conserved in *C. albicans* (Fig. 5.3). However, only the first three lysine residues (marked with red boxes), identified in *S. cerevisiae* as important residues to the MTS, are conserved in *C. albicans*, which could suggest that the fourth residue (K160) might be of limited importance to the mitochondrial targeting of the *S. cerevisiae* Erg11$^{\Delta 150}$ construct. This could be further examined by fluorescence microscopy analysis of individual lysine to alanine substitutions in the Erg11$^{\Delta 150}$ construct. Furthermore, the predicted role of this residue in the interaction of *S. cerevisiae* Erg11 with its redox partner might be minor, or alternatively, another residue of *C. albicans* Erg11 could fulfill this function.

The three lysine residues are found to be conserved not only from *S. cerevisiae* to *C. albicans* but in general from fungi to mammals. In addition, the lysine at position 164 is conserved in all species, except for *C. glabrata* (indicated by the first red asterisk on top). Remarkably, other positively charged residues in the MTS region (indicated by red asterisks) are not conserved between fungi and mammals. One bacterial CYP51 sequence has also been included in the alignment but little sequence conservation could be detected in the MTS region between the prokaryote and fungal sequences. Overall, these results suggest that the MTS, and especially the first positively charged lysine residues in this region, are important to the CYP51 protein, as these are conserved from yeast to mammals. Based on the crystallization data that have predicted the involvement of the lysines in the interaction of *S. cerevisiae* Erg11 with the redox partner (Fig. 3.15), it is hypothesized that this interaction is also dependent on the conserved lysine residues in mammals.

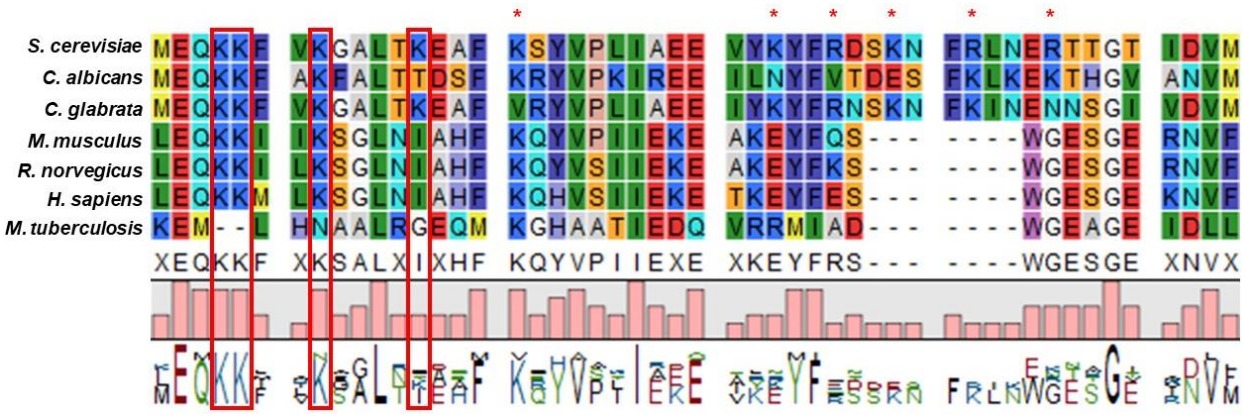


Fig. 5.3. Alignment of the CYP51 sequences of several fungal and mammalian species and of one bacterial species. The fungal CYP51 sequences of *S. cerevisiae*, *C. albicans* and *C. glabrata* have been aligned in addition to the mammalian CYP51 sequences of *Mus musculus*, *Rattus norvegicus*, *Homo sapiens* and the bacterial CYP51 sequence of *Mycobacterium tuberculosis*. In general, the CYP51 MTS is fairly conserved among the fungal species. Furthermore, the three first positively charged lysine residues (indicated by red boxes) and K164 but not the last five positively charged residues (indicated by asterisks) are conserved from fungi to mammals.

5.3 Creation of null mutants of the *Candida albicans* homologs to the *Saccharomyces cerevisiae* proteases responsible for Erg11 cleavage products

In this section, it is investigated whether the additional Erg11 bands observed on western blot in *C. albicans* cells are also produced during proteolytic cleavage events by vacuolar proteases. For this, the *C. albicans* homologs of Pep4 and Prb1 have been searched via BLAST, both on nucleotide sequence level and on amino acid sequence level (Basic Local Alignment Search Tool, https://blast.ncbi.nlm.nih.gov/Blast.cgi). The same hits have been identified through both searches, of which the results of the BLAST search on protein level have been included in Table 5.1. *S. cerevisiae* Pep4 has one close homolog in *C. albicans*, which is Apr1. *S. cerevisiae* Prb1 has two close homologs in *C. albicans*, both described as Prb1 but also as Prb12 and Prb11. The latter names will be used to avoid confusion.

Table 5.1. Closest *C. albicans* homologs to *S. cerevisiae* Pep4 and Prb1, identified through a BLAST search.

S. cerevisiae	*C. albicans* homolog	Length of *C. albicans* protein	Identical AA to *S. cerevisiae* protein	Similar AA to *S. cerevisiae* protein
Pep4	CaO19.1891 (*APR1*)	419 AA	276/417 or 66%	315/417 or 75%
Prb1	CaO19.7196 (*PRB12* also *PRB1*)	493 AA	295/458 or 64%	353/458 or 77%
Prb1	CaO19.2242 (*PRB11* also *PRB1*)	465 AA	213/424 or 50%	285/424 or 67%

It has been examined whether the identified *C. albicans* proteases are involved in the generation of the Erg11 protein bands on western blot by creating deletion strains for these three genes in the wild type AFA79a background. First, the *PRB12* gene has been deleted by use of the *SAT1* flipper cassette, in which both alleles of the diploid strain are deleted sequentially (Reuss *et al.*, 2004). This cassette contains both a dominant nourseothricin resistance marker (encoded by *SAT1*) and a recombinase *FLP* gene inserted between FRT regions (FLP recombination target), flanked by homologous regions to delete the gene of interest (GOI). The FRT sites allow efficient excision of the deletion cassette out of the *C. albicans* genome by the *FLP* recombinase gene, which is under control of the *MAL2* promoter, leaving nothing but one FRT site in the genome when cells are grown on maltose, or even glucose. This step is repeated once to obtain homozygous deletion mutants. This protocol is time-consuming but efficient. However, around the time this experiment has been performed, the CRISPR-Cas9 system has been introduced to *C. albicans* genetics (Vyas *et al.*, 2015). As this system introduces a gene mutation in both alleles of the diploid at once, it has been

decided to continue the construction of the mutants with this technique, as it is expected to be less time consuming. It is based on the Cas9 protein, which is a nuclease that introduces a double-stranded break in the DNA near a protospacer adjacent motif (PAM) site, when it is guided there by the single guide RNA (sgRNA), containing a protospacer sequence which can hybridize to complementary DNA. The double-stranded break at the GOI can be repaired by homology-directed repair (HDR). In the CRISPR-Cas9 technique, the repair template or donor DNA is provided, flanked by homologous regions to the site of the double-stranded break, to introduce specific mutations into the *C. albicans* genome. Specifically in this experiment, a double STOP codon has been introduced early in the ORF sequences of the proteases, inhibiting their formation and thus creating null mutants. The used vector (pV1524) has been kindly provided by the authors and has been published recently (Vyas *et al.*, 2018). It is an optimized system that contains both the Cas9 and the sgRNA sequences on one vector, instead of on two separate plasmids. The vector integrates at an intergenic region, *NEUT5L*, as extrachromosomal plasmids are not stably maintained in *C. albicans* (Gerami-Nejad *et al.*, 2013). Both methods are schematically represented in Fig. 5.4.

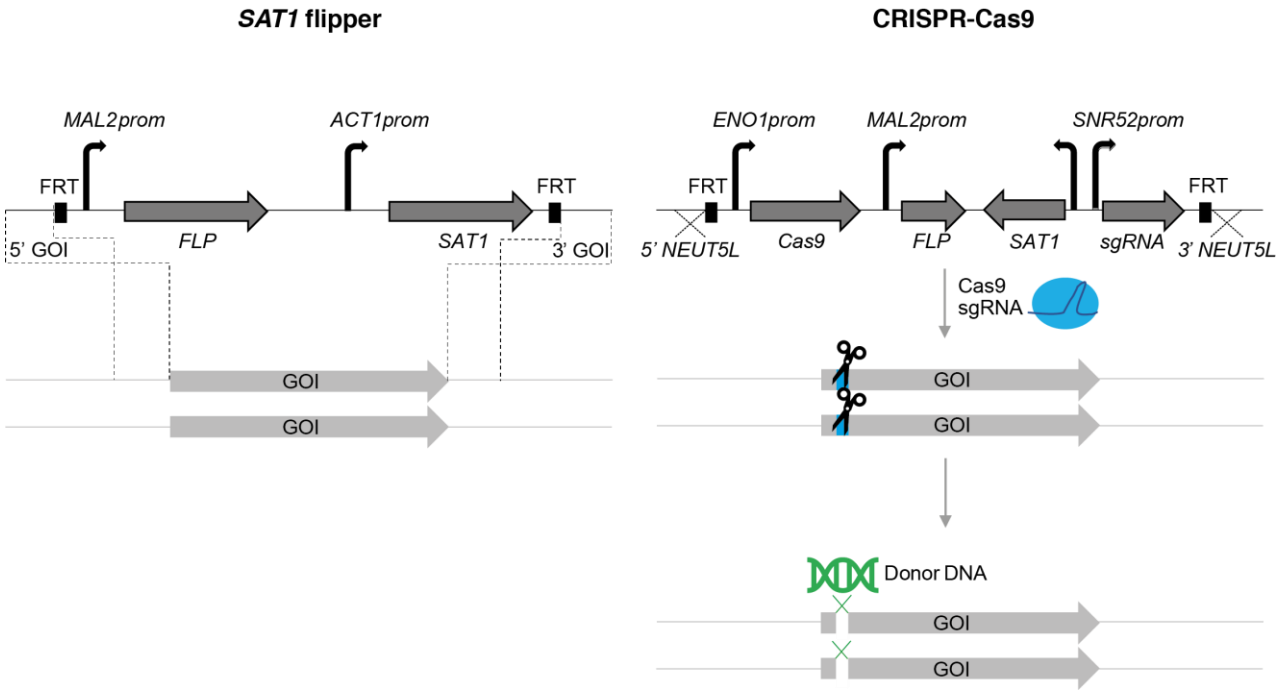


Fig. 5.4. Schematic representation of the *SAT1* flipper method (left) and the CRISPR-Cas9 method (right), used to generate deletion and null mutants, respectively. The *SAT1* flipper method relies on homologous recombination to swap the gene of interest with the deletion cassette, which can be subsequently lost by inducing *FLP* recombinase expression from the *MAL2* promoter, leaving nothing but one FRT site at the GOI. In the CRISPR method, the Cas9/sgRNA cassette is introduced to the *NEUT5L* locus, from which the Cas9 is expressed and guided by the sgRNA to the GOI, introducing double-stranded breaks near PAM sites. The co-transformed donor DNA containing a double STOP codon and homologous flanking regions can be used to repair these breaks, creating null mutants of the GOI. Similar to the *SAT1* flipper method, this cassette can be flipped out of the *NEUT5L* locus by the FLP recombinase, leaving an FRT site.

A series of optimization steps has been carried out to finally obtain CRISPR-Cas9 generated mutants, especially with regard to the transformation of the AFA79a strain to obtain null mutants and the subsequent loss of the Cas9/sgRNA cassette. It has been suggested by Vyas V. K. to use a hybrid protocol of lithium acetate and electroporation to transform *C. albicans* with the vector and the repair template, which has shown sufficient to obtain protease null mutants, although with low efficiency (Vyas *et al.*, 2018). The inability to flip out the Cas9/sgRNA cassette and thus also the dominant nourseothricin resistance marker at the *NEUT5L* locus could however not be solved. This has prohibited the construction of consecutive, multiple deletions, *i.e.* the construction of ***apr1Δ/Δ prb12Δ/Δ*** or ***apr1Δ/Δ prb11Δ/Δ*** double mutants or the simultaneous knock down of both *PRB1* homologs or the construction of ***apr1Δ/Δ prb12Δ/Δ prb11Δ/Δ*** triple mutants. Recently, our lab has started using a different CRISPR-Cas9 system, with a much higher success rate for generating mutants (Nguyen *et al.*, 2017). Moreover, the dominant selection marker is easily lost, so that multiple deletions can be made. If possible, this system would have been preferred over the used CRISPR-Cas9 system. Nevertheless, this approach has resulted in the isolation of a handful of ***prb12Δ/Δ*** and ***prb11Δ/Δ*** mutants and one ***apr1Δ/Δ*** mutant. These have been examined on western blot for their Erg11 pattern (Fig. 5.5). Interestingly, some additional Erg11 bands are observed in all the deletion mutants. However, the Erg11 pattern is different from that of the wild type in the ***apr1Δ/Δ*** and ***prb12Δ/Δ*** mutants, which complement each other for the additional Erg11 bands. This suggests that both Apr1 and Prb12 are involved in the cleavage of Erg11 in *C. albicans*, unlike the results obtained in *S. cerevisiae* where only Prb1 seems involved. The *prb11* null mutant shows a similar Erg11 pattern as the wild type strain, indicating that Prb11 is not involved in the generation of the additional bands. One of the ***prb12Δ/Δ*** mutants obtained with the classical *SAT1* flipper method has been included on the western blot. No differences are observed between the *prb12* mutants generated by the two different methods.

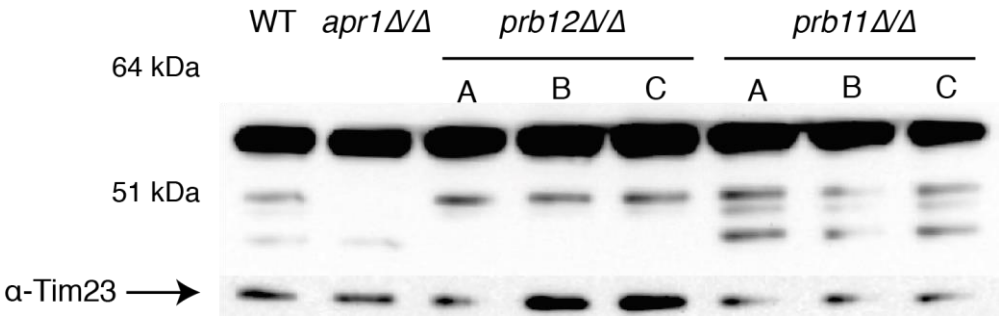


Fig. 5.5. Western blot of Erg11-HA detected in protease mutants deficient in *apr1*, *prb12* and *prb11*, generated through the *SAT1* flipper method or CRISPR-Cas9 in the AFA79a wild type strain. The protease mutants and wild type strain have been grown overnight in rich medium in the presence of FLC. The *apr1* and *prb12* mutants lack some of the additional Erg11 bands in a complementary manner, suggesting that both are involved in the generation of the Erg11 bands. For the *prb12* mutants, both methods have been represented on western blot, leading to similar Erg11 patterns, where A and B have been generated by the CRISPR-Cas9 method and C by the *SAT1* flipper method. The anti-Tim23 antibody is used as loading control.

Subsequently, it has been tested whether the absence of some of the Erg11 forms in the null mutants affects the susceptibility or tolerance of the strains to FLC (Fig. 5.6). Similar to what has been observed in *S. cerevisiae*, these mutations and the concomitant absence of truncated Erg11 forms do not affect the examined properties, as the MIC of all the strains is similar, *i.e.* 0.19 µg/mL for the *apr1* null mutant and 0.125 µg/mL for all other mutants, in agreement with the MIC of the AFA79a wild type strain (Fig. 5.1 B). Also for the tolerance to FLC, visualized by growth inside the halo of inhibition, no notable differences are observed. This suggests that also in *C. albicans*, the observed Erg11 forms on western blot are degradation products. If aberrant MIC values or tolerance levels would have been observed, it would not have been possible to determine whether this would be caused by the loss of the Erg11 truncations or the loss of the gene product in the mutant strain.

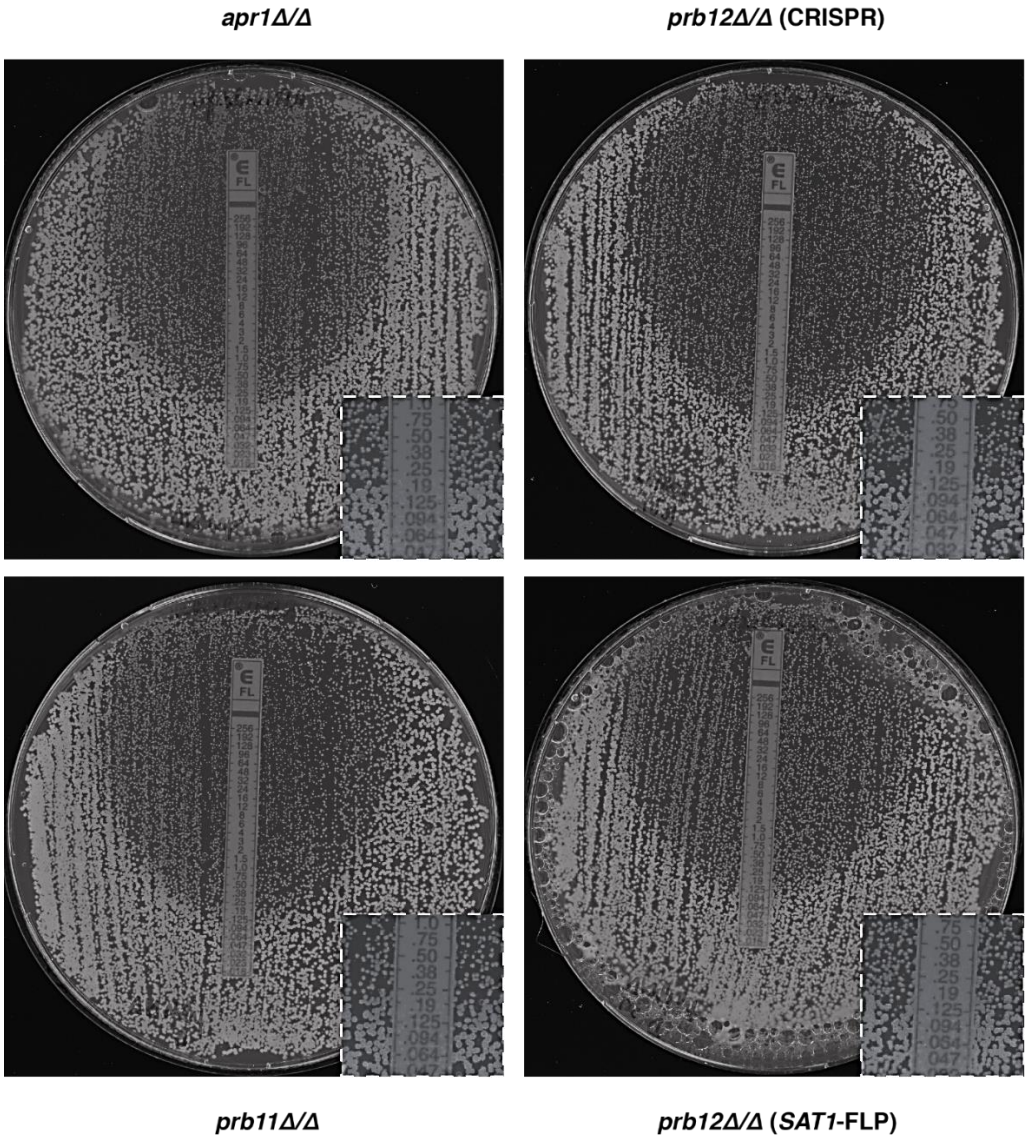


Fig. 5.6. FLC Etests of *apr1* and *prb11* mutants, generated by CRISPR and *prb12* mutants, generated by CRISPR and the *SAT1* flipper method. The MICs of the strains are similar, with a value of 0.125 µg/mL for the *prb11* and *prb12* mutants and of 0.19 µg/mL for the *apr1* mutant. The areas around the MIC have been enlarged in the insets.

5.4 Discussion

Initially, the additional Erg11 forms observed on western blot in the presence of FLC have been detected in the opportunistic human pathogen *C. albicans*. In this section we have further identified similarities between *S. cerevisiae* and *C. albicans* Erg11. We have confirmed that the Erg11 bands are more easily detected on western blot in the presence of FLC treatment. Furthermore, they appear in a similar time frame as for *S. cerevisiae*. However, the molecular weights of the *C. albicans* Erg11 bands are different from those observed in *S. cerevisiae*.

Furthermore, the alignment of primary sequences of fungal CYP51s has shown that the MTS region is well conserved. Moreover, alignment of fungal and mammalian CYP51 sequences shows the conservation of the first three lysine residues in this region, which have been identified in *S. cerevisiae* as important to the biology of the CYP51 protein, presumably because of a role in the interaction of Erg11 with the redox partner (Chapter 3). For *C. albicans* specifically, it has been reported that the lysine residue at position 143, which corresponds to the *S. cerevisiae* K151 residue, is altered to a glutamine or arginine residue in clinical isolates, which increases the resistance to azoles (Xiang *et al.*, 2013; Sagatova *et al.*, 2015). This further signifies the role of this residue to the overall CYP51 structure, of which the coordination around the heme group has been reported to be conserved in fungi, as mentioned in paragraph 3.4 (Monk *et al.*, 2014). The conservation of these lysine residues from fungi to mammals suggests that their role to the CYP51 protein could be conserved.

Additionally, in this chapter the closest *C. albicans* homologs to the *S. cerevisiae* Pep4 and Prb1 proteases have been tested for their involvement in the generation of truncated Erg11 protein bands on western blot. They have been identified as *C. albicans* Apr1, and Prb11 and Prb12 respectively, through a BLAST search. However, both Prb11 and Prb12 have not been characterized in *C. albicans*, so it is unclear whether these proteins are indeed vacuolar proteases. Furthermore, only a limited number of studies have been published on the Apr1 protein (Bauerova *et al.*, 2012; Bauerova *et al.*, 2014; Amri Saroukolaei *et al.*, 2016). Some functional similarities have been described between *S. cerevisiae* Pep4 and *C. albicans* Apr1, such as the upregulation of *APR1* under starvation conditions. On the other hand, differences have also been observed, as the *apr1Δ/Δ* mutant has no defect in the maturation of the carboxypeptidase Y (CPY) protein, unlike what has been described for *S. cerevisiae pep4* mutants.

Examination of the corresponding null mutants on western blot has led to the conclusion that both Apr1 and Prb12 are involved in the generation of additional Erg11 bands. This contrasts the findings in *S. cerevisiae*, where only Prb1 is suggested to be important in the generation of Erg11 bands. The construction of an *apr1Δ/Δ prb12Δ/Δ* null mutant could further demonstrate this. The Prb11 protein does not seem to be involved in Erg11 cleavage. As these mutants have no altered

susceptibility or tolerance to FLC, the possibility that the additional forms of Erg11 are important for increased resistance or tolerance to azoles can be excluded. It is more likely that these additional bands observed on western blot are degradation products, similar to what has been suggested in *S. cerevisiae*.

CHAPTER 6

GENERAL CONCLUSION AND FUTURE PERSPECTIVES

In this study, we have identified several aspects concerning the biology of the Erg11 protein in *S. cerevisiae* and in *C. albicans*. This includes the characterization of an MTS region in the *S. cerevisiae* protein, which is largely conserved in *C. albicans*, the identification of the involved degradation processes in both species and the (non-)essentiality of the *S. cerevisiae ERG11* gene for growth on different media. Furthermore, we have disproved the hypothesis that the Erg11 truncated forms, as observed on western blot in FLC-treated wild type cells, play a role in the susceptibility or tolerance of the strain to the drugs. The principal findings of this study are further discussed below.

6.1 The Erg11 MTS: a determinant of mitochondrial localization?

In both the model organism *S. cerevisiae* and the opportunistic human pathogen *C. albicans*, additional forms of the Erg11 protein are observed on western blot, especially when the expression of *ERG11* is induced, *e.g.* by FLC treatment. In analogy to the process of bimodal targeting to the ER and mitochondria, described for several mammalian CYPs, it has been hypothesized that these additional forms of Erg11 might localize to mitochondria. Indeed, it has been found that an Erg11 construct (Erg11$^{\Delta 150}$) with a molecular weight similar to that of the largest observed additional Erg11 forms on western blot inarguably localizes to mitochondria, validated by confocal and electron microscopy and by the *ARG8* assay, by which robust growth on arginine limiting medium indicated efficient mitochondrial targeting of the Erg11$^{\Delta 150}$-Arg8$^{\Delta 13}$ chimeric protein. It has been specified that the amino acids from position 148 to 197 are sufficient to target the MTS-free Arg8$^{\Delta 13}$ passenger protein to mitochondria when this region is fused to its N-terminus, confirming that this sequence represents a true MTS. FIB-SEM data have further indicated that the Erg11$^{\Delta 150}$ construct localizes inside mitochondria, as the complete mitochondria are stained. Combined with the results of the *ARG8* assay, that requires localization of the chimeric protein to the mitochondrial matrix to restore arginine auxotrophy, it has been hypothesized that the Erg11$^{\Delta 150}$ construct is targeted as a soluble protein to the matrix or inserted at the inner mitochondrial membrane, exposing its C-terminus to the matrix. The latter conformation would be consistent with that of mammalian mitochondrial CYPs (Avadhani *et al.*, 2011). It will be interesting to test which factors of mitochondrial import machineries are important for the mitochondrial targeting of Erg11$^{\Delta 150}$, *e.g.* by fluorescence microscopy analysis of mCherry-tagged Erg11$^{\Delta 150}$ localization in mitochondrial import mutants, in the presence of appropriate FP-tagged control proteins of which the import mechanisms are known. As a starting point, mutants of the translocase of the outer mitochondrial membrane (TOM) complex could be tested, except for Tom40, which is essential (Baker *et al.*, 1990). As such, this assay could also identify possible mitochondrial interaction partners of the full-length protein, which might be more difficult to analyze, as full-length Erg11 does not clearly localize to mitochondria (as discussed below).

Although the MTS of *S. cerevisiae* and *C. albicans* is conserved, its function remains unclear. The results obtained in this study challenge the initial idea of Erg11 bimodal targeting to ER and mitochondria. FIB-SEM imaging of full-length Erg11 only visualizes its presence in the ER and in the vacuole. An alternative hypothesis to bimodal targeting might be that the MTS of Erg11 directs the protein to an ER-mitochondria interface, rather than truly localizing the protein to the mitochondria. Organelle contact sites have been intensely studied in recent years in various species and between various organelles and have become an emerging topic in molecular cell biology (Eisenberg-Bord *et al.*, 2016; Herrera-Cruz and Simmen, 2017). Their importance and the molecular machinery will undoubtedly become increasingly clear in the coming years. A relevant example is the tight interplay between ER and mitochondria with regard to lipid synthesis and homeostasis in mammals, *e.g.* the biosynthesis of steroid hormones in vertebrates depends on the ER for cholesterol production and on the mitochondria for conversion of this sterol to pregnenolone, which is subsequently redirected to the ER to produce steroid hormones. Although the transport mechanisms are still obscure, ER-mitochondria membrane proximity is important (Elbaz-Alon, 2017). Interestingly, some overlap has been observed between the ER-localized full-length Erg11-mCherry and the GFP-marked mitochondria during fluorescence microscopy studies. Similarly, full-length Erg11 grown in the presence of FLC shows close apposition to mitochondria in electron micrographs. Despite the need for additional experiments, the idea that Erg11 could be present at ER-mitochondria contact sites is credible and is supported by other examples. As discussed in Chapter 3, several lipid biosynthesis genes have been characterized to localize to MAMs, which are ER subdomains that are in close contact to mitochondrial membranes. The finding that the mammalian protein DGAT2 localizes to MAMs is based on fluorescence microscopy data, similar to our approach and on purification of MAMs by biochemical fractionation and subsequent analysis of the protein of interest in the isolated fractions through western blotting. Similarly, the identification of the yeast enzymes phosphatidylserine and phosphatidylinositol synthase to MAMs is based on isolation of the MAMs. This could be a valuable approach to examine whether the MTS has a role in the possible association of Erg11 with mitochondrial membranes. Interestingly, preliminary results obtained in our lab from purification experiments of mitochondria have shown that full-length Erg11 can be detected in mitochondrial fractions, as also described by Craven *et al.* (2007), further validating the hypothesis that Erg11 could be associated in its full-length form with mitochondria at organelle contact sites. Additionally, the redox partner of Erg11, Ncp1 has been identified in the most recent mitochondrial proteome study as a mitochondria-associated protein, indicating that both could localize to MAM domains (Morgenstern *et al.*, 2017).

Also in DGAT2, an MTS has been identified, that when fused to RFP could target this moiety to mitochondria. Similar to the conservation of the CYP51 MTS across species, the identified positively charged residues that constitute the MTS in DGAT2 are highly conserved, which stresses their importance to the biology of the protein (Stone *et al.*, 2009). Ideally, when more information on proteins with non-canonical MTSs is available, these data could be gathered in a database to

potentially predict such sites in other proteins. This could complement the available tools that already exist to predict 'canonical' N-terminal mitochondrial targeting signals.

Nevertheless, the option remains that the MTS has no significance to the localization of Erg11 *in vivo*. It has been shown that about 25% of randomly generated sequences of 26 nucleotides are sufficient to serve as an MTS when placed in front of MTS-devoid cytochrome oxidase subunit IV (Lemire *et al.*, 1989). As such, the presence of the MTS in Erg11 could be accidental and not of physiological importance to its localization. Including the Erg11**** mutant during MAM purification studies could shed more light on this issue. This mutant carries lysine to alanine substitutions at K151, K152, K155 and K160, which have been identified as determinants for the mitochondrial targeting of Erg11$^{\Delta 150}$. Also in the full-length protein, these lysine residues have been shown to affect Erg11 biology, as cells expressing Erg11**** produce low levels of ergosterol. Based on crystallization data, it has been predicted that these lysine residues are important to the interaction of wild type Erg11 with its redox partner, and hence determine the functionality of the Erg11 protein. The importance of each individual lysine residue to ergosterol production on one hand and to mitochondrial targeting of the Erg11$^{\Delta 150}$ construct on the other hand could be tested, which should increase the understanding of the physiological role of these residues to Erg11 biology. As three of the four lysines of *S. cerevisiae* Erg11 are conserved within the fungal lineage and from fungi to mammals, it has been suggested that these may also play a role in the redox partner binding of other CYP51s.

The truncated version of Erg11 that exposes its MTS (Erg11$^{\Delta 150}$) is expected to lack lanosterol demethylase activity, as spores expressing this construct do not germinate. The deletion of the first 150 amino acids likely exposes the heme group of Erg11 to the environment, probably resulting in a catalytically inactive variant. Alternatively, the protein itself could be functional but lack an appropriate redox partner or substrate inside mitochondria. Unexpectedly, we have noticed that the sporulation of a diploid strain containing nothing but an HA-epitope at one of both *ERG11* alleles has resulted in colony formation of all four spores after tetrad dissection on SD medium, supplemented with auxotrophic amino acids. This result suggests that under these specific conditions the essentiality of the *ERG11* gene has been overcome, which is interesting for future *erg11* null studies. So far, the study of *erg11* mutants is restricted to working in an ***erg3Δ*** background, accepting its unwanted side effects, or working under anaerobic conditions to induce the uptake of necessary sterols from the environment (Bard *et al.*, 1993). Our preliminary data indicate that these hurdles can be overcome in an aerobic environment, however further experiments are necessary to validate this idea and to pinpoint the mechanisms that can explain this phenotype. Survival assays should be performed to test whether the obtained *erg11* null mutants remain viable. The genotypes of viable mutants should be examined, to exclude the possibility that these cells have accumulated mutations, *e.g.* in the *ERG3* gene and to test whether certain auxotrophy markers are associated with survival of the *erg11* mutants. It has been described by Crowley *et al.* (1996) for the ***erg24Δ*** mutant that YPD has an inhibitory effect on

growth of spores deleted for this ergosterol biosynthesis gene. Similarly, germination of *erg11* mutants is only obtained on minimal medium and not on complete synthetic medium or YPD. Moreover, we have observed that the size of the germinating Erg11**** colonies is clearly smaller on YPD and CSM compared to minimal medium, indicating that the phenotype might be related to amino acid availability.

6.2 Multiple Erg11 protein forms: a story of degradation

The process that generates the truncated Erg11 protein products has been examined, from the perspective of proteolytic processing. A screening has been set up in which deletion mutants of all non-essential proteases and peptidases of *S. cerevisiae* have been tested for a possible role in the formation process, through the detection of their Erg11 pattern on western blot. This has resulted in the identification of Pep4 and Prb1, which are well-characterized proteases executing the lysosomal activity of the vacuole (Moehle *et al.*, 1987; Nebes and Jones, 1991; Hirsch *et al.*, 1992; Rupp and Wolf, 1995; Wolff *et al.*, 1996; Naik *et al.*, 1997; Hecht *et al.*, 2014). Typically, Pep4 and Prb1 cleave a protein into shorter peptides, which are subsequently degraded to individual amino acids by vacuolar carboxypeptidases and aminopeptidases (Shen *et al.*, 2008). This could explain why truncated forms of Erg11 are visible on western blot. The hypothesis that Erg11 is degraded by Pep4 and Prb1 is further supported by i) an MS analysis of purified Erg11, which has identified 23 possible Erg11 N-termini. This high amount suggests that they are created in a cleavage process rather than by processes of alternative transcription or translation initiation. As such, these N-termini represent putative cleavage sites. The importance of the identified residues could be investigated further by mutational analysis. ii) Moreover, similar patterns of protein bands have been observed on western blot for other proteins and have been associated with Prb1 and Pep4 activity (Ziegler and Schwartz, 1991; Onodera and Ohsumi, 2004; Schuck *et al.*, 2014). iii) The use of the *pep4Δ prb1Δ* deletion strain allows experiments to be performed in the absence of additional Erg11 forms. It has been found that this strain has no remarkable deficiencies and behaves similar to the wild type under the conditions tested, *i.e.* growth, respiration and FLC susceptibility or tolerance. This further supports the idea that the additional Erg11 bands have no functional significance to the tested parameters.

The closest *C. albicans* homologs of *S. cerevisiae* Pep4 and Prb1 have been identified as Apr1 and Prb11/12, respectively. Examination of the corresponding null mutants has shown the importance of Apr1 and Prb12 for the turnover of *C. albicans* Erg11. Similar as observed for the *S. cerevisiae* protease mutants, the absence of Erg11 bands does not result in an altered susceptibility or tolerance towards FLC in the *C. albicans* mutants. Ultimately, as suggested by Prof. Sanglard, *C. albicans* clinical isolates with varying levels of azole tolerance (for example one with very high levels of tolerance and one with very low levels) could be HA-tagged at the *ERG11* locus and investigated on western blot to check for differences in the pattern of additional Erg11 bands, to definitely exclude the involvement of truncated Erg11 products in azole tolerance. However, the results obtained in this study are already convincing.

Pep4 is the key proteolytic activator, that initiates the maturation cascade of other vacuolar proteases, which are delivered to the vacuole as precursors. Remarkably, all other vacuolar

proteases, such as CPY have also been tested in our screening and have not shown involvement in the formation of additional Erg11 forms on western blot. It is assumed that Prb1 is the actual cleaver of Erg11. In a *pep4Δ* deletion strain, very little to no active Prb1 is produced. This is not true the other way around, where active Pep4 can be present in a *prb1Δ* deletion mutant (Rupp and Wolf, 1995). Both *pep4Δ* and *prb1Δ* are in fact thus defective in Prb1, resulting in a similar phenotype on western blot, *i.e.* the absence of Erg11 forms. A closer look at the western blot results of the single deletion strains indicates a shifted pattern of very faint additional Erg11 bands in the *prb1Δ* mutant, where active Pep4 or another protease might take over some of the Erg11 processing, leading to bands of a different size. On the other hand, the very faint additional Erg11 bands observed in the *pep4Δ* mutant are similar to those observed in wild type cells, likely produced by residual very low amounts of a catalytically active form of Prb1 (Mechler *et al.*, 1988). Moreover, qRT-PCR analysis of *ERG11*, *PRB1* and *PEP4* expression in the absence or presence of FLC demonstrates a significant upregulation of *ERG11* and *PRB1* expression but not of *PEP4* expression under FLC treatment in wild type cells, indicating that the increased transcription of *PRB1* might be partly responsible for the generation of the additional Erg11 products. However, no additional studies on the direct cleavage of Erg11 by Prb1 have been performed. This could be done, *e.g.* by purifying both proteins and testing cleavage of the purified Erg11 protein *in vitro*, by subsequently investigating the samples on western blot.

In literature, two ways have been described to directly measure ER stress, one of which is electron microscopy, as used here (Oslowski and Urano, 2011). It has already been described that overproduction of certain CYPs leads to ER expansion, in various species (Sandig *et al.*, 1999). In this study, it has been shown for the first time that upregulation of *S. cerevisiae* Erg11 leads to a similar effect. For the first time, protein localization studies by FIB-SEM have been performed in *S. cerevisiae*, by fusing Erg11 to the APEX2-tag. Full-length Erg11-APEX2 localizes to the ER and to ER whorls, which are concentric, multilayered ER membrane structures. It thus seems that overexpression of Erg11 causes ER abnormalities that are coped with by ER proliferation. Interestingly, overexpression of other ER-localized enzymes important to lipid biosynthesis, such as Hmg1/2 and cytochrome b_5 has also been described to lead to ER expansion and the observation of multilayered ER membrane structures (Wright *et al.*, 1988; Vergeres *et al.*, 1993). In this regard, FLC can be seen as an ER stress inducing agent, which has also been indicated by others, as it induces Erg11 production (Dudgeon *et al.*, 2008; Kim *et al.*, 2012). To restore ER homeostasis, excess Erg11 will be delivered to the vacuole for degradation by transport through whorls, a process described as ER-phagy by Schuck *et al.* (2014), following the hypothesis that the additional Erg11 forms are non-functional degradation products. FIB-SEM further supports this hypothesis as the Erg11-APEX2 signal in whorls is partly observed inside vacuoles. As specifically Prb1 is important for the clearance of autophagic bodies in the vacuole, it might also be responsible for the clearance of whorls (Takeshige *et al.*, 1992).

6.3 The contribution of this study to optimized antifungal therapy

The major findings in this study focus on the identification of the Erg11 MTS and the degradation of the Erg11 protein by the vacuolar Prb1 and Pep4 proteases. Both aspects open up new possibilities towards enhanced efficacy of azole antifungal therapy. i) The MTS of Erg11 might be important to the localization of the protein. Further analysis could identify interacting proteins or molecular requirements of this process that could be targeted simultaneously with azole treatment, to further enhance the antifungal effect, if the localization of Erg11 or its interaction with mitochondrial partners is important to its function. This idea is based on the fact that azole-treated cells can still produce low levels of ergosterol (as depicted in Fig. 3.14), which might control cell survival under azole drug treatment. ii) Even if the MTS is not important to Erg11 localization, it is important to the functionality of the protein, as demonstrated by the strong reduction in ergosterol biosynthesis of the Erg11**** mutant. The analysis of the importance of the lysine residues to the activity of Erg11 might be useful information for the synthesis of azole drugs with enhanced activity. iii) The deletion of *PRB1* and *PEP4* has no remarkable effect on *S. cerevisiae* cell growth in the presence of FLC, which is surprising as FLC induces ER stress. A similar observation has been made in a previous study, where a strain deficient for *PEP4* shows no growth defect under TUN-induced ER stress (Bernales *et al.*, 2006). However, cells that are unable to form autophagosomes could not grow under TUN treatment. Therefore, it has been suggested by the authors that the sequestration of excess ER by autophagic mechanisms is more important for cell survival than the actual degradation of the excess material. Further analysis of the ER-phagy machinery could thus be valuable to future antifungal therapies, as the targeting of earlier steps in ER-phagy could enhance the ER stressor effect of FLC and therefore could enhance azole therapy.

CHAPTER 7
MATERIALS AND METHODS

7.1 Materials

7.1.1 Growth media and conditions

S. cerevisiae cells were grown in rich yeast peptone dextrose (YPD) medium (1% yeast extract, 2% bacto peptone and 2% glucose), complete synthetic defined or drop out medium (0.079% CSM or 0.067% - 0.077% CSM drop out medium (MP Biomedicals) depending on the missing amino acid(s), 0.17% Difco yeast nitrogen base without amino acids and ammonium sulphate, 0.5% ammonium sulphate and 2% glucose, pH 5.5) or minimal synthetic defined (SD) medium (same composition as CSM, minus the amino acid source) supplemented with the necessary amino acids to complement the auxotrophies of the *S. cerevisiae* strains as described by (Sherman, 1991). For fluorescence microscopy, cells were cultured with 2% galactose instead of glucose, to induce the expression of the *ERG11-mCherry* constructs. To induce respiration, cells were grown on YP medium supplemented with 3% ethanol and 3% glycerol, instead of glucose. *C. albicans* cells were grown in YPD or SD medium. *C. albicans* FLC susceptibility assays were performed with RPMI medium (1640, Sigma) buffered with 0.165 M MOPS to pH 7 and with a final glucose concentration of 2%. Media were solidified by adding 1.5% agar and the pH was buffered to 6.5 for CSM and SD media. Cells were incubated at 30°C, except when cells were induced to sporulate on sporulation medium (1% KAc, 0.05% $KHCO_3$, 1.5% agar, adjusted to pH 6 by HCl) at 23°C or during *C. albicans* Etests at 37°C. Fluconazole (Sigma) was added at a concentration of 20 µg/mL for *S. cerevisiae* experiments, unless specified otherwise and at 10 µg/mL for *C. albicans* experiments. Voriconazole (Sigma) was used at a concentration of 1 and 5 µg/mL and ketoconazole (Sigma) at 1, 10 and 20 µg/mL. Amphotericin B (Sigma) was added to cells at a concentration of 1 and 5 µg/mL and caspofungin (Merck Sharp & Dohme) at a concentration of 1, 5 or 10 µg/mL. Tunicamycin (Sigma) was added at 5, 10 or 20 µg/mL. Anhydrotetracycline (ATC) hydrochloride was added at 3 µg/mL (Sigma). Cultures treated with these chemicals were grown in the dark.

7.1.2 Strains

The strains used in this study are listed in Table 7.1. The ***arg8Δ*** strain was created by amplifying a KanMX deletion cassette with primers B-5 and B-6 and transforming the PCR product to the BY4742 strain, generating strain AFC206a.

One of both *ERG11* alleles of BY4743 was replaced by a G1-flanked nourseothricin marker, amplified from plasmid 2589 with primers C-2429 and C-2430, creating strain IP-S1. The G1 sites are targeted by Cas9 expressed from plasmid 2539, so that the nourseothricin marker can be replaced by a donor template. The Cas9 is guided to the G1 sites by the sgRNA present on plasmid 2586. The donor templates were amplified from pBEVY-L plasmids carrying *ERG11-HA*, *ERG11****-HA*, *Erg11$^{\Delta 150}$-HA*, *Erg11$^{\Delta 150****}$-HA* and *Erg11$^{\Delta 74}$-HA*, with C-3423, C-3425, C-3426 or C-3424 as

forward primer and C-3428 as reverse primer. The HA-tag only was amplified with primers C-3427 and C-3428. The Cas9 plasmid, the sgRNA plasmid and the donor template were simultaneously transformed to IP-S1. Correct transformants were serially grown in YPD until both plasmids were lost. This resulted in the diploid strains IP-S2, IP-S3, IP-S4, IP-S5, IP-S6 and IP-S7, containing one wild type *ERG11* allele and the other replaced by *ERG11-HA*, *ERG11****-HA*, *Erg11$^{\Delta 150}$-HA*, *Erg11$^{\Delta 150****}$-HA* or *Erg11$^{\Delta 74}$-HA* or solely the HA-tag, respectively.

KanMX deletion cassettes for *SOM1*, *HSP32* and *HSP33* were amplified from plasmid 2593 with primers B-8029/B-8031, B-8030/B-8033 and B-8030/B-8032, respectively and transformed to AFC202, creating strains IP-S8, IP-S9 and IP-S10. Correct transformants were tested on western blot for the presence of additional Erg11 forms.

Deletion cassettes for *PRB1* and *PEP4* were amplified from plasmids 2591 and 2593 with primers C-2501/C-2502 and C-2503/C-2504, respectively and transformed to AFC202, generating strains WK-S1 and WK-S2. WK-S2 was subsequently transformed with a *PRB1* deletion cassette and the other way around, generating double mutants WK-S3 and WK-S4. The Erg11 pattern of three independent *prb1Δ*, *pep4Δ* and *prb1 pep4Δ* transformants was examined on western blot.

AFA79a was created by amplifying the 3xHA-tag associated to a *URA3* marker from plasmid pFA-3xHA-URA with primers B-1544 and B-1545 and transforming this cassette to the wild type CAI4 strain. *prb12* mutants were obtained via the *SAT1* flipper method and CRISPR-Cas9. For the *SAT1* flipper method, the pSFS2 plasmid was used (Reuss *et al.*, 2004). The promoter and terminator of *PRB12* were inserted 5' and 3' of the deletion cassette on pSFS2, which is flanked by FRT sites. The *PRB12* promoter was amplified from SC5314 genomic DNA (gDNA) with the primer pair B-7946/B-7947 with flanking ApaI-XhoI restriction sites. Both pSFS2 and the PCR were cut with ApaI and XhoI, ligated and transformed to *E. coli* DH5α. The resulting plasmid was verified. Similarly, the *PRB12* terminator was amplified from SC5314 gDNA with the primer pair B-7950/B-7951 with SacII-SacI flanking sites. The *PRB12*prom-containing pSFS2 and the PCR were cut with SacII and SacI, ligated and transformed to DH5α. The resulting plasmid was verified and subsequently transformed after linearization to AFA79a for the deletion of *PRB12*. Transformants were obtained on 200 µg/mL nourseothricin. Transformants carrying the *prb12* deletion were induced to lose the deletion cassette by growth on non-selective medium and were subsequently plated on 25 µg/mL nourseothricin to isolate those transformants that did. Subsequently, the heterozygous *PRB12*/*prb12Δ* strain was retransformed with the *PRB12* linearized deletion vector and all steps were repeated to obtain *prb12Δ/Δ* mutants, creating strain WK-C1.

Alternatively, *prb12* as well as *apr1* and *prb11* null mutants were obtained by the method of CRISPR-Cas9, where a double STOP codon was introduced early in the gene sequence. Complementary sgRNA oligos were duplexed and ligated in BsmBI-cut pV1524, using the NEBuilder HiFi DNA Assembly Cloning Kit and transformed to *E. coli* DH5α, with selection on ampicillin and nourseothricin, as suggested by the authors (Vyas *et al.*, 2015; Vyas *et al.*, 2018).

The oligos for the sgRNA for *prb12* are C-1448/C-1449, for *apr1* are C-1446/C-1447 and for *prb11* are C-1450/C-1451. Correct plasmids were linearized with SacI/KpnI restriction and transformed to AFA79a in combination with the donor DNA by a hybrid protocol of lithium acetate and electroporation as described in (Vyas *et al.*, 2018). Donor DNA was obtained by amplifying oligos on each other with primer pairs C-1520/C-1521 for *prb12*, C-1518/C-1519 for *apr1* and C-1522/C-1523 for *prb11* mutants. Transformants were obtained on 200 µg/mL nourseothricin, generating strains WK-C2/3/4. Loss of the integrated Cas9/sgRNA cassette could not be induced, not even when cells were grown in YP with 2% maltose for several generations.

7.1.3 Plasmids

The plasmids used in this study are listed in Table 7.2. To examine the Erg11-V5 constructs on western blot, plasmids pAFC122, pAFC124, pAFC125 and pAFC123 were constructed by cloning BamHI-PstI PCR-amplified *ERG11-3xV5* DNA fragments in pCM252. All fragments were amplified with the same reverse primer B-1610 and with construct-specific forward primers B-1608, B-3362, B-3363 and B-3361, respectively. *ERG11-3xV5* was also amplified with B-1608/B-1610 and cloned BamHI-PstI in pBEVY-L, creating pAFC118. In pAFC118, the four lysines of the cryptic *ERG11* MTS were replaced by alanines, creating pAFC142, by *in vivo* cloning of a B-5030/B-5031 primer-extended fragment into XbaI-cut pAFC118. BamHI-*ERG11******-3xV5*-PstI from pAFC142 was cut and ligated into pCM252, creating pIP1. Subsequently, plasmids pAFC122, pAFC124, pAFC125, pAFC123 and pIP1 were transformed to W303.

Full-length *ARG8* was amplified from BY4742 gDNA with primers B-8727 and B-386 and BamHI-PstI cloned into pBEVY-U, creating pIP2. Similarly, plasmid pAFC108 was made by BamHI-PstI cloning of PCR-amplified *ARG8*$^{\Delta 13}$ from BY4742 gDNA with primers B-385 and B-386 in pBEVY-U. These plasmids, as well as the empty vector pBEVY-U were transformed to strain AFC206a. The *ERG11-ARG8*$^{\Delta 13}$ chimeras were made by *in vivo* cloning. For the full-length *ERG11- ARG8*$^{\Delta 13}$ construct, *ERG11* was PCR amplified from BY4742 gDNA with primers B-8728/B-8729 and transformed to AFC206a together with BamHI-cut pAFC108, creating pIP3. Similarly, for the *ERG11*$^{\Delta 150****}$*-ARG8*$^{\Delta 13}$ construct, *ERG11*$^{\Delta 150****}$ was amplified with primers B-8732 and B-8729 from plasmid pAFC142 and co-transformed with BamHI-cut pAFC108 in AFC206a, creating pIP6. For the *ERG11*$^{\Delta 74}$*-ARG8*$^{\Delta 13}$ construct, *ERG11*$^{\Delta 74}$ was amplified from gDNA with primers B-8731 and B-8729 and co-transformed with BamHI-cut pAFC108 in AFC206a, creating pIP7. The negative control plasmid pAFC110, containing *SEC61-ARG8*$^{\Delta 13}$ was created by amplifying *SEC61* from BY4742 gDNA with primers B-387 and B-388 and co-transforming the PCR with BamHI-cut pAFC108 in AFC206a. Plasmid pAFC136 was created by amplifying the MTS region of *ERG11* with primers B-4106 and B-4107 from BY4742 gDNA and transforming it together with BamHI-cut pAFC108 in AFC206a. The *ERG11******-ARG8*$^{\Delta 13}$, *ERG11*$^{\Delta 150}$*- ARG8*$^{\Delta 13}$ and MTS*****- ARG8*$^{\Delta 13}$ constructs were made with NEBuilder. *ERG11***** was amplified from plasmid pAFC142 with primers B-9670 and B-9671 and ligated into BamHI-cut pAFC108 and transformed to *E. coli* TOP10,

creating pIP4. Similarly, pIP5 was constructed by amplifying *ERG11*$^{\Delta 150}$ from BY4742 gDNA with primers B-9672 and B-9671 and ligating it into BamHI-cut pAFC108 and transforming it to *E. coli* TOP10. Similarly, plasmid pIP8 was created by amplifying the MTS**** from pAFC142 with primers B-4106 and C-5589 and ligating it into BamHI-cut pAFC108 and transforming it to *E. coli* TOP10. Correct plasmids were subsequently transformed to AFC206a.

For FIB-SEM imaging, the *ERG11-V5* and *ERG11*$^{\Delta 150}$*-V5* portions were amplified from plasmids pAFC122 and pAFC124, respectively with primer pairs B-9943/B-9947 and B-9944/B-9947. The PCRs were ligated into BamHI-XbaI-cut pBEVY-L. APEX2 with XbaI and PstI restriction sites was ordered as a gBlock (Integrated DNA Technologies) and ligated into pBEVY-L to create pIP9. Next, APEX2 was PCR amplified with primers C-22 and C-23 from pIP9 and ligated C-terminally to the *ERG11-V5* and *ERG11*$^{\Delta 150}$*-V5* constructs in pBEVY-L, that were cut with SalI-PstI, generating the *ERG11-V5-APEX2* and *ERG11*$^{\Delta 150}$*-V5-APEX2* plasmids using NEBuilder (pIP10 and pIP11). The control construct pIP12 with *ERG11-V5* lacking the APEX2-tag was constructed by amplifying *ERG11-V5* from plasmid pAFC122 with primers B-9943 and C-29 and ligating it into BamHI-XbaI-cut pBEVY-L with NEBuilder. The ligations were transformed to *E. coli* TOP10 and correct plasmids were subsequently transformed to AFC202.

The 3xV5 tag was replaced for mCherry in PstI-cut plasmids pAFC122, pAFC124, pAFC125 and pAFC123 by *in vivo* cloning of a DNA-amplified fragment with primers A-9921 and B-3784 on template yEpGAP-Cherry. The resulting fusions were extracted as BamHI fragments from the corresponding plasmids and cloned into pBEVY-GL, creating pAFC130, pAFC132, pAFC133 and pAFC131, respectively. *ERG11******-mCherry* was constructed by amplifying *ERG11* from pAFC130 with overlapping primer sets C-2505/C2508 and C-2506/C-2507 and ligating these into BamHI-cut pAFC130 with NEBuilder, creating pIP13. The constructed plasmids were transformed to W303.

The BamHI-PstI *ERG11-3xV5* fragments from plasmids pAFC122-125 and pAFC142 were cut and ligated into BamHI-PstI-cut pBEVY-L and transformed to *E. coli* DH5α. Next, these plasmids were cut by PstI and HindIII and ligated with NEBuilder to a 3xHA-tag DNA fragment with *ERG11* flanking regions obtained from AFC202 gDNA with the forward primer C-562 and the reverse primer C-1075, generating plasmids that contain *ERG11-HA*, *ERG11******-HA*, *Erg11*$^{\Delta 150}$*-HA*, *Erg11*$^{\Delta 150****}$*-HA* and *Erg11*$^{\Delta 74}$*-HA* in pBEVY-L, pWK1 – pWK5. Plasmids pWK1 and pWK3 were subsequently transformed to AFC202 for a FLC tolerance assay and pWK1 to BY4742 for the MS analysis of purified Erg11.

PRB1 was amplified including its promoter and terminator region from BY4742 gDNA with flanking XbaI-BamHI restriction sites with primers B-7839 and B-7840. Next, the PCR and yCplac111 were XbaI/BamHI-cut, ligated and transformed to *E. coli* DH5α, creating plasmid pWK6. *PEP4* was amplified with its promoter and terminator regions from gDNA with primer pair C-3334/C-3335 and primer pair C-3336/C-3335 to ligate it into BamHI-cut yCplac111 or *PRB1*-containing yCplac111 (pWK6), respectively with NEBuilder and subsequently transform it to *E. coli* TOP10, creating

plasmids pIP14 and pIP15. The constructed plasmids were verified and subsequently transformed to *prb1Δ*, *pep4Δ* or *prb1Δ pep4Δ* strains or to the wild type AFC202 strain.

7.1.4 Primers

The primers used in this study, as well as other DNA sequences are listed in Table 7.3.

Table 7.1. *S. cerevisiae* and *C. albicans* strains used in this study.

Strain	Genotype	Source or Ref
S. cerevisiae		
BY4742	MATα *his3Δ1 leu2Δ0 lys2Δ0 ura3Δ0*	Euroscarf
BY4743	MATa/α *his3Δ1/his3Δ1 leu2Δ0/leu2Δ0 LYS2/lys2Δ0 met15Δ0/MET15 ura3Δ0/ura3Δ0*	Euroscarf
W303	MATa *ura3-1 leu2-3,112 trp1-1 his3-11,15 ade2-1 can1-100*	Lange *et al.* (2000)
AFC202	Same as BY4742 with *ERG11::ERG11-3xHA*	Demuyser *et al.* (2017)
AFC206a	Same as BY4742 with *ARG8::KANMX*	Fiori A. (unpublished)
IP-S1	Same as BY4743 with *ERG11/ERG11::NAT*	This study
IP-S2	Same as BY4743 with *ERG11/ERG11::ERG11-HA*	This study
IP-S3	Same as BY4743 with *ERG11/ERG11::ERG11****-HA*	This study
IP-S4	Same as BY4743 with *ERG11/ERG11::ERG11$^{\Delta 150}$-HA*	This study
IP-S5	Same as BY4743 with *ERG11/ERG11::ERG11$^{\Delta 150****}$-HA*	This study
IP-S6	Same as BY4743 with *ERG11/ERG11::ERG11$^{\Delta 74}$-HA*	This study
IP-S7	Same as BY4743 with *ERG11/ERG11::3xHA*	This study
IP-S8A	Same as AFC202 but *SOM1::KANMX*	This study
IP-S8B	Same as AFC202 but *SOM1::KANMX*	This study
IP-S8C	Same as AFC202 but *SOM1::KANMX*	This study
IP-S9A	Same as AFC202 but *HSP32::KANMX*	This study
IP-S9B	Same as AFC202 but *HSP32::KANMX*	This study
IP-S9C	Same as AFC202 but *HSP32::KANMX*	This study
IP-S10A	Same as AFC202 but *HSP33::KANMX*	This study
IP-S10B	Same as AFC202 but *HSP33::KANMX*	This study
IP-S10C	Same as AFC202 but *HSP33::KANMX*	This study
WK-S1A	Same as AFC202 but *PRB1::HPH*	This study
WK-S1B	Same as AFC202 but *PRB1::HPH*	This study
WK-S1C	Same as AFC202 but *PRB1::HPH*	This study
WK-S2A	Same as AFC202 but *PEP4::KANMX*	This study
WK-S2B	Same as AFC202 but *PEP4::KANMX*	This study
WK-S2C	Same as AFC202 but *PEP4::KANMX*	This study
WK-S3A	Same as WK-S2 with *PRB1::HPH*	This study
WK-S3B	Same as WK-S2 with *PRB1::HPH*	This study
WK-S4	Same as WK-S1 with *PEP4::KANMX*	This study
WK-S5A	Spore of IP-S2, MATα *his3Δ1; leu2Δ0; ura3Δ0; ERG11::ERG11-3xHA*	This study

WK-S5B	Spore of IP-S2, MATα *his3Δ1; leu2Δ0; ura3Δ0; ERG11::ERG11-3xHA*	This study
WK-S5C	Spore of IP-S2, MATα *his3Δ1; leu2Δ0; ura3Δ0; ERG11::ERG11-3xHA*	This study
WK-S5D	Spore of IP-S2, MATα *his3Δ1; leu2Δ0; ura3Δ0; ERG11::ERG11-3xHA*	This study
WK-S6A	Spore of IP-S3, MATα *his3Δ1; leu2Δ0; ura3Δ0; ERG11::ERG11****-3xHA*	This study
WK-S6B	Spore of IP-S3, MATα *his3Δ1; leu2Δ0; ura3Δ0; ERG11::ERG11****-3xHA*	This study
WK-S6C	Spore of IP-S3, MATα *his3Δ1; leu2Δ0; ura3Δ0; ERG11::ERG11****-3xHA*	This study
WK-S6D	Spore of IP-S3, MATα *his3Δ1; leu2Δ0; ura3Δ0; ERG11::ERG11****-3xHA*	This study
C. albicans		
CAI4	*URA3::imm434/URA3::imm434 IRO1/IRO1::imm434*	Fonzi and Irwin (1993)
AFA79a	Same as CAI4 with *ERG11/ERG11::ERG11-3xHA-URA3*	Fiori A. (unpublished)
WK-C1	Same as AFA79a with *PRB12::FRT/PRB12::FRT*	This study
WK-C2A	Same as AFA79a with *PRB12::prb12/PRB12::prb12*	This study
WK-C2B	Same as AFA79a with *PRB12::prb12/PRB12::prb12*	This study
WK-C3A	Same as AFA79a with *PRB11::prb11/PRB11::prb11*	This study
WK-C3B	Same as AFA79a with *PRB11::prb11/PRB11::prb11*	This study
WK-C3C	Same as AFA79a with *PRB11::prb11/PRB11::prb11*	This study
WK-C4	Same as AFA79a with *APR1::apr1/APR1::apr1*	This study

Table 7.2. Plasmids used in this study.

Plasmid	Description	Vector	Source or Ref
2539	Cas9-KanMX	pTEF	MCB collection
2586	sgRNA G1	pgRNA	MCB collection
2589	A1-G1-B-NAT-P-G1-A2	pTOPO2.1	MCB collection
2591	A1-G1-B-HPH-P-G1-A2	pTOPO2.1	MCB collection
2593	A1-G2-B-KanMX-P-G2-A2	pTOPO2.1	MCB collection
pAFC88	*ERG11*	yEplac181	Fiori and Van Dijck (2012)
pAFC108	*GPD1prom::ARG8$^{\Delta 13}$*	pBEVY-U	Fiori A. (unpublished)
pAFC110	*GPD1prom::SEC61- ARG8$^{\Delta 13}$*	pBEVY-U	Fiori A. (unpublished)
pAFC118	*GPD1prom::ERG11-3xV5*	pBEVY-L	Fiori A. (unpublished)
pAFC122	*tetO$_7$prom::ERG11-3xV5*	pCM252	Fiori A. (unpublished)
pAFC123	*tetO$_7$prom::ERG11$^{\Delta 74}$-3xV5*	pCM252	Fiori A. (unpublished)
pAFC124	*tetO$_7$prom::ERG11$^{\Delta 150}$-3xV5*	pCM252	Fiori A. (unpublished)
pAFC125	*tetO$_7$prom::ERG11$^{\Delta 150****}$-3xV5*	pCM252	Fiori A. (unpublished)
pAFC130	*GAL1,10prom::ERG11-mCherry*	pBEVY-GL	Fiori A. (unpublished)
pAFC131	*GAL1,10prom::ERG11$^{\Delta 74}$- mCherry*	pBEVY-GL	Fiori A. (unpublished)
pAFC132	*GAL1,10prom::ERG11$^{\Delta 150}$- mCherry*	pBEVY-GL	Fiori A. (unpublished)
pAFC133	*GAL1,10prom::ERG11$^{\Delta 150****}$-mCherry*	pBEVY-GL	Fiori A. (unpublished)
pAFC136	*GPD1prom::MTS^{ERG11}-ARG8$^{\Delta 13}$*	pBEVY-U	Fiori A. (unpublished)
pAFC142	*GPD1prom::ERG11****-3xV5*	pBEVY-L	Fiori A. (unpublished)
pIP1	*tetO$_7$prom::ERG11****-3xV5*	pCM252	This study
pIP2	*GPD1prom::ARG8*	pBEVY-U	This study
pIP3	*GPD1prom::ERG11- ARG8$^{\Delta 13}$*	pBEVY-U	This study
pIP4	*GPD1prom::ERG11****- ARG8$^{\Delta 13}$*	pBEVY-U	This study
pIP5	*GPD1prom::ERG11$^{\Delta 150}$- ARG8$^{\Delta 13}$*	pBEVY-U	This study
pIP6	*GPD1prom::ERG11$^{\Delta 150****}$- ARG8$^{\Delta 13}$*	pBEVY-U	This study
pIP7	*GPD1prom::ERG11$^{\Delta 74}$- ARG8$^{\Delta 13}$*	pBEVY-U	This study
pIP8	*GPD1prom::MTS^{ERG11****}-ARG8$^{\Delta 13}$*	pBEVY-U	This study
pIP9	APEX2	pBEVY-L	This study
pIP10	*GPD1prom::ERG11-V5-APEX2*	pBEVY-L	This study
pIP11	*GPD1prom::ERG11$^{\Delta 150}$-V5-APEX2*	pBEVY-L	This study
pIP12	*GPD1prom::ERG11-V5*	pBEVY-L	This study
pIP13	*GAL1,10prom::ERG11****-mCherry*	pBEVY-GL	This study
pIP14	*PEP4*	yCplac111	This study
pIP15	*PRB1 and PEP4*	yCplac111	This study
pWK1	*GPD1prom::ERG11-3xHA*	pBEVY-L	This study
pWK2	*GPD1prom::ERG11****-3xHA*	pBEVY-L	This study
pWK3	*GPD1prom::ERG11$^{\Delta 150}$-3xHA*	pBEVY-L	This study
pWK4	*GPD1prom::ERG11$^{\Delta 150****}$-3xHA*	pBEVY-L	This study
pWK5	*GPD1prom::ERG11$^{\Delta 74}$-3xHA*	pBEVY-L	This study
pWK6	*PRB1*	yCplac111	This study

Table 7.3. Primers and other nucleotide sequences used in this study.

Primer	Sequence	Description in database
A-9921	CCGGTCCAGCCAAGATCATCTGGGAAAAGAGAAATCCAG AACAAAAGATCATGGTTTCAAAAGGTGAAGAAG	CHERRY-ERG11-fus-f
B-5	TGCGAACATTTTTTTCGTTTGTTAGAATAATTCAAGAATCG CTACCAATCCGTACGCTGCAGGTCGAC	ARG8-S1
B-6	AGACGCACCACATGTACATATCACGTAAGATGTTCCTATG TGTCTCTGACATCGATGAATTCGAGCTCG	ARG8-S2
B-385	GGGGGATCCATGTTTACAAGCATTTTAGAGGAAAAG	ARG8short-s
B-386	GGCTGCAGTTAAGCGTAAACCGCTTCAATA	ARG8-as
B-387	TTATAGTTAGTCTTTTTTTTTAGTTTTAAAACACCAAGAACT TAGTTTCGATGTCCTCCAACCGTGTTCT	SEC61-ARG8short fus_f
B-388	CTAGAGTAAGTGGTCACTTGAAAGGCCTTTTCCTCTAAAAT GCTTGTAAACATCAAATCAGAAAATCCTGGA	SEC61-ARG8short fus_r
B-1544	TGATGGTTATAAAGTGCCTGACCCTGATTATAGTTCAATG GTGGTTTTACCTACTGAACCAGCAGAAATCATTTGGGAAA AAAGAGAAACTTGTATGTTTGGTGCTGGCGCAGGTGCTTC	CAERG11-3XHA-S1
B-1545	TATGTATATGTATATGTGTATATGTGTATATGTGTTAATCCA ACTAAGTAACAAAATGAAAACAATCTGAACACTGAATCGAA AGAAAGTTGCCGTTTTATCTGATATCATCGATGAATTCGAG	CAERG11-3XHA-S2
B-1608	GGGGGATCCATGTCTGCTACCAAGTCAATC	ERG11-Bam_s
B-1610	GGCTGCAGTTAACTAGTTGTTGAATCAAGTCC	ERG11-Pst-as
B-3361	GGGGGATCCATGAAGCCATACGAGTTTTTCG	ERG11-Bam-74_s
B-3362	GGGGGATCCATGAAGAAGTTTGTTAAGGGTGCTC	ERG11-Bam150_s
B-3363	GGGGGATCCATGGCTGCTTTTGTTGCTGGTGCTCTAACC GCTGAAGCCTTCAAGAGCTACGT	ERG11-Bam150MTSko_s
B-3784	CGTGAATGTAAGCGTGACATAACTAATTACATGATGCGGC CCTCCTGCAGCGAAGGAAGGAGCACAGAC	CHERRY-ERG11-fus-r2
B-4106	TCACTTGAAAGGCCTTTTCCTCTAAAATGCTTGTAAACATc acgtcaatagtaccagtagt	ERGMTSARGs
B-4107	AGTTTTAAAACACCAAGAACTTAGTTTCGACGGATCCatgga gcaaaagaagtttgttaa	ERGMTSARGas
B-5030	TCGGTAAAGGTGTTATTTACGATTGTCCAAATTCTAGATTG ATGGAGCAAGCTGCTTTTGTTGCTGGTGCTCTAA	ERG11-MTSko-s
B-5031	TACTTGTACACTTCTTCAGCAATCAATGGAACGTAGCTCTT GAAGGCTTCAGCGGTTAGAGCACCAGCAACAAAA	ERG11-MTSko-as
B-7839	gctctagaCCTACTATGCACTTATGCC	PRB1-Xba-For
B-7840	cgcggatccTGATCAGATAAGTGATCTGC	PRB1-BamH-Rev
B-7946	aatttgggcccGATAAGGACTTGCTGTTG	CaPRB12prom-F
B-7947	ccgctcgagCAATAGAAGTGTAAGCAGG	CaPRB12prom-R
B-7950	tccccgcggTTCAATGGTGCTGGTCA	CaPRB12term-F
B-7951	cgagctcGGTTTATAGTATGAAGGG	CaPRB12term-R
B-8029	AAGAGAAGGAAAGAAAGACTCATCTATCGCAGATAAGACA ATCAACCCTCAGCCGTTATGGCGGGCATC	SOM1del-Fw
B-8030	TATTTCTAGAACACTTTTCTCCTTCATTCAAAAAGAAAACT GGCCTTGCAAGCCGTTATGGCGGGCATC	HSP32/33del-Fw
B-8031	AAAATTTTTTATTTATCACACTACTGTGCTATATAGAGTATA TGTAATTTGTGGTCGGCTGGAGATCGG	SOM1del-Rev
B-8032	ACTGAAAGTCATTAAAAGCCTCCCCTTCAACAATTCCCTTG TCTTTTGTTGTGGTCGGCTGGAGATCGG	HSP33del-Rev

B-8033	ACTGAAAGCCATTAGAAGCCTCCCCTTCAACAATTCCCTTGTCTTTTGTTGTGGTCGGCTGGAGATCGG	HSP32del-Rev
B-8727	cgcggatccATGTTTAAAAGATATTTATCC	ARG8-Fw
B-8728	AGTTTTAAAACACCAAGAACTTAGTTTCGACGGATCCATGTCTGCTACCAAGTCAATC	FL_ERG11-ARG8N13_FW
B-8729	TCACTTGAAAGGCCTTTTCCTCTAAAATGCTTGTAAAGATCTTTTGTTCTGGATTTC	FL_ERG11-ARG8N13_Rev
B-8731	AGTTTTAAAACACCAAGAACTTAGTTTCGACGGATCCATGAAGCCATACGAGTTTTTCG	74ERG11-ARG8N13_FW
B-8732	AGTTTTAAAACACCAAGAACTTAGTTTCGACGGATCCATGGCTGCTTTTGTTGCTGGTGCTCTAACCGCTGAAGCCTTCAAGAGCTACGT	150ERG11MTSko-ARG8N13_FW
B-9670	CACCAAGAACTTAGTTTCGACGGATCCATGTCTGCTACCAAGTCAATC	FL_ERG11-ARG8N13_FW short
B-9671	TCCTCTAAAATGCTTGTAAAGATCTTTTGTTCTGGATTTC	FL_ERG11-ARG8N13_Rev short
B-9672	CACCAAGAACTTAGTTTCGACGGATCCATGAAGAAGTTTGTTAAGGGTGCTC	150ERG11-ARG8N13_FW short
B-9943	AGAACTTAGTTTCGACGGATCCATGTCTGCTACCAAGTCAATC	Gibson_Erg11-V5
B-9944	AGAACTTAGTTTCGACGGATCCATGAAGAAGTTTGTTAAGGGTGCTC	Gibson_N150Erg11-V5
B-9947	TGCCTGCAGGTCGACTCTAGAACTAGTTGTTGAATCAAGTCC	Gibson_V5-Rev
C-22	GGACTTGATTCAACAACTAGTGCAGCAGGAAAGTCTTACCCAACTGT	ScAPEX2_Fw
C-23	GAAGTCCAAAGCTTGCATGCCTGCAGGTCGACTCTAGATTAGGCATCAGCAAACCCAAG	ScAPEX2_Rev
C-29	TGCCTGCAGGTCGACTCTAGATTAACTAGTTGTTGAATCAAGTCC	Erg11-V5_STOP-Rev
C-562	ACAGGAAACAGCTATGACCATGATTACGCCCTGCAGTTAAGCGTAATCTGGAACGTCAT	ScErg11-V5-HA_Rev
C-1075	TGGGAAAAGAGAAATCCAGAACAAAAGATCGGGTACCCATACGATGTTCCTG	HAtag_Erg11inpBEVY-L
C-2429	CCACGTGAATGTACAACTTCTCTCTTTTTCTGTTTTTTTTTTTTTTCTCAGTTACAAACCGTGGTCGGCTGGAGATCGG	ERG11 deletion A1 - FW
C-2430	TTTTTTCCTTCACAATTGCAGCAGGCTTGAATAGAAACAGAACAAACGAGTAATACAAGGAGCCGTTATGGCGGGCATC	ERG11 deletion A2 - RV
C-2501	AGTCCAATTAGCTTCATCGCCAATAAAAAAACAAACTAAACCTAATTCTAACAAGCAAAGGTGGTCGGCTGGAGATCGG	ScPRB1del_Fw
C-2502	GAGACGCCTAAGGAAAGAAAAAGAAAAAAAAAAGCAGCTGAAATTTTTCTAAATGAAGAAAGCCGTTATGGCGGGCATC	ScPRB1del_Rev
C-2503	AAAAAGCCTAGTGACCTAGTATTTAATCCAAATAAAATTCAAACAAAAACCAAAACTAACGTGGTCGGCTGGAGATCGG	ScPEP4del_Fw
C-2504	CTTATAAAAGCTCTCTAGATGGCAGAAAAGGATAGGGCGGAGAAGTAAGAAAAGTTTAGCAGCCGTTATGGCGGGCATC	ScPEP4del_Rev
C-2505	AGCGGTTAGAGCACCAGCAACAAAAGCAGCTTGCTCCATCAATCTAGAAT	Erg11MTSko rv
C-2506	GCTGCTTTTGTTGCTGGTGCTCTAACCGCTGAAGCCTTCAAGAGCTACGT	Erg11MTSko fw
C-2507	CTTGCATGCCTGCAGGTCGA	pBEVY-GL-FW
C-2508	CTTCTTTGCGTCCATCCAAA	pBEVY-GL-RV
C-3334	GCTTGCATGCCTGCAGGTCGACTCTAGAGGATCCGAGCTCCTCAATTGTATTTGCTGAGG	Pep4only_Fw

C-3335	GACGTTGTAAAACGACGGCCAGTGAATTCGAGCTCGAAG TTGATCGTACAGAGGGCGATT	Pep4_Rev
C-3336	AAGTAACGTTGAGTATAGATACAGAAGCGGATCCGAGCTC CTCAATTGTATTTGCTGAGG	Pep4Prb1_Fw
C-3423	TTTTTTCCTTCACAATTGCAGCAGGCTTGAATAGAAACAGA ACAAACGAGTAATACAAGGATGTCTGCTACCAAGTCAATC	ERG11-HA-FW
C-3424	TTTTTTCCTTCACAATTGCAGCAGGCTTGAATAGAAACAGA ACAAACGAGTAATACAAGGATGAAGCCATACGAGTTTTTC G	delta 74 ERG11-HA FW
C-3425	TTTTTTCCTTCACAATTGCAGCAGGCTTGAATAGAAACAGA ACAAACGAGTAATACAAGGATGAAGAAGTTTGTTAAGGGT GCTC	delta 150 ERG11-HA FW
C-3426	TTTTTTCCTTCACAATTGCAGCAGGCTTGAATAGAAACAGA ACAAACGAGTAATACAAGGATGGCTGCTTTTGTTGCTGGT	delta 150 MTS ERG11-HA FW
C-3427	TTTTTTCCTTCACAATTGCAGCAGGCTTGAATAGAAACAGA ACAAACGAGTAATACAAGGATGgggtacccatacgatgttcc	only HA FW (no ERG11)
C-3428	CCACGTGAATGTACAACTTCTCTCTTTTTCTGTTTTTTTTTT TTTTCTCAGTTACAAACCTTAagcgtaatctggaacgtc	ERG11-HA-RV
C-5589	TTTTAAAACACCAAGAACTTAGTTTCGACGGATCCatggagca aGCTGCTTTTGTTGCT	ERGMTSko-ARG8as
sgRNA	**Sequence**	**Description in database**
C-1446	ACTTGCGTAAACTATTTTTAATTTGATGGGCCTTAGCGTCG ACTAGTTTTAGAGCTAGAAATAGCAAGTT	Gibson_Apr1_Fw
C-1447	AACTTGCTATTTCTAGCTCTAAAACTAGTCGACGCTAAGG CCCATCAAATTAAAAATAGTTTACGCAAGT	Gibson_Apr1_Rev
C-1448	ACTTGCGTAAACTATTTTTAATTTGTCAATAATATCACCAAC AGAGTTTTAGAGCTAGAAATAGCAAGTT	Gibson_Prb12_Fw
C-1449	AACTTGCTATTTCTAGCTCTAAAACTCTGTTGGTGATATTA TTGACAAATTAAAAATAGTTTACGCAAGT	Gibson_Prb12_Rev
C-1450	ACTTGCGTAAACTATTTTTAATTTGTAATGGATTAGAAAGA ATACGTTTTAGAGCTAGAAATAGCAAGTT	Gibson_Prb11_Fw
C-1451	AACTTGCTATTTCTAGCTCTAAAACGTATTCTTTCTAATCCA TTACAAATTAAAAATAGTTTACGCAAGT	Gibson_Prb11_Rev
Donor DNA	**Sequence**	**Description in database**
C-1518	TCATTGTCTGCCTTAACAACCGTAGCATTAGCTTTGACTTC TTAATAAGAATTCGCTAA	CaApr1Repair_Fw
C-1519	TCCTCATTTGATAATTTGGATAATTTGATGCTATGGGCCTT AGCGAATTCTTATTAAGA	CaApr1Repair_Rev
C-1520	TTCTATTTTAACATCCCTTATTGGTGTTCAAGGTTTACTCAT TTAATAAGAATTCGATA	CaPrb12Repair_Fw
C-1521	TGATTTGTTTTTGAACAGAATCACCAAATACATCAATAATAT CGAATTCTTATTAAATG	CaPrb12Repair_Rev
C-1522	GATGCGCATTTGCCCTCTGATGACAACCAACCAGATACTA AATAATAAGAATTCTCTAA	CaPrb11Repair_Fw
C-1523	ACAACAATGTAATGATTTGGAATTATTTTATTTAATGGATTA GAGAATTCTTATTATTT	CaPrb11Repair_Rev
qPCR primer	**Sequence**	**Description in database**
6068	CACTTCTTAGAGGGACTATCGGTTTC	18S_Fw
6069	CAGAACGTCTAAGGGCATCACA	18S_Rev
A-9854	TGGGATGGGATACGTTGAGAA	SCR1_Fw
A-9855	CTAGCCGCGAGGAAGGATT	SCR1_Rev

B-7958	GAGGTACCCGATAAAGTG	PRB1_Rev
C-542	CCTCTTATTCCGTCGGTGAA	ERG11_Fw
C-543	TGTGTCTACCACCACCGAAA	ERG11_Rev
C-766	GTATGTGTAAAGCCGGTTTTG	ACT1 fwd
C-767	CATGATACCTTGGTGTCTTGG	ACT1 rev
C-768	CTACAGATACAGCATTTCCAAGA	COX1 FWD
C-769	GTGGCCTGAATAGATGATAATGGT	COX1 REV
C-3060	CCACGTTGAGCGATGACAGA	PRB1_Fw
C-3063	GAAGGTATCGGTTTAGGCGA	PEP4_Fw
C-4114	TAGAGTATATTGACCGGTCC	PEP4_Rev
gBlock	**Sequence**	**Description in database**
	GCATCTAGAGCAGGAAAGTCTTACCCAACTGTGAGTGCTG ATTACCAGGACGCCGTTGAGAAGGCGAAGAAGAAGCTCA GAGGCTTCATCGCTGAGAAGAGATGCGCTCCTCTAATGCT CCGTTTGGCATTCCACTCTGCTGGAACCTTTGACAAGGGC ACGAAGACCGGTGGACCCTTCGGAACCATCAAGCACCCT GCCGAACTGGCTCACAGCGCTAACAACGGTCTTGACATC GCTGTTAGGCTTTTGGAGCCACTCAAGGCGGAGTTCCCTA TTTTGAGCTACGCCGATTTCTACCAGTTGGCTGGCGTTGT TGCCGTTGAGGTCACGGGTGGACCTAAGGTTCCATTCCA CCCTGGAAGAGAGGACAAGCCTGAGCCACCACCAGAGG GTCGCTTGCCCGATCCCACTAAGGGTTCTGACCATTTGAG AGATGTGTTTGGCAAAGCTATGGGGCTTACTGACCAAGAT ATCGTTGCTCTATCTGGGGGTCACACTATTGGAGCTGCAC ACAAGGAGCGTTCTGGATTTGAGGGTCCCTGGACCTCTAA TCCTCTTATTTTCGACAACTCATACTTCACGGAGTTGTTGA GTGGTGAGAAGGAAGGTCTCCTTCAGCTACCTTCTGACAA GGCTCTTTTGTCTGACCCTGTATTCCGCCCTCTCGTTGAC AAATATGCAGCGGACGAAGATGCCTTCTTTGCTGATTACG CTGAGGCTCACCAAAAGCTTTCCGAGCTTGGGTTTGCTGA TGCCTAACTGCAGCCAATGCATTGGAA	gBlock XbaI-APEX2-PstI

7.2 Methods

7.2.1 Protein extraction and western blotting

An overnight preculture was diluted to $O.D._{600nm}$ 0.2 with or without the addition of FLC (20 µg/mL for *S. cerevisiae* cultures and 10 µg/mL for *C. albicans* cultures) and grown overnight for 16 hours, after which the cells were harvested for protein extraction. For Fig. 3.1, the cells were also treated with 3 µg/mL ATC. In Fig. 2.4, a range of FLC concentrations was added to the cells (0 – 30 µg/mL). For Fig. 4.6, cells were treated with VOR (1 or 5 µg/mL), KETO (1, 10 or 20 µg/mL), AmB (1 or 5 µg/mL), CASP (1, 5 or 10 µg/mL) or TUN (5, 10 or 20 µg/mL). For Fig. 2.5 and 5.2, 10 O.D. units were isolated at the indicated time points and the pelleted cells were resuspended in 15% glycerol and frozen until all samples were taken. Crude membrane protein fractions were extracted according to the protocol of (Diekert *et al.*, 2001). Briefly, the cells were washed once in lysis buffer (0.6 M sorbitol, 20 mM Hepes-KOH, pH 7.4) supplemented with Complete EDTA-free protease inhibitor (Roche) and subsequently broken in a FastPrep machine (MP Biomedicals) by glass beads (three cycles of 20''). Next, the samples were centrifuged for 5' at 3,000 rpm (revolutions per minute) to separate the supernatant containing the protein fraction, from the cell debris. The lysis step was repeated once. The proteins in the isolated supernatant were pelleted at maximum speed for 10', to obtain the crude membrane protein fraction. The amount of protein in the sample was determined using the Pierce 660 nm protein assay (ThermoFisher Scientific). Equal amounts of protein were loaded on NuPAGE 4-12% Bis-Tris gels (Life Technologies) for electrophoretic separation, except for Fig. 2.3 and 5.2 where a range of protein amounts was loaded. The proteins were blotted onto Protran 0.45 µm nitrocellulose membranes (Amersham), which were subsequently blocked in 5% non-fat milk in Tris-buffered saline (TBS) and probed overnight at 4°C with 1:3,000 anti-HA-Peroxidase (Roche), 1:10,000 anti-V5-Peroxidase (Life Technologies) or with 1:500 of a custom-made polyclonal antibody raised by GenScript against the internal Erg11 peptide 'STYKDGVKMTDQEI' (purity of >85% and buffered in phosphate buffered saline (pH 7.4) with 0.02% sodium azide). Blots immune decorated with anti-Erg11 needed incubation with a 1:10,000 secondary anti-rabbit peroxidase-conjugated antibody (GE Healthcare). Blots were stripped and incubated with a loading control, 1:2,000 anti-Dpm1 (A-6429, Life Technologies), 1:3,000 anti-Pgk1 (459250, ThermoFisher) or 1:2,000 anti-Tim23 (a kind gift of Dr. T. Lithgow, Monash University), followed by incubation with a 1:10,000 secondary anti-mouse or anti-rabbit peroxidase-conjugated antibody (GE Healthcare). Western blots were visualized using the WesternBright Quantum HRP Substrate kit (Advansta) and chemiluminescence detection by a CCD camera-equipped LAS-4000 Mini Imaging System (Fuji). For optimal detection of the additional Erg11 forms, it was necessary to overexpose full-length Erg11 on western blot, except for Fig. 2.2, where a semi-quantitative

analysis of the western blot results has been performed by using ImageJ software (https://imagej.nih.gov/ij/).

7.2.2 Spot assay

Cells expressing the *ERG11-ARG8*$^{\Delta 13}$ chimera's or controls were cultured overnight in liquid CSM-Ura drop out medium. For all other experiments, cells were cultured in YPD. The cultures were diluted to O.D. 1 and 1:5 serially diluted in a microtiter plate. Next, the dilution series were spotted onto non-limiting and arginine limiting medium for Fig. 3.2 and on YPD or YPEG for the other experiments. Results are shown after three days of growth, except when specified otherwise.

7.2.3 Fluorescence microscopy

Cells were grown overnight in liquid -Leu-Ura drop out medium supplemented with 2% galactose, to induce the expression of the mCherry-tagged *ERG11* constructs. The strains were simultaneously transformed with a GFP marker plasmid (*SEC63-GFP* (property of FB lab), *GFP-CPS1* (JTPL40544, MCB collection) and mtGFP (pVT100U-mtGFP, Addgene 45054)). Cells expressing the full-length *ERG11-mCherry* construct were grown both in the absence and presence of FLC (20 µg/mL), when transformed with the mtGFP marker. Cells were visualized using a FluoView FV1000 confocal laser-scanning microscope (Olympus). The Erg11-mCherry constructs were detected by a 568-nm laser and BA575-675 emission filter and the GFP markers by a 488-nm argon laser and BA505-540 emission filter through a 60× 1.35 NA objective.

7.2.4 Focused ion beam scanning electron microscopy

Precultures were grown in -Leu drop out medium. Next, cells were diluted to O.D. 0.2 and grown overnight (or for 2 days for the *ERG11*$^{\Delta 150}$ construct) in the absence or presence of FLC (20 µg/mL). Spheroplasts were prepared by incubating the cells in a 0.1 M Tris-SO_4 – 10 mM DTT solution for 20' at 30°C, while shaking. The cells were resuspended in sorbitol buffer (1.2 M sorbitol and 20 mM KPi at pH 7.4) and 0.25 mg of lyticase was added per g wet weight. The cells were incubated at 30°C for 30' to 60', until about 70% to 80% of the cells had become spheroplasts, as measured by spectrophotometric analysis. The cells were harvested and washed in sorbitol buffer. Next, a 1:1 ratio of spheroplasts and fixative 1 (3% paraformaldehyde (PFA, EMS) and 6% glutaraldehyde (GA, EMS) in 0.05 M sodium cacodylate (pH 7.2)) was incubated on ice for ten minutes. Next, the pelleted spheroplasts were carefully resuspended in fixative 2 (1.5% PFA and 3% GA in 0.05 M sodium cacodylate) in a 1:1 ratio and incubated overnight at 4°C. The next day, the fixative was removed by washing with 0.05 M sodium cacodylate. The samples were stained 20' in a 0.054% diaminobenzidine (DAB)-HCl solution with 1:1,000 of 30% H_2O_2, to obtain an electron dense staining of the APEX2-tag that was fused to the *ERG11* constructs. The staining was stopped by washing the spheroplasts in 0.1 M sodium cacodylate. Next, samples were fixed for 2 h in 1.5%

PFA, 3% GA in 0,05 M sodium cacodylate at 4°C. Fixative was removed by washing with 0.05 M sodium cacodylate. To protect the spheroplasts during the following EM preparation steps, a pellet of yeast cells was embedded in 2% low-melting agarose (Sigma) in 0.05 M sodium cacodylate. After an additional washing step, the pellets were incubated in 6% potassium permanganate for 1 h and again washed in 0.05 M sodium cacodylate. Next, samples were dehydrated using solutions of increasing EtOH concentration for 15' each (7%, 30%, 50%, 70% and 2x 100% EtOH). After the 50% EtOH step, samples were additionally incubated in 1% OsO_4 (EMS), 50% EtOH for 1 h. Subsequent resin embedding was done using Low Viscosity Spurr's solution (EMS). Embedded cells were mounted on aluminium SEM stubs (diameter 12 mm) and samples were coated with ±20 nm of platinum (Quorum Q150T ES). FIB-SEM imaging was performed using a Zeiss Crossbeam 540 system with Atlas5 software. The FIB was set to remove 5 nm sections by propelling gallium ions at the surface (probe current: 700 pA). Imaging was done at 1.5 kV and 600 pA using an EsB (Energy selective Backscattered) detector, with the ESB grid set at -1200 V. Registration of the resulting dataset was done using IMOD (http://bio3d.colorado.edu/imod/). This experiment was performed in collaboration with the VIB BioImaging Core in Ghent.

7.2.5 Tetrad analysis

Diploid strains were generated that contained an HA-tagged *ERG11* variant (*ERG11*, *ERG11*****, *ERG11*$^{\Delta 150}$, *ERG11*$^{\Delta 150****}$ or *ERG11*$^{\Delta 74}$) or solely the HA-tag in one of both *ERG11* alleles of the BY4743 strain (see 7.1.2). The strains were induced to sporulate on sporulation medium at 23°C. After 4 days, tetrads were dissected with a micromanipulator (Singer Instruments), either on YPD medium, on CSM or $SD_{HisLysLeuUraMet}$ medium buffered with 50 mM succinate-KOH to pH 6.5, based on (Crowley *et al.*, 1996) or on $SD_{HisLysLeuUraMet}$. Results are shown after 3 days of growth. PCR analysis confirmed that the smaller germinating colonies contained the HA-tagged *ERG11* constructs or the HA-tag only.

7.2.6 Ergosterol measurement

Precultures of four different isogenic *ERG11-HA* spores and *ERG11******-HA* spores were started in liquid YPD medium. The next day, cells were diluted to O.D. 0.2 and grown for 16 hours, after which the cells were harvested. The protocol for sterol extraction is based on (Arthington-Skaggs *et al.*, 1999). In short, isolated cell pellets were washed with water and their wet weight was determined after filtration. Cell pellets were transferred to glass screwcap test tubes and 3 mL of a 25% alcoholic potassium hydroxide solution was added. Samples were mixed by vortexing for 90'', until the pellet was resuspended. Next, the samples were incubated for 1 hour in an 85°C water bath. The suspension was cooled to room temperature (RT). Next, 1 mL of water and 3 mL of *n*-heptane were added. The suspension was vortexed for 3' to extract the sterols. After settlement of the layers, the heptane fraction was transferred to a new glass screwcap tube. 3 technical replicates of each biological sample were immediately loaded into a UV-transparent 96-well flat bottom plate

(Corning), together with pure heptane, as a blanc control. The absorbance was measured at 281 nm and 230 nm. The percentage of ergosterol was determined, as described by the reference method, taking into account the wet weight of the cell pellet and subtracting the blanc absorbance values from the measured absorbances of the samples. The distance of the light travelled in the wells of the microtiter plate was accounted for by amplifying the E-values (in percentages per centimeter) by a factor of 0.6111. Results were statistically analyzed in GraphPad Prism, by two-way ANOVA (analysis of variance) and corrected for multiple comparisons by the Bonferroni post-hoc test. Results are represented as the mean with a 95% confidence interval.

7.2.7 Real time quantitative reverse transcription PCR

Cells were precultured in liquid $SD_{HisLeuUra}$ and diluted to O.D. 0.2 the next day, with or without the addition of 20 µg/mL FLC. After 16 hours, the cells were harvested and washed. To obtain purified RNA, cell pellets were resuspended in TRIzol (ThermoFisher Scientific) and the cells were broken with glass beads using a FastPrep machine (MP Biomedicals). Chloroform was added to the supernatant and RNA was isolated from the resulting supernatant after centrifugation. Subsequently, the RNA was precipitated by the addition of isopropanol and 70% ethanol. The dried pellet was resuspended in nuclease-free water and treated with DNase (New England Biolabs). Next, RNA was reverse transcribed using the iScript cDNA synthesis kit (Bio-Rad). qRT-PCR was performed with GoTaq polymerase (Promega) in a StepOnePlus Real-Time PCR system (ThermoFisher Scientific). To analyze the mRNA levels of *ERG11*, *PRB1* and *PEP4* expression, primer pairs C-542/C-543, B-7958/C-3060 and C-4114/C-3063 were used respectively. The data was analyzed using qBase+ software (Biogazelle) in reference to two housekeeping genes, *18S* and *SCR1* for which primer pairs 6068/6069 and A-9854/A-9855 were used. Statistical analysis of the results was performed in GraphPad Prism using two-way ANOVA and correction for multiple comparisons by the Bonferroni post-hoc test. Results are represented as the mean with a 95% confidence interval.

7.2.8 Determination of the mitochondrial DNA copy number

To determine the mtDNA copy number, the protocol was followed as described in Taylor *et al.* (2005). Precultures of the diploid cells grown in $SD_{HisLysLeuUraMet}$ limiting medium were diluted to O.D. 0.2 with or without the addition of FLC (20 µg/mL) and grown for 16 hours. gDNA was extracted from the cells by the use of glass beads and a FastPrep machine, after resuspending the cells in a 1:1 solution of TE-buffer (1mM EDTA, 10 mM Tris-HCl pH 8.0) and a phenol/chloroform/isoamyl alcohol solution (25/24/1) (PCI). The isolated DNA was further purified by precipitation with sodium acetate (3 M, pH 5.2)/ethanol and subsequent treatment with RNase A. Next, qPCR was performed with primers that bind to *COX1* (C-768 and C-769), a mitochondrial gene and to *ACT1* (C-766 and C-767), a nuclear household gene. To determine the fold change compared to the wild type sample, first the difference in threshold cycle numbers (C_T) for *COX1*

and *ACT1* was calculated for each strain ($\Delta C_T = C_{TCOX1} - C_{TACT1}$). The relative mtDNA copy number is then determined as $2^{\Delta C_T}$. The fold change compared to the wild type strain is obtained by dividing the relative copy number of a specific strain by that of the wild type strain. Two technical repeats were included for each sample.

7.2.9 FLC susceptibility by Etest

Cells were grown overnight in YPD medium, diluted to O.D. 0.2 and washed with sterile water. Next, the cell suspensions were evenly streaked out over agar plates with a sterile swab. The FLC Etest strips were carefully placed in the middle of the plates, which were subsequently incubated at 30°C for *S. cerevisiae* cells and at 37°C for *C. albicans* cells for two days. YPD agar medium is used for *S. cerevisiae* Etests and RPMI agar medium is used for *C. albicans* Etests.

7.2.10 FLC susceptibility by MIC broth microdilution assay

Cells were grown overnight in -Leu drop out medium for Fig. 3.10 and in YPD for Fig. 4.3. Cells were diluted to a concentration of $1x10^3$ – $5x10^3$ cells/mL, as suggested by the CLSI guidelines and added to a sterile microtiter plate in a 1:2 dilution to a final concentration of $0.5x10^3$ – $2.5x10^3$ cells/mL. A twofold serial dilution series of FLC was prepared starting from 640 µg/mL. These 10x stock dilutions were further diluted 1:5 and added to the wells in a 1:2 dilution. The FLC dilutions were made in the corresponding growth medium, either -Leu drop out medium or YPD. The microtiter plates were incubated at 30°C for 48 hours in the dark, with visual inspection at 24 and 48 hour time points.

7.2.11 Tolerance assay

Cells were transferred after 48 hours of incubation in the MIC broth microdilution assay to a new sterile microtiter plate. They were diluted 1:10 to 1:100,000 by tenfold serial dilutions to obtain a countable number of surviving cells when plated on non-selective agar medium. The CFU/mL was determined for each strain for every FLC concentration tested and was calculated relative to the 0 µg/mL FLC growth condition of the strain to obtain a percentage of growth for each FLC concentration, when multiplied by 100. The average of three biological repeats is included in Fig. 4.3 but for Fig. 3.10 the experiment was done only once.

7.2.12 Protease/peptidase screening

To test the hypothesis that the Erg11 products are generated through a cleavage process, the Generic Genome Browser (GBrowse), integrated into the *Saccharomyces* Genome Database (http://www.yeastgenome.org) was used on a genome-wide scale to search for all genes that are annotated with a protease or peptidase function in *S. cerevisiae* (S288C) (consulted on 20/04/2015 and displayed in Appendix II). In total, 61 proteases and 44 peptidases were found, of which six

genes were annotated both as a protease and a peptidase, so in total 99 hits were found. Essential genes were excluded from this list. 96 out of the 99 hits were tested by use of the haploid deletion collection (Giaever and Nislow, 2014). An *ERG11-V5* overexpressing plasmid, pAFC118 was introduced to all haploid deletion strains and the Erg11 pattern was examined on western blot, to identify deletion strains with a decrease in additional Erg11 forms. Three gene deletions were not present in the haploid deletion collection and were made by us in the AFC202 background. The Erg11 pattern of three independent transformants of *som1*Δ, *hsp32*Δ and *hsp33*Δ was tested on western blot to see if additional Erg11 forms were lacking.

7.2.13 Growth analysis

Precultures were diluted to O.D. 0.1. and the cells were transferred to a 96-well microtiter plate, which was incubated at 30°C in a Multiskan FC Microplate Photometer (Thermo Scientific). The O.D. was measured every 30 minutes for 72 hours. The O.D. of the blanc medium was subtracted from the cell growth measurements to produce the growth curves. Four technical repeats were included for Fig. 2.5 and 5.2. Three biological repeats were measured in Fig. 4.3 and three technical repeats were included in Fig. 3.8. Two biological repeats were measured in Fig. 3.12.

7.2.14 *In silico* analysis of Erg11 structure

Crystal structures have been examined with PyMOL software and have been imported from the Protein Data Bank (https://www.rcsb.org/). The PDB entry of the *S. cerevisiae* Erg11 crystal structure is 4WMZ (Sagatova *et al.*, 2015). The PDB entry of the FMN binding domain of the *B. megaterium* cytochrome P450BM-3 is 1BVY (Sevrioukova *et al.*, 1999).

7.2.15 Alignment of CYP51 sequences

Verified CYP51 sequences were retrieved from UniProt (https://www.uniprot.org/) and aligned with CLC Main Workbench 7 software.

7.2.16 Mass spectrometry analysis of the free N-termini of purified *S. cerevisiae* Erg11

BY4742 was transformed with an *ERG11-HA* overexpressing plasmid (pWK1) or the empty vector, pBEVY-L. Precultures were diluted to O.D. 0.2 in -Leu drop out medium and incubated overnight at 30°C. The next day, proteins were extracted in triplicate for each sample, according to the protocol described in 7.2.1, with the addition of 0.1% Triton-X-100 to the lysis buffer. After centrifugation for 10' at maximal speed, the supernatant was retrieved instead of the pellet and again centrifuged at max speed for 10'. Next, 20 µL of TBS-TWEEN 20 (0.05%, TBST)-prewashed magnetic anti-HA beads (Thermo Scientific, Pierce) was added to the protein-containing supernatant and incubated for 30' at 25°C at 8 rpm. The beads were collected and washed in TBST. Next, the beads were washed three times in acetylation digestion buffer (20 mM triethylammonium

bicarbonate pH 8 (Sigma T7408) and 2 mM $CaCl_2$). The beads were resuspended in acetylation digestion buffer and sent to the PEC in Ghent for subsequent MS analysis. The protocol described below was followed.

20 mM trideutero N-hydroxysuccinimide acetyl was added and incubated for 1 hour while mixing at 30°C. This step was repeated to reach a final concentration of 40 mM NHS-trideutero-acetate. 2x excess of glycine was added and incubated for 60' at 30°C to quench any non-reacted NHS-trideutero-acetate. This step was repeated once. 1 µg of trypsin was added and incubated for 4 hours at 37°C. The beads were removed and another 1 µg of trypsin was added and incubated overnight at 37°C. Hydroxylamine (pH 8 and 4x molar excess of hydroxylamine over the NHS ester) was added and incubated for 10' at 30°C to revert possible O-acylation of Ser, Thr or Tyr residues (on the peptide level). The samples were acidified to 1% acetic acid and 2 µl of 100% acetic acid stock solution and immediate cleaned on C18 Omix tips in ammonium acetate buffers. The samples were dried to complete dryness. Dried peptides were re-dissolved in 20 µl 0.1% formic acid in water/acetonitrile (98:2, v/v), of which 2 µl was injected for LC-MS/MS analysis on an Ultimate 3000 RSLC nano LC (Thermo Fisher Scientific, Bremen, Germany) in-line connected to a Q Exactive mass spectrometer (Thermo Fisher Scientific). The peptides were first loaded on a trapping column (made in-house, 100 µm internal diameter (I.D.) × 20 mm, 5 µm beads C18 Reprosil-HD, Dr. Maisch, Ammerbuch-Entringen, Germany). After flushing the trapping column, peptides were loaded in solvent A (0.1% formic acid in water) on a reverse-phase column (made in-house, 75 µm I.D. x 250 mm, 3µm Reprosil-Pur-basic-C18-HD beads, Dr. Maisch, packed in the needle) and eluted by an increase in solvent B (0.1% formic acid in acetonitrile) in a linear gradient from 2% solvent B to 55% solvent B in 2 hours, followed by a washing step with 99% solvent B, all at a constant flow rate of 300 nl/min. The mass spectrometer was operated in data-dependent, positive ionization mode, automatically switching between MS and MS/MS acquisition for the 5 most abundant peaks in a given MS spectrum. The source voltage was set at 4.5 kV, and the capillary temperature at 275°C. One MS1 scan (m/z 400−2,000, AGC target 3 × 106 ions, maximum ion injection time 80 ms), acquired at a resolution of 70,000 (at 200 m/z), was followed by up to 5 tandem MS scans (resolution 17,500 at 200 m/z) of the most intense ions fulfilling predefined selection criteria (AGC target 5 × 104 ions, maximum ion injection time 80 ms, isolation window 2 Da, fixed first mass 140 m/z, spectrum data type: centroid, underfill ratio 2%, intensity threshold 1.3xE4, exclusion of unassigned, 1, 5-8, >8 positively charged precursors, peptide match preferred, exclude isotopes on, dynamic exclusion time 12 s). The HCD collision energy was set to 25% Normalized Collision Energy and the polydimethylcyclosiloxane background ion at 445.120025 Da was used for internal calibration (lock mass).

Data analysis was performed with mascot search engine (version 2.5.1). Spectra were searched against the yeast proteins in the Uniprot/Swiss-Prot database (database release version of 01-2017 containing 6721 yeast protein sequences, www.uniprot.org) supplemented with the Erg11-HA sequence. The mass tolerance for precursor and fragment ions were set to 10 ppm and 20 mmu

respectively, during the main search. Enzyme specificity was set as semi specific C-terminal to arginine, also allowing cleavage at proline bonds with a maximum of two missed cleavages. Variable modifications were set to oxidation of methionine residues, acetylation and trideutero-acetylation of peptide N-termini and cyclicsation of glutamine residues. Trideutero-acetylation on lysine residues was set as a fixed modification.

APPENDIX

Appendix I. MS data received from PEC Ghent regarding the identification of putative cleavage sites in *Saccharomyces cerevisiae* Erg11.

This table provides a summary of the AcD_3-labeled Erg11 peptides identified during MS analysis. The position of the amino acid residue in the full-length Erg11 protein to which the start site of the Erg11 peptide corresponds has been indicated under 'start' and the sequences of the peptides are provided. The PSM counts of the three replicate samples are included and averaged. Also, values for the integrated MS1 peak areas of the Erg11 peptides are included and averaged. If several peptides have been identified corresponding to the same start site, the values of PSM counts and MS1 areas have been added up within the same replicate sample and the sequence of the shortest peptide is included. It has been calculated that at least 94% of all lysine residues have been labeled with AcD_3.

Start	AcD_3-modified sequence	PSM count				MS1 peak area			
		ERG11-HA			AVERAGE	*ERG11-HA*			AVERAGE
		1	2	3		1	2	3	
147	AcD3-LMEQKKFVKGALTKE	1,00	3,00	1,00	**1,67**	1,79E+08	2,26E+08	1,42E+08	**1,82E+08**
190	AcD3-TTGTIDVMVTQPEMTIFTASR	0,00	0,00	5,00	**1,67**	2,61E+08	2,16E+07	4,83E+08	**2,55E+08**
229	AcD3-YSDLDKGFTPINFVFPNLPLEHYR	3,00	1,00	3,00	**2,33**	1,76E+08	5,56E+07	1,78E+08	**1,37E+08**
230	AcD3-SDLDKGFTPINFVFPNLPLEHYR	3,00	0,00	0,00	**1,00**	3,35E+08	1,20E+08	1,94E+08	**2,16E+08**
241	AcD3-FVFPNLPLEHYR	3,00	3,00	3,00	**3,00**	7,08E+08	4,39E+08	4,18E+08	**5,22E+08**
242	AcD3-VFPNLPLEHYR	1,00	1,00	2,00	**1,33**	2,47E+10	2,64E+10	2,94E+10	**2,68E+10**
255	AcD3-DHAQKAISGTYMSLIKER	1,00	2,00	4,00	**2,33**	6,40E+08	7,35E+08	1,57E+09	**9,81E+08**
328	AcD3-LHLAERPDVQQELYEEQMR	2,00	2,00	3,00	**2,33**	1,01E+09	9,02E+08	1,46E+09	**1,13E+09**
329	AcD3-HLAERPDVQQELYEEQMR	0,00	2,00	1,00	**1,00**	1,12E+08	3,70E+08	1,71E+08	**2,18E+08**
331	AcD3-AERPDVQQELYEEQMR	2,00	0,00	0,00	**0,67**	1,80E+08	8,61E+07	1,61E+08	**1,42E+08**
347	AcD3-VLDGGKKELTYDLLQEMPLLNQTIKETLR	22,00	1,00	23,00	**15,33**	1,25E+09	1,37E+08	1,19E+09	**8,56E+08**
357	AcD3-YDLLQEMPLLNQTIKETLR	0,00	0,00	3,00	**1,00**	5,14E+07	2,16E+07	5,90E+07	**4,40E+07**
360	AcD3-LQEMPLLNQTIKETLR	0,00	1,00	0,00	**0,33**	2,74E+07	3,85E+07	2,36E+07	**2,98E+07**
362	AcD3-EMPLLNQTIKETLR	0,00	0,00	1,00	**0,33**	4,08E+07	3,68E+06	4,14E+07	**2,86E+07**
386	AcD3-KVMKDMHVPNTSYVIPAGY	4,00	4,00	3,00	**3,67**	3,95E+09	4,74E+09	4,60E+09	**4,43E+09**
405	AcD3-HVLVSPGYTHLR	0,00	0,00	1,00	**0,33**	1,17E+08	6,83E+08	7,70E+08	**5,23E+08**
408	AcD3-VSPGYTHLR	1,00	3,00	5,00	**3,00**	1,70E+09	2,03E+09	2,26E+09	**2,00E+09**
417	AcD3-DEYFPNAHQFNIH	1,00	0,00	1,00	**0,67**	1,33E+08	7,27E+07	2,03E+08	**1,36E+08**

431	AcD3-WNKDSASSYSVGEEVDYGFGAISKGVSSPYLPFGGGR	0,00	0,00	2,00	**0,67**	0,00E+00	5,96E+07	0,00E+00	**1,99E+07**
440	AcD3-SVGEEVDYGFGAISKGVSSPYLPFGGGR	3,00	5,00	0,00	**2,67**	1,10E+09	1,91E+09	4,89E+08	**1,17E+09**
510	AcD3-VTLPTGPAKIIWEKR	7,00	7,00	7,00	**7,00**	9,76E+09	6,40E+09	8,90E+09	**8,35E+09**
511	AcD3-TLPTGPAKIIWEKR	11,00	10,00	11,00	**10,67**	2,76E+10	2,18E+10	3,23E+10	**2,73E+10**
512	AcD3-LPTGPAKIIWEKR	4,00	4,00	6,00	**4,67**	3,19E+09	1,50E+09	2,12E+09	**2,27E+09**

Appendix II. List of genes annotated with a protease or peptidase function. Essential genes have not been included in the screen.

Systematic name	Standard name	Description
PROTEASES		
YBR074W	*PFF1*	Multi-spanning vacuolar membrane protease; glycosylated transmembrane protein bearing homology to the M28 family of metalloproteases; has a lumenal-facing protease domain; proposed role in vacuole physiology
YDR144C	*MKC7*	GPI-anchored aspartyl protease; member of the yapsin family of proteases involved in cell wall growth and maintenance; shares functions with Yap3p and Kex2p; MKC7 has a paralog, YPS1, that arose from the whole genome duplication
YDR349C	*YPS7*	Putative GPI-anchored aspartic protease; member of the yapsin family of proteases involved in cell wall growth and maintenance; located in the cytoplasm and endoplasmic reticulum
YDR430C	*CYM1*	Lysine-specific metalloprotease of the pitrilysin family; metalloprotease of the intermembrane space; degrades proteins and presequence peptides cleaved from imported proteins; required for normal mitochondrial morphology
YIR039C	*YPS6*	Putative GPI-anchored aspartic protease; member of the yapsin family of proteases involved in cell wall growth and maintenance
YGL259W	*YPS5*	Protein with similarity to GPI-anchored aspartic proteases; such proteases are Yap1p and Yap3p
YLR120C	*YPS1*	Aspartic protease; member of the yapsin family of proteases involved in cell wall growth and maintenance; attached to the plasma membrane via a glycosylphosphatidylinositol (GPI) anchor; YPS1 has a paralog, MKC7, that arose from the whole genome duplication
YLR121C	*YPS3*	Aspartic protease; member of the yapsin family of proteases involved in cell wall growth and maintenance; attached to the plasma membrane via a glycosylphosphatidylinositol (GPI) anchor
YNL123W	*NMA111*	Serine protease and general molecular chaperone; involved in response to heat stress and promotion of apoptosis; may contribute to lipid homeostasis; sequence similarity to the mammalian Omi/HtrA2 family of serine proteases
YPL246C	*RBD2*	Possible rhomboid protease; has similarity to eukaryotic rhomboid proteases including Pcp1p
YBL067C	*UBP13*	Ubiquitin-specific protease that cleaves Ub-protein fusions; UBP13 has a paralog, UBP9, that arose from the whole genome duplication
YBL022C	*PIM1*	ATP-dependent Lon protease; involved in degradation of misfolded proteins in mitochondria; required for biogenesis and maintenance of mitochondria
YBR058C	*UBP14*	Ubiquitin-specific protease; specifically disassembles unanchored ubiquitin chains; involved in fructose-1,6-bisphosphatase (Fbp1p) degradation; similar to human isopeptidase T
YCL044C	*MGR1*	Subunit of the mitochondrial (mt) i-AAA protease supercomplex; i-AAA degrades misfolded mitochondrial proteins; forms a subcomplex with Mgr3p that binds to substrates to facilitate proteolysis; required for growth of cells lacking mtDNA
YCR045C	*RRT12*	Probable subtilisin-family protease; role in formation of the dityrosine layer of spore walls; localizes to the spore wall and also the nuclear envelope and ER region in mature spores
YDL122W	*UBP1*	Ubiquitin-specific protease; removes ubiquitin from ubiquitinated proteins; cleaves at the C terminus of ubiquitin fusions irrespective of their size; capable of cleaving polyubiquitin chains
YIL156W	*UBP7*	Ubiquitin-specific protease that cleaves ubiquitin-protein fusions; UBP7 has a paralog, UBP11, that arose from the whole genome duplication
YIL137C	*TMA108*	Ribosome-associated protein that is involved in ribosome biogenesis; putative metalloprotease
YIL015W	*BAR1*	Aspartyl protease; secreted into the periplasmic space of mating type a cell; helps cells find mating partners; cleaves and inactivates alpha factor allowing cells to recover from alpha-factor-induced cell cycle arrest

YEL060C	*PRB1*	Vacuolar proteinase B (yscB); serine protease of the subtilisin family; involved in protein degradation in the vacuole and required for full protein degradation during sporulation; activity inhibited by Pbi2p; protein abundance increases in response to DNA replication stress; PRB1 has a paralog, YSP3, that arose from the whole genome duplication
YER017C	*AFG3*	Component, with Yta12p, of mitochondrial inner membrane m-AAA protease; mediates degradation of misfolded or unassembled proteins and is also required for correct assembly of mitochondrial enzyme complexes; involved in cytoplasmic mRNA translation and aging
YER098W	*UBP9*	Ubiquitin-specific protease that cleaves ubiquitin-protein fusions; UBP9 has a paralog, UBP13, that arose from the whole genome duplication
YER144C	*UBP5*	Putative ubiquitin-specific protease; concentrates at the bud neck; UBP5 has a paralog, DOA4, that arose from the whole genome duplication
YER151C	*UBP3*	Ubiquitin-specific protease involved in transport and osmotic response; interacts with Bre5p to co-regulate anterograde and retrograde transport between the ER and Golgi; involved in transcription elongation in response to osmostress through phosphorylation at Ser695 by Hog1p; inhibitor of gene silencing; cleaves ubiquitin fusions but not polyubiquitin; also has mRNA binding activity; protein abundance increases in response to DNA replication stress
YFL010C	*WWM1*	WW domain containing protein of unknown function; binds to Mca1p, a caspase-related protease that regulates H2O2-induced apoptosis; overexpression causes G1 phase growth arrest and clonal death that is suppressed by overexpression of MCA1
YFR010W	*UBP6*	Ubiquitin-specific protease; situated in the base subcomplex of the 26S proteasome, releases free ubiquitin from branched polyubiquitin chains; negatively regulates degradation of ubiquitinated proteins by the proteasome; works in opposition to Hul5p polyubiquitin elongation activity; mutant has aneuploidy tolerance
YGL203C	*KEX1*	Cell death protease essential for hypochlorite-induced apoptosis; involved in the processing of killer toxin and alpha factor precursor; cleaves Lys and Arg residues from the C-terminus of peptides and proteins
YGR101W	*PCP1*	Mitochondrial serine protease; required for the processing of various mitochondrial proteins and maintenance of mitochondrial DNA and morphology; belongs to the rhomboid-GlpG superfamily of intramembrane peptidases
YHL013C	*OTU2*	Protein of unknown function; may interact with ribosomes, based on co-purification experiments; member of the ovarian tumor-like (OTU) superfamily of predicted cysteine proteases; shows cytoplasmic localization; protein abundance increases in response to DNA replication stress
YHR113W	*APE4*	Cytoplasmic aspartyl aminopeptidase with possible vacuole function; Cvt pathway cargo protein; cleaves unblocked N-terminal acidic amino acids from peptide substrates; forms a 12-subunit homo-oligomer; M18 metalloprotease family
YHR132C	*ECM14*	Putative metalloprotease with similarity to zinc carboxypeptidases; required for normal cell wall assembly
YJL197W	*UBP12*	Ubiquitin-specific protease; cleaves ubiquitin from ubiquitinated proteins; present in the nucleus and cytoplasm
YJR117W	*STE24*	Highly conserved zinc metalloprotease; functions in two steps of a-factor maturation, C-terminal CAAX proteolysis and the first step of N-terminal proteolytic processing; contains multiple transmembrane spans
YKR044W	*UIP5*	Protein of unknown function that interacts with Ulp1p; a Ubl (ubiquitin-like protein)-specific protease for Smt3p protein conjugates
YKR098C	*UBP11*	Ubiquitin-specific protease; cleaves ubiquitin from ubiquitinated proteins; UBP11 has a paralog, UBP7, that arose from the whole genome duplication
YLR389C	*STE23*	Metalloprotease; involved in N-terminal processing of pro-a-factor to the mature form; expressed in both haploids and diploids; member of the insulin-degrading enzyme family; homolog Axl1p is also involved in processing of pro-a-factor
YMR115W	*MGR3*	Subunit of the mitochondrial (mt) i-AAA protease supercomplex; i-AAA degrades misfolded mitochondrial proteins; forms a subcomplex with Mgr1p that binds to substrates to facilitate proteolysis; required for growth of cells lacking mtDNA

YMR154C	*RIM13*	Calpain-like cysteine protease; involved in proteolytic activation of Rim101p in response to alkaline pH; localizes to punctate structures in alkaline conditions and in vps4 mutant; has similarity to A. nidulans palB
YMR223W	*UBP8*	Ubiquitin-specific protease component of the SAGA acetylation complex; required for SAGA (Spt-Ada-Gcn5-Acetyltransferase)-mediated deubiquitination of histone H2B
YMR274C	*RCE1*	Type II CAAX prenyl protease; involved in the proteolysis and maturation of Ras and the a-factor mating pheromone
YMR304W	*UBP15*	Ubiquitin-specific protease involved in protein deubiquitination; catalytic activity regulated by an N-terminal TRAF-like domain and and C-terminal sequences; physically interacts with anaphase-promoting complex/cyclosome (APC/C) activator, Cdh1p; forms a complex with AAA peroxins Pex1p and Pex6p
YMR322C	*SNO4*	Possible chaperone and cysteine protease; similar to bacterial Hsp31 and yeast Hsp31p, Hsp32p, and Hsp33p; DJ-1/ThiJ/PfpI superfamily member; predicted involvement in pyridoxine metabolism; induced by mild heat stress and copper deprivation
YNL311C	*SKP2*	F-box protein of unknown function; predicted to be part of an SCF ubiquitin protease complex; involved in regulating protein levels of sulfur metabolism enzymes; may interact with ribosomes, based on co-purification experiments
YNL223W	*ATG4*	Conserved cysteine protease required for autophagy; cleaves Atg8p to a form required for autophagosome and Cvt vesicle generation
YNL186W	*UBP10*	Ubiquitin-specific protease, deubiquitinates Ub-protein moieties; interacts with proteins that function in rRNA production and ribosome biogenesis; stabilizes Rpa190p, the largest subunit of RNAP I, by mediating its deubiquitination; controls PCNA deubiquitylation; may regulate silencing by acting on Sir4p; involved in posttranscriptionally regulating Gap1p and possibly other transporters; localized to the nucleolus; human USP36 is a functional analog of Ubp10p
YNR020C	*ATP23*	Putative metalloprotease of the mitochondrial inner membrane; required for processing of Atp6p; has an additional role in assembly of the F0 sector of the F1F0 ATP synthase complex; substrate of the Mia40p-Erv1p disulfide relay system, and folding is assisted by Mia40p
YNR051C	*BRE5*	Ubiquitin protease cofactor; forms deubiquitination complex with Ubp3p that coregulates anterograde and retrograde transport between the endoplasmic reticulum and Golgi compartments; null is sensitive to brefeldin A
YOL098C	/	Putative metalloprotease
YOR003W	*YSP3*	Putative precursor to the subtilisin-like protease III; YSP3 has a paralog, PRB1, that arose from the whole genome duplication
YOR090C	*PTC5*	Mitochondrial type 2C protein phosphatase (PP2C); involved in regulation of pyruvate dehydrogenase activity by dephosphorylating the serine 133 of the Pda1p subunit; localizes to the intermembrane space and is imported via the presequence pathway and processed by the inner membrane protease (Imp1p-Imp2p); acts in concert with kinases Pkp1p and Pkp2p and phosphatase Ptc6p
YOR124C	*UBP2*	Ubiquitin-specific protease; removes ubiquitin from ubiquitinated proteins; deubiquitinates Rsp5p and is required for MVB sorting of membrane proteins; can cleave polyubiquitin and has isopeptidase activity
YOR197W	*MCA1*	Ca2+-dependent cysteine protease; may cleave specific substrates during the stress response; regulates apoptosis upon H2O2 treatment; required for clearance of insoluble protein aggregates during normal growth; implicated in cell cycle dynamics; undergoes autocatalytic processing; similar to mammalian metacaspases, but exists as a monomer due to an extra pair of anti-parallel beta-strands that form a continuous beta-sheet, blocking potential dimerization
YPL186C	*UIP4*	Protein that interacts with Ulp1p; a Ubl (ubiquitin-like protein)-specific protease for Smt3p protein conjugates; detected in a phosphorylated state in the mitochondrial outer membrane; also detected in ER and nuclear envelope
YPL154C	*PEP4*	Vacuolar aspartyl protease (proteinase A); required for the posttranslational precursor maturation of vacuolar proteinases; important for protein turnover after oxidative damage; synthesized as a zymogen, self-activates
YPR024W	*YME1*	Catalytic subunit of the i-AAA protease complex; complex is located in the mitochondrial inner membrane; responsible for degradation of unfolded or misfolded mitochondrial gene products; serves as a nonconventional translocation motor to pull PNPase into the intermembrane space; also has a

		role in intermembrane space protein folding; mutation causes an elevated rate of mitochondrial turnover
YPR122W	*AXL1*	Haploid specific endoprotease of a-factor mating pheromone; performs one of two N-terminal cleavages during maturation of a-factor mating pheromone; required for axial budding pattern of haploid cells
YEL052W	*AFG1*	Protein that may act as a chaperone for cytochrome c oxidase subunits; conserved protein; may act as a chaperone in the degradation of misfolded or unassembled cytochrome c oxidase subunits; localized to matrix face of the mitochondrial inner membrane; member of the AAA family but lacks a protease domain
YMR089C	*YTA12*	Mitochondrial inner membrane m-AAA protease component; mediates degradation of misfolded or unassembled proteins; also required for correct assembly of mitochondrial enzyme complexes
YNL238W	*KEX2*	Subtilisin-like protease (proprotein convertase); a calcium-dependent serine protease involved in the activation of proproteins of the secretory pathway
PEPTIDASES		
YER078C	*ICP55*	Mitochondrial aminopeptidase; cleaves the N termini of at least 38 imported proteins after cleavage by the mitochondrial processing peptidase(MPP), thereby increasing their stability; member of the aminopeptidase P family
YKL134C	*OCT1*	Mitochondrial intermediate peptidase; cleaves destabilizing N-terminal residues of a subset of proteins upon import, after their cleavage by mitochondrial processing peptidase (Mas1p-Mas2p); may contribute to mitochondrial iron homeostasis
YKR087C	*OMA1*	Metalloendopeptidase of the mitochondrial inner membrane; important for adaptive responses to various homeostatic insults and preservation of normal mitochondrial function under damage-eliciting conditions; involved in turnover of membrane-embedded proteins; mediates degradation of Cox1p in coa2 mutant cells; member of a family of predicted membrane-bound metallopeptidases in prokaryotes and higher eukaryotes
YBL091C	*MAP2*	Methionine aminopeptidase; catalyzes the cotranslational removal of N-terminal methionine from nascent polypeptides; function is partially redundant with that of Map1p
YCL057W	*PRD1*	Zinc metalloendopeptidase; found in the cytoplasm and intermembrane space of mitochondria; with Cym1p, involved in degradation of mitochondrial proteins and of presequence peptides cleaved from imported proteins; protein abundance increases in response to DNA replication stress
YGR101W	*PCP1*	Mitochondrial serine protease; required for the processing of various mitochondrial proteins and maintenance of mitochondrial DNA and morphology; belongs to the rhomboid-GlpG superfamily of intramembrane peptidases
YLR244C	*MAP1*	Methionine aminopeptidase; catalyzes the cotranslational removal of N-terminal methionine from nascent polypeptides; function is partially redundant with that of Map2p
YMR035W	*IMP2*	Catalytic subunit of mitochondrial inner membrane peptidase complex; required for maturation of mitochondrial proteins of the intermembrane space; complex contains two catalytic subunits (Imp1p and Imp2p that differ in substrate specificity), and Som1p
YMR150C	*IMP1*	Catalytic subunit of mitochondrial inner membrane peptidase complex; required for maturation of mitochondrial proteins of the intermembrane space; complex contains two catalytic subunits (Imp1p and Imp2p that differ in substrate specificty) and Som1p
YGR031W	*IMO32*	Conserved mitochondrial protein of unknown function; processed by both mitochondrial processing peptidase and mitochondrial octapeptidyl aminopeptidase; gene contains the nested antisense gene NAG1
YJR010C-A	*SPC1*	Subunit of the signal peptidase complex (SPC); SPC cleaves the signal sequence from proteins targeted to the endoplasmic reticulum (ER); homolog of the SPC12 subunit of mammalian signal peptidase complex; protein abundance increases in response to DNA replication stress
YDR415C	/	Putative aminopeptidase
YIL108W	/	Putative metalloendopeptidase; forms cytoplasmic foci upon DNA replication stress
YEL060C	*PRB1*	Vacuolar proteinase B (yscB) with H3 N-terminal endopeptidase activity; serine protease of the subtilisin family; involved in protein degradation in the vacuole

		and required for full protein degradation during sporulation; activity inhibited by Pbi2p; protein abundance increases in response to DNA replication stress; PRB1 has a paralog, YSP3, that arose from the whole genome duplication
YFR006W	/	Putative X-Pro aminopeptidase; green fluorescent protein (GFP)-fusion protein localizes to the cytoplasm; YFR006W is not an essential gene
YHR028C	*DAP2*	Dipeptidyl aminopeptidase; synthesized as a glycosylated precursor; localizes to the vacuolar membrane; similar to Ste13p
YHR113W	*APE4*	Cytoplasmic aspartyl aminopeptidase with possible vacuole function; Cvt pathway cargo protein; cleaves unblocked N-terminal acidic amino acids from peptide substrates; forms a 12-subunit homo-oligomer; M18 metalloprotease family
YHR132C	*ECM14*	Putative metalloprotease with similarity to zinc carboxypeptidases; required for normal cell wall assembly
YKL100C	*YPF1*	Intramembrane aspartyl protease of the perinuclear ER membrane; acts in a branch of ER-associated degradation (ERAD) that degrades functional proteins rather than misfolded proteins; regulates abundance of high-affinity plasma membrane transporters during the starvation response; has a presenilin fold; member of the GxGD family of intramembrane proteases; closest human homolog is signal peptide peptidase (SPP)
YML055W	*SPC2*	Subunit of signal peptidase complex; complex catalyzes cleavage of N-terminal signal sequences of proteins targeted to the secretory pathway; homologous to mammalian SPC25; other members of the complex are Spc1p, Spc1p, and Sec11p
YNL239W	*LAP3*	Cysteine aminopeptidase with homocysteine-thiolactonase activity; protects cells against homocysteine toxicity; has bleomycin hydrolase activity in vitro; transcription is regulated by galactose via Gal4p; orthologous to human BLMH
YOR124C	*UBP2*	Ubiquitin-specific protease; removes ubiquitin from ubiquitinated proteins; deubiquitinates Rsp5p and is required for MVB sorting of membrane proteins; can cleave polyubiquitin and has isopeptidase activity
YDL216C	*RRI1*	Catalytic subunit of the COP9 signalosome (CSN) complex; acts as an isopeptidase in cleaving the ubiquitin-like protein Nedd8 from SCF ubiquitin ligases; metalloendopeptidase involved in the adaptation to pheromone signaling
YFR044C	*DUG1*	Cys-Gly metallo-di-peptidase; forms a complex with Dug2p and Dug3p to degrade glutathione (GSH) and other peptides containing a gamma-glu-X bond in an alternative pathway to GSH degradation by gamma-glutamyl transpeptidase (Ecm38p)
YKL103C	*APE1*	Vacuolar aminopeptidase yscI; zinc metalloproteinase that belongs to the peptidase family M18; often used as a marker protein in studies of autophagy and cytosol to vacuole targeting (CVT) pathway; protein increases in abundance and relative distribution to cytoplasmic foci increases upon DNA replication stress
YBR281C	*DUG2*	Component of glutamine amidotransferase (GATase II); forms a complex with Dug3p to degrade glutathione (GSH) and other peptides containing a gamma-glu-X bond in an alternative pathway to GSH degradation by gamma-glutamyl transpeptidase (Ecm38p)
YBR286W	*APE3*	Vacuolar aminopeptidase Y; processed to mature form by Prb1p
YHR047C	*AAP1*	Arginine/alanine amino peptidase; overproduction stimulates glycogen accumulation; AAP1 has a paralog, APE2, that arose from the whole genome duplication
YKL157W	*APE2*	Aminopeptidase yscII; may have a role in obtaining leucine from dipeptide substrates; APE2 has a paralog, AAP1, that arose from the whole genome duplication
YLR262C	*YPT6*	Rab family GTPase; Ras-like GTP binding protein involved in the secretory pathway, required for fusion of endosome-derived vesicles with the late Golgi, maturation of the vacuolar carboxypeptidase Y; resides temporarily at the Golgi, dissociates into cytosol upon arrival of the Rab GTPaseYpt32p, which also functions in the late Golgi; Golgi-localized form is bound to GTP, while cytosolic form is GDP-bound; homolog of the mammalian Rab6
YLR299W	*ECM38*	Gamma-glutamyltranspeptidase; major glutathione-degrading enzyme; involved in detoxification of electrophilic xenobiotics; expression induced mainly by nitrogen starvation

YNL191W	*DUG3*	Component of glutamine amidotransferase (GATase II); forms a complex with Dug2p to degrade glutathione (GSH) and other peptides containing a gamma-glu-X bond in an alternative pathway to GSH degradation by gamma-glutamyl transpeptidase (Ecm38p)
YNL045W	*LAP2*	Leucyl aminopeptidase yscIV with epoxide hydrolase activity; metalloenzyme containing one zinc atom; green fluorescent protein (GFP)-fusion protein localizes to the cytoplasm and nucleus; also known as leukotriene A4 hydrolase
YOL057W	/	Dipeptidyl-peptidase III; cleaves dipeptides from the amino terminus of target proteins; highly active on synthetic substrate Arg-Arg-2-naphthylamide; mammalian ortholog may be a biomarker for some cancers
YMR297W	*PRC1*	Vacuolar carboxypeptidase Y (proteinase C, CPY); broad-specificity C-terminal exopeptidase involved in non-specific protein degradation in the vacuole; member of the serine carboxypeptidase family
YBR058C	*UBP14*	Ubiquitin-specific protease; specifically disassembles unanchored ubiquitin chains; involved in fructose-1,6-bisphosphatase (Fbp1p) degradation; similar to human isopeptidase T
YBR139W	/	Putative serine type carboxypeptidase; role in phytochelatin synthesis; green fluorescent protein (GFP)-fusion protein localizes to the vacuole; expression induced by nitrogen limitation in a GLN3, GAT1-independent manner
YJL172W	*CPS1*	Vacuolar carboxypeptidase S; expression is induced under low-nitrogen conditions
YLR178C	*TFS1*	Inhibitor of carboxypeptidase Y (Prc1p), and Ras GAP (Ira2p); phosphatidylethanolamine-binding protein (PEBP) family member and ortholog of hPEBP1/RKIP, a natural metastasis suppressor; targets to vacuolar membranes during stationary phase; acetylated by NatB N-terminal acetyltransferase; protein abundance increases in response to DNA replication stress
YLR360W	*VPS38*	Part of a Vps34p phosphatidylinositol 3-kinase complex; functions in carboxypeptidase Y (CPY) sorting; binds Vps30p and Vps34p to promote production of phosphatidylinositol 3-phosphate (PtdIns3P) which stimulates kinase activity; required for overflow degradation of misfolded proteins when ERAD is saturated
YOL082W	*ATG19*	Receptor protein for the cytoplasm-to-vacuole targeting (Cvt) pathway; delivers cargo proteins aminopeptidase I (Ape1p) and alpha-mannosidase (Ams1p) to the phagophore assembly site for packaging into Cvt vesicles
YOR219C	*STE13*	Dipeptidyl aminopeptidase; Golgi integral membrane protein that cleaves on the carboxyl side of repeating -X-Ala- sequences, required for maturation of alpha factor, transcription is induced by a-factor
YOR288C	*MPD1*	Member of the protein disulfide isomerase (PDI) family; interacts with and inhibits the chaperone activity of Cne1p; MPD1 overexpression in a pdi1 null mutant suppresses defects in Pdi1p functions such as carboxypeptidase Y maturation
Deletion mutants not present in database (created by us)		
YOR391C	*HSP33*	Possible chaperone and cysteine protease; similar to E. coli Hsp31 and S. cerevisiae Hsp31p, Hsp32p, and Sno4p; member of the DJ-1/ThiJ/PfpI superfamily, which includes human DJ-1 involved in Parkinson's disease
YPL280W	*HSP32*	Possible chaperone and cysteine protease; similar to E. coli Hsp31 and S. cerevisiae Hsp31p, Hsp33p, and Sno4p; member of the DJ-1/ThiJ/PfpI superfamily, which includes human DJ-1 involved in Parkinson's disease
YEL059C-A	*SOM1*	Subunit of the mitochondrial inner membrane peptidase (IMP); IMP is required for maturation of mitochondrial proteins of the intermembrane space; Som1p facilitates cleavage of a subset of substrates; contains twin cysteine-x9-cysteine motifs
Essential genes (not tested)		
YCL052C	*PBN1*	Component of glycosylphosphatidylinositol-mannosyltransferase I; essential component; required for the autocatalytic post-translational processing of the protease B precursor Prb1p; localizes to ER in lumenal orientation; homolog of mammalian PIG-X
YFR004W	*RPN11*	Metalloprotease subunit of 19S regulatory particle; part of 26S proteasome lid; couples the deubiquitination and degradation of proteasome substrates; involved, independent of catalytic activity, in fission of mitochondria and

		peroxisomes; protein abundance increases in response to DNA replication stress
YGR098C	*ESP1*	Separase, a caspase-like cysteine protease; promotes sister chromatid separation by mediating dissociation of the cohesin Scc1p from chromatin; inhibits protein phosphatase 2A-Cdc55p to promote mitotic exit; inhibited by Pds1p; relative distribution to the nucleus increases upon DNA replication stress
YHR024C	*MAS2*	Alpha subunit of the mitochondrial processing protease (MPP); essential processing enzyme that cleaves the N-terminal targeting sequences from mitochondrially imported proteins
YJL156C	*SSY5*	Serine protease of SPS plasma membrane amino acid sensor system; contains an inhibitory domain that dissociates in response to extracellular amino acids, freeing a catalytic domain to activate transcription factor Stp1p; other members are Ssy1p and Ptr3p
YLR163C	*MAS1*	Beta subunit of the mitochondrial processing protease (MPP); essential processing enzyme that cleaves the N-terminal targeting sequences from mitochondrially imported proteins
YPL020C	*ULP1*	Protease that specifically cleaves Smt3p protein conjugates; required for cell cycle progression; associates with nucleoporins and may interact with septin rings during telophase; sequestered to the nucleolus under stress conditions
YOR157C	*PUP1*	Beta 2 subunit of the 20S proteasome; endopeptidase with trypsin-like activity that cleaves after basic residues; synthesized as a proprotein before being proteolytically processed for assembly into 20S particle; human homolog is subunit Z
YIR022W	*SEC11*	18kDa catalytic subunit of the Signal Peptidase Complex (SPC); the Signal Peptidase Complex cleaves the signal sequence of proteins targeted to the endoplasmic reticulum; other members are Spc1p, Spc2p, Spc3p, and Sec11p
YLR066W	*SPC3*	Subunit of signal peptidase complex; complex catalyzes cleavage of N-terminal signal sequences of proteins targeted to the secretory pathway; homologous to mammalian SPC22/23; other members of the complex are Spc1p, Spc2p, and Sec11p
YIL031W	*ULP2*	Peptidase that deconjugates Smt3/SUMO-1 peptides from proteins; plays a role in chromosome cohesion at centromeric regions and recovery from checkpoint arrest induced by DNA damage or DNA replication defects; potential Cdc28p substrate

REFERENCES

Amri Saroukolaei S., Ghabaee M., Shokri H., Khosravi A. and Badiei A. (2016). Evaluation of APR1 Gene Expression in Candida albicans Strains Isolated From Patients With Multiple Sclerosis. *Jundishapur J Microbiol* **9**: e33292.

Anderson T.M., Clay M.C., Cioffi A.G., Diaz K.A., Hisao G.S., Tuttle M.D., Nieuwkoop A.J., Comellas G., Maryum N., Wang S., Uno B.E., Wildeman E.L., Gonen T., Rienstra C.M. and Burke M.D. (2014). Amphotericin forms an extramembranous and fungicidal sterol sponge. *Nat Chem Biol* **10**: 400-406.

Antinori S., Milazzo L., Sollima S., Galli M. and Corbellino M. (2016). Candidemia and invasive candidiasis in adults: A narrative review. *Eur J Intern Med* **34**: 21-28.

Armstrong-James D., Brown G.D., Netea M.G., Zelante T., Gresnigt M.S., van de Veerdonk F.L. and Levitz S.M. (2017). Immunotherapeutic approaches to treatment of fungal diseases. *Lancet Infect Dis* **17**: e393-e402.

Arthington-Skaggs B.A., Jradi H., Desai T. and Morrison C.J. (1999). Quantitation of ergosterol content: novel method for determination of fluconazole susceptibility of Candida albicans. *J Clin Microbiol* **37**: 3332-3337.

Avadhani N.G., Sangar M.C., Bansal S. and Bajpai P. (2011). Bimodal targeting of cytochrome P450s to endoplasmic reticulum and mitochondria: the concept of chimeric signals. *Febs J* **278**: 4218-4229.

Baker K.P., Schaniel A., Vestweber D. and Schatz G. (1990). A yeast mitochondrial outer membrane protein essential for protein import and cell viability. *Nature* **348**: 605-609.

Bard M., Lees N.D., Turi T., Craft D., Cofrin L., Barbuch R., Koegel C. and Loper J.C. (1993). Sterol synthesis and viability of erg11 (cytochrome P450 lanosterol demethylase) mutations in Saccharomyces cerevisiae and Candida albicans. *Lipids* **28**: 963-967.

Barnett J.A. (1998). A history of research on yeasts. 1: Work by chemists and biologists 1789-1850. *Yeast* **14**: 1439-1451.

Barnett J.A. and Robinow C.F. (2002a). A history of research on yeasts 4: cytology part I, 1890-1950. *Yeast* **19**: 151-182.

Barnett J.A. and Robinow C.F. (2002b). A history of research on yeasts 4: cytology part II, 1950-1990. *Yeast* **19**: 745-772.

Bauerova V., Hajek M., Pichova I. and Hruskova-Heidingsfeldova O. (2014). Intracellular aspartic proteinase Apr1p of Candida albicans is required for morphological transition under nitrogen-limited conditions but not for macrophage killing. *Folia Microbiol (Praha)* **59**: 485-493.

Bauerova V., Pichova I. and Hruskova-Heidingsfeldova O. (2012). Nitrogen source and growth stage of Candida albicans influence expression level of vacuolar aspartic protease Apr1p and carboxypeptidase Cpy1p. *Can J Microbiol* **58**: 678-681.

Bergman L.W. (2001). Growth and maintenance of yeast. *Methods Mol Biol* **177**: 9-14.

Berman J. and Sudbery P.E. (2002). Candida Albicans: a molecular revolution built on lessons from budding yeast. *Nat Rev Genet* **3**: 918-930.

Bernales S., McDonald K.L. and Walter P. (2006). Autophagy counterbalances endoplasmic reticulum expansion during the unfolded protein response. *PLoS Biol* **4**: e423.

Bongomin F., Gago S., Oladele R.O. and Denning D.W. (2017). Global and Multi-National Prevalence of Fungal Diseases-Estimate Precision. *J Fungi (Basel)* **3**.

Borman A.M., Fraser M., Palmer M.D., Szekely A., Houldsworth M., Patterson Z. and Johnson E.M. (2017). MIC Distributions and Evaluation of Fungicidal Activity for Amphotericin B, Itraconazole, Voriconazole, Posaconazole and Caspofungin and 20 Species of Pathogenic Filamentous Fungi Determined Using the CLSI Broth Microdilution Method. *J Fungi (Basel)* **3**.

Botstein D. and Fink G.R. (2011). Yeast: an experimental organism for 21st Century biology. *Genetics* **189**: 695-704.

Brown G.D., Denning D.W., Gow N.A., Levitz S.M., Netea M.G. and White T.C. (2012a). Hidden killers: human fungal infections. *Sci Transl Med* **4**: 165rv113.

Brown G.D., Denning D.W. and Levitz S.M. (2012b). Tackling human fungal infections. *Science* **336**: 647.

Cantu D., Govindarajulu M., Kozik A., Wang M., Chen X., Kojima K.K., Jurka J., Michelmore R.W. and Dubcovsky J. (2011). Next generation sequencing provides rapid access to the genome of Puccinia striiformis f. sp. tritici, the causal agent of wheat stripe rust. *PLoS One* **6**: e24230.

Chatton B., Walter P., Ebel J.P., Lacroute F. and Fasiolo F. (1988). The yeast VAS1 gene encodes both mitochondrial and cytoplasmic valyl-tRNA synthetases. *J Biol Chem* **263**: 52-57.

Chen X., Ren B., Chen M., Liu M.X., Ren W., Wang Q.X., Zhang L.X. and Yan G.Y. (2014). ASDCD: antifungal synergistic drug combination database. *PLoS One* **9**: e86499.

Claros M.G. and Vincens P. (1996). Computational method to predict mitochondrially imported proteins and their targeting sequences. *European journal of biochemistry* **241**: 779-786.

Craven R.J., Mallory J.C. and Hand R.A. (2007). Regulation of iron homeostasis mediated by the heme-binding protein Dap1 (damage resistance protein 1) via the P450 protein Erg11/Cyp51. *J Biol Chem* **282**: 36543-36551.

Crowley J.H., Smith S.J., Leak F.W. and Parks L.W. (1996). Aerobic isolation of an ERG24 null mutant of Saccharomyces cerevisiae. *J Bacteriol* **178**: 2991-2993.

Delarze E. and Sanglard D. (2015). Defining the frontiers between antifungal resistance, tolerance and the

concept of persistence. *Drug Resist Updat* **23**: 12-19.
Demuyser L., Swinnen E., Fiori A., Herrera-Malaver B., Vestrepen K. and Van Dijck P. (2017). Mitochondrial Cochaperone Mge1 Is Involved in Regulating Susceptibility to Fluconazole in Saccharomyces cerevisiae and Candida Species. *mBio* **8**.
Diekema D., Arbefeville S., Boyken L., Kroeger J. and Pfaller M. (2012). The changing epidemiology of healthcare-associated candidemia over three decades. *Diagn Microbiol Infect Dis* **73**: 45-48.
Diekert K., de Kroon A.I., Kispal G. and Lill R. (2001). Isolation and subfractionation of mitochondria from the yeast Saccharomyces cerevisiae. *Methods Cell Biol* **65**: 37-51.
Dinur-Mills M., Tal M. and Pines O. (2008). Dual targeted mitochondrial proteins are characterized by lower MTS parameters and total net charge. *PLoS One* **3**: e2161.
Doern G.V. and Brecher S.M. (2011). The Clinical Predictive Value (or Lack Thereof) of the Results of In Vitro Antimicrobial Susceptibility Tests. *Journal of Clinical Microbiology* **49**: S11-S14.
Dudgeon D.D., Zhang N.,Ositelu O.O., Kim H. and Cunningham K.W. (2008). Nonapoptotic death of Saccharomyces cerevisiae cells that is stimulated by Hsp90 and inhibited by calcineurin and Cmk2 in response to endoplasmic reticulum stresses. *Eukaryot Cell* **7**: 2037-2051.
Duina A.A., Miller M.E. and Keeney J.B. (2014). Budding yeast for budding geneticists: a primer on the Saccharomyces cerevisiae model system. *Genetics* **197**: 33-48.
Edwards J.E., Jr., Schwartz M.M., Schmidt C.S., Sobel J.D., Nyirjesy P., Schodel F., Marchus E., Lizakowski M., DeMontigny E.A., Hoeg J., Holmberg T., Cooke M.T., Hoover K., Edwards L., Jacobs M., Sussman S., Augenbraun M., Drusano M., Yeaman M.R., Ibrahim A.S., Filler S.G. and Hennessey J.P., Jr. (2018). A Fungal Immunotherapeutic Vaccine (NDV-3A) for Treatment of Recurrent Vulvovaginal Candidiasis-A Phase 2 Randomized, Double-Blind, Placebo-Controlled Trial. *Clin Infect Dis* **66**: 1928-1936.
Eisenberg-Bord M., Shai N., Schuldiner M. and Bohnert M. (2016). A Tether Is a Tether Is a Tether: Tethering at Membrane Contact Sites. *Dev Cell* **39**: 395-409.
Elbaz-Alon Y. (2017). Mitochondria-organelle contact sites: the plot thickens. *Biochem Soc Trans* **45**: 477-488.
Enache-Angoulvant A. and Hennequin C. (2005). Invasive Saccharomyces infection: a comprehensive review. *Clin Infect Dis* **41**: 1559-1568.
Ewen K.M., Ringle M. and Bernhardt R. (2012). Adrenodoxin--a versatile ferredoxin. *IUBMB Life* **64**: 506-512.
Fiori A. and Van Dijck P. (2012). Potent synergistic effect of doxycycline with fluconazole against Candida albicans is mediated by interference with iron homeostasis. *Antimicrob Agents Chemother* **56**: 3785-3796.
Fonzi W.A. and Irwin M.Y. (1993). Isogenic strain construction and gene mapping in Candida albicans. *Genetics* **134**: 717-728.
Foresti O., Rodriguez-Vaello V., Funaya C. and Carvalho P. (2014). Quality control of inner nuclear membrane proteins by the Asi complex. *Science* **346**: 751-755.
Fumagalli F., Noack J., Bergmann T.J., Cebollero E., Pisoni G.B., Fasana E., Fregno I., Galli C., Loi M., Solda T., D'Antuono R., Raimondi A., Jung M., Melnyk A., Schorr S., Schreiber A., Simonelli L., Varani L., Wilson-Zbinden C., Zerbe O., Hofmann K., Peter M., Quadroni M., Zimmermann R. and Molinari M. (2016). Translocon component Sec62 acts in endoplasmic reticulum turnover during stress recovery. *Nat Cell Biol* **18**: 1173-1184.
Gaigg B., Simbeni R., Hrastnik C., Paltauf F. and Daum G. (1995). Characterization of a microsomal subfraction associated with mitochondria of the yeast, Saccharomyces cerevisiae. Involvement in synthesis and import of phospholipids into mitochondria. *Biochim Biophys Acta* **1234**: 214-220.
Galluzzi L., Baehrecke E.H., Ballabio A., Boya P., Bravo-San Pedro J.M., Cecconi F., Choi A.M., Chu C.T., Codogno P., Colombo M.I., Cuervo A.M., Debnath J., Deretic V., Dikic I., Eskelinen E.L., Fimia G.M., Fulda S., Gewirtz D.A., Green D.R., Hansen M., Harper J.W., Jaattela M., Johansen T., Juhasz G., Kimmelman A.C., Kraft C., Ktistakis N.T., Kumar S., Levine B., Lopez-Otin C., Madeo F., Martens S., Martinez J., Melendez A., Mizushima N., Munz C., Murphy L.O., Penninger J.M., Piacentini M., Reggiori F., Rubinsztein D.C., Ryan K.M., Santambrogio L., Scorrano L., Simon A.K., Simon H.U., Simonsen A., Tavernarakis N., Tooze S.A., Yoshimori T., Yuan J., Yue Z., Zhong Q. and Kroemer G. (2017). Molecular definitions of autophagy and related processes. *EMBO J* **36**: 1811-1836.
Gao Y., Zhang C., Lu C., Liu P., Li Y., Li H. and Sun S. (2013). Synergistic effect of doxycycline and fluconazole against Candida albicans biofilms and the impact of calcium channel blockers. *FEMS Yeast Res* **13**: 453-462.
Gerami-Nejad M., Zacchi L.F., McClellan M., Matter K. and Berman J. (2013). Shuttle vectors for facile gap repair cloning and integration into a neutral locus in Candida albicans. *Microbiology* **159**: 565-579.
Giaever G., Chu A.M., Ni L., Connelly C., Riles L., Veronneau S., Dow S., Lucau-Danila A., Anderson K., Andre B., Arkin A.P., Astromoff A., El-Bakkoury M., Bangham R., Benito R., Brachat S., Campanaro S., Curtiss M., Davis K., Deutschbauer A., Entian K.D., Flaherty P., Foury F., Garfinkel D.J., Gerstein M., Gotte D., Guldener U., Hegemann J.H., Hempel S., Herman Z.,

Jaramillo D.F., Kelly D.E., Kelly S.L., Kotter P., LaBonte D., Lamb D.C., Lan N., Liang H., Liao H., Liu L., Luo C., Lussier M., Mao R., Menard P., Ooi S.L., Revuelta J.L., Roberts C.J., Rose M., Ross-Macdonald P., Scherens B., Schimmack G., Shafer B., Shoemaker D.D., Sookhai-Mahadeo S., Storms R.K., Strathern J.N., Valle G., Voet M., Volckaert G., Wang C.Y., Ward T.R., Wilhelmy J., Winzeler E.A., Yang Y., Yen G., Youngman E., Yu K., Bussey H., Boeke J.D., Snyder M., Philippsen P., Davis R.W. and Johnston M. (2002). Functional profiling of the Saccharomyces cerevisiae genome. *Nature* **418**: 387-391.

Giaever G. and Nislow C. (2014). The yeast deletion collection: a decade of functional genomics. *Genetics* **197**: 451-465.

Goffeau A., Barrell B.G., Bussey H., Davis R.W., Dujon B., Feldmann H., Galibert F., Hoheisel J.D., Jacq C., Johnston M., Louis E.J., Mewes H.W., Murakami Y., Philippsen P., Tettelin H. and Oliver S.G. (1996). Life with 6000 genes. *Science* **274**: 546, 563-547.

Grahl N. and Cramer R.A., Jr. (2010). Regulation of hypoxia adaptation: an overlooked virulence attribute of pathogenic fungi? *Med Mycol* **48**: 1-15.

Grau S., Pozo J.C., Roma E., Salavert M., Barrueta J.A., Peral C., Rodriguez I., Rubio-Rodriguez D. and Rubio-Terres C. (2015). Cost-effectiveness of three echinocandins and fluconazole in the treatment of candidemia and/or invasive candidiasis in nonneutropenic adult patients. *Clinicoecon Outcomes Res* **7**: 527-535.

Guinea J. (2014). Global trends in the distribution of Candida species causing candidemia. *Clin Microbiol Infect* **20 Suppl 6**: 5-10.

Hamill R.J. (2013). Amphotericin B formulations: a comparative review of efficacy and toxicity. *Drugs* **73**: 919-934.

Hanna D.A., Hu R., Kim H., Martinez-Guzman O., Torres M.P. and Reddi A.R. (2018). Heme bioavailability and signaling in response to stress in yeast cells. *J Biol Chem* **293**: 12378-12393.

He S. and Fox T.D. (1999). Mutations affecting a yeast mitochondrial inner membrane protein, pnt1p, block export of a mitochondrially synthesized fusion protein from the matrix. *Mol Cell Biol* **19**: 6598-6607.

Hecht K.A., O'Donnell A.F. and Brodsky J.L. (2014). The proteolytic landscape of the yeast vacuole. *Cell Logist* **4**: e28023.

Henry K.W., Nickels J.T. and Edlind T.D. (2002). ROX1 and ERG regulation in Saccharomyces cerevisiae: implications for antifungal susceptibility. *Eukaryot Cell* **1**: 1041-1044.

Herrera-Cruz M.S. and Simmen T. (2017). Of yeast, mice and men: MAMs come in two flavors. *Biol Direct* **12**: 3.

Hirsch H.H., Schiffer H.H., Muller H. and Wolf D.H. (1992). Biogenesis of the yeast vacuole (lysosome). Mutation in the active site of the vacuolar serine proteinase yscB abolishes proteolytic maturation of its 73-kDa precursor to the 41.5-kDa pro-enzyme and a newly detected 41-kDa peptide. *European journal of biochemistry* **203**: 641-653.

Hooper R.W., Ashcraft D.S. and Pankey G.A. (2018). In vitro synergy with fluconazole plus doxycycline or tigecycline against clinical Candida glabrata isolates. *Med Mycol*.

Hurt E.C. and Schatz G. (1987). A cytosolic protein contains a cryptic mitochondrial targeting signal. *Nature* **325**: 499-503.

Jacquier N. and Schneiter R. (2012). Mechanisms of sterol uptake and transport in yeast. *J Steroid Biochem Mol Biol* **129**: 70-78.

Joseph-Strauss D., Zenvirth D., Simchen G. and Barkai N. (2007). Spore germination in Saccharomyces cerevisiae: global gene expression patterns and cell cycle landmarks. *Genome Biol* **8**: R241.

Juneau K., Nislow C. and Davis R.W. (2009). Alternative splicing of PTC7 in Saccharomyces cerevisiae determines protein localization. *Genetics* **183**: 185-194.

Karenlampi S.O., Marin E. and Hanninen O.O. (1981). Effect of carbon source on the accumulation of cytochrome P-450 in the yeast Saccharomyces cerevisiae. *Biochem J* **194**: 407-413.

Karniely S. and Pines O. (2005). Single translation--dual destination: mechanisms of dual protein targeting in eukaryotes. *EMBO Rep* **6**: 420-425.

Keniya M.V., Sabherwal M., Wilson R.K., Woods M.A., Sagatova A.A., Tyndall J.D.A. and Monk B.C. (2018). Crystal structures of full-length lanosterol 14alpha-demethylases of prominent fungal pathogens Candida albicans and Candida glabrata provide tools for antifungal discovery. *Antimicrob Agents Chemother*.

Kerstens W. and Van Dijck P. (2018). A Cinderella story: how the vacuolar proteases Pep4 and Prb1 do more than cleaning up the cell's mass degradation processes. *Microb Cell* **5**: 438-443.

Kim H., Kim A. and Cunningham K.W. (2012). Vacuolar H+-ATPase (V-ATPase) promotes vacuolar membrane permeabilization and nonapoptotic death in stressed yeast. *J Biol Chem* **287**: 19029-19039.

Kizilyaprak C., Daraspe J. and Humbel B.M. (2014). Focused ion beam scanning electron microscopy in biology. *J Microsc* **254**: 109-114.

Klug L. and Daum G. (2014). Yeast lipid metabolism at a glance. *FEMS Yeast Res* **14**: 369-388.

Kohler J.R., Casadevall A. and Perfect J. (2014). The spectrum of fungi that infects humans. *Cold Spring Harb Perspect Med* **5**: a019273.

Korber M., Klein I. and Daum G. (2017). Steryl ester synthesis, storage and hydrolysis: A contribution to sterol homeostasis. *Biochim Biophys Acta* **1862**: 1534-1545.
Kornmann B., Currie E., Collins S.R., Schuldiner M., Nunnari J., Weissman J.S. and Walter P. (2009). An ER-mitochondria tethering complex revealed by a synthetic biology screen. *Science* **325**: 477-481.
Kumar A., Zarychanski R., Pisipati A., Kumar A., Kethireddy S. and Bow E.J. (2018). Fungicidal versus fungistatic therapy of invasive Candida infection in non-neutropenic adults: a meta-analysis. *Mycology* **9**: 116-128.
Kuranda K., Francois J. and Palamarczyk G. (2010). The isoprenoid pathway and transcriptional response to its inhibitors in the yeast Saccharomyces cerevisiae. *FEMS Yeast Res* **10**: 14-27.
Kursu V.A., Pietikainen L.P., Fontanesi F., Aaltonen M.J., Suomi F., Raghavan Nair R., Schonauer M.S., Dieckmann C.L., Barrientos A., Hiltunen J.K. and Kastaniotis A.J. (2013). Defects in mitochondrial fatty acid synthesis result in failure of multiple aspects of mitochondrial biogenesis in Saccharomyces cerevisiae. *Mol Microbiol* **90**: 824-840.
Kwast K.E., Lai L.C., Menda N., James D.T., 3rd, Aref S. and Burke P.V. (2002). Genomic analyses of anaerobically induced genes in Saccharomyces cerevisiae: functional roles of Rox1 and other factors in mediating the anoxic response. *J Bacteriol* **184**: 250-265.
Lagrou K., Maertens J., Van Even E. and Denning D.W. (2015). Burden of serious fungal infections in Belgium. *Mycoses* **58 Suppl 5**: 1-5.
Lah L., Krasevec N., Trontelj P. and Komel R. (2008). High diversity and complex evolution of fungal cytochrome P450 reductase: cytochrome P450 systems. *Fungal Genet Biol* **45**: 446-458.
Lahiri S., Chao J.T., Tavassoli S., Wong A.K., Choudhary V., Young B.P., Loewen C.J. and Prinz W.A. (2014). A conserved endoplasmic reticulum membrane protein complex (EMC) facilitates phospholipid transfer from the ER to mitochondria. *PLoS Biol* **12**: e1001969.
Lam S.S., Martell J.D., Kamer K.J., Deerinck T.J., Ellisman M.H., Mootha V.K. and Ting A.Y. (2015). Directed evolution of APEX2 for electron microscopy and proximity labeling. *Nat Methods* **12**: 51-54.
Lamb D.C., Kelly D.E., Manning N.J., Kaderbhai M.A. and Kelly S.L. (1999a). Biodiversity of the P450 catalytic cycle: yeast cytochrome b5/NADH cytochrome b5 reductase complex efficiently drives the entire sterol 14-demethylation (CYP51) reaction. *FEBS Lett* **462**: 283-288.
Lamb D.C., Kelly D.E., Venkateswarlu K., Manning N.J., Bligh H.F., Schunck W.H. and Kelly S.L. (1999b). Generation of a complete, soluble, and catalytically active sterol 14 alpha-demethylase-reductase complex. *Biochemistry* **38**: 8733-8738.
Lamb D.C. and Waterman M.R. (2013). Unusual properties of the cytochrome P450 superfamily. *Philos Trans R Soc Lond B Biol Sci* **368**: 20120434.
Lange H., Kaut A., Kispal G. and Lill R. (2000). A mitochondrial ferredoxin is essential for biogenesis of cellular iron-sulfur proteins. *Proc Natl Acad Sci U S A* **97**: 1050-1055.
Lasserre J.P., Dautant A., Aiyar R.S., Kucharczyk R., Glatigny A., Tribouillard-Tanvier D., Rytka J., Blondel M., Skoczen N., Reynier P., Pitayu L., Rotig A., Delahodde A., Steinmetz L.M., Dujardin G., Procaccio V. and di Rago J.P. (2015). Yeast as a system for modeling mitochondrial disease mechanisms and discovering therapies. *Dis Model Mech* **8**: 509-526.
Leber R., Landl K., Zinser E., Ahorn H., Spok A., Kohlwein S.D., Turnowsky F. and Daum G. (1998). Dual localization of squalene epoxidase, Erg1p, in yeast reflects a relationship between the endoplasmic reticulum and lipid particles. *Mol Biol Cell* **9**: 375-386.
Lemire B.D., Fankhauser C., Baker A. and Schatz G. (1989). The Mitochondrial Targeting Function of Randomly Generated Peptide Sequences Correlates with Predicted Helical Amphiphilicity. *J Biol Chem* **264**: 20206-20215.
Lenney J.F. (1956). A study of two yeast proteinases. *J Biol Chem* **221**: 919-930.
Lepesheva G.I. and Waterman M.R. (2007). Sterol 14alpha-demethylase cytochrome P450 (CYP51), a P450 in all biological kingdoms. *Biochim Biophys Acta* **1770**: 467-477.
Lepesheva G.I. and Waterman M.R. (2011). Structural basis for conservation in the CYP51 family. *Biochim Biophys Acta* **1814**: 88-93.
Lewis J.S., 2nd and Graybill J.R. (2008). Fungicidal versus Fungistatic: what's in a word? *Expert Opin Pharmacother* **9**: 927-935.
Li M., Zhong Z., Zhu J., Xiang D., Dai N., Cao X., Qing Y., Yang Z., Xie J., Li Z., Baugh L., Wang G. and Wang D. (2010). Identification and characterization of mitochondrial targeting sequence of human apurinic/apyrimidinic endonuclease 1. *J Biol Chem* **285**: 14871-14881.
Li S.C. and Kane P.M. (2009). The yeast lysosome-like vacuole: endpoint and crossroads. *Biochim Biophys Acta* **1793**: 650-663.
Liao M., Zgoda V.G., Murray B.P. and Correia M.A. (2005). Vacuolar degradation of rat liver CYP2B1 in Saccharomyces cerevisiae: further validation of the yeast model and structural implications for the degradation of mammalian endoplasmic reticulum P450 proteins. *Mol Pharmacol* **67**: 1460-1469.
Lipatova Z. and Segev N. (2015). A Role for Macro-ER-Phagy in ER Quality Control. *PLoS Genet* **11**: e1005390.
Longo V.D., Shadel G.S., Kaeberlein M. and Kennedy B. (2012). Replicative and chronological aging in Saccharomyces cerevisiae. *Cell Metab* **16**: 18-31.

Lyons C.N. and White T.C. (2000). Transcriptional analyses of antifungal drug resistance in Candida albicans. *Antimicrob Agents Chemother* **44**: 2296-2303.
Marques A.C., Vinckenbosch N., Brawand D. and Kaessmann H. (2008). Functional diversification of duplicate genes through subcellular adaptation of encoded proteins. *Genome Biol* **9**: R54.
Mason D.A., Shulga N., Undavai S., Ferrando-May E., Rexach M.F. and Goldfarb D.S. (2005). Increased nuclear envelope permeability and Pep4p-dependent degradation of nucleoporins during hydrogen peroxide-induced cell death. *FEMS Yeast Res* **5**: 1237-1251.
Mayer F.L., Wilson D. and Hube B. (2013). Candida albicans pathogenicity mechanisms. *Virulence* **4**: 119-128.
Mechler B., Hirsch H.H., Muller H. and Wolf D.H. (1988). Biogenesis of the yeast lysosome (vacuole): biosynthesis and maturation of proteinase yscB. *EMBO J* **7**: 1705-1710.
Miura F., Kawaguchi N., Sese J., Toyoda A., Hattori M., Morishita S. and Ito T. (2006). A large-scale full-length cDNA analysis to explore the budding yeast transcriptome. *Proc Natl Acad Sci U S A* **103**: 17846-17851.
Mo C. and Bard M. (2005). A systematic study of yeast sterol biosynthetic protein-protein interactions using the split-ubiquitin system. *Biochim Biophys Acta* **1737**: 152-160.
Moehle C.M., Aynardi M.W., Kolodny M.R., Park F.J. and Jones E.W. (1987). Protease B of Saccharomyces cerevisiae: isolation and regulation of the PRB1 structural gene. *Genetics* **115**: 255-263.
Moehle C.M. and Jones E.W. (1990). Consequences of growth media, gene copy number, and regulatory mutations on the expression of the PRB1 gene of Saccharomyces cerevisiae. *Genetics* **124**: 39-55.
Monk B.C., Tomasiak T.M., Keniya M.V., Huschmann F.U., Tyndall J.D., O'Connell J.D., 3rd, Cannon R.D., McDonald J.G., Rodriguez A., Finer-Moore J.S. and Stroud R.M. (2014). Architecture of a single membrane spanning cytochrome P450 suggests constraints that orient the catalytic domain relative to a bilayer. *Proc Natl Acad Sci U S A* **111**: 3865-3870.
Morgenstern M., Stiller S.B., Lubbert P., Peikert C.D., Dannenmaier S., Drepper F., Weill U., Hoss P., Feuerstein R., Gebert M., Bohnert M., van der Laan M., Schuldiner M., Schutze C., Oeljeklaus S., Pfanner N., Wiedemann N. and Warscheid B. (2017). Definition of a High-Confidence Mitochondrial Proteome at Quantitative Scale. *Cell Rep* **19**: 2836-2852.
Mortimer R.K. (2000). Evolution and variation of the yeast (Saccharomyces) genome. *Genome Res* **10**: 403-409.
Muhsain S.N., Lang M.A. and Abu-Bakar A. (2015). Mitochondrial targeting of bilirubin regulatory enzymes: An adaptive response to oxidative stress. *Toxicol Appl Pharmacol* **282**: 77-89.
Muller F.M., Staudigel A., Salvenmoser S., Tredup A., Miltenberger R. and Herrmann J.V. (2007). Cross-resistance to medical and agricultural azole drugs in yeasts from the oropharynx of human immunodeficiency virus patients and from environmental Bavarian vine grapes. *Antimicrob Agents Chemother* **51**: 3014-3016.
Muller M., Schmidt O., Angelova M., Faserl K., Weys S., Kremser L., Pfaffenwimmer T., Dalik T., Kraft C., Trajanoski Z., Lindner H. and Teis D. (2015). The coordinated action of the MVB pathway and autophagy ensures cell survival during starvation. *Elife* **4**: e07736.
Murray B.P., Zgoda V.G. and Correia M.A. (2002). Native CYP2C11: heterologous expression in Saccharomyces cerevisiae reveals a role for vacuolar proteases rather than the proteasome system in the degradation of this endoplasmic reticulum protein. *Mol Pharmacol* **61**: 1146-1153.
Naik R.R., Nebes V. and Jones E.W. (1997). Regulation of the proteinase B structural gene PRB1 in Saccharomyces cerevisiae. *J Bacteriol* **179**: 1469-1474.
Natsoulis G., Hilger F. and Fink G.R. (1986). The HTS1 gene encodes both the cytoplasmic and mitochondrial histidine tRNA synthetases of S. cerevisiae. *Cell* **46**: 235-243.
Nebes V.L. and Jones E.W. (1991). Activation of the proteinase B precursor of the yeast Saccharomyces cerevisiae by autocatalysis and by an internal sequence. *J Biol Chem* **266**: 22851-22857.
Nguyen N., Quail M.M.F. and Hernday A.D. (2017). An Efficient, Rapid, and Recyclable System for CRISPR-Mediated Genome Editing in Candida albicans. *mSphere* **2**.
Nobile C.J. and Johnson A.D. (2015). Candida albicans Biofilms and Human Disease. *Annu Rev Microbiol* **69**: 71-92.
Ohsumi Y. (2014). Historical landmarks of autophagy research. *Cell Res* **24**: 9-23.
Oliver B.G., Song J.L., Choiniere J.H. and White T.C. (2007). cis-Acting elements within the Candida albicans ERG11 promoter mediate the azole response through transcription factor Upc2p. *Eukaryot Cell* **6**: 2231-2239.
Onodera J. and Ohsumi Y. (2004). Ald6p is a preferred target for autophagy in yeast, Saccharomyces cerevisiae. *J Biol Chem* **279**: 16071-16076.
Opalinska M. and Meisinger C. (2015). Metabolic control via the mitochondrial protein import machinery. *Curr Opin Cell Biol* **33**: 42-48.
Oslowski C.M. and Urano F. (2011). Measuring ER stress and the unfolded protein response using mammalian tissue culture system. *Methods Enzymol* **490**: 71-92.
Ostrosky-Zeichner L., Casadevall A., Galgiani J.N., Odds F.C. and Rex J.H. (2010). An insight into the antifungal pipeline: selected new molecules and beyond. *Nat Rev Drug Discov* **9**: 719-727.

Ota M., Gonja H., Koike R. and Fukuchi S. (2016). Multiple-Localization and Hub Proteins. *PLoS One* **11**: e0156455.
Ott R.G., Athenstaedt K., Hrastnik C., Leitner E., Bergler H. and Daum G. (2005). Flux of sterol intermediates in a yeast strain deleted of the lanosterol C-14 demethylase Erg11p. *Biochim Biophys Acta* **1735**: 111-118.
Outten C.E. and Culotta V.C. (2004). Alternative start sites in the Saccharomyces cerevisiae GLR1 gene are responsible for mitochondrial and cytosolic isoforms of glutathione reductase. *J Biol Chem* **279**: 7785-7791.
Palmer G.E., Askew D.S. and Williamson P.R. (2008). The diverse roles of autophagy in medically important fungi. *Autophagy* **4**: 982-988.
Palmer G.E., Kelly M.N. and Sturtevant J.E. (2007). Autophagy in the pathogen Candida albicans. *Microbiology* **153**: 51-58.
Parks L.W. and Casey W.M. (1995). Physiological implications of sterol biosynthesis in yeast. *Annu Rev Microbiol* **49**: 95-116.
Pereira C., Bessa C., Soares J., Leao M. and Saraiva L. (2012). Contribution of yeast models to neurodegeneration research. *J Biomed Biotechnol* **2012**: 941232.
Perez-Torrado R. and Querol A. (2015). Opportunistic Strains of Saccharomyces cerevisiae: A Potential Risk Sold in Food Products. *Front Microbiol* **6**: 1522.
Perfect J.R. (2017). The antifungal pipeline: a reality check. *Nat Rev Drug Discov* **16**: 603-616.
Perlin D.S., Rautemaa-Richardson R. and Alastruey-Izquierdo A. (2017). The global problem of antifungal resistance: prevalence, mechanisms, and management. *Lancet Infect Dis* **17**: e383-e392.
Pfaller M., Diekema D. and Merz W.G., (2009) Infections caused by non-Candida, non-Cryptococcus yeasts. In: Clinical Mycology. Elsevier Inc., pp. 251-270.
Pfaller M.A. (2012). Antifungal drug resistance: mechanisms, epidemiology, and consequences for treatment. *Am J Med* **125**: S3-13.
Pfaller M.A. and Diekema D.J. (2007). Epidemiology of invasive candidiasis: a persistent public health problem. *Clin Microbiol Rev* **20**: 133-163.
Pfaller M.A. and Diekema D.J. (2010). Epidemiology of invasive mycoses in North America. *Crit Rev Microbiol* **36**: 1-53.
Phadke S.S., Maclean C.J., Zhao S.Y., Mueller E.A., Michelotti L.A., Norman K.L., Kumar A. and James T.Y. (2018). Genome-Wide Screen for Saccharomyces cerevisiae Genes Contributing to Opportunistic Pathogenicity in an Invertebrate Model Host. *G3* **8**: 63-78.
Pichler H., Gaigg B., Hrastnik C., Achleitner G., Kohlwein S.D., Zellnig G., Perktold A. and Daum G. (2001). A subfraction of the yeast endoplasmic reticulum associates with the plasma membrane and has a high capacity to synthesize lipids. *European journal of biochemistry* **268**: 2351-2361.
Pierson C.A., Eckstein J., Barbuch R. and Bard M. (2004). Ergosterol gene expression in wild-type and ergosterol-deficient mutants of Candida albicans. *Med Mycol* **42**: 385-389.
Pino P., Foth B.J., Kwok L.Y., Sheiner L., Schepers R., Soldati T. and Soldati-Favre D. (2007). Dual targeting of antioxidant and metabolic enzymes to the mitochondrion and the apicoplast of Toxoplasma gondii. *PLoS Pathog* **3**: e115.
Porras P., Padilla C.A., Krayl M., Voos W. and Barcena J.A. (2006). One single in-frame AUG codon is responsible for a diversity of subcellular localizations of glutaredoxin 2 in Saccharomyces cerevisiae. *J Biol Chem* **281**: 16551-16562.
Prokisch H., Scharfe C., Camp D.G., 2nd, Xiao W., David L., Andreoli C., Monroe M.E., Moore R.J., Gritsenko M.A., Kozany C., Hixson K.K., Mottaz H.M., Zischka H., Ueffing M., Herman Z.S., Davis R.W., Meitinger T., Oefner P.J., Smith R.D. and Steinmetz L.M. (2004). Integrative analysis of the mitochondrial proteome in yeast. *PLoS Biol* **2**: e160.
Qian W. and Zhang J. (2009). Protein subcellular relocalization in the evolution of yeast singleton and duplicate genes. *Genome Biol Evol* **1**: 198-204.
Qu Y., Jelicic B., Pettolino F., Perry A., Lo T.L., Hewitt V.L., Bantun F., Beilharz T.H., Peleg A.Y., Lithgow T., Djordjevic J.T. and Traven A. (2012). Mitochondrial sorting and assembly machinery subunit Sam37 in Candida albicans: insight into the roles of mitochondria in fitness, cell wall integrity, and virulence. *Eukaryot Cell* **11**: 532-544.
Reggiori F. and Klionsky D.J. (2013). Autophagic processes in yeast: mechanism, machinery and regulation. *Genetics* **194**: 341-361.
Reiners J.J., Jr., Kleinman M., Kessel D., Mathieu P.A. and Caruso J.A. (2011). Nonesterified cholesterol content of lysosomes modulates susceptibility to oxidant-induced permeabilization. *Free Radic Biol Med* **50**: 281-294.
Reuss O., Vik A., Kolter R. and Morschhauser J. (2004). The SAT1 flipper, an optimized tool for gene disruption in Candida albicans. *Gene* **341**: 119-127.
Rex J.H. and Pfaller M.A. (2002). Has antifungal susceptibility testing come of age? *Clin Infect Dis* **35**: 982-989.
Rodriguez R.J. and Parks L.W. (1983). Structural and physiological features of sterols necessary to satisfy bulk membrane and sparking requirements in yeast sterol auxotrophs. *Arch Biochem Biophys* **225**:

861-871.
Roemer T. and Krysan D.J. (2014). Antifungal drug development: challenges, unmet clinical needs, and new approaches. *Cold Spring Harb Perspect Med* **4**.
Rupp S. and Wolf D.H. (1995). Biogenesis of the yeast vacuole (lysosome). The use of active-site mutants of proteinase yscA to determine the necessity of the enzyme for vacuolar proteinase maturation and proteinase yscB stability. *European journal of biochemistry* **231**: 115-125.
Rutter J. and Hughes A.L. (2015). Power(2): the power of yeast genetics applied to the powerhouse of the cell. *Trends Endocrinol Metab* **26**: 59-68.
Sagatova A.A., Keniya M.V., Wilson R.K., Monk B.C. and Tyndall J.D. (2015). Structural Insights into Binding of the Antifungal Drug Fluconazole to Saccharomyces cerevisiae Lanosterol 14alpha-Demethylase. *Antimicrob Agents Chemother* **59**: 4982-4989
Sandig G., Kargel E., Menzel R., Vogel F., Zimmer T. and Schunck W.H. (1999). Regulation of endoplasmic reticulum biogenesis in response to cytochrome P450 overproduction. *Drug Metab Rev* **31**: 393-410.
Sanglard D., Ischer F., Parkinson T., Falconer D. and Bille J. (2003). Candida albicans mutations in the ergosterol biosynthetic pathway and resistance to several antifungal agents. *Antimicrob Agents Chemother* **47**: 2404-2412.
Sanguinetti M. and Posteraro B. (2017). New approaches for antifungal susceptibility testing. *Clin Microbiol Infect* **23**: 931-934.
Schneiter R. (2007). Intracellular sterol transport in eukaryotes, a connection to mitochondrial function? *Biochimie* **89**: 255-259.
Schreiber K., Csaba G., Haslbeck M. and Zimmer R. (2015). Alternative Splicing in Next Generation Sequencing Data of Saccharomyces cerevisiae. *PLoS One* **10**: e0140487.
Schuck S. (2016). On keeping the right ER size. *Nat Cell Biol* **18**: 1118-1119.
Schuck S., Gallagher C.M. and Walter P. (2014). ER-phagy mediates selective degradation of endoplasmic reticulum independently of the core autophagy machinery. *J Cell Sci* **127**: 4078-4088.
Sevrioukova I.F., Li H., Zhang H., Peterson J.A. and Poulos T.L. (1999). Structure of a cytochrome P450-redox partner electron-transfer complex. *Proc Natl Acad Sci U S A* **96**: 1863-1868.
Shapiro R.S., Robbins N. and Cowen L.E. (2011). Regulatory circuitry governing fungal development, drug resistance, and disease. *Microbiol Mol Biol Rev* **75**: 213-267.
Shen Y., Hixson K.K., Tolic N., Camp D.G., Purvine S.O., Moore R.J. and Smith R.D. (2008). Mass spectrometry analysis of proteome-wide proteolytic post-translational degradation of proteins. *Anal Chem* **80**: 5819-5828.
Sherman F. (1991). Getting started with yeast. *Methods Enzymol* **194**: 3-21.
Shingu-Vazquez M. and Traven A. (2011). Mitochondria and fungal pathogenesis: drug tolerance, virulence, and potential for antifungal therapy. *Eukaryot Cell* **10**: 1376-1383.
Song J.L., Harry J.B., Eastman R.T., Oliver B.G. and White T.C. (2004). The Candida albicans lanosterol 14-alpha-demethylase (ERG11) gene promoter is maximally induced after prolonged growth with antifungal drugs. *Antimicrob Agents Chemother* **48**: 1136-1144.
Sorger D. and Daum G. (2002). Synthesis of triacylglycerols by the acyl-coenzyme A:diacyl-glycerol acyltransferase Dga1p in lipid particles of the yeast Saccharomyces cerevisiae. *J Bacteriol* **184**: 519-524.
Spitzer M., Robbins N. and Wright G.D. (2017). Combinatorial strategies for combating invasive fungal infections. *Virulence* **8**: 169-185.
Steele D.F., Butler C.A. and Fox T.D. (1996). Expression of a recoded nuclear gene inserted into yeast mitochondrial DNA is limited by mRNA-specific translational activation. *Proc Natl Acad Sci U S A* **93**: 5253-5257.
Stone S.J., Levin M.C., Zhou P., Han J., Walther T.C. and Farese R.V., Jr. (2009). The endoplasmic reticulum enzyme DGAT2 is found in mitochondria-associated membranes and has a mitochondrial targeting signal that promotes its association with mitochondria. *J Biol Chem* **284**: 5352-5361.
Synnott J.M., Guida A., Mulhern-Haughey S., Higgins D.G. and Butler G. (2010). Regulation of the hypoxic response in Candida albicans. *Eukaryot Cell* **9**: 1734-1746.
Takeshige K., Baba M., Tsuboi S., Noda T. and Ohsumi Y. (1992). Autophagy in yeast demonstrated with proteinase-deficient mutants and conditions for its induction. *J Cell Biol* **119**: 301-311.
Tang H.L., Yeh L.S., Chen N.K., Ripmaster T., Schimmel P. and Wang C.C. (2004). Translation of a yeast mitochondrial tRNA synthetase initiated at redundant non-AUG codons. *J Biol Chem* **279**: 49656-49663.
Taylor S.D., Zhang H., Eaton J.S., Rodeheffer M.S., Lebedeva M.A., O'Rourke T W., Siede W. and Shadel G.S. (2005). The conserved Mec1/Rad53 nuclear checkpoint pathway regulates mitochondrial DNA copy number in Saccharomyces cerevisiae. *Mol Biol Cell* **16**: 3010-3018.
Teichert U., Mechler B., Muller H. and Wolf D.H. (1989). Lysosomal (vacuolar) proteinases of yeast are essential catalysts for protein degradation, differentiation, and cell survival. *J Biol Chem* **264**: 16037-16045.
Truan G., Epinat J.C., Rougeulle C., Cullin C. and Pompon D. (1994). Cloning and characterization of a yeast cytochrome b5-encoding gene which suppresses ketoconazole hypersensitivity in a NADPH-

P-450 reductase-deficient strain. *Gene* **142**: 123-127.
Turi T.G. and Loper J.C. (1992). Multiple regulatory elements control expression of the gene encoding the Saccharomyces cerevisiae cytochrome P450, lanosterol 14 alpha-demethylase (ERG11). *J Biol Chem* **267**: 2046-2056.
Van Den Hazel H.B., Kielland-Brandt M.C. and Winther J.R. (1996). Review: biosynthesis and function of yeast vacuolar proteases. *Yeast* **12**: 1-16.
Vembar S.S. and Brodsky J.L. (2008). One step at a time: endoplasmic reticulum-associated degradation. *Nat Rev Mol Cell Biol* **9**: 944-957.
Vergeres G., Yen T.S., Aggeler J., Lausier J. and Waskell L. (1993). A model system for studying membrane biogenesis. Overexpression of cytochrome b5 in yeast results in marked proliferation of the intracellular membrane. *J Cell Sci* **106 (Pt 1)**: 249-259.
Vermes A., Guchelaar H.J. and Dankert J. (2000). Flucytosine: a review of its pharmacology, clinical indications, pharmacokinetics, toxicity and drug interactions. *J Antimicrob Chemother* **46**: 171-179.
Vongsamphanh R., Fortier P.K. and Ramotar D. (2001). Pir1p mediates translocation of the yeast Apn1p endonuclease into the mitochondria to maintain genomic stability. *Mol Cell Biol* **21**: 1647-1655.
Vyas V.K., Barrasa M.I. and Fink G.R. (2015). A Candida albicans CRISPR system permits genetic engineering of essential genes and gene families. *Sci Adv* **1**: e1500248.
Vyas V.K., Bushkin G.G., Bernstein D.A., Getz M.A., Sewastianik M., Barrasa M.I., Bartel D.P. and Fink G.R. (2018). New CRISPR Mutagenesis Strategies Reveal Variation in Repair Mechanisms among Fungi. *mSphere* **3**.
Wald-Dickler N., Holtom P. and Spellberg B. (2018). Busting the Myth of "Static vs Cidal": A Systemic Literature Review. *Clin Infect Dis* **66**: 1470-1474.
Wang M., Roberts D.L., Paschke R., Shea T.M., Masters B.S. and Kim J.J. (1997). Three-dimensional structure of NADPH-cytochrome P450 reductase: prototype for FMN- and FAD-containing enzymes. *Proc Natl Acad Sci U S A* **94**: 8411-8416.
Werck-Reichhart D. and Feyereisen R. (2000). Cytochromes P450: a success story. *Genome Biol* **1**: REVIEWS3003.
Williams C.C., Jan C.H. and Weissman J.S. (2014). Targeting and plasticity of mitochondrial proteins revealed by proximity-specific ribosome profiling. *Science* **346**: 748-751.
Winzeler E.A., Shoemaker D.D., Astromoff A., Liang H., Anderson K., Andre B., Bangham R., Benito R., Boeke J.D., Bussey H., Chu A.M., Connelly C., Davis K., Dietrich F., Dow S.W., El Bakkoury M., Foury F., Friend S.H., Gentalen E., Giaever G., Hegemann J.H., Jones T., Laub M., Liao H., Liebundguth N., Lockhart D.J., Lucau-Danila A., Lussier M., M'Rabet N., Menard P., Mittmann M., Pai C., Rebischung C., Revuelta J.L., Riles L., Roberts C.J., Ross-MacDonald P., Scherens B., Snyder M., Sookhai-Mahadeo S., Storms R.K., Veronneau S., Voet M., Volckaert G., Ward T.R., Wysocki R., Yen G.S., Yu K., Zimmermann K., Philippsen P., Johnston M. and Davis R.W. (1999). Functional characterization of the S. cerevisiae genome by gene deletion and parallel analysis. *Science* **285**: 901-906.
Wolff A.M., Din N. and Petersen J.G. (1996). Vacuolar and extracellular maturation of Saccharomyces cerevisiae proteinase A. *Yeast* **12**: 823-832.
Woolford C.A., Daniels L.B., Park F.J., Jones E.W., Van Arsdell J.N. and Innis M.A. (1986). The PEP4 gene encodes an aspartyl protease implicated in the posttranslational regulation of Saccharomyces cerevisiae vacuolar hydrolases. *Mol Cell Biol* **6**: 2500-2510.
Woolford C.A., Noble J.A., Garman J.D., Tam M.F., Innis M.A. and Jones E.W. (1993). Phenotypic analysis of proteinase A mutants. Implications for autoactivation and the maturation pathway of the vacuolar hydrolases of Saccharomyces cerevisiae. *J Biol Chem* **268**: 8990-8998.
Wright R., Basson M., D'Ari L. and Rine J. (1988). Increased amounts of HMG-CoA reductase induce "karmellae": a proliferation of stacked membrane pairs surrounding the yeast nucleus. *J Cell Biol* **107**: 101-114.
Yang H., Tong J., Lee C.W., Ha S., Eom S.H. and Im Y.J. (2015). Structural mechanism of ergosterol regulation by fungal sterol transcription factor Upc2. *Nat Commun* **6**: 6129.
Yogev O. and Pines O. (2011). Dual targeting of mitochondrial proteins: mechanism, regulation and function. *Biochim Biophys Acta* **1808**: 1012-1020.
Zahedi R.P., Sickmann A., Boehm A.M., Winkler C., Zufall N., Schonfisch B., Guiard B., Pfanner N. and Meisinger C. (2006). Proteomic analysis of the yeast mitochondrial outer membrane reveals accumulation of a subclass of preproteins. *Mol Biol Cell* **17**: 1436-1450.
Zane L.T., Chanda S., Coronado D. and Del Rosso J. (2016). Antifungal agents for onychomycosis: new treatment strategies to improve safety. *Dermatol Online J* **22**.
Zavrel M., Hoot S.J. and White T.C. (2013). Comparison of sterol import under aerobic and anaerobic conditions in three fungal species, Candida albicans, Candida glabrata, and Saccharomyces cerevisiae. *Eukaryot Cell* **12**: 725-738.
Zhang Z. and Dietrich F.S. (2005). Mapping of transcription start sites in Saccharomyces cerevisiae using 5' SAGE. *Nucleic Acids Res* **33**: 2838-2851.
Ziegler K.J. and Schwartz A.C. (1991). Participation of proteinase yscA in the in vitro formation of the smaller

subunit of glycogen phosphorylase in extracts of Saccharomyces cerevisiae. *Yeast* **7**: 925-931.
Zinser E., Paltauf F. and Daum G. (1993). Sterol composition of yeast organelle membranes and subcellular distribution of enzymes involved in sterol metabolism. *J Bacteriol* **175**: 2853-2858.

CV AND LIST OF PUBLICATIONS

CV Winnie Kerstens

winnie.kerstens@gmail.com

Working experience

Doctoral student at VIB Department of Molecular Microbiology, KU Leuven	2013 - 2019
Master thesis in the lab of Functional Genomics and Proteomics, KU Leuven (1 year) Research on genes involved in the reproduction of nematodes	2012 - 2013
Summer job - **Assistent researcher** ADx NeuroSciences, Ghent (1 month) Identifying biomarkers Alzheimer's disease	2012
Master internship ADx NeuroSciences, Ghent (5 months) Identifying biomarkers Alzheimer's disease	2012
Summer jobs commercial sector (yearly, 1 month)	2006 - 2011

Education

PhD in Science in Biochemistry and Biotechnology, KU Leuven	2019
Master of Science in Biochemistry and Biotechnology, KU Leuven Graduated magna cum laude	2013
Bachelor of Science in Biochemistry and Biotechnology, KU Leuven Graduated magna cum laude	2011

Scientific expertise

Microbiology
Saccharomyces cerevisiae, *Candida albicans*

Biochemistry
extraction methods, purifying proteins, SDS-PAGE, western blotting, UV-VIS spectroscopy

Molecular biology
plasmid construction, homologous recombination techniques, CRISPR-Cas9, transformation methods, (qRT-)PCR

Microscopy

IT skills
Microsoft Office, Illustrator, Photoshop, Fiji/ImageJ, GraphPad Prism, ELN, CLC

Scientific grants
FEMS Young Scientists Grant to the 13th Yeast Lipid Conference (17 - 19 May 2017, Paris)

Additional trainings
Teacher assistant training (KU Leuven)
Laboratory Animal Science: FELASA Cat. B certificate (KU Leuven)
State-of-the-art Research Methods in Biology (KU Leuven)
Basic bioinformatics concepts, databases and tools (VIB)
The emerging power of quantitative proteomics in life sciences (VIB)
Tools for the analysis of membrane proteins (VIB)

List of publications

Kerstens W. and Van Dijck P. (2018). A Cinderella story: how the vacuolar proteases Pep4 and Prb1 do more than cleaning up the cell's mass degradation processes. *Microb Cell* **5**: 438-443.